TECHNISCHE UNIVERSITÄT MÜNCHEN

Lehrstuhl für Molekulare Ernährungsmedizin

The Role of the Parkinson's Disease associated Protein DJ-1 in the Development of Diet-induced Obesity in Mice

Katrin Seyfarth

Vollständiger Abdruck der von der Fakultät Wissenschaftszentrum Weihenstephan für Ernährung, Landnutzung und Umwelt der Technischen Universität München zur Erlangung des akademischen Grades eines

Doktors der Naturwissenschaften

genehmigten Dissertation.

Vorsitzender: Univ.-Prof. Dr. D. Haller

Prüfer der Dissertation:

1. Univ.-Prof. Dr. M. Klingenspor
2. Univ.-Prof. A. Schnieke, Ph.D.

Die Dissertation wurde am 07.05.2013 bei der Technischen Universität München eingereicht und durch die Fakultät Wissenschaftszentrum Weihenstephan für Ernährung, Landnutzung und Umwelt am 19.09.2013 angenommen.

You cannot help dealing with the limited information you have as if it were all there is to know. You build the best possible story from the information available to you, and if it is a good story, you believe it. Paradoxically, it is easier to construct a coherent story when you know little, when there are fewer pieces to fit into the puzzle. …

- Daniel Kahneman (Nobel Laureate in Economics 2002) in 'Thinking, fast and slow' -

CONTENTS

ABBREVIATIONS

$\Delta\Psi_m$	Membrane potential
2D-DIGE	Two-dimensional difference gel electrophoresis
ADP	Adenosine diphosphate
AGRP	agouti-related protein
α-MSH	α-melanocyte stimulating hormone
ANCOVA	Analysis of covariance
ANOVA	Analysis of variation
ARC	Arcuate nucleus
ATP	Adenosine triphosphate
BMR	Basal metabolic rate
BSA	Bovine serum albumin
CART	cocaine and amphetamine related transcript
cDNA	Complementary deoxyribonucleic acid
CV	Coefficient of variation
DIO	Diet-induced obesity
DNA	Deoxyribonucleic acid
DTT	Dithiothreitol
EDTA	Ethylenediaminetetraacetic acid
EGTA	Ethylene glycol tetraacetic acid
EI	Energy intake
ER	Endoplasmic reticulum
eWAT	Epididymal white adipose tissue
FCCP	Carbonyl cyanide-4-(trifluoromethoxy)phenylhydrazone
FOXO1	Forkhead box protein O1
GABA	γ-aminobutyric acid
HEPES	4-(2-hydroxyethyl)-1-piperazineethanesulfonic acid
HF	High fat
HF/HS	High-fat, high-sugar
HOMA-IR	Homeostatic model assessment - insulin resistance
HP	Heat production
HPLC-ESI	High-performance liquid chromatography - Electrospray ionization
i.p.	Intraperitoneal
IEF	Isoelectric focusing
IKK	Inhibitor of nuclear factor kappa-B kinase
IL	Interleukin
JNK	c-Jun-N-terminal kinase
KHE	KCl-HEPES-EGTA
MC4R	Melanocortin 4 receptor
M. gastroc	Musculus gastrocnemius

MR	Metabolic rate
mTOR	Mammalian target of rapamycin
MW	Molecular weight
NAC	N-acetylcysteine
NF-κB	Nuclear factor-κB
NMR	Nuclear magnetic resonance
NPY	Neuropeptide Y
OXPHOS	Oxidative phosporylation system
PAGE	Polyacrylamide gel electrophoresis
PCR	Polymerase chain reaction
PD	Parkinson's disease
pI	Isoelectric point
PI3K	Phosphatidylinositol-3-kinase
PKB/PKC	Protein kinase B (AKT)/ Protein kinase C
POMC	Pro-opiomelanocortin
poWAT	Periovarial white adipose tissue
psWAT	Posterior subcutaneous white adipose tissue
PTP1B	Protein-tyrosine phosphatase 1B
qRT-PCR	Quantitative real-time PCR
RCR	Respiratory control ratio
RER	Respiratory exchange ratio
RFU	Relative fluorescence units
RNA	Ribonucleic acid
ROS	Reactive oxygen species
SDS	Sodium dodecyl sulfate
SOCS3	Suppressor of cytokine signaling 3
STAT3	Signal transducer and activator of transcription 3
SUMO	Small ubiquitin-like modifier
TBS	Tris-buffered saline
TBST	Tris-buffered saline with Tween® 20
TLR	Toll-like receptor
TNF-α	Tumor necrosis factor-alpha
Tris	2-Amino-2-hydroxymethyl-propane-1,3-diol
UV	Ultraviolet
V̇O$_2$	Oxygen consumption rate

SUMMARY

DJ-1 is a multifunctional, evolutionarily ancient protein which is ubiquitously expressed in humans and mice. The diverse functions of DJ-1 including the protection from oxidative stress and apoptosis as well as maintenance of mitochondrial integrity can be attributed to its ability to interact with RNA as well as with numerous proteins. Moreover, mutations in the *DJ-1* (*PARK7*) gene are associated with inherited forms of Parkinson's disease (PD) and oxidatively damaged DJ-1 plays a role in aging and neurodegenerative diseases including Alzheimer and sporadic PD. Mouse lines deficient in *Dj-1* (*Dj-1*$^{-/-}$), however, do not show the age-dependent degeneration of dopaminergic neurons typical for PD.

In the present study, DJ-1 emerged as a candidate from a proteome analysis investigating alterations in the hypothalamus in response to a short-term diet intervention. Three mouse strains differing in their susceptibility to diet-induced obesity (DIO) were fed a high-fat (HF) or control diet for 10 days. Among the differentially expressed proteins, DJ-1 was more abundant in the HF diet groups of all strains as compared to the respective control groups. The DJ-1 protein pool comprises different post-translational modified isoforms. Therefore, we separated hypothalamic protein extracts based on their isoelectric point with subsequent immunodetection of DJ-1. Quantification revealed an increase in acidic DJ-1 isoforms in the hypothalamus of HF diet-fed mice relative to the control group, validating the initial proteome result. A similar shift in the DJ-1 isoform pattern was detected in the brain, skeletal muscle, pancreas, and liver but not in epididymal white adipose tissue.

We furthermore investigated the gene-diet interaction in mice lacking *Dj-1*. The susceptibility of *Dj-1*$^{-/-}$ mice to DIO is similar to wildtype mice with regard to body mass development but HF diet-feeding for 14 weeks resulted in higher fat accumulation in *Dj-1*$^{-/-}$ mice at the expense of lean mass. This effect was transient: With a prolonged feeding duration and/or advanced age, the fat mass was similar to wildtype mice, while the muscle mass was reduced in *Dj-1*$^{-/-}$ mice independent of diet. The altered body composition was not caused by measurable changes in energy intake or expenditure while locomotor activity was generally lower in *Dj-1*$^{-/-}$ mice. Our data imply that *Dj-1* deficiency and HF feeding interact to influence glucose levels and hypothalamic STAT3 phosphorylation without affecting glucose tolerance or anorectic leptin action. In a transciptome analysis of the ventral hypothalamus, however, we illustrate that HF diet-feeding has a greater impact on gene regulation in the absence of *Dj-1*.

Based on these results, we speculate that DJ-1 plays a role in the metabolic adaptation to a change in nutrient abundance or composition: HF diet-feeding modulates DJ-1 resulting in the maintenance of normal cellular homeostasis. When DJ-1 and its stabilizing function are absent, mice cope less efficient with metabolic changes induced by HF diet-feeding but are

finally able to compensate for the missing mechanisms. Our findings furthermore support a possible convergence or interaction of molecular pathways involved in obesity as well as neurodegeneration. Finally, obesity-associated metabolic changes might contribute to lower the threshold and therefore accelerate the development of age-related neurodegenerative diseases.

ZUSAMMENFASSUNG

DJ-1 ist ein multifunktionales, evolutionär frühzeitig entstandenes Protein, das sowohl im Menschen als auch in der Maus ubiquitär exprimiert wird. Unter anderem schützt DJ-1 vor oxidativem Stress und Apoptose und trägt zum Erhalt mitochondrialer Integrität bei. Die vielfältigen Funktionen von DJ-1 lassen sich auf die Fähigkeit, sowohl mit RNA als auch mit zahlreichen Proteinen interagieren zu können, zurückführen. Mutationen im *DJ-1 (PARK7)*-Gen wurden ferner mit erblichen Formen von Parkinson-Krankheit assoziiert und oxidativ geschädigtes DJ-1 spielt eine Rolle beim Altern und neurodegenerativen Erkrankungen wie der Alzheimer- und der sporadischen Parkinson-Erkrankung. *Dj-1* defiziente Mauslinien zeigen hingegen keine der für die Parkinson-Krankheit typischen altersabhängigen Degeneration dopaminerger Neurone.

In der vorliegenden Arbeit wurde DJ-1 als Kandidat einer Proteomstudie identifiziert, in der Veränderungen im Hypothalamus durch eine kurzzeitige Futterumstellung untersucht wurden. Hierbei erhielten drei Mausstämme mit unterschiedlicher Anfälligkeit gegenüber Diät-induzierter Adipositas für 10 Tage entweder fettreiches oder Kontrollfutter. Unter den differentiell exprimierten Proteinen war DJ-1 in den fettreich gefütterten Gruppen aller Stämme verstärkt im Vergleich zur jeweiligen Kontrollgruppe zu finden. Die Gesamtheit des DJ-1-Proteins setzt sich aus mehreren post-translational modifizierten Isoformen zusammen. Um die einzelnen Isoformen zu quantifizieren, trennten wir hypothalamische Proteinextrakte nach dem isoelektrischen Punkt auf und detektierten DJ-1 anschließend immunologisch. Die Quantifizierung zeigte ein Anstieg der saureren DJ-1 Isoformen im Hypothalamus von fettreich gefütterten Mäusen relativ zur Kontrollgruppe und bestätigte damit den initialen Proteombefund. Eine ähnliche Verschiebung des DJ-1 Isoformenmusters wurde im Gehirn, im Skelettmuskel, im Pankreas und der Leber, nicht aber im epididymalen weißen Fettgewebe detektiert.

Darüber hinaus untersuchten wir die Interaktion des Gens mit einer fettreichen Fütterung in *Dj-1* defizienten (*Dj-1$^{-/-}$*) Mäusen. Im Hinblick auf die Körpergewichts-entwicklung war die Anfälligkeit gegenüber diät-induzierter Adipositas in *Dj-1$^{-/-}$* Mäusen ähnlich der von wildtypischen Mäusen. Nach 14-wöchiger Fütterung mit fettreichem Futter

war jedoch eine höhere Fettakkumulation in *Dj-1^{-/-}* Mäusen auf Kosten der fettfreien Masse zu beobachten. Dieser Effekt war transient: Die Fettmasse glich sich mit längerer Fütterungsdauer und/oder fortgeschrittenem Alter der von Wildtyp-Mäusen an, während die Muskelmasse in *Dj-1^{-/-}* Mäusen unabhängig von der Futterart reduziert war. Die veränderte Körperzusammensetzung konnte nicht auf messbare Änderungen in der Energieaufnahme oder dem Energieverbrauch zurückgeführt werden, wohingegen die lokomotorische Aktivität der *Dj-1^{-/-}* Mäuse generell niedriger war. Unsere Daten deuten darauf hin, dass die *Dj-1*-Defizienz in Wechselwirkung mit der fettreichen Fütterung sowohl die Plasmaglucosespiegel als auch die hypothalamische STAT3-Phosphorylierung beeinflusst, was jedoch keine Auswirkungen auf die Glucosetoleranz oder die anorektische Leptinantwort hat. In einer Transkriptomanalyse des ventralen Teils des Hypothalamus zeigen wir jedoch, dass die Fütterung mit fettreichem Futter einen größeren Einfluss auf die Genregulation in der Abwesenheit von *Dj-1* hat.

Ausgehend von diesen Ergebnissen spekulieren wir, dass DJ-1 eine Rolle bei der metabolischen Anpassung an eine veränderte Quantität oder Qualität der zugeführten Nährstoffe spielt: Durch die fettreiche Fütterung werden DJ-1-Modifikationen induziert und modifiziertes DJ-1 trägt so zur Aufrechterhaltung der normalen zellulären Homöostase bei. Fehlt DJ-1 und damit seine stabilisierende Funktion, können Mäuse weniger effizient mit den metabolischen Änderungen, die durch eine fettreiche Fütterung induziert werden, umgehen. Letztendlich sind sie aber in der Lage, die abwesenden Mechanismen zu kompensieren. Unsere Befunde unterstützen weiterhin eine mögliche Überschneidung oder Interaktion von molekularen Signalwegen, die sowohl bei Adipositas als auch bei Neurodegeneration eine Rolle spielen.

Adipositas-bezogene metabolische Veränderungen könnten dazu beitragen, die Schwelle der Entwicklung von altersabhängigen neurodegenerativen Erkrankungen herabzusetzen und deren Entstehung somit beschleunigen.

1   INTRODUCTION

1.1   Common obesity - A polygenic trait

Obesity and overweight have emerged to a worldwide public health challenge. Having more than doubled since 1980, global obesity has ceased from being considered a problem of merely high-income countries *[WHO 2012]*. According to the World Health Organization, a person with a body mass index (BMI = body weight [kg]/height [m]^2) higher than 25 is considered overweight, while a BMI exceeding 30 indicates obesity *[WHO 2012]*. In Germany the prevalence of obesity has continued to rise in the last two decades affecting about one quarter of men as well as woman according to the latest projection *[Mensink et al. 2012]*.

Obesity results from a chronic energy surplus of the organism majorly as a consequence of adverse lifestyle and environmental factors, including the unrestricted access to high caloric, energy dense foods and low physical activity. Notably, already a divergence of 1 % in calories consumed versus energy expended maintained over a few years is sufficient for extensive weight gain *[Brown 2008]*. With the exception of rare monogenic forms, the susceptibility to common forms of obesity is furthermore influenced by a large number of gene variants: 32 loci have been linked to obesity in genome-wide association studies *[Speliotes et al. 2010]*. However, based on an estimated BMI heritability of 0.4 to 0.7, the total identified variants explain only 2-4 % of the genetic variance *[Hebebrand et al. 2010]* indicating that each variant has only subtle effects.

Since overweight and obesity are associated with comorbidities like cardiovascular diseases, type 2 diabetes mellitus and several forms of cancer *[Daniels 2009; WHO 2012]*, a lot of work has been done trying to identify the factors that influence energy homeostasis in order to develop new drugs to treat obesity. Multiple central and peripheral components have been determined, resulting in a complex network of energy balance regulation. In this network, the hypothalamus is the brain area where many peripheral signals are first integrated. In fact, in all known monogenic forms of obesity, hypothalamic pathways are impaired affecting satiety and food intake *[Lee et al. 2010]*. One aim of the present thesis was to identify hypothalamic alterations associated with the development of diet-induced obesity (DIO) in mice.

1.2   Hypothalamus – Function and dysfunction in energy balance regulation

1.2.1   Physiological regulation of energy homeostasis

The hypothalamus plays a central role in controlling energy homeostasis, which aims to promote stable body fat stores regarded over a longer period of time, by regulating food intake and energy expenditure *[Morton et al. 2006]*. It integrates various hormonal and neuronal signals that inform about short-term changes in nutrient availability (e.g. satiety signals from the gastrointestinal tract) and long-term energy status (e.g. adipose tissue derived adipokines) (Fig. 1-1) *[Gale et al. 2004; Zeltser et al. 2012]*. Circulating factors need to overcome the blood-brain barrier via diffusion or saturable transport mechanisms in order to reach their central target sites. Within the ventral hypothalamus, the arcuate nucleus (ARC) is responsive to a wide variety of hormones and nutrients due to special properties of the blood-brain barrier in this region *[Schwartz et al. 2000; Cone et al. 2001; Varela & Horvath 2012]*. Additionally, some axonal processes of ARC neurons reach into the portal vein potentially having direct access to circulating factors and thereby circumventing the blood-brain barrier *[Cone et al. 2001; Münzberg 2008]*.

The ARC contains two distinct first-order neuron populations exerting opposing actions on energy balance regulation: Neurons coexpressing neuropeptide Y (NPY) and agouti-related protein (AgRP) have an orexigenic effect promoting food intake, while neurons coexpressing pro-opiomelanocortin (POMC) and cocaine and amphetamine related transcript (CART) exert anorexigenic action (Fig. 1-1) *[Bell et al. 2005]*. For instance, both neuron populations express receptors for leptin, a hormone secreted in proportion to the body fat stores *[Maffei et al. 1995]*. While the binding of leptin inhibits NPY/AgRP neurons, it stimulates POMC/CART neurons *[Schwartz et al. 2000]*. Additionally, NPY/AgRP neurons inhibit POMC/CART neurons via the release of the neurotransmitter γ-aminobutyric acid (GABA) *[Bell et al. 2005]*. In addition, a wide range of further nutrient and hormonal signals including insulin, ghrelin, glucose, amino acids and free fatty acids are sensed by POMC/CART and NPY/AgRP neurons (Fig.1-1). Consequently, the balance of the activity between the two neuron sets is a major regulator of feeding behavior and body weight *[Zeltser et al. 2012]*. Orexigenic and anorexigenic signals are relayed to second order neurons in other hypothalamic nuclei (Fig. 1-1). POMC is cleaved post-translationally into several products one of which is α-melanocyte stimulating hormone (α-MSH) that activates the melanocortin 4 receptor (MC4R) in other hypothalamic areas thereby inhibiting appetite *[Gale et al. 2004]*. AgRP, on the other hand, acts through the inhibition of the MC4R and, together with the action of NPY, promotes food intake *[Fan et al. 1997; Broberger et al. 1998]*. Moreover, the hypothalamus interacts with satiety circuits located in the brainstem *[Schwartz et al. 2000]*. The hypothalamic integration of these signals together with reward and motivation-related signals

from the midbrain-dopamine system and cognitive information from the forebrain in a concerted manner result in the overall balance of food intake and energy expenditure (Fig. 1-1) *[Blouet & Schwartz 2010]*. Efferent output is realized by the autonomic or motoric nervous system or by hormone signaling via the hypothalamic-pituitary-adrenal axis. However, neural circuits of higher brain regions have the potential to override the homeostatic mechanisms, resulting in obesity or anorexia as extreme cases *[Palmiter 2007]*.
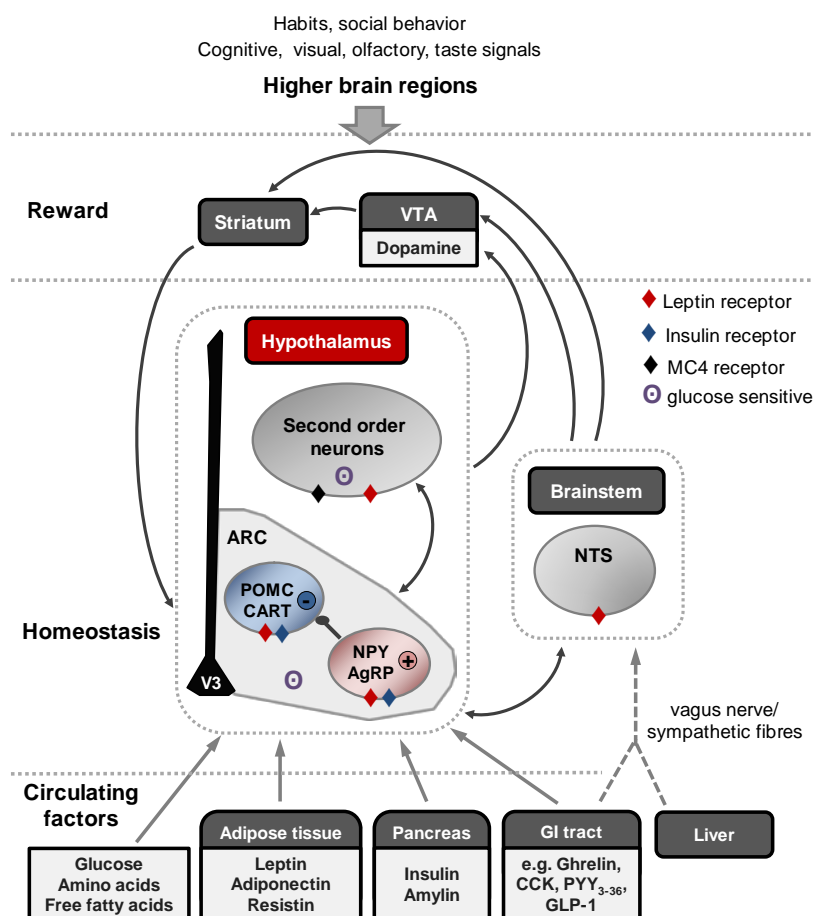
Fig. 1-1. Homeostatic control of food intake. Circulating factors from the periphery are sensed by first order neurons within the arcuate nucleus (ARC): POMC/CART neurons exert anorexigenic action (-) while the activation of NPY/AgRP neurons leads to orexigenic effects (+) and the inhibition of POMC/CART neurons via the neurotransmitter γ-aminobutyric acid (GABA). Orexigenic and anorexigenic signals are relayed to second order neurons within the hypothalamus. The hypothalamus cross-talks with the brainstem that receives afferent input from the liver or GI tract transmitted through the vagus nerve and sympathetic fibres. Homeostatic circuits are modulated by dopaminergic pathways of the reward system and signaling from higher brain regions. Dark grey arrows indicate projections between brain areas. VTA - ventral tegmental area. NTS - nucleus of the solitary tract. GLP-1 - glucagon-like peptide 1. PYY_{3-36} - peptide YY residues 3–36. CCK – cholecystokinin. MC4 - melanocortin 4. 3V - third ventricle. GI tract – gastrointestinal tract. Modified from *Schwartz et al. [2000]; Varela & Horvath [2012]; Yeo & Heisler [2012]*.

1.2.2 Alterations in the hypothalamus associated with high fat intake and obesity

To develop overweight, the homeostatic system of energy balance regulation needs to be disturbed. Established obesity, however, involves an active defence of the elevated level of adiposity, hence the homeostatic pathways likely act on a shifted 'set-point' of body fat *[Wisse et al. 2007; Leibel 2008]*. The current state of knowledge regarding changes in the hypothalamus associated with high fat intake, which were also subject of this thesis, are summarized in the following focusing on findings from DIO rodent models.

Leptin and insulin resistance

One aspect of the pathophysiology of obesity is the loss of sensitivity towards leptin and insulin, both known to be negative feedback signals for adiposity *[Bagdade et al. 1967; Considine et al. 1996; Schwartz et al. 1996; Münzberg et al. 2004; De Souza et al. 2005]*. Since intracellular pathways exist that can be activated both by insulin and leptin, the impairment of one such mechanism may cause resistance to both hormones. Leptin and insulin signaling namely converge at the phosphatidylinositol-3-kinase (PI3K) pathway resulting in the activation of protein kinase B (PKB, also known as AKT) *[Niswender & Schwartz 2003; Niswender et al. 2004; Varela & Horvath 2012]* (Fig. 1-2). Activated PKB phosphorylates numerous substrates including the transcription factor Forkhead box protein O1 (FOXO1). FOXO1 is inhibited by phosphorylation and exported from the nucleus giving way to the binding of signal transducer and activator of transcription 3 (STAT3) to the *Pomc* and *Agrp* promoter, respectively, thereby stimulating *Pomc* and inhibiting *Agrp* expression *[Morrison et al. 2005; Kim et al. 2006; Kitamura et al. 2006]*. PKB further regulates the mammalian target of rapamycin (mTOR) *[Cota et al. 2006]*, which responds to changes in nutrient availability. Moreover, a PI3K-dependent activation of the ATP-sensitive potassium channel (KATP) in response to insulin and leptin has been shown in hypothalamic neurons leading to a reduced firing rate *[Spanswick et al. 1997; Niswender & Schwartz 2003]*. The activation of KATP channels by physiological insulin levels is blunted in obese compared to lean leptin receptor-deficient rats *[Spanswick et al. 2000]*.

As a mechanism underlying the hypothalamic resistance to leptin, an impaired negative feedback inhibition of the leptin receptor in the presence of chronically elevated leptin levels has been suggested *[Maffei et al. 1995; Considine et al. 1996; Velloso & Schwartz 2011]*. Binding of leptin to its receptor consequently leads to the induction of suppressor of cytokine signaling 3 (SOCS3) expression, an inhibitor of proximal leptin and insulin signalling (Fig.1-2) *[Bjorbaek et al. 1999; Emanuelli et al. 2000; Rui et al. 2002; Mori et al. 2004]*.

In DIO, SOCS3 levels are increased in hypothalamic neurons likely leading to a blunted response to neuronal leptin and insulin action *[Howard et al. 2004; Howard & Flier 2006; Ernst et*

al. 2009; Velloso & Schwartz 2011]. Another inhibitor of leptin and insulin signal transduction is the protein-tyrosine phosphatase 1B (PTP1B, Fig. 1-2) *[Zabolotny et al. 2002; Picardi et al. 2008; Picardi et al. 2010]*. Similar to SOCS3, PTP1B expression is increased in the hypothalamus of obese rodents *[Cheng et al. 2002; White et al. 2009]*. Neuronal PTP1B knockout mice and rats deficient of PTP1B in hypothalamic areas are resistant to DIO and show enhanced sensitivity to hypothalamic leptin and insulin *[Bence et al. 2006; Picardi et al. 2008]*.
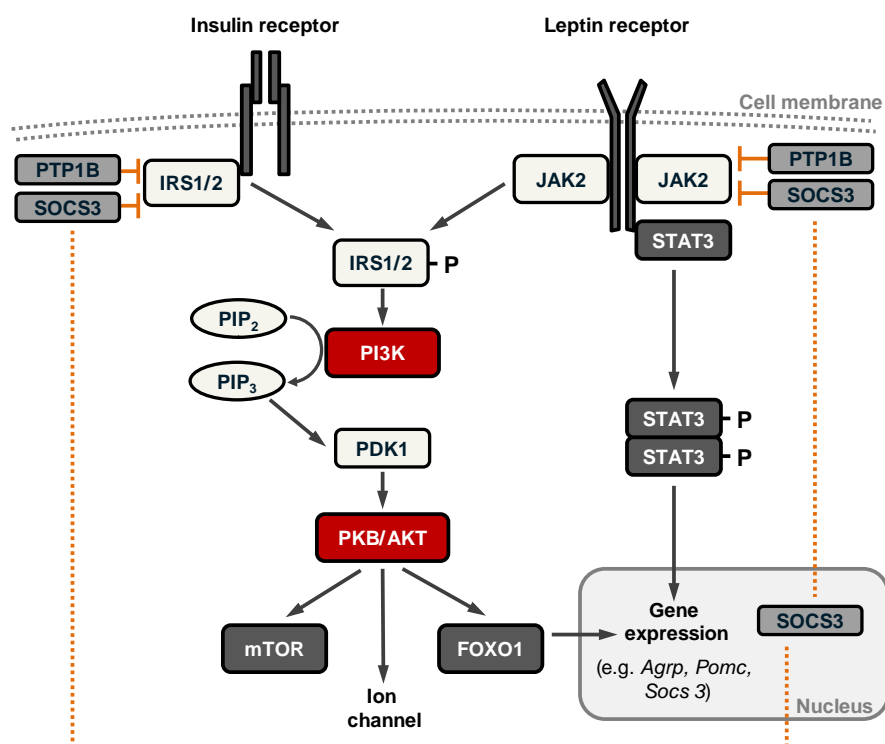
Fig. 1-2. Insulin and leptin receptor-dependent activation of the PI3K pathway. The phosphatidylinositol-3-kinase (PI3K) is activated by phosphorylated insulin receptor substrate 1 or 2 (IRS1/2). IRS1/2 phosphorylation is mediated directly by the insulin receptor or indirectly by the leptin receptor through the janus kinase 2 (JAK2), upon binding of their respective substrate. Activated PI3K phosphorylates the second messenger phosphatidylinositol (4,5) bisphosphate (PIP_2) converting it into phosphatidylinositol (3,4,5) triphosphate (PIP_3). PIP_3 recruits and activates the phosphatidylinositol-dependent kinase 1 (PDK1), which in turn phosphorylates and thereby activates the protein kinase B (PKB, also known as AKT). Active PKB regulates the mammalian target of rapamycin (mTOR) pathway and activates ion channels. PKB further phosphorylates and thereby inhibits the transcription factor Forkhead box protein O1 (FOXO1). Leptin receptor induced activation of JAK2 further results in the phosphorylation of the signal transducer and activator of transcription 3 (STAT3) which forms dimers that act as a transcription factor. FOXO1 and STAT3 reciprocally regulate gene expression e.g. of the neuropeptides *Agrp* and *Pomc* or of the suppressor of cytokine signaling 3 (*Socs3*). SOCS3 and the protein-tyrosine phosphatase 1B (PTP1B) inhibit insulin and leptin receptor signaling via IRS1/2 or JAK2, respectively. Modified from *Morton et al. [2006]; Velloso & Schwartz [2011]*.

Inflammatory processes

Leptin and insulin resistance may result from processes linked to inflammation which are well documented to occur within the hypothalamus as a consequence of HF diet-consumption and obesity *[De Souza et al. 2005; Posey et al. 2009; Wisse & Schwartz 2009; Thaler et al. 2010; Thaler et al. 2012]*. The increased expression of the inflammatory cytokines TNF-α, IL-1β and IL-6 in the hypothalamus of rats after several weeks of HF diet has been reported repeatedly *[De Souza et al. 2005; Milanski et al. 2009; Moraes et al. 2009; Thaler et al. 2012]* and central TNF-α administration is able to affect leptin and insulin signaling *[Romanatto et al. 2007]*.

Inflammation-responsive signaling components activated by HF intake include (I) the serine/threonine kinase c-Jun-N-terminal kinase (JNK) that is involved in various processes such as neuronal proliferation and apoptosis *[De Souza et al. 2005]*, (II) the inhibitor of nuclear factor kappa-B kinase (IKK), a serine kinase which activates the transcription factor nuclear factor-κB (NF-κB) *[Zhang et al. 2008]* and (III) the protein kinase C-theta (PKC-theta), a serine/threonine kinase that mediates T-cell receptor signaling *[Benoit et al. 2009]*. Analogue to SOCS3 and PTP1B, the kinases IKK, JNK and PKC-theta are able to inhibit leptin and insulin signaling via inhibition of STAT3 as well as the insulin receptor substrate 1 and 2 (IRS1/2), proteins that are phosphorylated upon activation of the leptin or insulin receptor, respectively *[Velloso & Schwartz 2011]*. Moreover, SOCS3 and PTP1B can also be induced by inflammatory processes *[Zabolotny et al. 2002; Velloso & Schwartz 2011]*.

Several mechanisms have been suggested to trigger hypothalamic inflammation. Saturated fatty acids, a main component of HF diets, increase the expression and activity of the toll-like receptor 4 (TLR4) *[Milanski et al. 2009]* which leads to IKKβ activation and NF-κB-dependent expression of inflammatory cytokines *[Akira 2003; Kleinridders et al. 2009]*. TLR4 signaling as well as the direct action of saturated fatty acids can induce endoplasmic reticulum (ER) stress *[Zhang et al. 2008; Milanski et al. 2009]*. Increased ER stress has been shown to inhibit leptin signaling in the hypothalamus of obese mice and activate the unfolded protein response *[Ozcan et al. 2009]*, a pathway aiming to restore ER homeostasis *[Schroder & Kaufman 2005]*. Under prolonged stress, however, an overloaded unfolded protein response is capable of initiating apoptosis *[Schroder & Kaufman 2005]*. The induction of apoptosis by dietary fats has indeed been shown to occur in hypothalamic neurons of rats *[Moraes et al. 2009]*.

Autophagy

Hypothalamus-linked autophagy [1], a cellular recycling process for cytoplasmic material and excess or defective organelles *[Shintani & Klionsky 2004]*, has recently been shown to be involved in the pathogenesis of obesity *[Coupe & Bouret 2012]*. As an alternative energy source during starvation, autophagy is negatively regulated by the mTOR pathway *[Pattingre et al. 2008; Kaushik et al. 2011]* and dysfunction of autophagy may result in abnormal mitochondrial function and oxidative or nitrative stress *[Lee et al. 2012]*. Mice in which autophagy was selectively deactivated in AgRP neurons reduce food intake and adiposity *[Kaushik et al. 2011]*. In contrast, in POMC neurons, this defect resulted in higher body weights with increased adiposity and leptin resistance along with hyperphagia and impaired glucose tolerance *[Coupe & Bouret 2012; Kaushik et al. 2012; Quan et al. 2012]*. Mechanistically, loss of autophagy from POMC neurons decreases α-MSH levels *[Kaushik et al. 2011]* and reduces the density of POMC-containing projections *[Coupe & Bouret 2012]* suggesting a role of autophagy in promoting structural changes *[Varela & Horvath 2012]*.

Synaptic plasticity

The term 'synaptic plasticity' implies changes in the magnitude of a synaptic reaction regulated at different levels including synapse strength, synapse number and intrinsic neuronal excitability *[Zeltser et al. 2012]*. Hypothalamic neurons have the potential to undergo continuous rewiring, a process that is influenced by a variety of factors including leptin and nutrients *[Pinto et al. 2004; Horvath 2006]*. HF feeding leads to hypothalamic alterations in synaptic plasticity: A high dietary fat intake reduces the amount of nerve terminals in the ARC and lateral hypothalamus of rats *[Moraes et al. 2009]* and the amount of synapses on POMC neurons is altered in DIO rats and mice compared to control diet-fed animals *[Horvath et al. 2010; Ravussin et al. 2011]*.

Taken together, there is convincing evidence that HF feeding affects the hypothalamus at several levels (Fig. 1-3). However, many open questions remain to be answered. One aspect is the contribution of microglia and their interaction with neurons and other glial cells to HF diet-induced inflammation, as the TLR4 is predominantly expressed by microglia in the central nervous system *[Lehnardt et al. 2003]*. In addition, microglia play a role in synaptic remodeling *[Cullheim & Thams 2007; Ransohoff & Perry 2009]*. Another issue is the influence of the diet composition on different outcomes associated with HF feeding in the hypothalamus. As shown in pair-feeding experiments, HF diet-induced apoptosis is not caused by increased energy intake and weight gain *per se [Moraes et al. 2009]*. Finally, the cause-consequence

---

[1] The term 'autophagy' used in this thesis refers to macroautophagy.

relationship of alterations in the central nervous system associated with a HF diet is not well elucidated. It was demonstrated that hypothalamic inflammation and reactive gliosis were present before extensive weight gain, subsided in the following but returned permanently with continued HF feeding *[Thaler et al. 2012]*. Alterations occurring early during HF feeding are more likely to be causal for the development of obesity and should thus be separated from chronic manifestations of the disease.
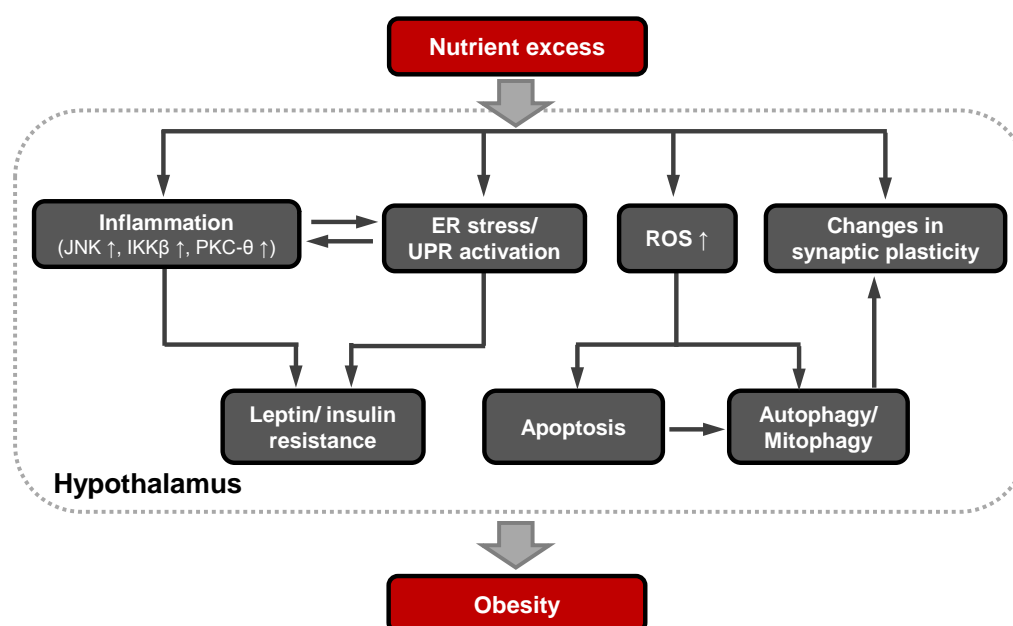
Fig. 1-3. Cellular mechanisms shown to occur in the hypothalamus upon excess nutrient intake. Arrows indicate putative causal connections. Whether the suggested mechanisms are causal for or consequences of obesity remains to be clarified. ER – Endoplasmic reticulum. ROS – Reactive oxygen species. UPR – Unfolded protein response.

1.3 Obesity and neurodegeneration

It has long been suggested that obesity may accelerate brain aging *[Bruce-Keller et al. 2009]* and cognitive decline in humans *[Sorensen et al. 1983; Jeong et al. 2005; Gunstad et al. 2007; Singh-Manoux et al. 2012]*. Experimental studies with rodent models investigating the putative influence of dietary energy intake on brain function show decreased spatial learning abilities in rats after several months of a diet rich in fat and sucrose *[Molteni et al. 2002; Stranahan et al. 2008]* as well as in leptin receptor-deficient mice and rats *[Li et al. 2002]* indicating a cognitive impairment. Cognitive performance was also reduced in old DIO mice *[Farr et al. 2008; Morrison et al. 2010]*. As a mechanism, elevated plasma triglyceride levels were suggested because the cognitive function was improved after triglyceride levels were lowered pharmacologically *[Farr et al. 2008]*.

Recently, obesity and metabolic dysfunction have also been recognized as a possible risk factor for neurodegenerative disorders such as Alzheimer's disease, depression or Parkinson's disease (PD) *[Doherty 2011; Lee 2011; Farooqui et al. 2012]*. Moreover, the susceptibility to chemically induced neurodegeneration was increased in mice and rats fed a HF diet *[Choi et al. 2005; Morris et al. 2010]* as well as in the genetically obese *ob/ob* mouse model *[Sriram et al. 2002]*.

PD is a neurodegenerative disorder subsuming the movement-related symptoms bradykinesia, rigidity, resting tremor and postural instability that result from a loss of dopaminergic neurons in the substantia nigra, a part of the ventral midbrain *[Thomas & Beal 2011]* . Although majorly a sporadic disorder, several genetic loci termed PARK1 to PARK16 have been linked to inherited forms of PD *[Thomas & Beal 2011]*. Increased measures of adiposity have been associated with an elevated risk for the development of PD in a Finish study population *[Hu et al. 2006]*, among Japanese-American men *[Abbott et al. 2002]* as well as in the Health Professional Follow-up study (HPFS) and the Nurses' Health Study (NHS) cohorts *[Chen et al. 2004]*. However, in the Cancer Prevention Study II Nutrition cohort no relationship between BMI, weight change or waist circumference and the risk of PD was found *[Palacios et al. 2011]*.

As an underlying mechanism linking metabolic disorders and neurodegeneration, an impairment of insulin and leptin signaling, respectively, has been suggested *[Doherty 2011; Kaidanovich-Beilin et al. 2012]*. Thus, the threshold for developing age-related neurodegenerative diseases may be lowered by obesity-associated metabolic changes.

1.4 DJ-1 (PARK7) – a multifunctional redox-regulated protein

In this thesis, we identified DJ-1 (PARK7) as a protein responsive to HF diet-feeding in mice. DJ-1 was first described in 1997 as an oncogene able to transform mouse embryonic fibroblast cells *[Nagakubo et al. 1997]*. Six years later, DJ-1 was linked to neurodegeneration when mutations in the *DJ-1* gene were associated with autosomal recessive early-onset parkinsonism *[Bonifati et al. 2003a]*. Later, oxidative damage of DJ-1 was shown in sporadic Parkinson's and Alzheimer's disease as well as in other neurodegenerative diseases and aging *[Choi et al. 2006; Zhong & Xu 2008; Natale et al. 2010]*. For this reason, the molecular impact of DJ-1 regarding oxidative stress-related neurodegeneration has been widely studied.

DJ-1 is an evolutionary ancient protein with homologs present in diverse organisms *[Bandyopadhyay & Cookson 2004; Kahle et al. 2009]*. In humans and mice, DJ-1 is ubiquitously expressed *[Nagakubo et al. 1997; Taira et al. 2001; Bonifati et al. 2003b; Niki et al. 2003; Zhang et al. 2005a]*. Within the brain, DJ-1 is present in neurons of different neurotransmitter type and in all glial cell types *[Bader et al. 2005]*. DJ-1 is further found in red blood cells and plasma and is secreted from various cancer cells, constituting a potential cancer biomarker *[Le Naour et al. 2001; MacKeigan et al. 2003; Hod 2004; Pardo et al. 2006; Shi et al. 2010; Xu et al. 2010; Lin et al. 2012]*.

Both the human and mouse DJ-1 protein consist of 189 amino acids, respectively, and show 91.5 % identity (Fig. 1-4 A). Human DJ-1 contains three cysteines (Cys) at position 46, 53 and 106 as well as five methionines that are all highly conserved *[Bandyopadhyay & Cookson 2004; Waak et al. 2009]*. Murine DJ-1 contains an additional cysteine at position 87 as well as three additional methionines (Fig. 1-4 A).

Fig. 1-4. Primary and quaternary structure of the DJ-1 protein. (**A**) Alignment of human and mouse DJ-1 amino acid sequence. Identical amino acids are highlighted dark grey. Cysteines are shown in yellow, methionines in blue. (**B**) Ribbon diagram of human dimeric DJ-1 (from *Wilson [2011]*). Monomers are shown in gold and blue, respectively. Cysteines are shown in yellow. C – carboxy terminus. N – amino terminus.

Crystal structures have shown that DJ-1 exists as a homodimer and dimerization is crucial for its stability and function *[Honbou et al. 2003; Huai et al. 2003; Miller et al. 2003; Tao & Tong 2003; Wilson et al. 2003; van der Brug et al. 2008].*Cys-45 and Cys-53 are located close to the dimer interface, while Cys-106 is located at the bottom of a narrow cleft (Fig. 1-4 B) *[Wilson et al. 2003; Canet-Aviles et al. 2004].* Cysteine and methionine residues are prone to post-translational oxidation yielding several possible isoforms[2] that can be separated according to their isoelectric points (pI). Multiple DJ-1 isoforms have been described with a pI ranging from 5.4 to 6.7 and low pI forms are increased in cultured cells exposed to oxidative stresses as well as in human brain under neurodegenerative conditions (Fig. 1-5 A) *[Mitsumoto & Nakagawa 2001; Bandopadhyay et al. 2004; Canet-Aviles et al. 2004; Kinumi et al. 2004; Taira et al. 2004; Zhou & Freed 2005; Choi et al. 2006; Kim et al. 2009b; Natale et al. 2010].* Among the DJ-1 cysteine residues, Cys-106 is the most sensitive to oxidative modification because it is accessible by small molecules like peroxides, and oxidized Cys-106 has been identified in low pI forms of DJ-1 *[Wilson et al. 2003; Canet-Aviles et al. 2004; Kinumi et al. 2004; Zhou et al. 2006; Inden et al. 2011].* Thus, Cys-106 is expected to be crucial for DJ-1 function, although there is no consent about to which extent its oxidation occurs *in vivo [Blackinton et al. 2009; Wilson 2011].* In addition to the post-translational modifications of cysteines, methionine residues can also be oxidized *[Choi et al. 2006]* and DJ-1 can undergo SUMOylation *[Shinbo et al. 2006].* Thus, it is sensible to recognize DJ-1 total protein as a pool of isoforms with different modifications and the relative amounts of these isoforms are likely of importance with respect to its overall activity *[Natale et al. 2010].*

The subcellular distribution of the DJ-1 pool is dynamic *[Kahle et al. 2009].* Predominantly, DJ-1 is a cytosolic protein with some nuclear and mitochondrial localization *[Taira et al. 2004; Zhang et al. 2005a].* However, in response to oxidative stress, some of the cytosolic DJ-1 pool translocates to the nucleus and mitochondria (Fig. 1-5 B) *[Nagakubo et al. 1997; Canet-Aviles et al. 2004; Blackinton et al. 2005; Lev et al. 2008; Blackinton et al. 2009; Zhong et al. 2009].*

DJ-1 plays a role in diverse biological processes (Fig. 1-5 C). As indicated above, DJ-1 is involved in the cellular oxidative stress response. It prevents cell death triggered by a variety of oxidative stresses in various *in vitro* models as well as in rodents *[Yokota et al. 2003; Kim et al. 2005b; Zhou & Freed 2005; Shinbo et al. 2006].* Down-regulation of DJ-1 on the other hand, renders cells more susceptible to such stimuli *[Yokota et al. 2003; Martinat et al. 2004; Taira et al. 2004; Junn et al. 2005; Zhou & Freed 2005].* The DJ-1 dependent protection from oxidative stress has been linked to the up-regulating of cellular glutathione levels in a rat dopaminergic cell line and primary rat midbrain cells *[Zhou & Freed 2005; Liu et al. 2008].* Moreover, knockdown of DJ-1 in human dopaminergic neuroblastoma cells decreases the

---

[2] The term ‚isoform‘ is herafter used to describe different posttranslational modified forms of one protein.

mRNA expression of genes involved in ROS removal, such as manganese superoxide dismutase, catalase and glutathione peroxidase 1 *[Zhong & Xu 2008]*.

Furthermore, DJ-1 interacts with the inhibitors of various transcription factors, including the androgen receptor, p53 and the nuclear factor erythroid 2-related factor 2 (Nrf2) *[Takahashi et al. 2001; Niki et al. 2003; Shinbo et al. 2005; Xu et al. 2005b; Clements et al. 2006; Zhong et al. 2006]*.

DJ-1 is also discussed as a molecular (co-)chaperone *[Wilson 2011]*. The chaperone activity thereby depends on the redox state as DJ-1 prevents the aggregation of several substrates *in vitro* only under oxidizing conditions *[Shendelman et al. 2004]* and the association of DJ-1 with mitochondrial Hsp70 is enhanced when cells are treated with H_2O_2 *[Li et al. 2005]*. DJ-1 has also been found in complex with alpha-synuclein *[Meulener et al. 2005b]* and, in a redox-dependent manner, prevents the abnormal aggregation of alpha-synuclein and neurofilament light subunits, two substrates found in Lewy body inclusions that are characteristic for PD *[Shendelman et al. 2004; Zhou & Freed 2005; Zhou et al. 2006]*.

Moreover, DJ-1 interacts with the PI3K pathway in response to oxidative stress, a pathway that is also activated through insulin and leptin receptor signaling amongst others (see 1.2.2). This action is exerted via oxidation-dependent binding of DJ-1 to the phosphatase and tensin homologue (PTEN), an inhibitor of the PI3K pathway, whereby it promotes PKB phosphorylation *[Kim et al. 2005a; Yang et al. 2005; Kim et al. 2009b; Aleyasin et al. 2010; Das et al. 2011]*.

DJ-1 inhibits several apoptotic pathways in response to oxidative stresses. First, DJ-1 competes with pro-caspase-8 to bind to the Fas-associated protein with death domain (FADD), an adaptor molecule of the death receptor *[Fu et al. 2012]*. Thereby procaspase 8 activation is repressed and the formation of the death-inducing signaling complex inhibited *[Fu et al. 2012]*. Second, DJ-1 represses the cleavage of caspase 3 induced by UV irradiation *[Fan et al. 2008b]* or hypoxia *[Vasseur et al. 2009]*. Third, UV irradiation increases the translocation of DJ-1 to mitochondria, where it binds to the anti-apoptotic Bcl-XL in an oxidation-dependent manner thereby preventing Bcl-XL degradation *[Ren et al. 2011]*. Fourth, DJ-1 suppresses JNK signaling through interacting with the mitogen-activated protein kinase kinase kinase 1 (MEKK1) *[Mo et al. 2008; Pham et al. 2010]*. JNK activity is increased by inflammatory processes e.g. such as induced by HF diet (see 1.2.2) and mediates apoptosis. Moreover, JNK can be activated by apoptosis signal-regulating kinase 1 (ASK1). DJ-1 inhibits ASK1 through (I) direct binding *[Gorner et al. 2007; Waak et al. 2009]*, (II) sequestering the pro-apoptotic Death domain-associated protein 6 (DAXX) in the nucleus whereby DAXX is stopped from translocating to the cytoplasm and activating ASK1 *[Junn et al. 2005; Karunakaran et al. 2007]* or (III) by preventing the dissociation of the negative regulator thioredoxin from ASK1 *[Im et al. 2010]*. On the other hand, JNK can activate p53

transcriptional activity. DJ-1 can directly interact with p53 and thereby it decreases Bax expression *[Fan et al. 2008b]* providing another mechanism for protecting against apoptosis.

Furthermore, DJ-1 plays a role in mitochondrial integrity at several levels. First, DJ-1 is implied in the maintenance of the correct function of complex I of the respiratory chain. DJ-1 directly binds to the NDUFA4 and ND1 subunits of complex I and its colocalization with complex I is enhanced by oxidative stress *[Hayashi et al. 2009]*. Knockdown of *Dj-1* in a mouse embryonic fibroblast cell line, HEK293 cells or *Dj-1* null dopaminergic neurons lead to reduced complex I activity *[Hayashi et al. 2009; Kwon et al. 2011]*. Moreover, loss of *Dj-1* in mice, flies and C. elegans increases the vulnerability to mitochondrial complex I inhibition *[Kim et al. 2005b; Meulener et al. 2005a; Ved et al. 2005]*. Second, the H_2O_2 production is increased in isolated mitochondria from brain or skeletal muscle of $Dj-1^{-/-}$ mice as well as in *Dj-1* knockdown mouse insulinoma cells *[Andres-Mateos et al. 2007; Irrcher et al. 2010; Jain et al. 2012]*. Increased ROS production of DJ-1 deficient mouse embryonic fibroblasts results in elevated mitochondrial permeability transition pore opening and reduced mitochondrial membrane potential as well as reduced ATP production *[Andres-Mateos et al. 2007; Krebiehl et al. 2010; Giaime et al. 2012]*. Third, $Dj-1^{-/-}$ mice further show reduced expression of the two uncoupling proteins UCP4 and UCP5 in the substantia nigra and increased oxidation of matrix proteins *[Guzman et al. 2010]*. And fourth, DJ-1 deficient cultured neurons, mouse brain, lymphoblast and beta cells display an abnormal mitochondrial phenotype including fragmentation *[Irrcher et al. 2010; Krebiehl et al. 2010; Jain et al. 2012]*. The induced mitochondrial fragmentation can be rescued by the coexpression of DJ-1 in human neuroblastoma cells *[Kamp et al. 2010]*.

As a last example, DJ-1 was proposed to be involved in autophagy, a process that has also been suggested to play a role in energy balance regulation (see 1.2.2). However, the exact function of DJ-1 in autophagy is unresolved since *Dj-1* silencing has been shown to upregulate *[Vasseur et al. 2009; Irrcher et al. 2010; Ren et al. 2010; Thomas et al. 2011]* but also downregluate autophagy *[Gonzalez-Polo et al. 2009; Krebiehl et al. 2010]*. It has been suggested that DJ-1 directly regulates upstream activators of autophagy including mTOR *[Vasseur et al. 2009]*.

The list of biological functions of DJ-1 is not complete as it is also associated with fertility, tumorigenesis, and neurodegeneration amongst others (reviewed in *da Costa [2007]; Kahle et al. [2009]*). However, the reason for these multiple functions can be attributed to DJ-1's ability to interact with RNA as well as with numerous proteins, a feature that is influenced by changes in the redox state in many cases (Fig. 1-5 C). Consequently, DJ-1 has been termed a multifunctional oxidative stress response protein that functions in regulating cellular organelle homeostasis *[Krebiehl et al. 2010; Wilson 2011]*. Thereby, it cross-talks with several

pathways, some of which are implicated in energy balance regulation and the development of obesity.
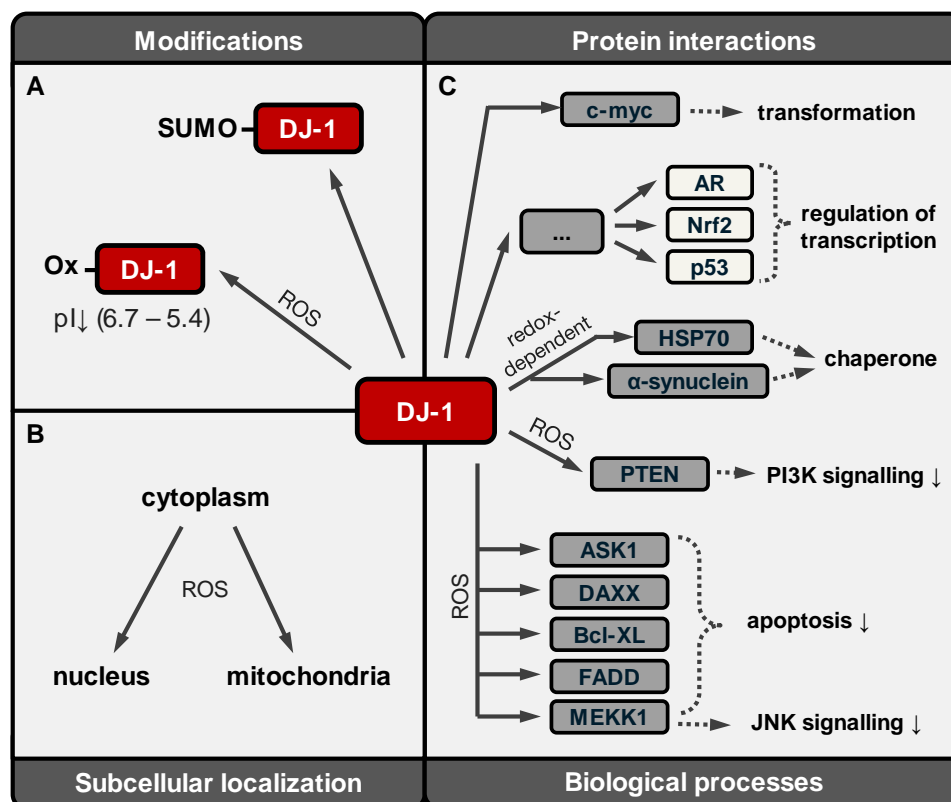
Fig. 1-5. DJ-1 constitutes a multifunctional oxidative stress responsive protein. (**A**) Post-translational modifications of DJ-1. In the presence of reactive oxygen species (ROS), DJ-1 is oxidized (Ox) at cysteine and/or methionine residues decreasing its isoelectric point (pI). DJ-1 can further be SUMOylated (SUMO). (**B**) The subcellular distribution of DJ-1 is dynamic. The major DJ-1 pool is located in the cytoplasm but nuclear and mitochondrial translocation can be enhanced in response to ROS. (**C**) DJ-1 interacts with numerous proteins involved in diverse biological processes. Several protein interactions can be influenced by changes in ROS levels or redox state. AR – androgen receptor. Nrf2 - nuclear factor erythroid 2-related factor 2. HSP70 – heat shock 70 kDa protein. PTEN - phosphatase and tensin homologue. PI3K - phosphatidylinositol-3-kinase. ASK1 - apoptosis signal-regulating kinase 1. DAXX - Death domain-associated protein 6. FADD - Fas-associated protein with death domain. MEKK1 - mitogen-activated protein kinase kinase kinase 1. JNK - serine/threonine kinase c-Jun-N-terminal kinase. Modified from Cookson *[2003]*.

1.5 Aims and scope

It is well established that obesity is caused by disturbances in the neuronal control of energy balance and the hypothalamus is an important regulator of food intake and energy expenditure. We therefore investigated, whether alterations occur in the murine hypothalamic proteome in response to a short-term diet intervention. Indeed, several differentially expressed proteins emerged from the comparison of hypothalamic protein expression patterns between HF and control diet-fed mice. The most promising candidate, DJ-1, was followed up using two approaches: First, the responsiveness of DJ-1 to HF diet feeding was validated in the same mouse model focusing on the composition of the DJ-1 protein pool. Second, a *Dj-1* deficient mouse line was phenotypically and metabolically characterized under a HF diet challenge.

The present Ph.D. thesis arose within the framework of the NGFN-Plus network 'Molecular Mechanisms in Obesity' that targets the identification of polygenes predisposing to obesity and their subsequent evaluation under epidemiological, clinical, functional and therapeutic aspects. Complementary to the identification of new candidate genes in humans and mice, our strategy aimed to contribute towards the identification of new obesity candidates in mice on the protein level utilizing a discovery-oriented proteomics approach.

Potentially, the altered proteins represent candidates for studies in humans that cannot be detected via genome wide association studies. The relevance of these candidates could then be validated in human epidemiologic and obesity-specific study populations.

Viewed in a broader context, this work contributes to unravel the underlying molecular mechanisms in the central nervous system dealing with energy-balance regulation. The understanding of how energy homeostasis is shifted out of balance during the development of overweight might provide new insight into the susceptibility of humans to become obese and thus enables preemptive intervention.

2 METHODS

2.1 Animals

Studies were performed on mice bred in house[3] and kept under specific pathogen-free conditions (with regular hygiene monitoring according to FELASA[4] criteria) unless otherwise stated. Mice were housed in individually ventilated cages (IVC, type II, 540 cm^2) and kept on a 12-hour light/dark cycle. Rooms were maintained at 22 ± 1°C with a relative humidity of 50-60 %. Mice were fed a standard chow diet (V1124) until assigned to the feeding experiments (see below). Diets were obtained from Ssniff Spezialdiäten GmbH, Soest, Germany (Appendix I.I Fig. A1). Procedures were carried out in accordance with the German animal welfare law and approved by the government of Oberbayern, Germany.

Short-term high-fat diet-feeding of three different inbred mouse strains for proteome analyses of hypothalami[5]

Seven-week-old male SWR/J, C57BL/6N or AKR/J mice were either fed a control (11 cal% fat, soybean oil; E15000-047) or a high-fat diet (40 cal% fat, palm oil; S0372-E712) for ten days (n = 5-6 per diet group). Mice were kept at the German Mouse Clinic, Munich, Germany and housed in groups of 3-4 animals per cage. Body mass was determined at the beginning and the end of the feeding period. The diet groups were matched for body mass. Body composition was measured in the abdominal part using micro computer tomography (LaThetaTM LCT-100, Aloka; obtained from Zinsser Analytic GmbH, Germany) after the 10-day challenge. Mice were killed by cervical dislocation before collection of hypothalami.

Short-term high-fat diet-feeding of mice for candidate validation experiments

Seven-week-old male C57BL/6N or AKR/J mice were either fed a control (12 cal% fat, soybean oil; S5745-E702) or a high-fat diet (48 cal% fat, soybean oil and palm oil; S5745-E712, HF) for two or ten days (Appendix I.I Fig. A1: diet composition). Mice were singly housed during the feeding period. Body mass and body composition via nuclear magnetic resonance (NMR) spectroscopy (Bruker) were measured at the beginning and the end of the feeding period. The diet groups were matched for body mass. Mice were euthanized with carbon dioxide before collection of plasma and tissues. Different cohorts were used for different follow-up experiments (Supplementary Table S1). In one cohort, 1 % N-

---

[3] TU München, Kleintierforschungszentrum, Freising, Germany

[4] Federation of European Laboratory Animal Science Associations

[5] The experiment was performed at the German Mouse Clinic, Munich, Germany by Dr. Jan Rozman, Monja Willershäuser and Dr. Michael Helwig.

acetylcysteine (NAC, pH 7.2) was supplied in the drinking water. NAC water was changed twice and mice, food racks and water bottles were weight four times during the 10-day feeding period to assure an adequate water and food intake.

High-fat diet challenge of *Dj-1* deficient (*Dj-1*$^{-/-}$) mice

The *Dj-1* deficient mouse line (XE726 DJ-1) was kindly provided by Prof. Dr. Wolfgang Wurst (Helmholtz Zentrum München, Munich, Germany) for breeding in our facility. The mouse line was generated using the gene trap method *[Pham et al. 2010]*. Briefly, the gene trap vector (pGT1Lxf) containing a beta-galactosidase/neomycin fused gene was integrated between exon 6 and exon 7 of the murine *Dj-1* gene of the embryonic stem cell clone XE726. Clones were injected into blastocystes of C57BL/6J mice and resulting chimeras were crossed with C57BL/6J mice *[Pham et al. 2010]*. Mice derived from heterozygous breeding pairs after the mutation had been backcrossed 11 times onto C57BL/6J background. At four weeks of age, male and female *Dj-1*$^{-/-}$ mice and wildtype littermates mice were assigned to either a control (12 cal% fat, soybean oil; S5745-E702) or a HF diet (48 cal% fat, soybean oil and palm oil; S5745-E712; Appendix I.I Fig. A1). Mice remained on the diet for 14 weeks. For a part of the animals, the feeding period was extended to 32 weeks. Every fortnight, mice were weight and fat and lean mass were determined using a NMR spectrometer (Bruker) which had been calibrated with mouse adipose tissue and chicken breast. Glucose tolerance, food intake, locomotor activity, energy expenditure and sensitivity towards leptin were measured during the last two weeks of the feeding periods in subgroups of animals (see below).

2.1.1   Genotyping of the *Dj-1* deficient mouse line

DNA was prepared from tail tips that were incubated in 500 µl tail buffer supplemented with 0.4 mg/ml Proteinase K (Fermentas) at 55°C until dissolved. DNA was precipitated with 500 µl isopropanol, washed with 70 % ethanol and dissolved in 40 µl nuclease-free water. Centrifugation steps were performed at 16000 *g* for 2-3 min at room temperature. A PCR was carried out according to Table 2-1 and 2-2 using the primers (5'-3') AGGCAGTGGAGAAGTCCATC (wildtype forward); AACATACAGACCCGGGATGA (wildtype reverse) and CGGTACCAGACTCTCCCATC (mutant reverse) yielding product sizes of 457 bp (wildtype) or 231 bp (mutant).

Tail buffer: 100 mM Tris, 5 mM EDTA, 0.2 % (w/v) SDS, 200 mM NaCl; pH 8.5

Table 2-1. PCR reaction mixture for genotyping of *Dj-1* deficient mice.

	Volume per reaction [µl]
2x ImmoMix (Bioline)	10.0
Primer wildtype forward (10 pmol/l)	1.0
Primer wildtype reverse (10 pmol/l)	1.0
Primer mutant reverse (10 pmol/l)	1.0
Nuclease-free water	5.5
DNA	1.5
Total	20.0

Table 2-2. PCR program for genotyping of *Dj-1* deficient mice.

Step	Temperature [°C]	Time [s]	Cycle
Initialization	95	600	
Denaturation	94	30	
Annealing	58	40	35 x
Elongation	72	60	
Final elongation	72	420	

2.1.2 Intraperitoneal glucose tolerance test (i.p. GTT)

Animals were deprived of food for 6 hours (8 am to 2 pm). Fasting blood glucose levels (= 0 minutes) were measured from tail blood using a blood glucose meter (Abbott) with disposable test strips. Following i.p. injection of 2 mg glucose*kg^{-1} body mass, blood glucose was monitored after 15, 30, 60 and 120 minutes.

2.1.3 Food intake and locomotor activity measurements

Food intake and spontaneous locomotor activity was measured using a feeding-drinking-activity system (TSE Systems). Up to 16 animals were kept separately in type III cages (820 cm^2) with *ad libitum* access to food and water, while the consumption was automatically registered with a resolution of one data point per minute. Locomotor activity was recorded as counts of beam breaks of surrounding light barriers in X, Y and Z direction (Fig. 2-1). Activity can be differentiated into ambulatory (beam breaks of two consecutive light barriers) or fine movement (successive beam breaks of the same light barrier). Mice were accustomed to the system for one day. Energy intake (kJ) was calculated from food intake and energy content of the diet and expressed per 24 hours or per dark phase. Only the dark phases were analyzed for activity parameters. Data of 2-3 days or nights were averaged. If the intra-individual coefficient of variation exceeded 33 % (for energy intake) or 40 % (for activity), mice were excluded to increase the statistical power.

Fig. 2-1. Feeding-drinking-activity system. Individual cages are surrounded by sensor frames containing emitter and receiver diodes. Diodes of the Z-frame are located above the Y-frame. Counts of beam breaks of the X- and Y-frame constitute horizontal activity, counts of beam breaks of the Z-frame refer to rearing activity. Food was supplied in one basket.

2.1.4 Energy expenditure measurement (indirect calorimetry)

The chemical energy of nutrients is utilized by the body through oxidation, whereby oxygen is consumed and carbon dioxide and water are produced. The metabolic rate indicates the rate at which chemical energy is converted into heat and external work and is most commonly measured indirectly as the oxygen consumption rate *[Hill et al. 2012]*. During indirect calorimetry, the energy expenditure is determined by means of the caloric equivalent indicating the energy per liter oxygen consumed which ranges from 19-21 kJ*l O_2^{-1} depending on the oxidized substrate.

Indirect calorimetry was performed using the LabMaster system from TSE Systems, Bad Homburg, Germany. Up to eight animals were kept separately in modified home cages and placed in a temperature-controlled climate chamber (Feutron®). With a constant flow rate of 0.7 l*min^{-1} air was pulled from the cages and volumes of oxygen consumed (Δvol% O_2) and carbon dioxide produced (Δvol% CO_2) were determined once every 9 min. For three days, animals were measured with *ad libitum* access to food and water at 21.5 ± 0.5°C. The oxygen consumption rate ($\dot{V}O_2$) was calculated according to the following equation *[Heldmaier & Ruf 1992]*:

$$\dot{V}O_2 \text{ [ml*h}^{-1}] = \Delta\text{vol\% } O_2 * \text{flow [l*h}^{-1}] * 10.$$

The carbon dioxide production rate ($\dot{V}CO_2$) was calculated accordingly:

$$\dot{V}CO_2 \text{ [ml*h}^{-1}] = \Delta\text{vol\% } CO_2 * \text{flow [l*h}^{-1}] * 10.$$

The respiratory exchange ratio (RER) was calculated according the equation:

$$RER = \dot{V}CO_2 \, [ml*h^{-1}] \, / \, \dot{V}O_2 \, [ml*h^{-1}].$$

The RER differs between carbohydrates (1.0), proteins (0.81) and lipids (0.705) and thus is indicative for the substrate oxidized for energy generation *[Even & Nadkarni 2012]*. As a measure of energy expenditure, heat production (HP) was calculated according to *Heldmaier [1975]*:

$$HP_{22°C,ad\text{-}lib} \, [mW] = (4.44 + 1.43 * RER) * \dot{V}O_2 \, [ml*h^{-1}],$$

whereby $\dot{V}O_2$ corresponds to the sum of the hourly means over 24 hours and RER corresponds to the daily mean. For the final result the mean HP of day 2 and 3 were averaged. On the fourth day, food was removed in the morning and temperature was set to $30 \pm 0.5°C$ (thermoneutral zone) *[Meyer et al. 2004]*. During the following 6 hours, the basal metabolic rate (BMR) was determined as the minimal $\dot{V}O_2$ of data smoothed over 20 min with a coefficient of variation below 5 %. HP under thermoneutral, postabsorptive conditions ($HP_{30°C,pa}$) was calculated from BMR and the corresponding RER. HP was normalized to the sum of lean mass + 0.2 * fat mass [g] *[Even & Nadkarni 2012]* whereby lean and fat mass was determined shortly before the experiment using NMR spectroscopy (Bruker). Mice and food racks were weighed daily.

2.1.5 Determination of sensitivity towards intraperitoneally administered leptin

The food intake in response to an intraperitoneal (i.p.) leptin injection was used as a physiological marker for leptin sensitivity. Mice were accustomed to the feeding-drinking-activity system (TSE Systems) for at least 24 hours. On three consecutive days, mice received i.p. injections of PBS followed by 5 mg*kg^{-1} body mass mouse leptin [6] (solved in PBS) the day after. The leptin dose was chosen according to Münzberg *et al. [2004]*. Injections were given shortly before the onset of the dark phase. Food intake was measured automatically throughout the whole experiment. Body mass of mice was surveyed daily.

---

[6] Leptin was kindly provided by Prof. Dr. Arne Skerra, TU München, Freising, Germany.

2.1.6 Tissue dissection

At the end of the feeding periods, mice were euthanized with carbon dioxide. For dissection of the hypothalamus, sacrificed mice were decapitated. The brain was quickly removed and placed in a custom-made brain blocker with the ventral side facing up (Fig. 2-2 A). The about 3-mm-thick coronary section containing the hypothalamus was dissected and the hypothalamus was cut out of this section with a preformed metal punch. For collection of the ventral part of the hypothalamus containing the arcuate nucleus, the hypothalamus was divided in the horizontal plane into two parts of approximately the same size (Fig. 2-2 B). Samples termed 'forebrain' refer to the remaining tissue after removing the hypothalamus, cerebellum, brainstem, and olfactory bulbs. Left and right posterior subcutaneous (psWAT) and epididymal (eWAT) or periovarial white adipose tissue depots (poWAT) as well as gastrocnemius muscles (M. gastroc) were combined. Collected tissues were frozen in liquid nitrogen and stored at -80°C.
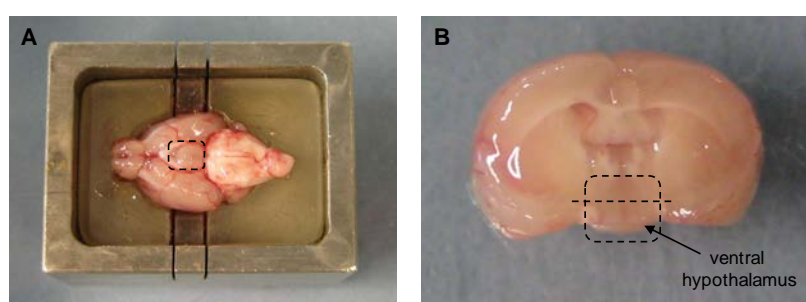
Fig 2-2. Dissection of mouse hypothalamus. (**A**) The brain was placed in the brain blocker with the ventral side facing up. The coronal section between the two incisions containing the hypothalamus (dashed box) was cut out using a razor blade. (**B**) From this section, the hypothalamus (dashed box) was dissected with a metal punch. For collection of the ventral hypothalamus, the hypothalamus was divided in the horizontal plane (dashed line).

2.2   Plasma glucose, insulin and leptin level determination

After euthanization with carbon dioxide, cardiac blood was collected from non-fasted mice in a heparin-coated tube and centrifuged for 5 min at 2000 *g.* The time window of blood collection did not exceed 3.5 hours during the day time. The supernatant was frozen in liquid nitrogen and stored at -80°C. Plasma glucose was determined using a blood glucose meter (Abbott). Plasma insulin levels were measured by ELISA (Mercodia) in samples diluted 1:5. Insulin sensitivity was estimated from glucose and insulin levels applying the homeostatic model assessment of insulin resistance (HOMA-IR = (insulin [µU/ml] * glucose [mmol/l]) * 22.5^{-1}) *[Hoeks et al. 2011]*. Plasma leptin levels were determined by ELISA (BioVendor).

2.3 Glutathione assay

Reduced (GSH) and oxidized (GSSG) glutathione were measured with a kit based on an enzymatic recycling method (Cayman) according to the manufacturer's instructions. Samples were prepared according to Rahman *et al. [2006]*. In short, frozen tissue was grinded in liquid nitrogen and a part of the tissue powder was homogenized in 5 ml*g^{-1} potassium phosphate buffer (pH 7.5) supplemented with 5 mM EDTA, 0.1 % Triton X-100, 0.6 % sulfosalicylic acid and centrifuged for 10 min at 8000 *g* (4°C). Protein concentration of the supernatant was determined by Bradford assay.

2.4 Western blot analysis

Frozen tissue was homogenized in lysis buffer 1. Forebrain, muscle and WAT samples were grinded in liquid nitrogen using mortar and pestle prior to homogenization. Homogenates were treated in an ultrasonic bath for 1 min, centrifuged at 16000 *g* for 15 min (4°C) and supernatants were collected. Precipitates were resuspended in lysis buffer 1 and the procedure repeated. Supernatants were combined. Protein concentrations were assayed according to Bradford. A defined amount of protein per sample was separated according to the molecular weight via sodium dodecyl sulfate polyacrylamide gel electrophoresis (SDS-PAGE) based on the discontinuous Laemmli system *[Laemmli 1970]* in a vertical electrophoresis system (Bio-Rad). Separated proteins were transferred from SDS gels onto nitrocellulose membranes (LI-COR Biosciences) using either a semi-dry system (Bio-Rad) with 0.8 mA*cm^{-2} for 45 min or, in case of OXPHOS immunoblots, a tank system (Bio-Rad) with 100 V for 1 h. After blocking for 1 h with 3 % BSA in TBS, immunoblots were incubated with primary antibody solution in TBST over night at 4°C (Appendix I.II Table A1: Primary antibodies). Afterwards, membranes were incubated for 1 h with infrared dye-conjugated secondary antibody solution (1:20 000, LI-COR Biosciences) in TBST at room temperature. Target proteins were detected using the Odyssey® Infrared Imaging System (LI-COR Biosciences).

Lysis buffer 1 30 mM Tris, 2 M thiourea, 7 M urea, 4 % (w/v) CHAPS, 1 % (w/v) DTT, 1 % (v/v) protease and phosphatase inhibitor cocktail (Sigma-Aldrich); pH 8

TBS 0.02 M Tris (pH 7.6), 0.137 M NaCl

TBST TBS + 1% (v/v) Tween® 20

2.5   Protein concentration determination according to Bradford

Protein concentrations were assayed in duplicates in 96-well plates using the Roti®-Quant solution (Carl Roth) according to the manufacturer's protocol. For the standard curve, BSA concentrations of 0, 0.02, 0.04, 0.06, 0.08 and 0.1 mg*ml^{-1} were used. Samples and standards were diluted in distilled water. Absorbance at 590 nm was measured using a microplate reader (Tecan).

2.6   Proteome analysis of hypothalami from high-fat or control diet-fed mice

Proteome analysis was carried out by Dr. Gereon Poschmann from the group of Prof. Dr. Kai Stühler, Molecular Proteomics Laboratory (MPL), Heinrich-Heine-Universität Düsseldorf, Germany *[Poschmann et al., in preparation]*. In short, hypothalamic protein expression patterns between HF and control diet groups were compared independently for each strain using two-dimensional difference gel electrophoresis (2D-DIGE) and differential proteins were identified by mass spectrometry. For this, frozen hypothalami were homogenized in lysis buffer 2 as described in Chapter 2.4. Proteins were labeled with fluorescent CyDyes (GE Healthcare, minimal labeling). One HF/control pair of animals was analyzed in one gel together with an internal standard prepared as a pool of all samples from one mouse strain. Carrier ampholyte isoelectric focusing (first dimension) was carried out in tube gels, after which proteins were separated in the second dimension by 15.2 % acrylamide/1.3 % bisacrylamide SDS gels *[Klose & Kobalz 1995; Poschmann et al. 2012]*. Gels were scanned on a Typhoon Trio laser scanner (GE Healthcare) and gel images were processed by the DeCyder-2D-V6.5 software suite (GE Healthcare) run in batch mode. For spot detection the estimated spot number was set to 10 000 and spots < 20 000 arbitrary units were removed. Spots were matched across the gels and normalized to the internal standard. Only spots matched in at least 4 gels, showing a ratio between HF and control diet of < 0.8 or > 1.25 and a p-value < 0.05 (two-sided Student's t-test performed on log-transformed data) were considered.

Protein spots found to be differentially abundant between HF and control diet-fed mice were manually excised from the preparative gel and in-gel digested with trypsin (Promega) in 10 mM ammonium bicarbonate buffer (pH 7.8) at 37°C overnight. Tryptic peptides were extracted twice with acetonitrile/ 5 % formic acid (50:50, v/v), acidified by addition of 5 % formic acid after removal of acetonitrile and subjected to nano-HPLC-ESI tandem mass spectrometry (Appendix II). Peptides and proteins were identified using MASCOT 2.4.1

software and the UniProtKB database release 12/2012 with shuffled decoy version of all entries.

Lysis buffer 2   30 mM Tris-HCl, 2 M thiourea; 7 M urea; 4 % CHAPS (w/v); pH 8.0

2.7   Separation of DJ-1 isoforms by isoelectric focusing (IEF) followed by immunodetection

For the separation of proteins based on their isoelectric point (pI) with subsequent immunodetection of DJ-1 two different methods were applied:

(I) Gel-based IEF followed by western blotting

This method was carried out by Dr. Gereon Poschmann from the group of Prof. Dr. Kai Stühler, Molecular Proteomics Laboratory (MPL), Heinrich-Heine-Universität Düsseldorf, Germany *[Poschmann et al., in preparation]*. IEF was performed as described in Chapter 2.6 applying 50 µg of unlabeled protein. The gel was incubated for 20 min in 125 mM Tris, 40 % (w/v) glycerin, 65 mM DTT and 104 mM SDS and the proteins were transferred onto a nitrocellulose membrane using a semi-dry system. Subsequently, the membrane was probed with a rabbit monoclonal anti DJ-1 antibody (1:2000, Biomol, #2398-1). The target was detected with an IRDye 800-conjugated anti-rabbit antibody (1:15 000, LI-COR Biosciences, #926-32213) using the Odyssey® Infrared Imaging System (LI-COR Biosciences) or an Alexa Fluor 555-conjugated anti-rabbit antibody (1:5000, Life Technologies, #A21429) in combination with a Typhoon 9400 Scanner (GE Healthcare). Protein isoforms were quantified using the gel analyzer plug-in of the ImageJ 1.45s software *[Schneider et al. 2012]*.

(II) Capillary IEF immunoassay

This method was carried out by Dr. Daniela Besong Agbo and Dr. Hans Klafki from the group of Prof. Dr. Jens Wiltfang, LVR-Klinikum Essen, Germany *[Besong Agbo et al. 2013]*. The assay was performed on a NanoPro™ 1000 Instrument (Protein Simple, Santa Barbara, CA, USA). Briefly, lysates were prepared as described in Chapter 2.6, denatured (40 mM DTT, 9 M urea) and mixed 1:2 with an ampholyte premix (separation gradient pH 5-8) containing a fluorescent pI standard ladder and a protease and phosphatase inhibitor mix. Samples, primary antibody targeting DJ-1 (1:50, Biomol, #2398-1), biotinylated anti-rabbit antibody, streptavidin-horseradish peroxidase conjugate (1:100, Protein Simple), and luminol/peroxide

mix were loaded on a 384-well plate and transferred to the NanoPro™ 1000 instrument. The automatically run assay was programmed with the Compass software (Protein Simple, version 1.3.7). Capillaries were loaded with 400 nl sample solution and IEF was performed at 21 mW for 40 minutes. Afterwards, analytes and standards were immobilized to the capillary wall by applying UV-light for 100 seconds followed by incubations with primary DJ-1 antibody (120 min), biotinylated anti-rabbit antibody (60 min), streptavidin-horseradish peroxidase conjugate (120 min) and luminol/peroxide mix (30 to 960 seconds). Peak integration and pI marker calibration for peak alignment were performed using Compass software.

2.8 Isolation of mitochondria and cytosolic fraction from brain tissue for analysis of DJ-1 localization

Brains without olfactory bulbs, brain stem and cerebellum were placed in icecold isolation buffer, cut into smaller pieces using scissors and cleaned from blood. The tissue was homogenized in 5 ml isolation buffer in a 15-ml glass-glass homogenizer with 12 strokes and centrifuged at 1300 g for 6 min at 4°C in a 50-ml centrifuge tube precipitating crude cell debris and nuclei (pellet P1, Fig. 2-3 A). The supernatant was transferred into a new centrifuge tube and centrifuged at 13000 g for 10 min at 4°C separating a crude mitochondrial fraction. The supernatant was transferred into a 12-ml ultracentrifuge tube for further centrifugation at 100000 g for 1 h (4°C). The obtained supernatant is referred to as cytosolic fraction to which 2.5 µl*ml^{-1} protease inhibitor and phophatase inhibitor cocktail (Sigma-Aldrich) were added, respectively. The pellet represents the microsomal fraction containing ER and other membranes *[Darios et al. 2003]*. The crude mitochondrial fraction was resuspended in 500 µl 20 µM Na$_2$CO$_3$ in 25 mM HEPES buffer (pH 7.5) and incubated for 30 min on ice to detach loosely associated proteins from the mitochondria *[Blackinton et al. 2009]*. Mitochondrial suspension was ultracentrifuged at 60000 g for 30 min (4°C). Precipitated mitochondria were washed once in isolation buffer and resuspended in 250 µl isolation buffer (Fig. 2-3 A). Protease and phosphatase inhibitor cocktails (10 µl*ml^{-1}, Sigma-Aldrich) were added to mitochondria and mitochondrial supernatant. Protein concentrations were determined by the Bradford method (Chapter 2.5). The purity of the different fractions was analyzed by immunodetecting cell organell specific markers (Fig. 2-3 B).

Isolation buffer   215 mM mannitol, 75 mM sucrose, 20 mM HEPES, 1 mM EGTA; pH 7.2
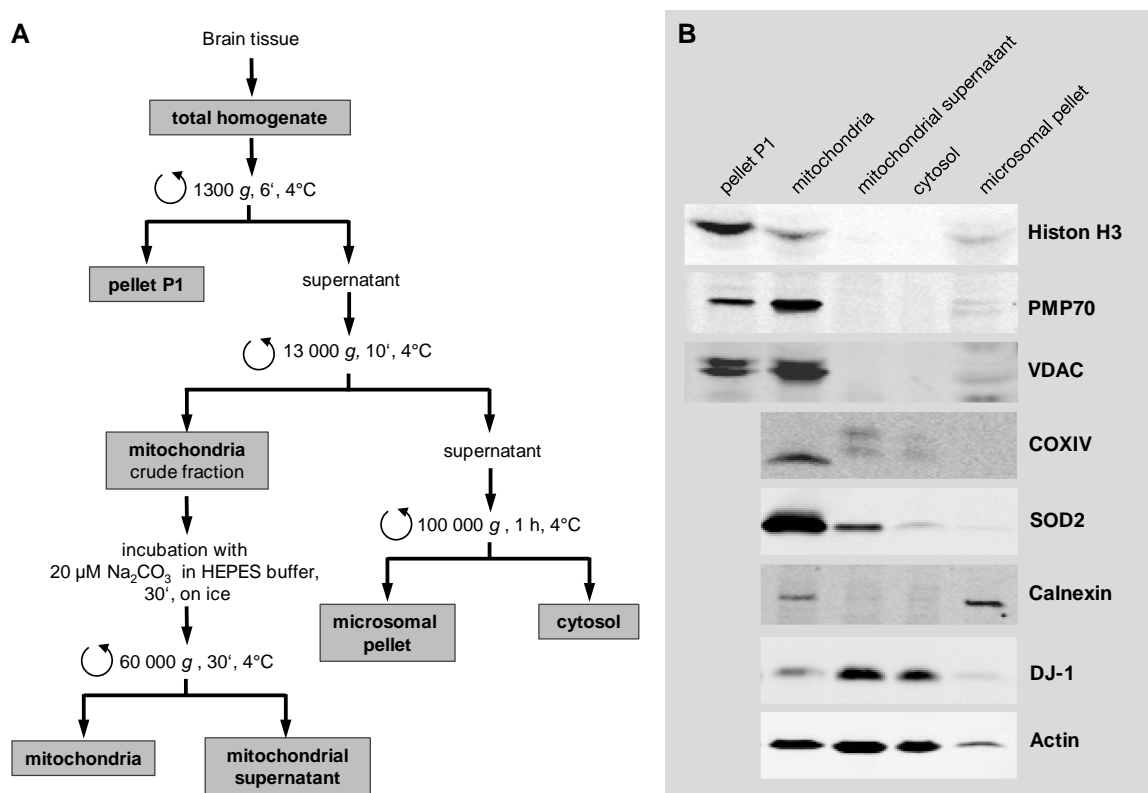
Fig. 2-3. Preparation of subcellular fractions from mouse brain tissue. (**A**) Flow chart showing the preparation steps of mitochondrial and cytosolic fractions. (**B**) Western blot targeting specific markers for individual cell organelles: Histon H3 (nucleus), peroxisomal membrane protein 70 (PMP70, peroxisomal membrane), voltage-dependent anion channel (VDAC, outer mitochondrial membrane), cytochrome c oxidase subunit 4 (COXIV, inner mitochondrial membrane), superoxide dismutase 2 (SOD2, mitochondrial matrix).

2.9 Characterization of isolated brain mitochondria from HF or control diet-fed mice

For functional characterization of mitochondria, the crude mitochondrial fraction was isolated from brain tissue according to Chapter 2.8 with the following modifications: use of a 15-ml glass-teflon homogenizer with 7 to 8 strokes, addition of 0.1 % fatty-acid free BSA to the isolation buffer and resuspension of mitochondria in 500 µl KHE buffer (see Chapter 2.9.1).

2.9.1 Oxygen consumption measurements of isolated mitochondria using a Clark electrode

The Clark electrode (Rank Brothers) consists of a platinum cathode and a silver anode that are surrounded by 3 M KCl and separated from an incubation chamber by an oxygen permeable Teflon membrane. The platinum cathode is polarized with -0.6 V relative to the silver anode. Under this condition, the oxygen partial pressure inside the incubation chamber is proportional to the electric current between anode and cathode (Fig. 2-4) which is amplified (PowerLab 26T, ADInstruments) and recorded by the Labchart 5 software.

$$\text{Oxidation:} \quad 4\,Ag + 4\,Cl^- + 4\,e^- \longrightarrow 4\,AgCl$$

$$\text{Reduction:} \quad O_2 + 2\,H_2O + 4\,e^- \longrightarrow 4\,OH^-$$

$$\text{Redox:} \quad 4\,Ag + O_2 + 2\,H_2O + 4\,Cl^- \longrightarrow 4\,AgCl + 4\,OH^-$$
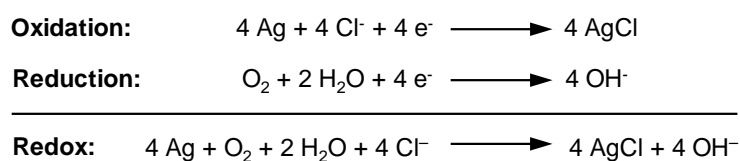
Fig. 2-4. Redox reaction inside the Clark electrode. Oxidation occurs at the silver anode, reduction at the platinum cathode.

The electrode was calibrated with sodium dithionite in KHE buffer (0 µM O_2) and air saturated KHE buffer (240 µM O_2). Measurements were carried out with 500 µg mitochondrial protein in 1 ml air saturated KHE buffer at 37°C under continuous stirring (level 6). As substrate, either 5 mM succinate or a combination of 5 mM glutamate and 5 mM malate was used (in H_2O, pH 7). After closing the incubation chamber, 8 µM rotenone (in ethanol, only for succinate respiration) followed by substrate, 1 mM ADP (in H_2O, pH 7), 2 µg*ml^{-1} oligomycin (in ethanol) and 2.5 µM FCCP (in DMSO) were added in 1.5-min intervals using a Hamilton syringe. Oxygen consumption rates under the different conditions were determined from the recorded slopes and expressed as nmol O_2*min^{-1}*mg protein^{-1}. The respiratory control ratio (RCR) was calculated by dividing the oxygen consumption rate in the presence of substrate and ADP (state 3 respiration) by the oxygen consumption rate in the presence of substrate only (state 4 respiration). The RCR provides a measure of mitochondrial integrity by indicating the fold increase of respiration under phosphorylating conditions relative to non-phosphorylating respiration under substrate excess.

KHE buffer   120 mM KCl, 3 mM HEPES, 1 mM EGTA, 5 mM KH_2PO_4, 0.3 % fatty-acid free BSA; pH 7.2

2.9.2 Mitochondrial membrane potential ($\Delta\Psi_m$) measurements in isolated brain mitochondria using Safranin O

The method utilizes the cationic membrane-permeant fluorescent dye Safranin O that accumulates inside energized mitochondria where its fluorescence is quenched due to a spectral shift *[Akerman & Wikstrom 1976]*. The relative decrease of the total fluorescence with hyperpolarization is considered to be proportional to the membrane potential *[Toime & Brand 2010]*. Measurements were performed in 96-well plates (FLUOTRACTM 200, Greiner Bio-One) at 37°C in triplicates. Fluorescence was measured at 495 nm excitation and 586 nm emission wavelength in a microplate reader (Tecan). In a final volume of 200 µl/well, 100 µg of mitochondrial protein, 2 µM rotenone and 8 µM Safranin O were combined in KHE buffer and measured over 30 min. Subsequently, mitochondria were energized by the injection of substrate (5 mM succinate or a combination of 5 mM glutamate and 5 mM malate) and measured for further 30 min before adding the artificial uncoupler FCCP (0.3 µM). The resulting time course of fluorescence intensities is expressed in percent defining the last time-point prior to substrate injection as 100 % to adjust for different baseline levels of the samples. The maximal decrease of Safranin O fluorescence after the addition of substrate was calculated as a measure of membrane potential.

2.9.3 Detection of mitochondrial superoxide production using Amplex® Red

Superoxide ($O_2^{\bullet-}$) produced by isolated mitochondria is converted to hydrogen peroxide by superoxide dismutase (SOD). Horseradish peroxidase subsequently reduces H_2O_2 to water oxidizing the non-fluorescent dye Amplex® Red (Invitrogen) into the fluorescent resorufin (Fig. 2-5) *[Zhou et al. 1997]*.
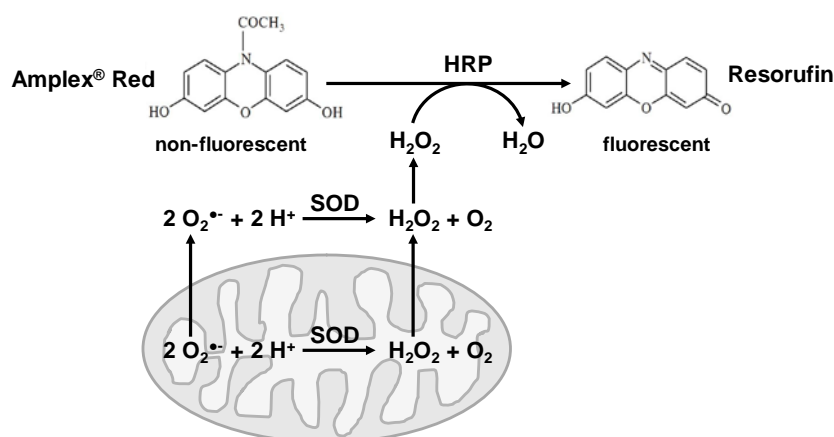
Fig. 2-5. Indirect detection of mitochondrial superoxide ($O_2^{\bullet-}$) production using Amplex® Red. HRP - Horseradish peroxidase. SOD - Superoxide dismutase.

Measurements were performed in 96-well plates (FLUOTRACTM 200, Greiner Bio-One) at 37°C in triplicates. Fluorescence was measured at 560 nm excitation and 590 nm emission wavelength in a microplate reader (Tecan). In a final volume of 200 µl/well, 50 µg of mitochondrial protein, 0.4 U SOD, 1.2 U HRP and 50 µM Amplex® Red were combined in KHE buffer with or without 2 µM rotenone. Fluorescence intensity was detected over 30 min with injection of 5 mM succinate or a combination of 5 mM glutamate and 5 mM malate after 10 min. From the resulting time course, for each sample the increase of the slopes before and after the addition of substrate was calculated and divided by the slope of the standard curve and the protein amount (Fig. 2-6). DMSO and ethanol solvent controls were run simultaneously. For the standard curve, 50 µg of mitochondria were inactivated by three freeze-thaw cycles. A point measurement was carried out in the reaction mixture described above supplemented with 0, 1, 2, 3, 4 and 5 nmol H_2O_2 in duplicates.

$$H_2O_2 \text{ production } [nmol*min^{-1}*mg^{-1}] = \frac{slope_{substrate} [RFU*min^{-1}] - slope_{no\,substrate} [RFU*min^{-1}]}{slope_{standard} [RFU*nmol^{-1}] * m_{mitochondria} [mg]}$$

Fig. 2-6. Calculation of the H_2O_2 production rate.

2.10   RNA isolation from hypothalamic tissue

For isolation of total RNA, a complete or ventral hypothalamus was homogenized in 800 µl TRIsure (Bioline) for 20 s using an Ultra-Turrax (IKA), incubated for 5 min at room temperature, mixed with 160 µl chloroform, incubated for further 3 min and centrifuged for 15 min at 12000 g at 4°C. The clear top phase was mixed with 500 µl 75 % ethanol, transferred to columns of the SV Total RNA Isolation System (Promega) and proceeded according to the manual. RNA was eluted in 60 µl nuclease-free water and concentration was measured spectrophotometrically (Infinite® 200 NanoQuant, Tecan). For quality assessment, 2 µl of isolated RNA were mixed with 8 µl RNA loading buffer, incubated at 65°C for 10 min and separated by size on a denaturing formaldehyde agarose gel (1 %) for ~40 min at 100 V to visualize the 28S and 18S rRNA bands. RNA was stored at -80°C.

RNA loading buffer	200 µl formamide, 64 µl 37 % formaldehyde, 40 µl 10x MOPS, 8 µl H_2O, 8 µl ethidium bromide
Formaldehyde agarose gel	1 g agarose in 72 ml H_2O, 10 ml 10x MOPS buffer, 18 ml 37 % formaldehyde
10x MOPS buffer	400 mM MOPS, 100 mM sodium acetate, 10 mM EDTA; pH 7

2.11   Quantitative real-time polymerase chain reaction (qRT-PCR)

Isolated hypothalamic RNA was reverse-transcribed into cDNA using the QuantiTect®
Reverse Transcription Kit (Qiagen) utilizing oligo-dT and random primers in a 10 µl reaction
mixture containing 500 ng RNA. The cDNA was stored at -20°C. Primer sequences
(Appendix I.III Table A2) were designed using the Primer3 algorithm (SDSC Biology
Workbench). Primer sequences were tested in a non-quantitative PCR and only primer pairs
that generated a single, sharp product band were applied in the qRT-PCR analysis. For
analysis of gene expression, the SYBR Green-based qRT-PCR was performed either on 96-
well (Mastercycler® ep realplex epgradient S, Eppendorf) or 384-well format (Roche
LightCycler® 480) according to table 2-3 and 2-4. A melting curve was recorded at the end of
the program to confirm the quality of the amplified product and identify possible non-specific
reaction products.

Table 2-3. qRT-PCR reaction mixture for analysis of gene expression.

	Volume per reaction [µl]	
	96-well	384-well
Sensimix SYBR NoRox (Bioline)	12.5	6.25
Primer forward	1.0 (10 pmol/l)	1.0 (5 pmol/l)
Primer reverse	1.0 (10 pmol/l)	1.0 (5 pmol/l)
Nuclease-free water	9.5	3.25
cDNA	1.0	1.0
Total	25.0	12.5

Table 2-4. qRT-PCR program for analysis of gene expression.

Step	Temperature [°C]	Time [s]	Cycles
Initialization	95	600	
Denaturation	97	10	
Annealing	52	15	45 x
Elongation	72	20	
Melting curve	60 to 95	1200	

Gene expression levels of the samples were calculated from a standard curve that was
generated from pooled cDNA of all samples (n = 12) and diluted by 2^n in 8 steps. Standards
were measured in duplicates. Sample cDNAs were diluted 1:10 to 1:50 and measured in
triplicates. The mean expression of the technical replicates was normalized by the mean
expression of *Heat shock protein 90* (*Hsp90*) that was selected as housekeeping gene.

2.12 Transcriptome analysis of ventral hypothalamus comparing high-fat or control diet-fed *Dj-1$^{-/-}$* and *Dj-1$^{+/+}$* mice

Transcriptome next generation sequencing (RNA-Seq) was carried out by Dr. Karol Szafranski and Dr. Marco Groth from the group of Dr. Matthias Platzer, Fritz Lipmann Institute Jena, Germany. RNA of ventral hypothalami was isolated as described in Chapter 2.10 and the integrity was assessed using a RNA 6000 Nano chip (Agilent, Santa Clara, CA, USA). RNA-Seq was performed on the Illumina HiSeq 2000 platform (Illumina, San Diego, CA, USA). RNA-Seq libraries were prepared using TruSeq RNA Sample Prep kit v2, pooled to up to 7 libraries per lane and sequenced 50 nt single-sided (plus barcode) using TruSeq SBS kit v3-HS to result in a depth of at least 25 million read pairs per sample. Primary data was processed using CASAVA version 1.8.2.

Gene expression analysis

Next generation sequencing reads were mapped to the mouse genome (Genomatix Mining station; Genomatix, Munich, Germany) applying the library version NCBI build 37 and the ElDorado Version 08-2011 (seed mapping type 'deep', 92 % minimum alignment quality). Only unique hits (> 82 % of total hits) were subjected to differential expression analysis utilizing the Genomatix Genome Analyzer. Two groups were compared at once using both DESeq 1.10.1 and edgeR 3.0.4 algorithms, respectively. The p-value threshold was set to 0.05 with the use of a multiple testing correction introduced by Benjamini & Hochberg *[1995]*. A fold change of log2 ≥ 0.263 indicated upregulation and log2 ≤ -0.263 downregulation in the 'treated' vs. the 'control' group corresponding to a fold change of 1.2 or -1.2, respectively. Only differentially expressed genes found significant with both DESeq and edgeR algorithms and displaying a minimal expression level of 10 reads for the majority of animals in one group were considered.

Additionally, we performed a t-test statistic with log-transformed normalized expression (NE) values of the individual transcripts (log(NE+1)). Genes for which at least one transcript was found different between two groups with a significance level of $p < 0.01$ and a mean NE fold change of log2 > 0.263 (upregulation) or log2 < -0.263 (downregulation), corresponding to a fold change of 1.2 or -1.2, respectively, were subjected to a pathway analysis using the Genomatix Pathway System.

2.13   Mitochondrial genome copy number quantification in mouse tissue

Frozen forebrain, gastrocnemius muscle and eWAT samples were grinded in liquid nitrogen using mortar and pestle. DNA was isolated from powdered tissue using the Wizard SV Genomic DNA Purification System (Promega) according to the manufacturer's protocol. DNA concentrations were measured spectrophotometrically (Infinite® 200 NanoQuant, Tecan) and diluted to 40 ng/µl with nuclease-free water.

The mitochondrial genome copy number is quantified relative to the nuclear genome copy number and provides a measure for mitochondria per cell. This is achieved by a qRT-PCR directed against targets exclusively found in the murine nuclear or mitochondrial genome (Table 2-5)[7]. The qRT-PCR was performed in a Roche LightCycler® on 96-well plates according to table 2-6 and 2-7 in duplicates. As a result, the relative DNA amount for each replicate was obtained according to the following equation:

$$DNA [AU] = 10^6 * (2^{Cp})^{-1}; AU – Arbitrary Unit, Cp – Crossing point.$$

Subsequently, the quotient of the mean mitochondrial DNA amount and the mean nuclear DNA amount was calculated.

Table 2-5. Primer-probe pairs for quantification of mitochondrial genome copy number designed for the Roche LightCycler®.

Primer pairs

Target genome	Location	Forward (3'-5')	Reverse (3'-5')
Nuclear	chr8: 1000128+31000199	tttacaggatctccaagattcaga	gatcaccccatgtgaacaaa
Mitochondrial	chrM: 4343+4452	caaatttacccgctactcaactc	gctataattttcgtatttgtgtttgg

Probes

Target genome	No.	Sequence	Length [nt]	Cat. No.
Nuclear	26	tttacaggatctccaagattcagagtcagcccagcttggacattgtt agaaatttgttcacatggggtgatc	72	04687574001
Mitochondrial	101	caaatttacccgctactcaactctactatcattttaatactagcaatt acttctattttcataggggcatgaggaggacttaaccaaacacaa atacgaaaaattatagc	110	04692195001

Table 2-6. qRT-PCR reaction mixture for analysis of mitochondrial genome copy number.

	Volume per reaction [µl]
2x Mastermix (LightCycler® 480 ProbesMaster, Roche)	5.0
Primer forward (20 µmol/l)	0.2
Primer reverse (20 µmol/l)	0.2
Probe	0.2
DNA (40 ng/µl)	4.4
Total	10.0

[7] The method was established by Dr. Tobias Fromme, Molecular Nutritional Medicine, TU München, Freising.

Table 2-7. qRT-PCR program for analysis of mitochondrial genome copy number.

Step	Temperature [°C]	Time [s]	Cycles
Initialization	95	300	
Denaturation	95	10	
Annealing	60	20	45 x
Elongation	72	2	
Final elongation	72	180	

2.14 Statistics

For comparison of two groups, significance was determined using two-sided Student's t-test with a p-value < 0.05 indicating significant differences. A Bonferroni correction was conducted manually for multiple comparisons by dividing the significance level by the number of comparisons. Equal variances were tested applying F-tests.

The phenotypic data of HF or control diet-fed *Dj-1$^{-/-}$* and *Dj-1$^{+/+}$* mice was analyzed by two-way ANOVA inclusive of testing for genotype:diet interactions. Male and female mice were regarded separately. ANOVA analysis was followed by post-hoc Bonferroni correction. Differences with p < 0.05 were considered significant. In case the data was not normally distributed, a log-transformation was performed. Analysis of covariance (ANCOVA) was performed to adjust fat and lean mass, respectively, to the mean body mass of each diet group. For this, fat or lean mass was plotted against body mass. From the linear regression functions for the diet-genotype groups, the predicted fat or lean mass was calculated from the body mass of individual animals as well as the mean body mass per diet group. Residuals were calculated for each animal and added to the predicted fat or lean mass of the diet group. Residuals were tested for normality using the Shapiro-Wilk test.

Whiskers of box plots indicate the minimum and maximum value, respectively.

T-tests and ANCOVA analysis were performed using Microsoft Office Excel 2007. Two-way ANOVA was performed using the software GraphPad PRISM 4 or SigmaPlot 12.3.

3   RESULTS

3.1   Alterations in the hypothalamic proteome associated with a short-term high-fat diet intervention

We aimed to detect alterations in the murine hypothalamic proteome in response to a short-term high-fat (HF) diet. Three inbred mouse strains with different susceptibility to diet-induced obesity (DIO) were compared: the obesity-prone AKR/J and C57BL/6N mice and the SWR/J mice that are resistant to DIO *[Hesse et al. 2010]*. Male 7-week-old mice of each strain were fed a HF or a control diet for 10 days. After this time, the body mass of HF diet-fed AKR/J and C57BL/6N mice was significantly increased compared to mice maintained on control diet (Fig. 3-1). This was due to elevated body fat as well as lean mass with a more pronounced level of DIO in AKR/J mice. In SWR/J mice, only very mild DIO was detectable as indicated by an increased fat mass (Fig. 3-1).
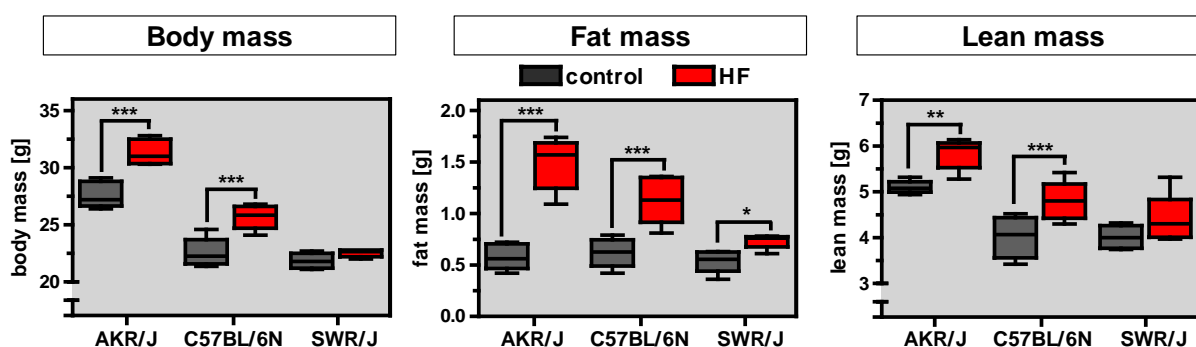
Fig. 3-1. Body mass, fat and lean mass of AKR/J, C57BL/6N and SWR/J mice after 10 days of HF or control diet. Mice were male and 7 weeks old (n = 5-6). Fat and lean mass were assessed in the abdominal part via Micro-CT. ANOVA indicated significant effects for diet and strain for body mass, fat and lean mass ($p < 0.001$) and a significant strain:diet interaction for body mass ($p = 0.001$) and fat mass ($p = < 0.001$). Bonferroni posttest: ***$p < 0.001$, **$p < 0.01$, *$p < 0.05$ HF vs. control diet-fed mice.

After 10 days of HF or control diet, hypothalami were dissected and protein expression patterns between the diet groups were compared within each strain using two-dimensional difference gel electrophoresis (2D-DIGE). Protein spots showing differential abundance between HF and control diet-fed mice were excised and mass spectrometrically identified. In AKR/J mice, 7 differentially abundant proteins were found, 6 in C57BL/6N and 3 in SWR/J mice with HF/control ratios ranging from 0.6 to 2.0 (Table 3-1). Thus, the number of HF diet-regulated proteins within a strain seems to correlate positively with the level of adiposity.

Table 3-1. Alterations in the hypothalamic proteome induced by a 10-day HF feeding in AKR/J, C57BL/6N and SWR/J mice. HF and control diet-fed mice were compared within each strain using 2D-DIGE. Listed are spots with significantly differential volumes that were identified by nano-HPLC-ESI tandem mass spectrometry.

Master spot no.	Gene Symbol	UniProtKB accession no.	Ratio* HF/control	T-Test p-value	Protein name
AKR/J					
3646	Sh3bgrl3	Q91VW3	2.0	0.0016	SH3 domain-binding glutamic acid-rich-like protein 3
2652	Park7	Q99LX0	1.5	0.0001	Protein DJ-1
2880	Cfl1	P18760	1.4	0.0047	Cofilin-1
2995	Sncb	Q91ZZ3	1.3	0.0195	Beta-synuclein
3209	Ppp3r1	Q63810	0.8	0.0465	Calcineurin subunit B type 1
3310	Acot13	Q9CQR4	0.7	0.0470	Acyl-coenzyme A thioesterase 13
3282	Acot13	Q9CQR4	0.7	0.0071	Acyl-coenzyme A thioesterase 13
3417	Hbb-b1	P02088	0.6	0.0351	Hemoglobin subunit beta-1
C57BL/6N					
3695	Park7	Q99LX0	1.4	0.0002	Protein DJ-1
3374	Pbh	P67778	1.3	0.0184	Prohibitin
3374	Tceal5	Q8CCT4	1.3	0.0184	Transcription elongation factor A protein-like 5
3730	Psmb6	Q60692	0.8	0.0372	Proteasome subunit beta type-6
4423	Snca	O55042	0.8	0.0094	Alpha-synuclein
4737	Hrsp12	P52760	0.7	0.0093	Ribonuclease UK114
SWR/J					
3673	Ndufv2	Q9D6J6	1.4	0.0082	NADH dehydrogenase [ubiquinone] flavoprotein 2, mitochondrial
3673	Apoa1	Q00623	1.4	0.0082	Apolipoprotein A-I
3619	Park7	Q99LX0	1.3	0.0003	Protein DJ-1

*Ratio of normalized and standardized 2D-DIGE spot volumes. Data generated by Dr. Gereon Poschmann, MPL, Düsseldorf, Germany.

Strikingly, the protein DJ-1 (PARK7) was found to be more abundant in the HF groups of all strains as compared to the respective control groups (Fig. 3-2) and was thus chosen for validation.
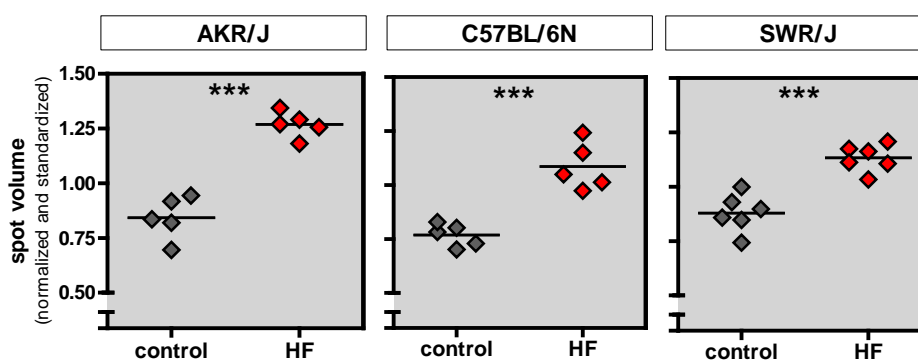
Fig. 3-2. 2D-DIGE spot volumes of the spot identified as DJ-1. Data points represent individual animals. Student's t-test: ***$p < 0.001$.

3.2 High-fat feeding alters the isoform composition of the DJ-1 pool

3.2.1 The DJ-1 pool shifts towards more acidic isoforms in the brain upon high-fat feeding

Total protein expression and *Dj-1* transcript levels in hypothalami were comparable between HF or control diet-fed C57BL/6N mice (Fig. 3-3). Due to post-translational modifications, the intracellular DJ-1 protein pool comprises multiple isoforms varying in their isoelectric point (pI) *[Natale et al. 2010]*. The above result was obtained after hypothalamic protein homogenates were separated two-dimensionally by the isoelectric point (pI) in the first dimension and molecular weight in the second. Accordingly, the higher abundance of DJ-1 in HF animals likely represents only one specific DJ-1 isoform. We therefore investigated, whether the composition of the DJ-1 pool changes upon HF feeding. In order to quantify the different DJ-1 pI isoforms, we separated hypothalamic extracts via gel-based isoelectric focusing (IEF) with subsequent membrane transfer and DJ-1 immunodetection. With this approach, a total of 7 DJ-1 isoforms were detected within the hypothalamus of AKR/J and C57BL6/N mice (Fig. 3-4 A, B). Quantification revealed that one DJ-1 isoform in the lower pI range was increased in HF diet-fed AKR/J mice relative to the control group (Fig. 3-4 C) confirming the initial proteome result. In HF diet-fed C57BL/6N mice, the same spot was also increased but lost significance after Bonferroni correction (Fig. 3-4 D).
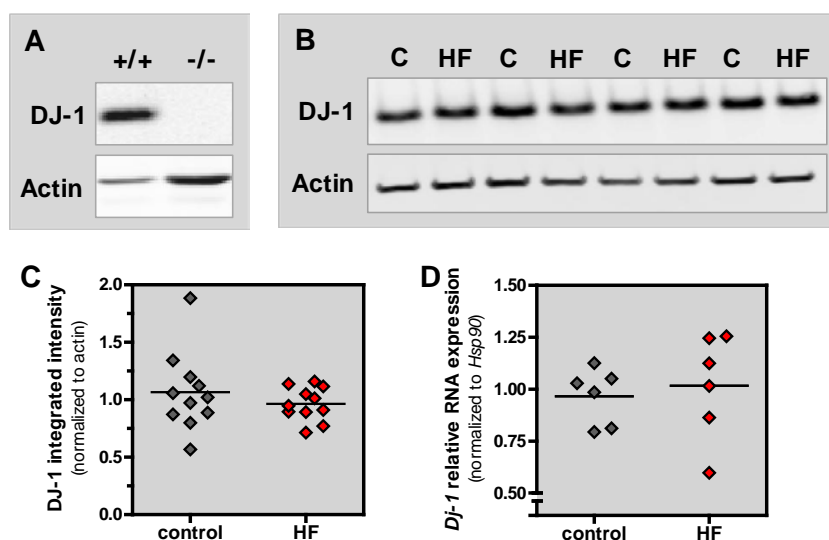
Fig. 3-3. Total DJ-1 expression in the hypothalamus of male C57BL/6N mice after 10 days of HF or control diet. (**A**) Validation of the anti-DJ-1 antibody in hypothalamic extracts of *Dj-1*$^{-/-}$ compared to *Dj-1*$^{+/+}$ mice. (**B**) Representative western blot showing DJ-1 and actin expression. Both target proteins were detected on the same membrane. (**C**) Densitometric analysis of western blot data. DJ-1 signals were normalized to actin (n = 11). (**D**) *Dj-1* gene expression measured by quantitative PCR. Transcript levels were normalized to *Hsp90* expression (n = 5). (**C, D**) Data points represent individual animals.
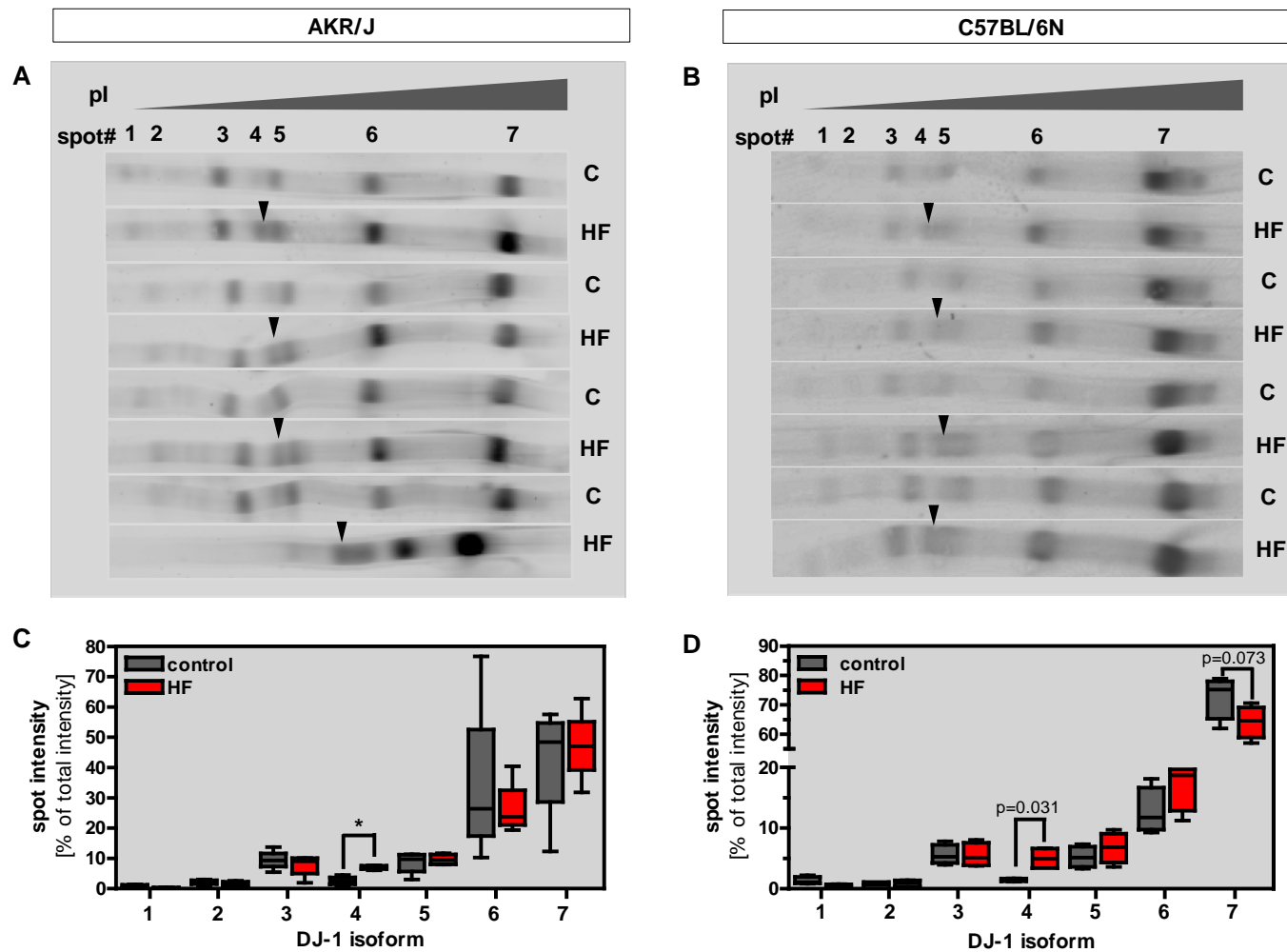
Fig. 3-4. Comparison of DJ-1 pI isoforms in the hypothalamus of male AKR/J and C57BL/6N mice after 10 days of HF or control diet. (**A, B**) Hypothalamic extracts were separated in an IEF gel and transferred to a membrane followed by immunodetection of DJ-1. Arrows indicate the DJ-1 isoform found increased in HF diet-fed mice. (**C, D**) Densitometric quantification of the signal intensities of individual DJ-1 spots (n = 4). Student's t-test with Bonferroni correction: *p < 0.0071 control vs. HF diet-fed mice. Data generated by Dr. Gereon Poschmann, MPL, Düsseldorf, Germany.

Because DJ-1 is expressed ubiquitously (Fig. 3-5) *[Nagakubo et al. 1997; Taira et al. 2001;*
Bonifati et al. 2003b; Niki et al. 2003; Bader et al. 2005; Zhang et al. 2005a], we next investigated
whether the increase in acidic DJ-1 isoforms can also be observed in other brain areas.
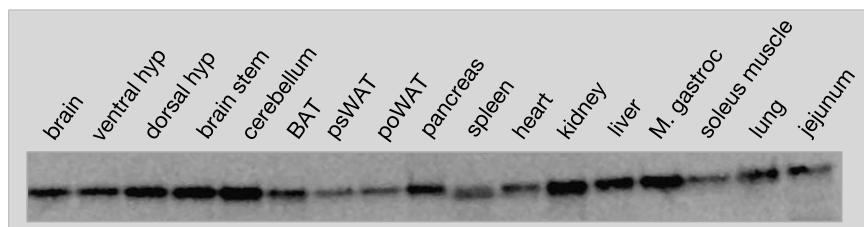
Fig. 3-5. DJ-1 expression in selected mouse tissues. Western blot showing protein homogenates from tissues
of a female C57BL/6J mouse (10 µg protein/lane). hyp – hypothalamus. BAT - brown adipose tissue. psWAT -
posterior subcutaneous white adipose tissue. poWAT - periovarial white adipose tissue. M. gastroc -
gastrocnemius muscle.

For this, we utilized an automated high-throughput capillary IEF immunoassay (NanoPro™,
ProteinSimple) with DJ-1 immunodection. This method has two major advantages: Up to 96
samples can be processed simultaneously and the use of pI standards allows a precise
allocation of pI-values to the individual isoforms. Applying this assay to the hypothalamus, we
detected 7 DJ-1 isoforms (Fig. 3-6 A). The distribution of signal intensities differed from the
spot pattern obtained with the gel-based IEF-immunoblot method probably due to method-
dependent separation characteristics. Thus, the numbering of the individual isoforms does
not allow an inter-method comparison.

The pI values of the DJ-1 isoforms detected with the capillary IEF immunoassay ranged
from 5.6 to 6.7 (Fig. 3-6 A) in accordance with published data *[Natale et al. 2010]*. The relative
peak areas indicated higher abundances of isoform 3 (pI 5.8) and isoform 4 (pI 5.9) within
the hypothalamus of HF diet-fed mice (Fig. 3-6 B). Additionally, isoform 6 (pI 6.5) was
significantly decreased compared to the control group. We further examined the DJ-1 isoform
distribution in brain stem, cerebellum and forebrain. All brain areas showed a similar signal
distribution as in the hypothalamus with higher abundances of isoform 3 and 4 in mice fed
the HF diet (Fig. 3-6 C-E). Isoform 6 was also significantly decreased by HF diet in the
cerebellum and forebrain. In the cerebellum, isoform 7 (pI 6.7) was additionally decreased in
the HF diet group.

These results demonstrate a HF diet-induced shift in the composition of the DJ-1 protein
pool with accumulation of more acidic isoforms throughout the brain.
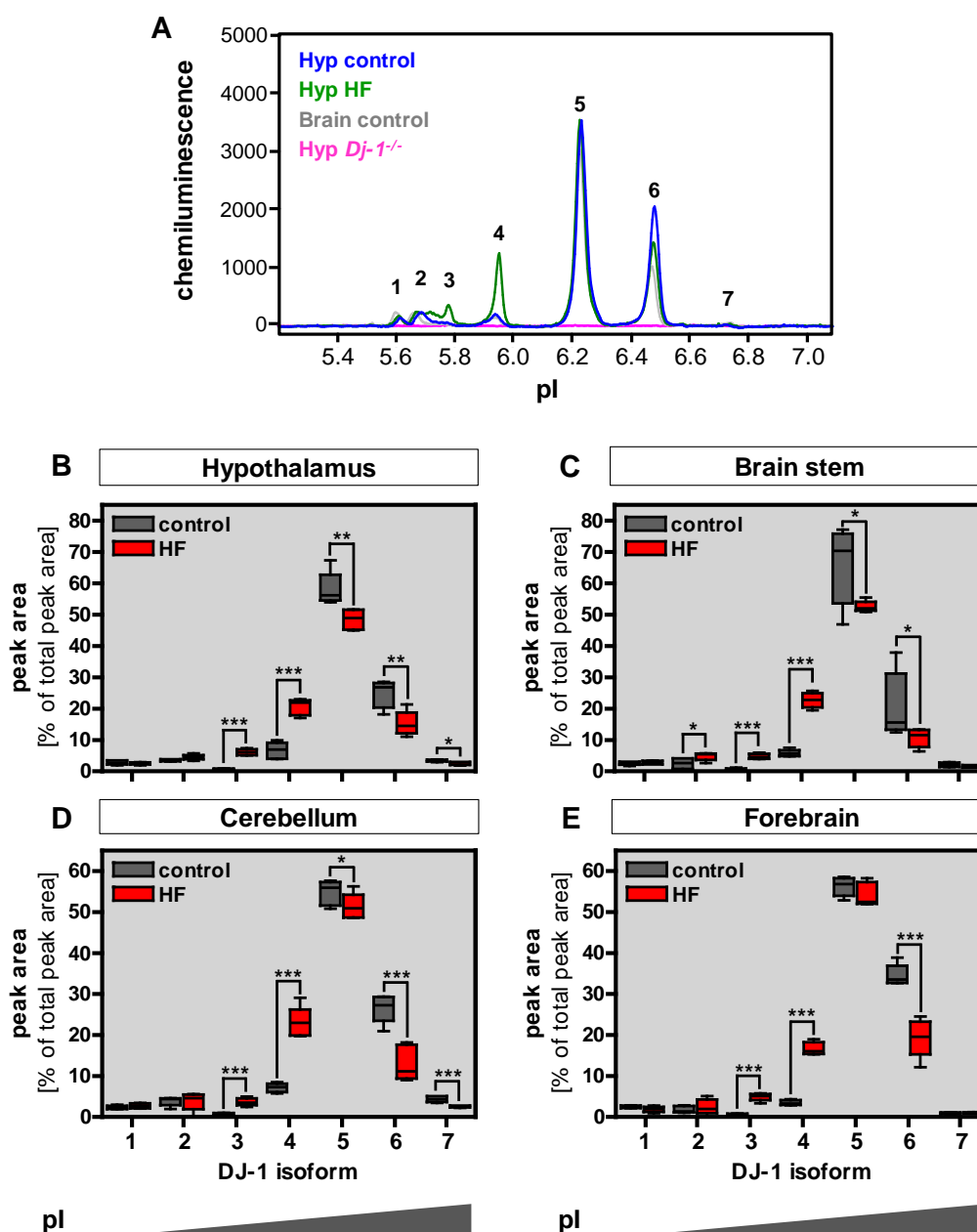
Fig. 3-6. Comparison of DJ-1 pI isoforms in selected brain areas of C57BL/6N mice maintained on a HF or control diet for 10 days. Protein extracts were analyzed using an automated capillary IEF immunoassay (NanoPro[TM] 1000, ProteinSimple). (**A**) Electropherogram exemplifying the pI distribution of DJ-1 isoforms in the hypothalamus and brain as detected via chemifluorescence. Each peak likely corresponds to one DJ-1 isoform. The hypothalamic extract of a *Dj-1* deficient mouse (Hyp *Dj-1*^{-/-}) served as negative control. (**B-E**) Quantification of peak areas. Forebrain excludes the hypothalamus. Student's t-test with Bonferroni correction: *$p < 0.0071$, **$p < 0.0014$, ***$p < 0.0001$ control vs. HF diet-fed mice. $n_{hypothalamus} = 5$, $n_{brain\ stem} = 6$, $n_{cerebellum} = 6$, $n_{forebrain} = 5\text{-}6$. Data generated by Dr. Daniela Besong Agbo and Dr. Hans Klafki, LVR-Klinikum Essen, Germany.

3.2.2 High-fat diet-induced accumulation of acidic DJ-1 isoforms in peripheral tissues

We furthermore applied the capillary IEF immunoassay to selected peripheral tissues. As in the brain, seven isoforms were detected with matching pIs. In gastrocnemius muscle and pancreas, DJ-1 isoforms 1 (pI 5.6), 2 (pI 5.7), 3 (pI 5.8) and 4 (pI 5.9) were increased in the HF diet-fed animals, while isoform 6 (pI 6.5) was decreased (Fig. 3-7 A, B). Gastrocnemius muscle showed an additional HF diet-induced decrease in isoform 7 (pI 6.7). In liver, only isoform 2 (pI 5.7) was significantly increased upon HF-feeding (Fig. 3-7 C). In contrast, a HF diet-induced shift of DJ-1 isoforms was absent in epididymal white adipose tissue (eWAT, Fig. 3-7 D). The result for eWAT was confirmed using the gel-based IEF method with subsequent membrane transfer and DJ-1 immunodetection (Supplementary Fig. S1).

These results clearly show tissue specific differences in the distribution of DJ-1 isoforms as well as in the susceptibility towards HF diet-induced changes of the DJ-1 protein pool composition.
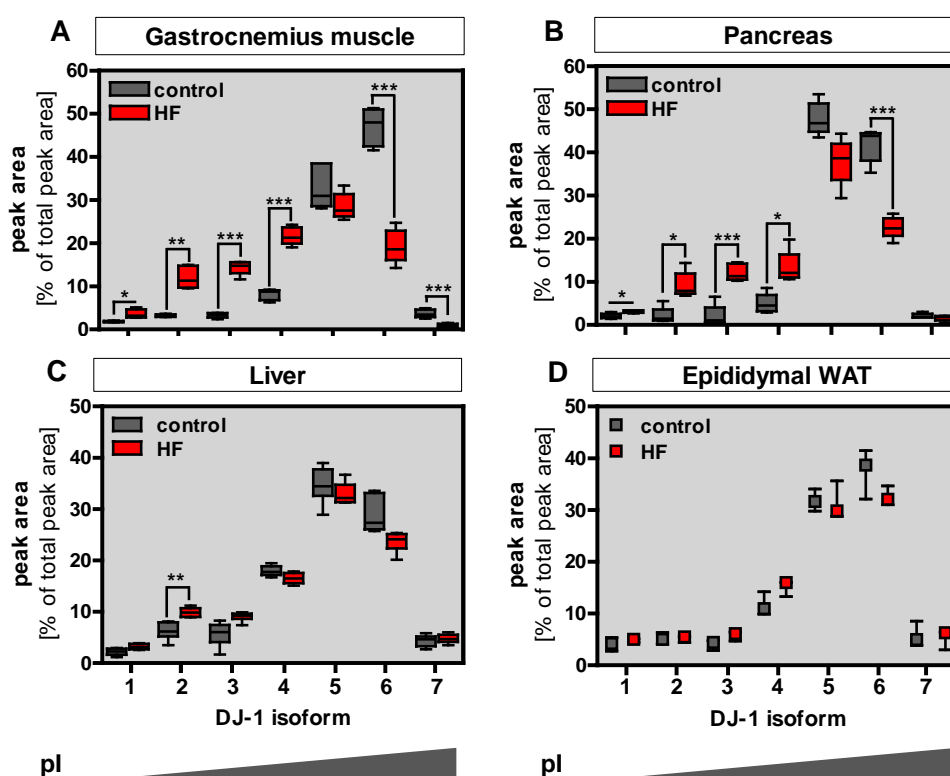
Fig. 3-7. Comparison of DJ-1 pI isoforms in peripheral tissues of C57BL/6N mice maintained on a HF or control diet for 10 days. Protein extracts were analyzed using an automated capillary IEF immunoassay (NanoPro[TM] 1000, ProteinSimple). Shown is the quantification of peak areas of electropherograms (see Supplementary Fig. S2). Student's t-test with Bonferroni correction: *p < 0.0071, **p < 0.0014, ***p < 0.0001 control vs. HF diet-fed mice. $n_{gastrocnemius\ muscle}$ = 5-6, $n_{pancreas}$ = 5, n_{liver} = 6, $n_{epididymal\ WAT}$ = 3 (median ± range). Data was generated by Dr. Daniela Besong Agbo and Dr. Hans Klafki, LVR-Klinikum Essen, Germany.

3.2.3 The high-fat diet-induced shift of DJ-1 isoforms is influenced by the length of feeding

The HF diet-induced increase of acidic DJ-1 isoforms in the hypothalamus observed after 10 days of feeding raised the question whether this effect can be detected at earlier timepoints and if the shift is stable when the feeding period is prolonged. We therefore examined the hypothalami of mice that were fed a HF or control diet for two days or three months. Two days of HF diet did not result in a significant increase in body mass or fat mass. However, body mass and fat mass of control diet-fed mice was slightly reduced resulting in a significant difference in body and fat mass gain between HF and control diet-fed mice after two days (Supplementary Table S1). Lean mass was unaffected by the diets. After three months of feeding, body mass, fat and lean mass were clearly elevated in HF diet-fed mice compared to controls (Supplementary Table S1).
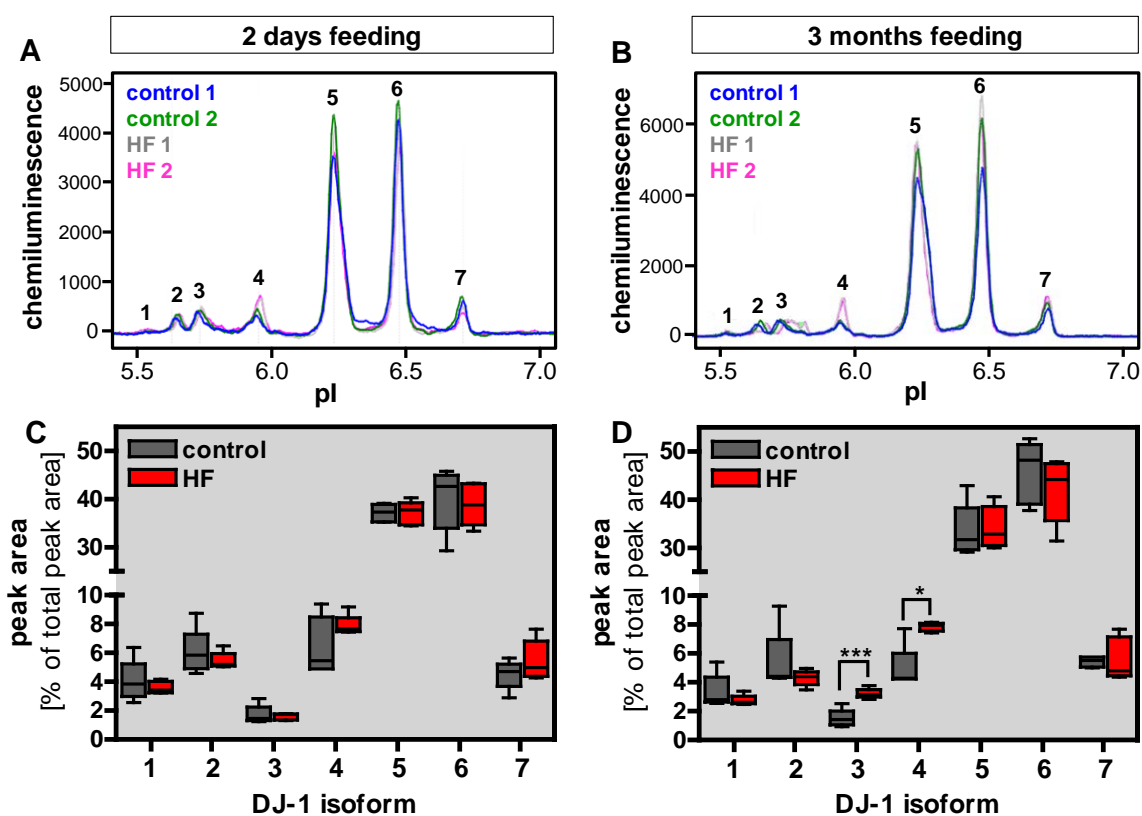
Fig. 3-8. Comparison of DJ-1 pI isoforms in the hypothalamus of C57BL/6N mice maintained on a HF or control diet for 2 days (A, C) or 3 months (B, D). Protein extracts were analyzed using an automated capillary IEF immunoassay (NanoPro[TM] 1000, ProteinSimple). (**A, B**) Electropherograms exemplifying the pI distribution of DJ-1 isoforms. (**C, D**) Quantification of peak areas (n = 5). Student's t-test with Bonferroni correction: *p < 0.0071, ***p < 0.0001 control vs. HF diet-fed mice. Data generated by Dr. Daniela Besong Agbo and Dr. Hans Klafki, LVR-Klinikum Essen, Germany.

Using the capillary IEF immunoassay, the detected DJ-1 isoforms were analogous to the hypothalamic samples after 10 days of feeding although the peaks in this sample set showed a slightly different pattern, with the peak of isoform 6 (pI 6.5) having a similar height as the peak for isoform 5 (pI 6.2) (compare Fig. 3-8 A, B and Fig. 3-6 A). However, due to high inter-assay coefficients of variation different runs cannot reliably be compared quantitatively *[Besong Agbo et al. 2013]*.

After two days, HF and control diet-fed mice showed comparable relative peak areas for all DJ-1 isoforms (Fig. 3-8 C). In contrast, after three months of feeding a significant difference between HF and control diet-fed animals for isoform 3 (pI 5.7) and isoform 4 (pI 5.9) was detected (Fig. 3-8 D). These results indicate that the shift of DJ-1 isoforms is not an acute effect but remains at least partly stable once established.

3.2.4 N-acetylcysteine increases glutathione levels but does not affect the abundances of DJ-1 isoforms in the brain

DJ-1 isoforms with a low pI are increased in cultured cells exposed to oxidative stresses *[Mitsumoto & Nakagawa 2001; Bandopadhyay et al. 2004; Canet-Aviles et al. 2004; Kinumi et al. 2004; Taira et al. 2004; Zhou & Freed 2005; Choi et al. 2006; Kim et al. 2009b; Natale et al. 2010]*. Furthermore, DJ-1 regulates glutathione levels through regulation of glutamate cysteine ligase, the rate limiting enzyme in glutathione synthesis *[Zhou & Freed 2005; Liu et al. 2008; Zhong & Xu 2008]* and many functions of DJ-1 are influenced by changes in the cellular redox state (see Fig. 1-5). Thus, we began to investigate whether the HF diet-induced increase of acidic DJ-1 isoforms can be reversed. Mice were treated with N-acetylcysteine (NAC) that is known to increase glutathione levels which in turn affect the cellular redox balance *[Fujii et al. 2011; Wilson 2011]*. NAC was supplied in the drinking water during the 10 days the mice received a HF or control diet. Mice showed no aversion to the NAC water as they consumed on average 4.5 g of water per day which is similar to what we observed in experiments without NAC supplementation. The cumulative water consumption for the 10-day-period did not differ between HF and control diet-fed mice (47.5 ± 5.1 g for control vs. 42.4 ± 8.0 g for HF diet-fed mice, Student's t-test p = 0.149). HF diet-induced gain of body mass and fat mass was comparable to other cohorts fed for 10 days without NAC treatment (Supplementary Table S1). The effect of NAC treatment on reduced (GSH) and oxidized glutathione (GSSG) was measured in brain tissue and gastrocnemius muscle. HF feeding increased reduced glutathione levels in skeletal muscle leading to a higher GSH to GSSG ratio while in the brain, glutathione levels were comparable between HF and control mice (Fig. 3-9). NAC treatment significantly elevated both GSH and GSSG levels in brain and gastrocnemius muscle resulting in a significantly reduced ratio of GSH to GSSG which was

more pronounced in muscle compared to brain tissue (Fig. 3-9 C, F). Glutathione levels were raised to a similar level in HF and control diet-fed mice.
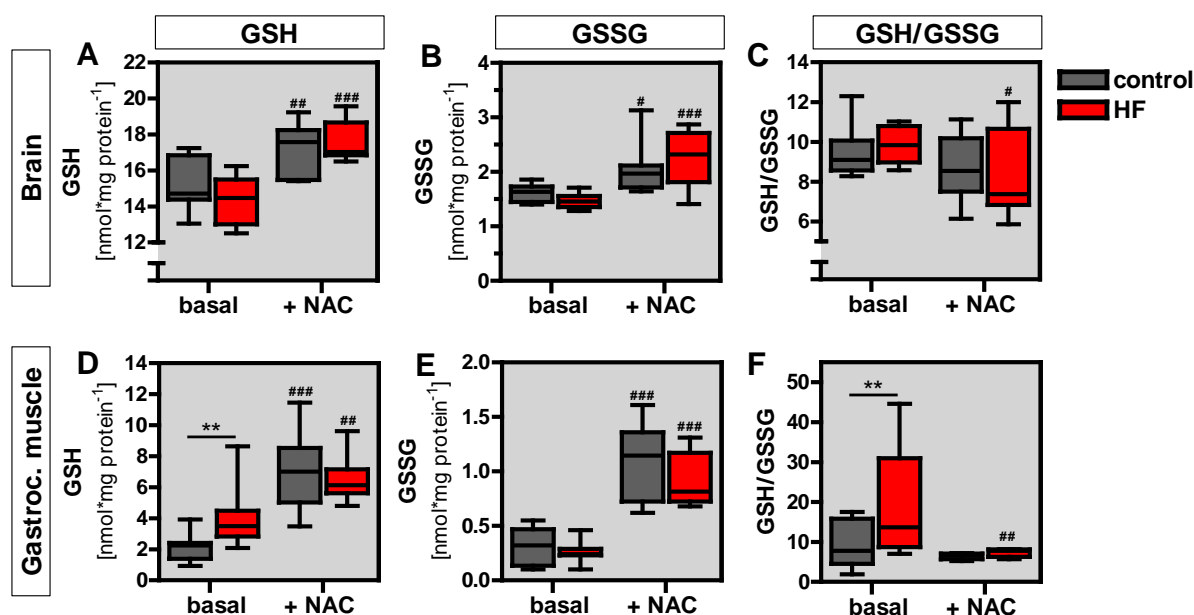
Fig. 3-9. Effect of N-acetylcysteine (NAC) on glutathione levels in brain and gastrocnemius muscle of C57BL/6N mice after 10 days of HF or control diet. NAC (1%) was supplied in the drinking water during the 10-day feeding period. Reduced (GSH) and oxidized glutathione (GSSG) were measured utilizing an enzymatic recycling method. ANOVA: significant effect of treatment on GSH and GSSG levels ($p < 0.0001$) as well as on GSH/GSSG ratios ($p < 0.05$) for both brain and muscle; effect of diet: significant for muscle GSH and GSH/GSSG ratio ($p < 0.5$); diet-treatment interaction: not significant. Bonferroni posttest: [#]p 0.05, [###]p < 0.001 basal vs. NAC treated; **p < 0.01 HF vs. control diet-fed mice. Statistics were performed on log-transformed data. n = 8.

Lysates prepared from hypothalami were separated by gel-based IEF with subsequent membrane transfer and DJ-1 immunodetection. The pattern of individual DJ-1 pI isoforms was comparable to the one obtained without NAC treatment (compare Fig. 3-10 A with Fig. 3-4 C). Furthermore, the same increase in the abundance of isoform 4 was detected in HF mice (compare Fig. 3-10 B with Fig. 3-4 D) although this was not significant after Bonferroni correction. This result suggests that NAC has no influence on the formation of lower pI isoforms of DJ-1 in the hypothalamus.
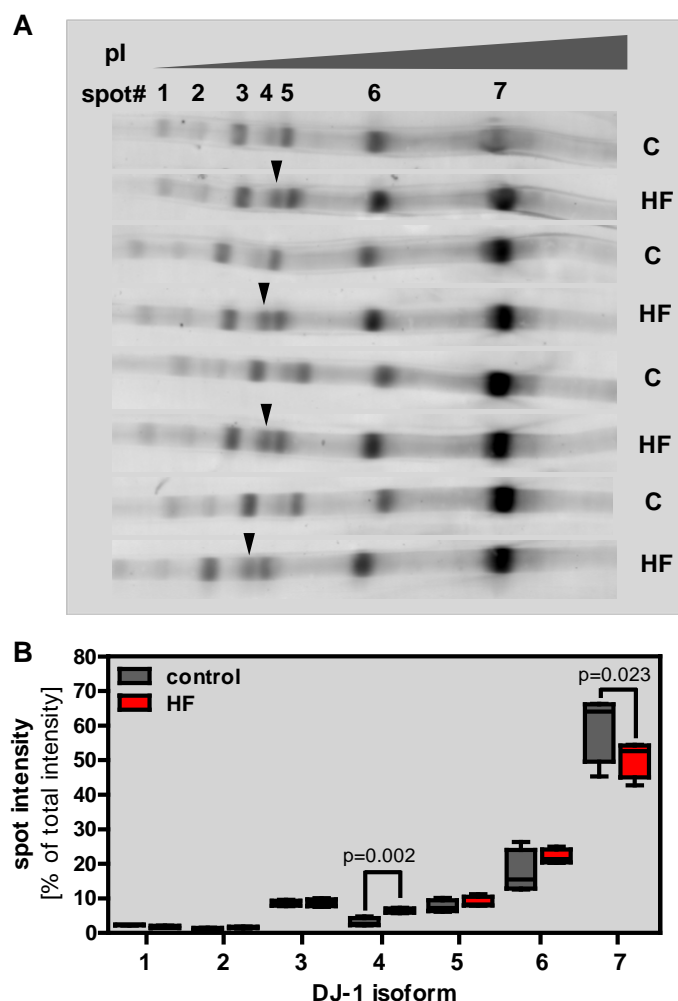
Fig. 3-10. Comparison of DJ-1 pI isoforms in the hypothalamus of male C57BL/6N mice treated with N-acetylcysteine (NAC) during 10 days of HF or control diet. NAC (1%) was supplied in the drinking water. (**A**) Hypothalamic extracts were separated via IEF. Gels were transferred to a membrane followed by immunodetection of DJ-1. Arrows indicate the DJ-1 isoform found increased in HF mice. (**B**) Densitometric quantification of the signal intensities of individual DJ-1 spots (n = 4). Student's t-test: no significances after Bonferroni correction. Data generated by Dr. Gereon Poschmann, MPL, Düsseldorf, Germany.

3.2.5 Influence of high-fat feeding on the mitochondrial localization of DJ-1 in the brain

DJ-1 is predominantly a cytosolic protein but increases its localization to mitochondria in response to oxidative stress as observed in human neuroblastoma cells as well as mouse brain *[Nagakubo et al. 1997; Canet-Aviles et al. 2004; Taira et al. 2004; Blackinton et al. 2005; Zhang et al. 2005a; Lev et al. 2008; Blackinton et al. 2009; Zhong et al. 2009]*. To investigate whether the localization of DJ-1 to mitochondria in the brain is affected by HF diet-feeding, mitochondrial and cytosolic fractions of brain tissue from C57BL6/N mice maintained on HF or control diet for 10 days were prepared. Crude mitochondrial fractions were treated with a sodium

carbonate buffer to detach loosely associated proteins, yielding the 'mitochondrial supernatant (mito SN)' as a third fraction (Fig. 2-3). Using conventional western blot analysis targeting total DJ-1, we detected about half of the DJ-1 pool localized in the cytosol, one fifth in the mitochondrial fraction and one third in the mito SN without differences between HF or control diet-fed mice (Fig. 3-11 A, B). Calculating the ratio of mitochondrial to cytosolic DJ-1 revealed a tendency towards decreased DJ-1 translocation to mitochondria upon HF diet-feeding (Fig. 3-11 C) which did not reach significance (Student's t-test p = 0.1825).
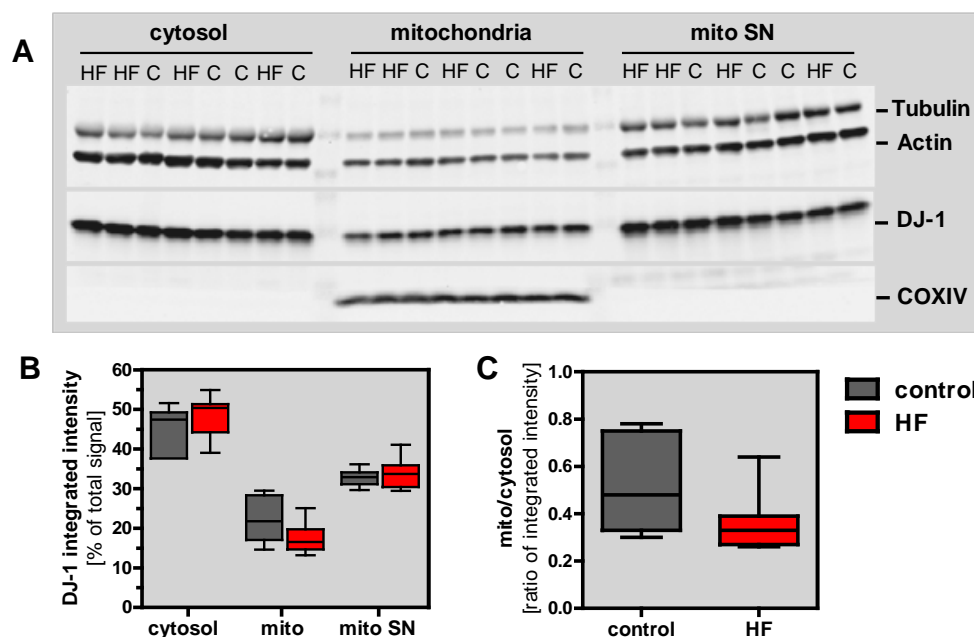
Fig. 3-11. DJ-1 expression of cytosolic and mitochondrial fractions obtained from brain tissue of C57BL/6N mice maintained on a HF or control diet for 10 days. (**A**) Example western blot of separated cytosolic and mitochondrial fractions as well as mitochondrial supernatant (mito SN, see Chapter 2.8 for explanation). Target proteins were immunodetected on the same membrane. The inner mitochondrial membrane protein Cytochrome c oxidase subunit 4 (COXIV) was used as quality control for fractionation efficiency. (**B**) Densitometric analysis quantifying the relative distribution of DJ-1 between the fractions. (**C**) Ratio of mitochondrial to cytosolic DJ-1 content. n = 7. Mito – mitochondria.

Next, we examined the distribution of individual DJ-1 isoforms between these cell compartments by subjecting mitochondrial and cytosolic fractions to the capillary IEF immunoassay. The peak distribution in mitochondria as well as in the cytosol differed from the isoform pattern observed in whole tissue extracts with mitochondria containing one dominant isoform (pI 6.2) (compare Fig. 3-12 A, B with Fig. 3-6 A). No differences were detected for any DJ-1 isoform between HF and control diet-fed mice (Fig. 3-12 C, D), although peak quantification was difficult in mitochondrial fractions due to lower DJ-1

abundance and thus higher signal-to-noise ratios. However, summing up the individual peak areas showed a tendency towards decreased DJ-1 content in mitochondria of HF mice as compared to controls (Fig. 3-12 E). This was significant when expressed as the ratio of mitochondrial to cytosolic DJ-1 (Fig. 3-12 F) confirming the trend seen in the western blot analysis. This suggests that the translocation of DJ-1 from the cytosol to mitochondria in brain tissue is attenuated by HF feeding.
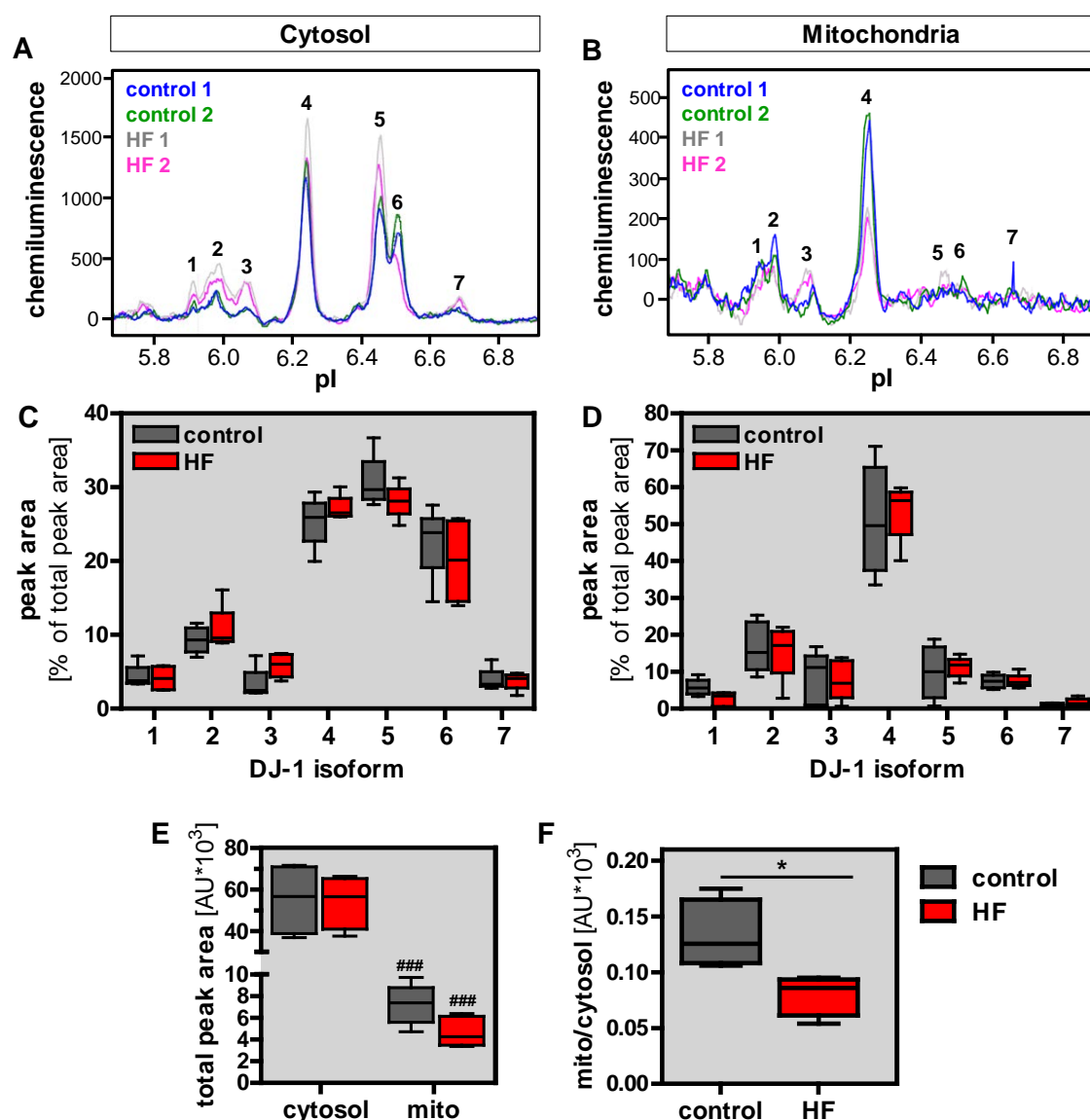
Fig. 3-12. Comparison of DJ-1 pI isoforms in the cytosolic and mitochondrial fraction obtained from brain tissue of C57BL/6N mice maintained on a HF or control diet for 10 days. Protein extracts were analyzed using an automated capillary IEF immunoassay (NanoPro[TM], ProteinSimple). (**A, B**) Electropherograms exemplifying the pI distribution of DJ-1 isoforms. (**C, D**) Quantification of individual peak areas. (**E**) Total peak area as the sum of individual peak areas. ANOVA: effect for fraction: $p < 0.0001$; effect for diet: not significant; Bonferroni posttest: [###]$p < 0.001$ cytosol vs. mitochondria. (**F**) Ratio of mitochondrial to cytosolic total peak area. Student's t-test: *$p < 0.05$. $n_{cytosol} = 4$, $n_{mitochondria} = 5$. Mito – mitochondria. AU – arbitrary units. Data generated by Dr. Daniela Besong Agbo and Dr. Hans Klafki, LVR-Klinikum Essen, Germany.

3.3 Brain mitochondrial function and ROS production are normal after 10 days of high-fat diet

DJ-1 plays a role in the integrity of mitochondria by contributing to the maintenance of a stable environment inside this organelle *[Zhang et al. 2005a; Zhong & Xu 2008; Krebiehl et al. 2010]*. Loss of *Dj-1* results in abnormal mitochondrial morphology, reduced mitochondrial respiration and membrane potential as well as elevated ROS levels (see Chapter 1-4) *[Andres-Mateos et al. 2007; Irrcher et al. 2010; Krebiehl et al. 2010]*. Apart from DJ-1, three further candidates from the initial proteome study investigating the influence of a 10-day HF diet on hypothalamic protein expression localize to mitochondria: Isoform 1 of NADH dehydrogenase flavoprotein 2 (upregulated by HF diet in SWR/J mice), prohibitin (upregulated by HF diet in C57BL/6N mice) and Acyl-coenzyme A thioesterase 13 (downregulated by HF diet in AKR/J mice). Moreover, alpha-synuclein (downregulated by HF diet in C57BL/6N mice), of which gene mutations are also associated with inherited forms of PD, can interact with mitochondria and its overexpression is discussed to impair mitochondrial function *[Nakamura et al. 2008]*.

Thus, we characterized the mitochondrial function after 10 days of HF or control diet in isolated brain mitochondria from 7-week-old male C57BL/6N mice. First, the assembly of respiratory chain complexes was examined. For each of the five complexes, the expression levels of one subunit known to be labile in the unassembled state of its complex was determined via western blot. Densitometric analysis showed that the assembly of respiratory chain complexes in the brains of HF mice is comparable to controls (Fig. 3-13).
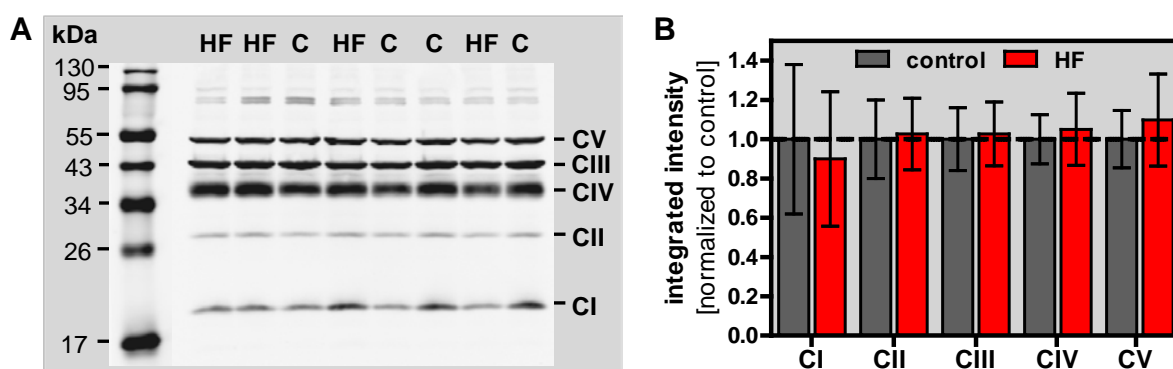
Fig. 3-13. Relative protein levels of respiratory chain complex subunits involved in complex assembly. One representative subunit of each of the five respiratory chain complexes was detected using a mixture of antibodies (OXPHOS, MitoScience). These subunits are labile when the respective complex is not assembled. (**A**) Western blot showing isolated brain mitochondria from C57BL/6N mice after 10 days of HF or control diet. (**B**) Densitometric analysis. Data was normalized to the mean of the control diet group for each complex. Values are means ± SD (n = 4). CI subunit: NDUFB8 ~ 20 kDa, CII subunit: 30 kDa ~ 30 kDa, CIII subunit: Core 2 ~ 47 kDa, CIV subunit I ~ 39 kDa, CV subunit: alpha ~ 53 kDa.

Second, respiration was measured in a Clark electrode. Succinate or a combination of glutamate and malate were used as substrates to measure complex II or complex I respiration, respectively. After the addition of substrate, ADP was added to measure state 3 (phosphorylating) respiration followed by oligomycin, an inhibitor of the ATP synthase, to measure state 4 (non-phosphorylating) respiration. Finally, adding the uncoupler FCCP allowed the determination of the maximal oxygen consumption rate. Mitochondria from HF or control diet-fed mice showed similar rates for complex I and II-dependent respiration under all conditions measured (Fig. 3-14 A, C) as well as similar respiratory control ratios (RCR) (Fig. 3-14 B, D).
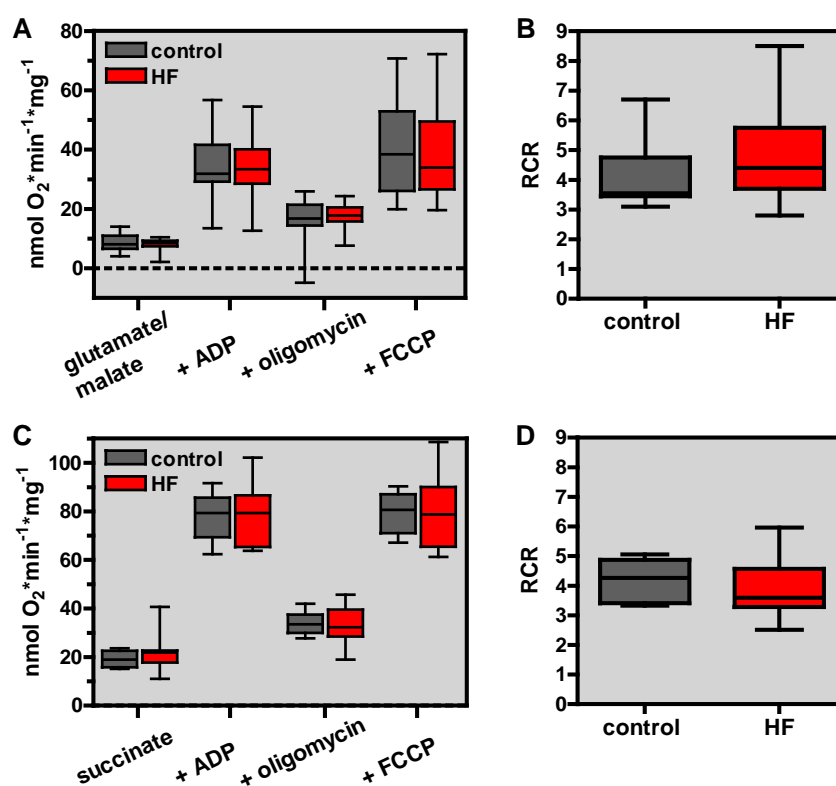
Fig. 3-14. Respiration of isolated brain mitochondria from C57BL/6N mice after 10 days of HF or control diet. (**A, C**) Oxygen consumption rate was measured with a Clark electrode in the presence of 5 mM glutamate + 5 mM malate (**A**) or 5 mM succinate (**C**). The addition of substrate was followed by 1 mM ADP, 2 mg/l oligomycin and 2.5 µM FCCP. Succinate-dependent respiration was measured in the presence of 8 µM rotenone. (**B, D**) Respiratory control ratios (RCR) under glutamate/malate (**B**) and succinate (**D**) respiration. The RCR represents the increase of phosphorylating respiration (+ ADP) over respiration in the presence of excess substrate. Data includes the results of 2-3 independent experiments. n = 16 (A, B); n = 10-11 (C, D).

Third, the mitochondrial membrane potential $\Delta\Psi_m$ was estimated using the fluorescence cationic dye Safranin O that accumulates inside energized mitochondria where its fluorescence is quenched *[Akerman & Wikstrom 1976]*. Isolated brain mitochondria from HF or control diet-fed mice equally increased their membrane potential as indicated by decreased

fluorescence after the addition of the substrates succinate or glutamate/malate (Fig. 3-15 B, E). Moreover, when uncoupled with FCCP, mitochondria from HF or control diet-fed animals decreased their $\Delta\Psi_m$ to the same extent (Fig. 3-15 C, F).
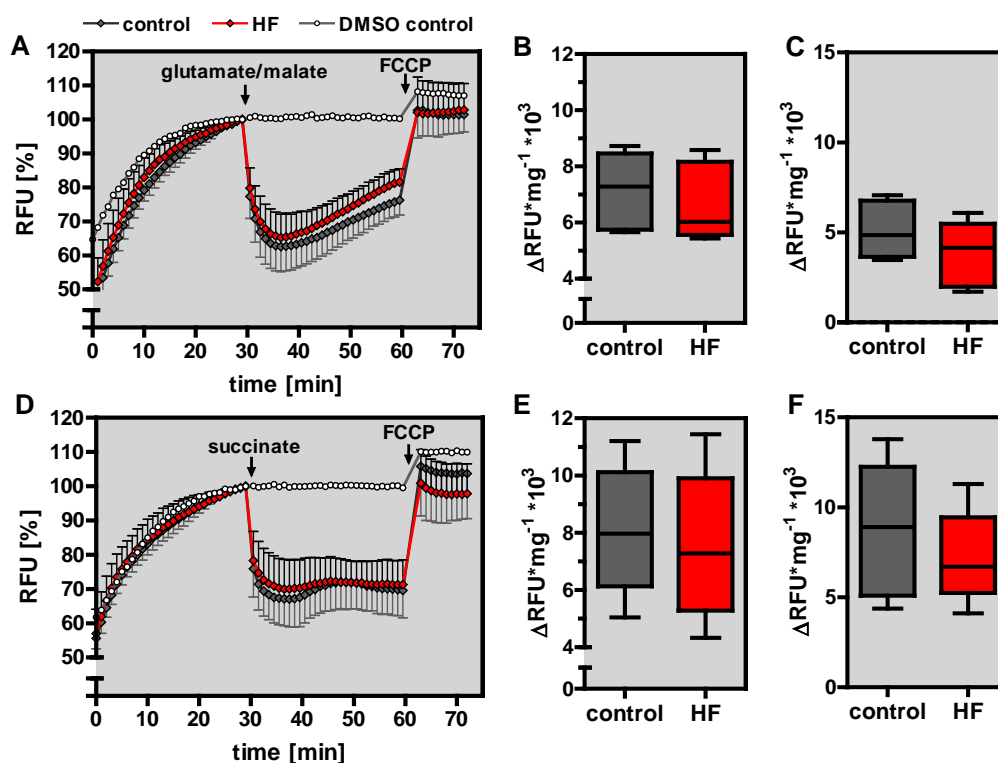
Fig. 3-15. Membrane potential $\Delta\Psi_m$ detected by Safranin O fluorescence in isolated brain mitochondria of C57BL6/N mice after 10 days of HF or control diet. (**A, D**) Course of Safranin O fluorescence over time. As substrates 5 mM glutamate + 5 mM malate (**A-C**) or 5 mM succinate (**C-E**) were injected after 30 minutes followed by 0.3 µM FCCP 30 minutes later. DMSO was added as solvent control for FCCP. The last data point before the addition of substrate was set to 100 %. Values are means ± SD (n = 6). (**B, E**) Maximal decrease of Safranin O fluorescence after the addition of glutamate/malate (**B**) or succinate (**D**). (**C, F**) Increase of Safranin O fluorescence after the addition of FCCP.

Fourth, the hydrogen peroxide production was assayed with the fluorescent dye Amplex[®] Red in brain mitochondria respiring on succinate or glutamate/malate. H_2O_2 production rates were determined at basal levels, after the inhibition of complex I with rotenone, after the inhibition of complex III with antimycin as well as under phosphorylating conditions (+ ADP) or after several combinations of the above. Under all conditions measured, H_2O_2 production was comparable between HF or control diet-fed mice (Fig. 3-16).
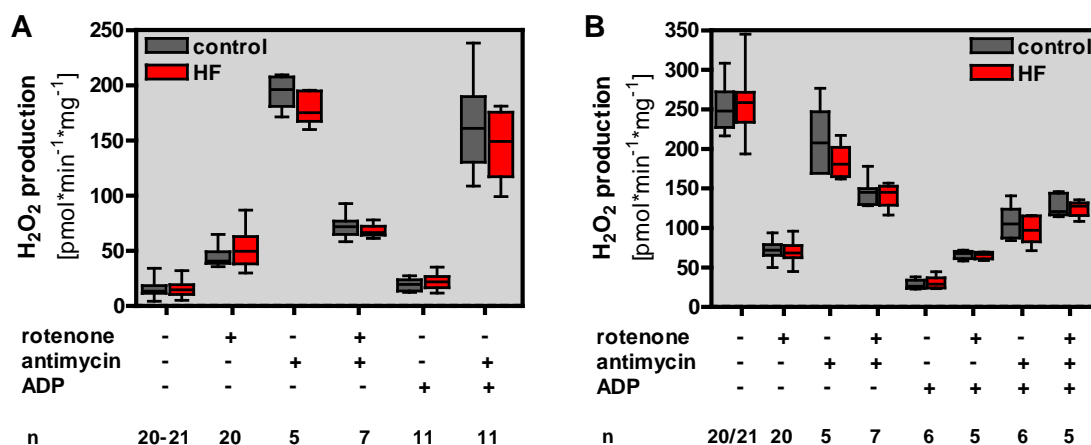
Fig. 3-16. H_2O_2 production in isolated brain mitochondria of C57BL6/N mice after 10 days of HF or control diet. The generation of H_2O_2 was detected with the fluorescent dye Amplex[®] Red in mitochondria respiring on 5 mM glutamate + 5 mM malate (**A**) or 5 mM succinate (**B**). In separate preparations, 2 µM rotenone, 50 µM antimycin A or 1 mM ADP were added. N-numbers are indicated for each condition.

Last, the expression levels of the mitochondrial antioxidant enzyme manganese superoxide dismutase (SOD2) that converts superoxide anion radicals to H_2O_2 and oxygen were unchanged upon HF feeding (Fig. 3-17).
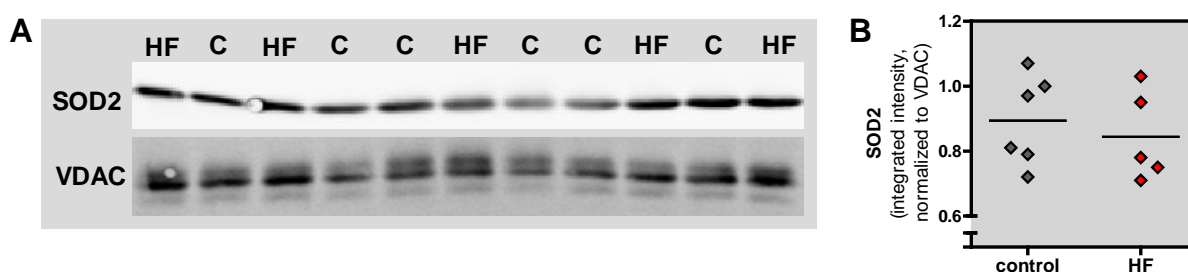
Fig. 3-17. SOD2 expression in isolated brain mitochondria of male C57BL/6N mice after 10 days of HF or control diet feeding. (**A**) Western blot of mitochondrial fraction targeting manganese superoxide dismutase (SOD2) and voltage-dependent anion channel (VDAC). Both targets were immunodetected on the same membrane. (**B**) Densitometric analysis of western blot data. SOD2 signals were normalized to VDAC (n = 5-6).

Conclusively, the function of brain mitochondria in terms of respiratory chain complex assembly, respiration, membrane potential, H_2O_2 production and SOD2 content is not influenced by a short-term HF diet-intervention and the associated changes of the intracellular DJ-1 pool composition.

3.4 Phenotypic characterization of high-fat diet challenged *Dj-1$^{-/-}$* mice

DJ-1 emerged as a candidate protein from the initial proteome analysis investigating acute alterations in the hypothalamus in response to a short-term diet intervention (Chapter 3.1). We therefore investigated the susceptibility of *Dj-1* deficient mice (*Dj-1$^{-/-}$*) to DIO.

3.4.1 Higher fat accumulation in *Dj-1$^{-/-}$* mice after 14 weeks of high-fat feeding

Male and female *Dj-1$^{-/-}$* mice and their wildtype littermates were fed a HF or control diet for 14 weeks. Body mass and body composition were recorded every two weeks (Fig. 3-18). At the age of 4 weeks when the feeding was started, there were no differences in body mass, fat or lean mass between the genotypes in male mice. In contrast, female *Dj-1$^{-/-}$* mice had a reduced lean mass at this age (Supplementary Table S3). The level of DIO was lower in female compared to male mice (Fig. 3-18 B and E) but HF diet-feeding resulted in a significant gain in body mass, fat and lean mass within 14 weeks in both sexes (Table 3-2). No significant genotype differences within the diet groups were observed for either of these parameters after 14 weeks of feeding (Table 3-2). Correlating fat or lean mass with body mass nevertheless suggested an increased HF diet-induced body fat accumulation in *Dj-1$^{-/-}$* mice compared to wildtype mice with a corresponding decrease in lean mass (Fig. 3-19).
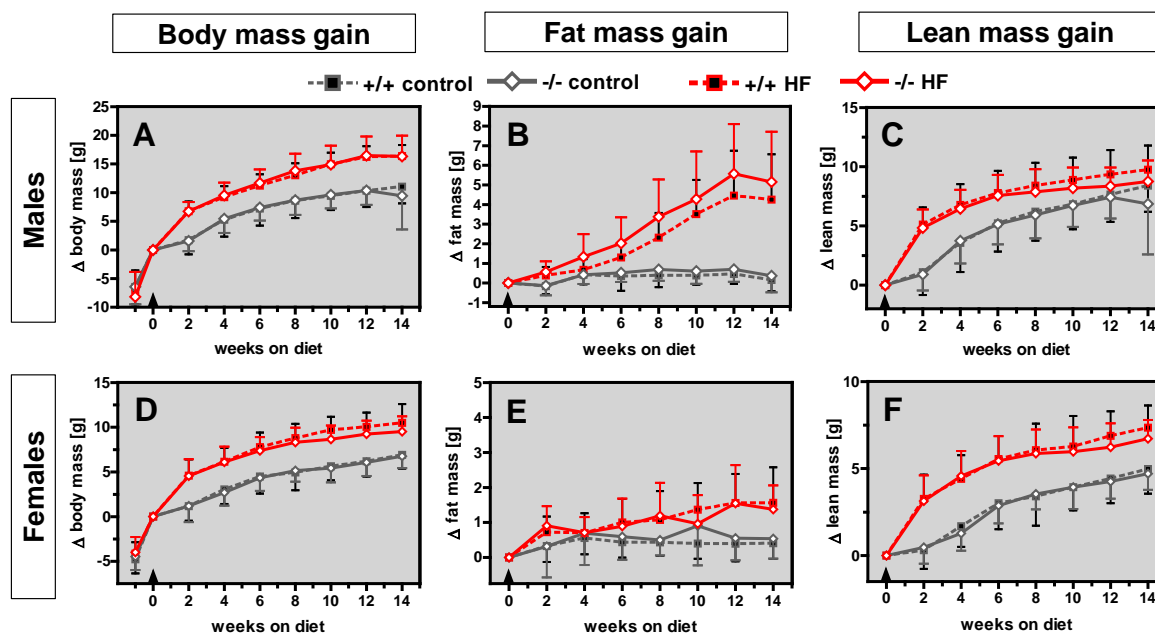
Fig. 3-18. Gain of body mass, fat and lean mass in male (top) and female (bottom) *Dj-1$^{-/-}$* and *Dj-1$^{+/+}$* mice maintained on HF or control diet for 14 weeks. Arrows indicate the diet change at the age of 4 weeks. Values are means ± SD (n$_{males}$ = 14-20; n$_{females}$ = 13-16).

Fig. 3-19. Fat and lean mass related to body mass in male (top) and female (bottom) *Dj-1⁻ᐟ⁻* and *Dj-1⁺ᐟ⁺* mice after 14 weeks of HF or control diet.

Hence, we performed an analysis of covariance (ANCOVA) to adjust fat and lean mass, respectively, to the body mass as a covariate. The adjusted fat mass was significantly increased while lean mass was significantly decreased in *Dj-1⁻ᐟ⁻* mice compared to *Dj-1⁺ᐟ⁺* mice of both sexes (Table 3-2). These effects were more pronounced under HF diet compared to control diet.

In male mice, additionally, two fat pads (epididymal, eWAT, and posterior subcutaneous white adipose tissue, psWAT) were weighed at the end of the feeding period. The absolute fat pad masses were significantly increased in HF diet-fed mice without a significant genotype difference (Table 3-3). When adjusted for body mass, the visceral eWAT was increased in HF diet-fed *Dj-1⁻ᐟ⁻* mice compared to wildtype mice on the same diet, while the increase in psWAT failed to reach significance (Fig. 3-20; Table 3-3). Taken together, these results demonstrate an altered partitioning of body energy resources in *Dj-1⁻ᐟ⁻* mice when fed a HF diet for 14 weeks characterized by higher storage of fat at the expense of lean mass.

Table 3-2. Gain of body mass, fat and lean mass in male (top) and female (bottom) *Dj-1⁻/⁻* and *Dj-1⁺/⁺* mice after 14 weeks of HF or control diet. §Adjusted fat and lean mass result from ANCOVA analysis with adjustment to the mean body mass of the respective diet group.

		+/+	-/-	ANOVA/ANCOVA p-value		
				genotype	diet	genotype:diet
Males						
Δ body mass [g]	control	11.1 ± 2.9	10.6 ± 2.3	0.7302	**<0.0001**	0.7955
	HF	16.4 ± 1.9	16.3 ± 3.6			
Δ fat mass [g]	control	0.2 ± 0.6	0.5 ± 0.6	0.1461	**<0.0001**	0.5098
	HF	4.3 ± 2.3	5.2 ± 2.6			
Δ lean mass [g]	control	8.4 ± 2.2	7.7 ± 1.8	0.0820	**0.0153**	0.7671
	HF	9.8 ± 2.0	8.6 ± 1.8			
fat mass*adjusted* [g]§	control	2.0 ± 0.3	2.4 ± 0.4	**0.0002**	**< 0.0001**	0.0779
	HF	6.0 ± 1.3	7.3 ± 1.2***			
lean mass*adjusted* [g]§	control	18.6 ± 0.4	18.1 ± 0.5	**< 0.0001**	**< 0.0001**	0.0559
	HF	20.9 ± 1.2	19.6 ± 1.0***			
Females						
Δ body mass [g]	control	6.9 ± 1.5	6.6 ± 1.3	0.2197	**<0.0001**	0.3728
	HF	1.0 ± 2.1	9.5 ± 1.7			
Δ fat mass [g]	control	0.4 ± 0.5	0.5 ± 0.6	0.8750	**<0.0001**	0.4033
	HF	1.6 ± 1.0	1.4 ± 0.7			
Δ lean mass [g]	control	5.0 ± 1.4	4.7 ± 0.9	0.1714	**<0.0001**	0.5670
	HF	7.4 ± 1.3	6.7 ± 1.1			
fat mass*adjusted* [g]§	control	2.2 ± 0.5	2.6 ± 0.3	**0.0028**	**< 0.0001**	0.4471
	HF	3.1 ± 0.7	3.6 ± 0.4*			
lean mass*adjusted* [g]§	control	29.0 ± 1.2	27.6 ± 1.0**	**< 0.0001**	**< 0.0001**	0.2062
	HF	33.4 ± 1.1	31.3 ± 0.6***			

Values are mean ± SD (n_{males} = 14-19, $n_{females}$ = 12-16). Bonferroni post-test: *p < 0.05, **p < 0.01, ***p < 0.001 *Dj-1⁻/⁻* vs. *Dj-1⁺/⁺* mice.

Fig. 3-20. Fat pad weights related to body mass of male *Dj-1⁻/⁻* and *Dj-1⁺/⁺* mice after 14 weeks of HF or control diet. eWAT - epididymal white adipose tissue. psWAT - posterior subcutaneous white adipose tissue.

Table 3-3. Weights of dissected fat pads of male $Dj-1^{-/-}$ and $Dj-1^{+/+}$ mice after 14 weeks of HF or control diet. §Adjusted fat pad weights result from ANCOVA analysis with adjustment to the mean body mass of the respective diet group.

		+/+	-/-	ANOVA/ANCOVA p-value		
				genotype	diet	genotype:diet
eWAT [g]	control	0.29 ± 0.09	0.31 ± 0.06	0.0979	**< 0.0001**	0.1730
	HF	0.79 ± 0.26	0.97 ± 0.24			
psWAT [g]	control	0.32 ± 0.10	0.30 ± 0.06	0.7561	**< 0.0001**	0.5839
	HF	0.69 ± 0.22	0.74 ± 0.23			
eWAT$_{adjusted}$ [g]§	control	0.27 ± 0.04	0.32 ± 0.05	**<0.0001**	**<0.0001**	**0.0010**
	HF	0.73 ± 0.15	1.01 ± 0.12***			
psWAT$_{adjusted}$ [g]§	control	0.30 ± 0.05	0.30 ± 0.04	0.0677	**<0.0001**	0.0669
	HF	0.64 ± 0.12	0.77 ± 0.18*			

Values are mean ± SD (n = 9-12). Bonferroni post-test: *p < 0.05, ***p < 0.001 $Dj-1^{-/-}$ vs. $Dj-1^{+/+}$ mice. eWAT - epididymal white adipose tissue. psWAT - posterior subcutaneous white adipose tissue.

3.4.2 Prolonged HF feeding does not aggravate fat storage in $Dj-1^{-/-}$ mice

To investigate whether the mild increase in fat storage in HF diet-fed $Dj-1^{-/-}$ mice increases with age, we extended the feeding period for part of the mice to 32 weeks (Fig. 3-21). Female mice fed a HF diet showed a drastic increase of body and fat mass from the 16th week on (Fig. 3-21 E). Within 32 weeks of feeding, both male and female mice gained significantly more body mass and fat mass on HF diet compared to control diet-fed mice, while the lean mass was unaffected (Table 3-4). The higher HF diet-induced fat accumulation in $Dj-1^{-/-}$ mice was abrogated after 32 weeks of feeding in male mice (Fig. 3-22 A, B; Table 3-4). In female mice, body mass-adjusted fat mass was significantly increased in control diet-fed $Dj-1^{-/-}$ mice (Table 3-4) while lean mass was reduced in $Dj-1^{-/-}$ mice compared to wildtype mice regardless of diet (Fig. 3-22 C, D; Table 3-4).
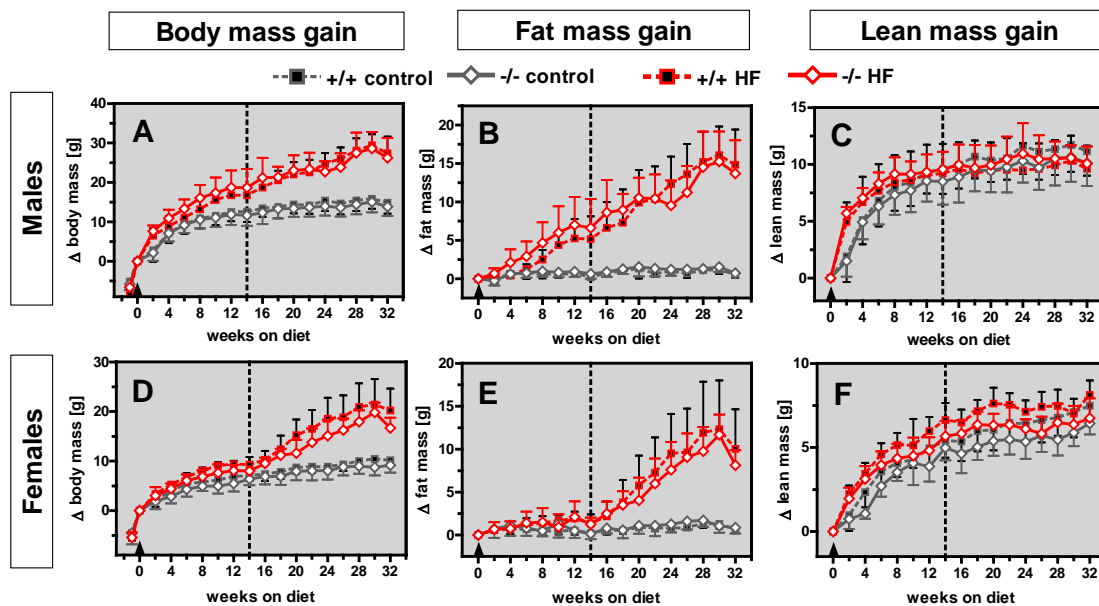
Fig. 3-21. Gain of body mass, fat and lean mass in male (top) and female (bottom) *Dj-1^{-/-}* and *Dj-1^{+/+}* mice maintained on HF or control diet for 32 weeks. Values are means ± SD (n_{males} = 5-8; $n_{females}$ = 4-7). Arrows indicate the diet change at the age of 4 weeks. The dotted line designates the 14-week time point.
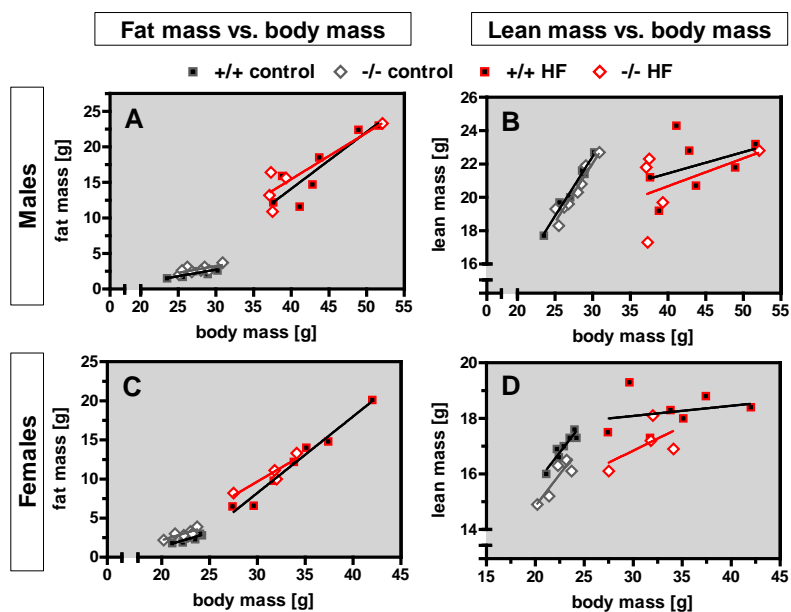
Fig. 3-22. Fat and lean mass related to body mass in male (top) and female (bottom) *Dj-1^{-/-}* and *Dj-1^{+/+}* mice after 32 weeks of HF or control diet.

58

Table 3-4. Gain of body mass, fat and lean mass in male (top) and female (bottom) *Dj-1^{-/-}* and *Dj-1^{+/+}* mice after 32 weeks of HF or control diet. [§]Adjusted fat and lean mass result from ANCOVA analysis with adjustment to the mean body mass of the respective diet group.

		+/+	-/-	ANOVA/ANCOVA p-value		
				genotype	diet	genotype:diet
Males						
Δ body mass [g]	control	14.9 ± 2.8	13.8 ± 2.4	0.4261	**< 0.0001**	0.9531
	HF	27.4 ± 4.2	26.2 ± 5.1			
Δ fat mass [g]	control	0.5 ± 0.4	0.8 ± 0.3	0.6862	**< 0.0001**	0.5695
	HF	14.8 ± 4.6	13.7 ± 4.3			
Δ lean mass [g]	control	11.2 ± 2.1	10.1 ± 2.0	0.7174	0.3151	0.3427
	HF	9.6 ± 2.0	10.1 ± 1.5			
fat mass$_{adjusted}$ [g][§]	control	2.3 ± 0.3	2.8 ± 0.3	0.1743	**< 0.0001**	0.6533
	HF	16.0 ± 2.1	17.0 ± 2.0			
lean mass$_{adjusted}$ [g][§]	control	20.7 ± 0.3	20.3 ± 0.4	0.2689	0.0664	0.7883
	HF	21.7 ± 1.6	21.1 ± 2.0			
Females						
Δ body mass [g]	control	10.2 ± 1.2	9.2 ± 1.5	0.0596	**< 0.0001**	0.2792
	HF	20.2 ± 4.4	16.7 ± 2.1			
Δ fat mass [g]	control	0.6 ± 0.3	0.9 ± 0.7	0.4610	**< 0.0001**	0.3453
	HF	10.0 ± 4.6	8.1 ± 1.8			
Δ lean mass [g]	control	7.5 ± 1.0	6.4 ± 0.7	**0.0045**	0.2218	0.6727
	HF	8.1 ± 0.9	6.8 ± 1.2			
fat mass$_{adjusted}$ [g][§]	control	2.3 ± 0.2	3.2 ± 0.3*	**0.0022**	**< 0.0001**	0.6135
	HF	11.1 ± 0.7	11.8 ± 0.8			
lean mass$_{adjusted}$ [g][§]	control	16.8 ± 0.2	16.0 ± 0.3*	**0.0006**	**< 0.0001**	0.8052
	HF	18.2 ± 0.7	17.3 ± 0.7*			

Values are mean ± SD (n_{males} = 5-8, $n_{females}$ = 4-7). Bonferroni post-test: *p < 0.05 *Dj-1^{-/-}* vs. *Dj-1^{+/+}* mice.

Weights of dissected fat pads revealed a HF diet-induced increase in subcutaneous WAT in female *Dj-1^{-/-}* mice after adjustment for body mass, while the visceral periovarial WAT (poWAT) was comparable to wildtype mice (Fig. 3-23 D, E; Table 3-5). No genotype differences were detected for fat pad weights in male mice (Fig. 3-23 A, B; Table 3-5). The gastrocnemius muscle wet weight was significantly decreased in male and female *Dj-1^{-/-}* mice compared to wildtype mice regardless of diet (Fig 3-23 C, F; Table 3-5).

Thus, the prolonged exposure to HF diet ameliorates the increased adiposity in male *Dj-1^{-/-}* mice. The HF diet-induced changes in body composition are delayed in female animals. After 32 weeks of feeding, female *Dj-1^{-/-}* mice have higher total fat mass under control diet conditions, but the subcutaneous WAT is increased by HF diet compared to wildtype mice. Moreover, *Dj-1^{-/-}* mice show an age-dependent decrease in lean mass that is

independent of diet. Conclusively, the altered body composition in *Dj-1$^{-/-}$* mice is a transient effect depending on the duration of HF diet-feeding and/or age.

Table 3-5: Weights of dissected fat pads and muscle of male (top) and female (bottom) *Dj-1$^{-/-}$* and *Dj-1$^{+/+}$* mice after 32 weeks of HF or control diet. [§]Adjusted fat pad weights result from ANCOVA analysis with adjustment to the mean body mass of the respective diet group.

		+/+	-/-	ANOVA/ANCOVA p-value		
				genotype	diet	genotype:diet
Males						
eWAT [g]	control	0.36 ± 0.10	0.43 ± 0.13	0.3389	**< 0.0001**	0.9865
	HF	2.17 ± 0.31	2.25 ± 0.23			
psWAT [g]	control	0.35 ± 0.09	0.41 ± 0.11	0.6225	**< 0.0001**	0.4482
	HF	2.62 ± 0.91	2.35 ± 0.63			
M. gastroc [g]	control	0.27 ± 0.02	0.23 ± 0.02**	**< 0.0001**	0.3693	0.4288
	HF	0.27 ± 0.03	0.22 ± 0.02***			
eWAT$_{adjusted}$ [g][§]	control	0.36 ± 0.09	0.43 ± 0.09	0.1604	**< 0.0001**	0.7202
	HF	2.16 ± 0.31	2.29 ± 0.17			
psWAT$_{adjusted}$ [g][§]	control	0.35 ± 0.08	0.41 ± 0.08	0.6705	**<0.0001**	0.9516
	HF	2.45 ± 0.51	2.49 ± 0.32			
M. gastroc$_{adjusted}$ [g][§]	control	0.27 ± 0.01	0.23 ± 0.02 ***	**< 0.0001**	0.3177	0.5184
	HF	0.27 ± 0.02	0.22 ± 0.02 ***			
Females						
poWAT [g]	control	0.15 ± 0.03	0.22 ± 0.10	0.5651	**< 0.0001**	0.3184
	HF	1.41 ± 0.67	1.15 ± 0.30			
psWAT [g]	control	0.30 ± 0.04	0.41 ± 0.12	0.8858	**< 0.0001**	0.8221
	HF	1.88 ± 1.17	1.86 ± 0.61			
M. gastroc [g]	control	0.22 ± 0.01	0.19 ± 0.02*	**< 0.0001**	**0.0012**	0.0900
	HF	0.26 ± 0.02	0.21 ± 0.01***			
poWAT$_{adjusted}$ [g][§]	control	0.15 ± 0.02	0.25 ± 0.05	0.3656	**< 0.0001**	0.2154
	HF	1.29 ± 0.11	1.27 ± 0.21			
psWAT$_{adjusted}$ [g][§]	control	0.30 ± 0.03	0.43 ± 0.07	**0.0073**	**< 0.0001**	0.1181
	HF	1.67 ± 0.33	2.13 ± 0.38*			
M.gastroc$_{adjusted}$ [g][§]	control	0.22 ± 0.01	0.20 ± 0.01*	**< 0.0001**	**0.0006**	**0.0277**
	HF	0.26 ± 0.02	0.21 ± 0.01***			

Values are mean ± SD (n_{males} = 5-8, $n_{females}$ = 4-7). Bonferroni post-test: *p < 0.05, **p < 0.01, ***p < 0.001 *Dj-1$^{-/-}$* vs. *Dj-1$^{+/+}$* mice. eWAT - epididymal white adipose tissue. poWAT – periovarial white adipose tissue psWAT - posterior subcutaneous white adipose tissue. M. gastroc –gastrocnemius muscle.
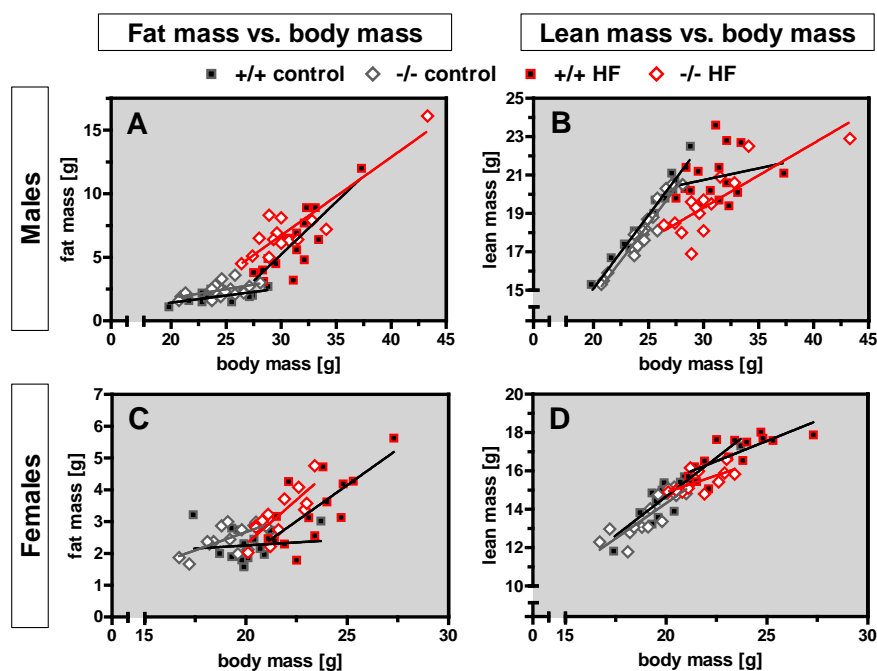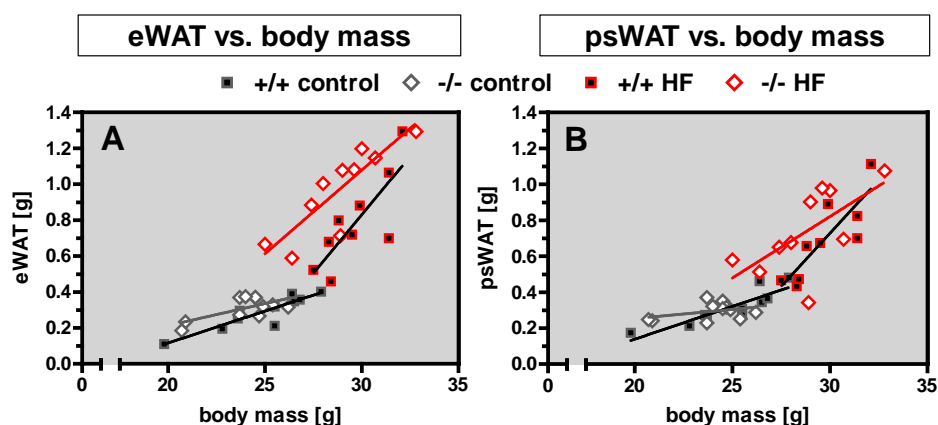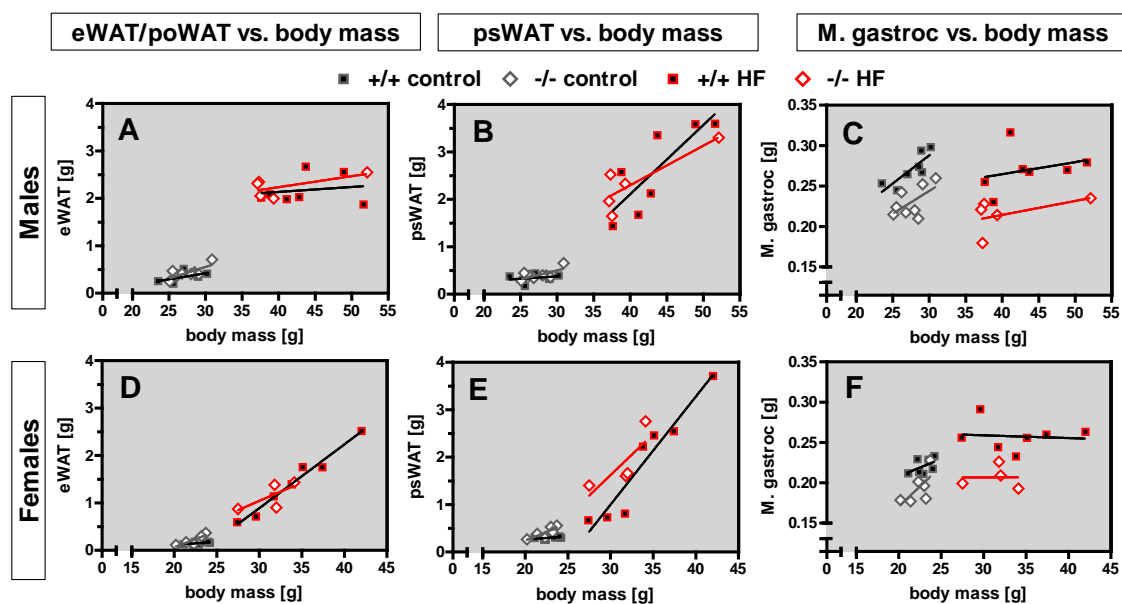
Fig. 3-23. Weights of dissected fat pads and muscle related to body mass in male (top) and female (bottom) *Dj-1^{-/-}* and *Dj-1^{+/+}* mice after 32 weeks of HF or control diet. eWAT/poWAT – epididymal/periovarial white adipose tissue. psWAT - posterior subcutaneous white adipose tissue. M. gastroc – gastrocnemius muscle.

3.4.3 *Dj-1^{-/-}* mice are hypoactive without detectable changes in energy intake and energy expenditure

To find possible causes underlying the altered body composition after 14 weeks of HF diet, we monitored the energy intake and spontaneous locomotor activity of male mice over 2-3 days. Towards the end of the 14-week feeding period, the energy intake over 24 hours or during the dark phase did not differ between HF or control diet-fed mice or between the genotypes (Table 3-6).

Dj-1^{-/-} mice displayed significantly less rearing activity, travelled a smaller distance and were slower compared to *Dj-1^{+/+}* mice (Table 3-6). A trend in the same direction was detected for total activity as the sum of all beam break counts. This genotype effect is more pronounced in control diet-fed animals because wildtype mice fed a HF diet tend to move less compared to their control diet-fed counterparts, bringing their activity level down to the level of *Dj-1^{-/-}* mice. When total counts were assigned to ambulatory or fine activity, it became apparent that the lower activity level resulted from reduced ambulatory movement of *Dj-1^{-/-}* mice, since fine movement was unaltered between the genotypes (Table 3-6). Thus, *Dj-1^{-/-}* mice were hypoactive independent of diet but this was not reflected in altered energy intake.

Table 3-6. Energy intake (EI) and spontaneous locomotor activity of male *Dj-1^{-/-}* and *Dj-1^{+/+}* mice maintained on a HF or control diet for 14 weeks. Animals were kept in the feeding-drinking-activity system (TSE Systems) for 2-3 days. EI is expressed per 24 hours or per dark-phase. Activity parameters are the mean of 2-3 consecutive dark-phases. Animals with a CV exceeding 33 % (for EI) or exceeding 40 % (for activity) were excluded. Total activity refers to beam break counts in X, Y and Z direction, horizontal activity to X and Y direction and rearing activity to Z direction (vertical movement).

		+/+	-/-	ANOVA p-value		
				genotype	diet	genotype:diet
EI - 24hr [kJ]	control	56.5 ± 5.9	59.4 ± 13.1	0.3725	0.2748	0.9183
	HF	52.2 ± 11.1	55.8 ± 7.3			
EI - dark phase [kJ]	control	40.2 ± 7.5	39.0 ± 11.1	0.5910	0.2092	0.3431
	HF	33.7 ± 6.9	38.1 ± 5.3			
total activity [counts x10³]	control	64.80 ± 13.71	46.25 ± 14.10	0.0620	0.5013	0.1378
	HF	53.00 ± 18.46	50.04 ± 11.15			
horizontal activity [counts x10³]	control	60.99 ± 13.27	43.80 ± 13.77	0.0718	0.4782	0.1395
	HF	49.64 ± 17.08	47.87 ± 11.09			
rearing activity [counts x10³]	control	3.77 ± 0.89	2.44 ± 1.02	**0.0380**	0.8127	0.4181
	HF	3.52 ± 1.49	2.91 ± 0.90			
ambulatory movement [counts x10³]	control	44.18 ± 11.05	29.79 ± 10.39	0.0545	0.4195	0.1328
	HF	34.60 ± 13.81	32.74 ± 8.79			
fine movement [counts x10³]	control	17.07 ± 2.34	14.01 ± 3.48	0.1034	0.6675	0.1514
	HF	15.22 ± 3.15	15.02 ± 2.12			
distance [m]	control	820 ± 205	556 ± 196*	**0.0378**	0.1873	0.1509
	HF	616 ± 234	565 ± 152			
mean speed [m*h⁻¹]	control	67.5 ± 17.2	45.5 ± 16.5*	**0.0391**	0.1860	0.1570
	HF	50.4 ± 19.8	46.1 ± 12.9			

Values are means ± SD (n = 7-9, n_{rearing activity} = 5-7). Bonferroni post-test: *p < 0.05 *Dj-1^{-/-}* vs. *Dj-1^{+/+}* mice.

We further performed indirect calorimetry measurements towards the end of the 14-week feeding period in male mice. The oxygen consumption ($\dot{V}O_2$) measured over 3 days at 22°C and the resulting mean metabolic rate expressed as heat production ($HP_{22°C,ad-lib}$) tended to be higher in HF compared to control diet-fed mice but was comparable between *Dj-1^{-/-}* and *Dj-1^{+/+}* mice within each diet group (Fig. 3-24; Table 3-7). Metabolic rate depends on body mass as well as body composition since lean mass and adipose tissue are not equally metabolically active. The specific metabolic activity of adipose tissue in mice is estimated to be 15-25 % of the metabolic activity of lean mass *[Arch et al. 2006]*. We normalized the energy expenditure data to the sum of lean mass + 0.2 * fat mass [g], as suggested by Even & Nadkarni *[2012]* because this method eliminated the body mass dependency (Fig. 3-25).

Normalization to body composition abolished the trend of increased $HP_{22°C,ad-lib}$ in HF diet-fed mice (Table 3-7).
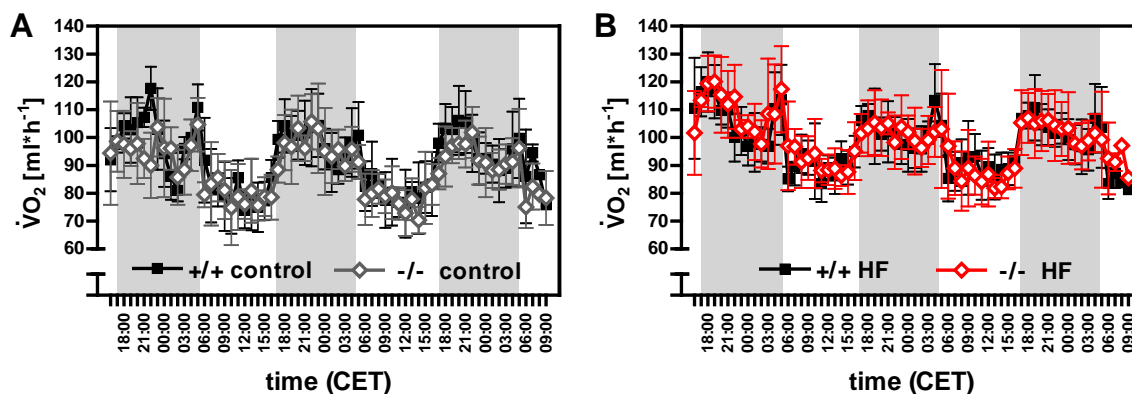
Fig. 3-24. Oxygen consumption $(\dot{V}O_2)$ of male *Dj-1*^{-/-} and *Dj-1*^{+/+} mice maintained on control (A) or HF (B) diet for 14 weeks. Indirect calorimetry was performed at 22°C. Shaded areas indicate dark phases. Values are means ± SD (n = 6).

Table 3-7. Respiratory exchange ratio (RER) and heat production (HP) of male *Dj-1*^{-/-} and *Dj-1*^{+/+} mice maintained on a HF or control diet for 14 weeks measured by indirect calorimetry. For RER and $HP_{22°C,ad-lib}$, the mean of two measuring days per animal was taken. $HP_{30°C,pa}$ was measured at thermoneutrality after animals were deprived of food for 6 hours.

		+/+	-/-	ANOVA/ANVOVA p-value		
				genotype	diet	genotype:diet
RER	control	0.90 ± 0.02	0.89 ± 0.02	0.8119	**<0.0001**	0.242
	HF	0.80 ± 0.01	0.81 ± 0.01			
$HP_{22°C,ad-lib}$ [mW]	control	472.7 ± 57.8	481.3 ± 33.7	0.6243	0.0599	0.3753
	HF	533.3 ± 21.3	504.0 ± 74.4			
$HP_{22°C,ad-lib}$ [mW *(LM+0.2FM)$^{-1}$]	control	24.2 ± 5.0	26.2 ± 2.3	0.4964	0.7352	0.686
	HF	24.9 ± 1.0	25.3 ± 2.4			
$HP_{30°C,pa}$ [mW]	control	182.4 ± 18.6	183.4 ± 9.0	0.5517	**0.0065**	0.643
	HF	202.1 ± 9.6	210.3 ± 29.9			
$HP_{30°C,pa}$ [mW *(LM+0.2FM)$^{-1}$]	control	9.5 ± 1.5	10.0 ± 0.5	0.0604	0.533	0.3805
	HF	9.4 ± 0.4	10.5 ± 0.8			
$HP_{22°C,ad-lib}$/$HP_{30°C,pa}$[#]	control	2.6 ± 0.3	2.6 ± 0.3	0.2088	0.2533	0.1031
	HF	2.6 ± 0.1	2.4 ± 0.2			

Values are means ± SD (n = 6). *Ad lib – ad libitum*. Pa – postabsorptive. LM – lean mass. FM – fat mass. [#]Ratio of $HP_{22°C,ad-lib}$ to $HP_{30°C,pa}$ was calculated using the values adjusted for body composition.
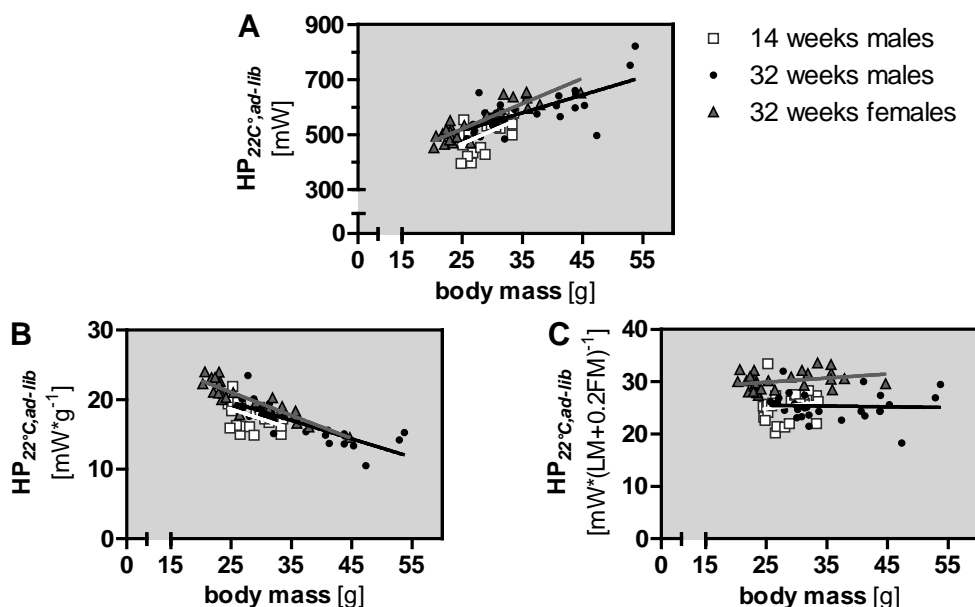
Fig. 3-25. Effect of adjustment method on body mass dependency of heat production (HP). Indirect calorimetry was performed at 22°C with *ad libitum* access to food. Subgroups include male or female *Dj-1$^{-/-}$* and *Dj-1$^{+/+}$* mice maintained on a HF or control diet for 14 or 32 weeks. Each data point represents an individual animal. (**A**) HP positively correlates with body mass (Pearson product-moment correlation, males14 weeks: r = 0.55, p = 0.0054; 32 weeks males: r = 0.7, p < 0.0001; 32 weeks females: r = 0.90, p < 0.0001). (**B**) HP normalized to g body mass negatively correlates with body mass (Pearson product-moment correlation, 14 weeks males: r = -0.46, p = 0.0237; 32 weeks males: r = -0.81, p < 0.0001; 32 weeks females: r = -0.90, p < 0.0001). (**C**) Normalization to lean mass (LM) + 0.2 * fat mass (FM) eliminates the dependency of HP from body mass (Pearson product-moment correlation, 14 weeks males: r = 0.15, not significant; 32 weeks males: r = -0.04, not significant; 32 weeks females: r = 0.30, not significant). Body composition was measured via NMR spectrometry shortly before performing indirect calorimetry.

To measure the basal metabolic rate (BMR), animals were deprived of food for 6 hours during the day while temperature was increased to 30°C. The resultant HP of this postabsorptive (pa) and thermoneutral state (HP$_{30°C,pa}$) was significantly increased in HF diet-fed mice compared to wildtype mice but the diet dependency was abolished after normalization to body composition (Table 3-7). BMR was not significantly different between the genotypes, but a trend towards higher HP$_{30°C,pa}$ in *Dj-1$^{-/-}$* mice was detected after normalization to body composition. The increase of HP$_{22°C,ad-lib}$ over basal conditions (HP$_{22°C,ad-lib}$/HP$_{30°C,pa}$) calculated from the body composition-adjusted values was comparable between *Dj-1$^{-/-}$* and *Dj-1$^{+/+}$* mice on both diets (Table 3-7). Thus, the changes in body composition of *Dj-1$^{-/-}$* mice are not attributed to measurable changes in the metabolic rate.

After 32 weeks of feeding, the oxygen consumption of HF diet-fed mice was clearly increased compared to controls (Fig. 3-26) and the resultant $HP_{22°C,ad\text{-}lib}$ and $HP_{30°C,pa}$ were significantly higher in HF diet-fed animals but similar between $Dj\text{-}1^{-/-}$ and $Dj\text{-}1^{+/+}$ mice (Table 3-8). When related to body composition, the diet effect of $HP_{22°C,ad\text{-}lib}$ was abolished in male mice but persisted in HF diet-fed female mice. Moreover, the diet effect persisted for HP under basal conditions ($HP_{30°C,pa}$) in male and female mice (Table 3-8). Similar to the trend observed in male mice after 14 weeks of HF diet-feeding, the body composition-corrected BMR was significantly higher in female $Dj\text{-}1^{-/-}$ mice compared to wildtype mice with a corresponding lower increase of $HP_{22°C,ad\text{-}lib}$ over basal conditions (Table 3-8). Thus, $HP_{30°C,pa}$ was increased in those HF diet-fed $Dj\text{-}1^{-/-}$ mice that showed a higher adiposity compared to wildtype mice.
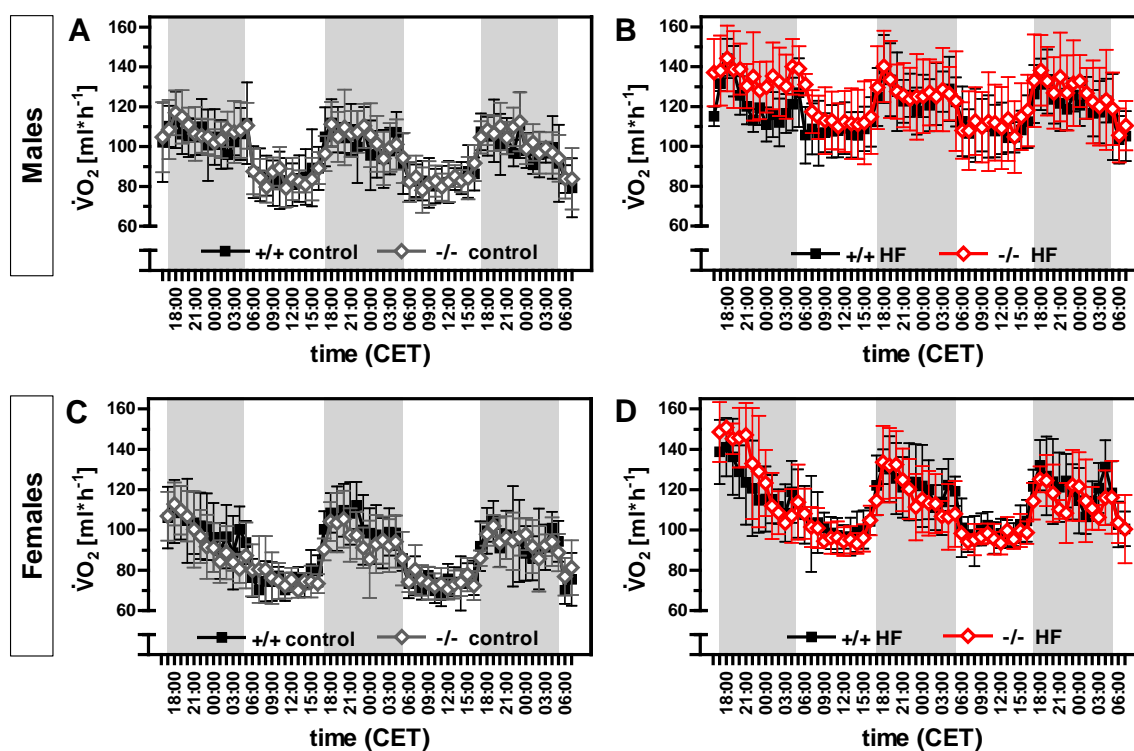
Fig. 3-26. Oxygen consumption ($\dot{V}O_2$) of male (top) and female (bottom) $Dj\text{-}1^{-/-}$ and $Dj\text{-}1^{+/+}$ mice maintained on control (A, C) or HF diet (B, D) for 32 weeks. Indirect calorimetry was performed at 22°C. Shaded areas indicate dark-phases. Values are means ± SD (n_{males} = 5-8; $n_{females}$ = 4-7).

Table 3-8. Respiratory exchange ratio (RER) and heat production (HP) of male (top) and female (bottom) _Dj-1-/-_ and _Dj-1+/+_ mice maintained on a HF or control diet for 32 weeks measured by indirect calorimetry. For RER and $HP_{22°C,ad-lib}$, the mean of two measuring days per animal was taken. $HP_{30°C,pa}$ was measured at thermoneutrality after animals were deprived of food for 6 hours.

		+/+	-/-	ANOVA/ANCOVA p-value		
				genotype	diet	genotype:diet
Males						
RER	control	0.92 ± 0.04	0.91 ± 0.05	0.2037	**<0.0001**	0.8619
	HF	0.82 ± 0.03	0.79 ± 0.03			
$HP_{22°C,ad-lib}$ [mW]	control	547.5 ± 14.9	548.6 ± 18.0	0.4002	**0.004**	0.4214
	HF	612.5 ± 35.4	657.8 ± 42.8			
$HP_{22°C,ad-lib}$ [mW *(LM+0.2FM)$^{-1}$]	control	25.5 ± 0.7	26.0 ± 0.9	0.1244	0.6518	0.2485
	HF	23.8 ± 1.2	26.7 ± 1.4			
$HP_{30°C,pa}$ [mW]	control	191.2 ± 5.9	197.6 ± 4.9	0.5282	**0.0002**	0.2827
	HF	268.1 ± 24.4	244.1 ± 17.0			
$HP_{30°C,pa}$ [mW *(LM+0.2FM)$^{-1}$]	control	8.9 ± 0.3	9.4 ± 0.2	0.9945	**0.0243**	0.3013
	HF	10.3 ± 0.7	9.9 ± 0.5			
$HP_{22°C,ad-lib}$/ $HP_{30°C,pa}$[#]	control	2.9 ± 0.1	2.8 ± 0.1	0.2836	**0.0201**	0.0885
	HF	2.4 ± 0.2	2.7 ± 0.1			
Females						
RER	control	0.90 ± 0.01	0.90 ± 0.04	0.6907	**<0.0001**	0.8685
	HF	0.84 ± 0.02	0.83 ± 0.03			
$HP_{22°C,ad-lib}$ [mW]	control	507.6 ± 26.6	484.0 ± 22.6	0.0782	**<0.0001**	0.9189
	HF	626.1 ± 31.1	605.0 ± 35.8			
$HP_{22°C,ad-lib}$ [mW *(LM+0.2FM)$^{-1}$]	control	29.4 ± 1.7	29.8 ± 1.7	0.5187	**0.0451**	0.9766
	HF	30.9 ± 1.6	31.3 ± 1.8			
$HP_{30°C,pa}$ [mW]	control	158.7 ± 18.9	173.1 ± 12.6	0.1662	**<0.0001**	0.5639
	HF	225.3 ± 13.4	231.3 ± 24.2			
$HP_{30°C,pa}$ [mW *(LM+0.2FM)$^{-1}$]	control	9.2 ± 0.9	10.7 ± 0.6**	**0.0019**	**<0.0001**	0.3606
	HF	11.1 ± 0.4	12.0 ± 1.2			
$HP_{22°C,ad-lib}$/ $HP_{30°C,pa}$[#]	control	3.2 ± 0.4	2.8 ± 0.2*	**0.0122**	**0.0072**	0.1958
	HF	2.8 ± 0.1	2.6 ± 0.3			

Values are means ± SD (n_{males} = 5-8, $n_{females}$ = 4-7). _Ad lib – ad libitum_. Pa – postabsorptive. LM – lean mass. FM – fat mass. [#]Ratio of $HP_{22°C,ad-lib}$ to $HP_{30°C,pa}$ was calculated using the values adjusted for body composition. Bonferroni post-test: *p < 0.05, **p < 0.01 _Dj-1-/-_ vs. _Dj-1+/+_ mice.

3.4.4 *Dj-1* deficiency influences glucose levels without affecting glucose tolerance

Since DIO negatively affects glucose metabolism, we tested whether the extent of this impairment varies between *Dj-1*^{-/-} and *Dj-1*^{+/+} mice. First, plasma glucose and insulin levels were measured in male *ad libitum* fed mice. Plasma glucose levels were not different between wildtype mice fed a HF or control diet for 14 weeks but were increased by HF diet in *Dj-1*^{-/-} mice, resulting in a significant diet effect which is dependent on genotype (Table 3-9). Plasma insulin levels were increased about twofold by HF diet as well as in mice lacking *Dj-1* in comparison to wildtype control diet-fed mice. Due to high intra-group variability this interaction failed to reach significance. Insulin sensitivity was estimated from glucose and insulin levels applying the homeostatic model assessment of insulin resistance (HOMA-IR) *[Hoeks et al. 2011]*. As for insulin levels, HOMA-IR indices tended to be doubled after 14 weeks of HF diet in wildtype mice as well as in *Dj-1* deficient mice compared to wildtype control-diet fed mice (Table 3-9). These results indicate that *Dj-1*^{-/-} mice are initially less insulin sensitive compared to wildtype mice. Wildtype mice reach this lower lever of insulin sensitivity after 14 weeks of HF diet-feeding, while insulin sensitivity is not further aggravated by HF diet in *Dj-1*^{-/-} mice.

Table 3-9. Plasma glucose and insulin levels of male *Dj-1*^{-/-} and *Dj-1*^{+/+} mice fed *ad libitum* with a HF or control diet for 14 (top) or 32 weeks (bottom). HOMA-IR = (insulin [$\mu U*ml^{-1}$]*glucose [$mmol*l^{-1}$])*22.5^{-1}.

	diet	+/+	-/-	ANOVA p-value		
				genotype	diet	genotype:diet
14 weeks						
glucose [mmol/l]	control	12.7 ± 2.7	11.0 ± 2.5	0.838	**0.008**	**0.015**
	HF	12.9 ± 1.4	15.0 ± 2.5			
insulin [pmol/l]*	control	177 ± 111	394 ± 330	0.402	0.508	0.094
	HF	345 ± 278	231 ± 110			
HOMA-IR*	control	12.0 ± 7.5	21.9 ± 14.0	0.389	0.143	0.247
	HF	23.7 ± 17.3	20.0 ± 11.1			
32 weeks						
glucose [mmol/l]	control	14.0 ± 2.3	14.4 ± 1.8	0.403	0.592	0.246
	HF	16.0 ± 4.6	13.7 ± 2.4			
insulin [pmol/l]*	control	278 ± 220	314 ± 219	0.700	**0.035**	0.942
	HF	606 ± 431	522 ± 177			
HOMA-IR*	control	22.8 ± 19.5	25.7 ± 19.7	0.835	**0.041**	0.756
	HF	59.6 ± 49.3	39.9 ± 14.0			

Values are means ± SD ($n_{14\ weeks}$ = 9-11; $n_{32\ weeks}$ = 4-8). *Statistic was performed with log-transformed data.

After 32 weeks of HF diet-feeding, plasma insulin levels and HOMA-IR indices were significantly increased in both genotypes indicating HF diet-induced insulin resistance (Table 3-9). The differences between control diet-fed $Dj-1^{-/-}$ and $Dj-1^{+/+}$ mice were less pronounced compared to 14 weeks of HF diet-feeding. This reflects the transient phenotype that was observed for body composition.

Second, we performed i.p. glucose tolerance tests (i.p. GTT) towards the end of the feeding periods in male and female mice. Glucose clearance was comparable between control diet-fed $Dj-1^{-/-}$ and $Dj-1^{+/+}$ mice (Fig. 3-27). In both sexes, HF diet-feeding for 14 or 32 weeks impaired the glucose tolerance of $Dj-1^{-/-}$ and $Dj-1^{+/+}$ mice to the same extent (Fig. 3-27).
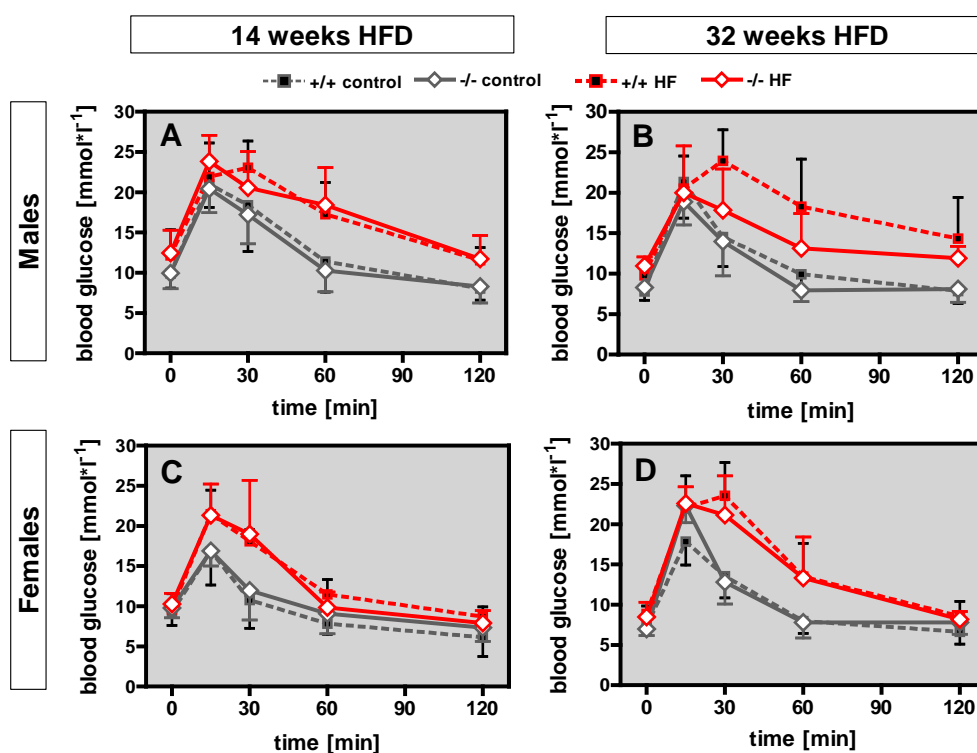
Fig. 3-27. Intraperitoneal glucose tolerance test (i.p.GTT) of male and female $Dj-1^{-/-}$ and $Dj-1^{+/+}$ mice maintained on a HF or control diet for 14 or 32 weeks. After animals were deprived of food for 6 hours, they received an i.p. injection of 2 g glucose*kg^{-1} body mass. Glucose was monitored in tail blood 15, 30, 60 and 120 min after glucose administration. Values are means ± SD ($n_{males;14weeks}$ = 8-12; $n_{females;14weeks}$ = 7-8; $n_{males;32weeks}$ = 3-7; $n_{females;32weeks}$ = 4-7). Areas under the curve were increased in HF mice (ANOVA diet effect: p < 0.0001, except males 32 weeks p < 0.0003) without any genotype effects.

The effect of *Dj-1* deficiency on glucose tolerance was additionally evaluated in mice fed a HF diet for 12 months and in male 8-month-old mice maintained on a high-fat, high-sugar diet (HF/HS, Appendix I.I Fig. A1) for 6 weeks (Fig. 3-28). We did not observe any differences in glucose tolerance of male or female *Dj-1*$^{-/-}$ mice compared to their wildtype littermates.

Consequently, loss of *Dj-1* transiently influences insulin levels without affecting glucose tolerance.
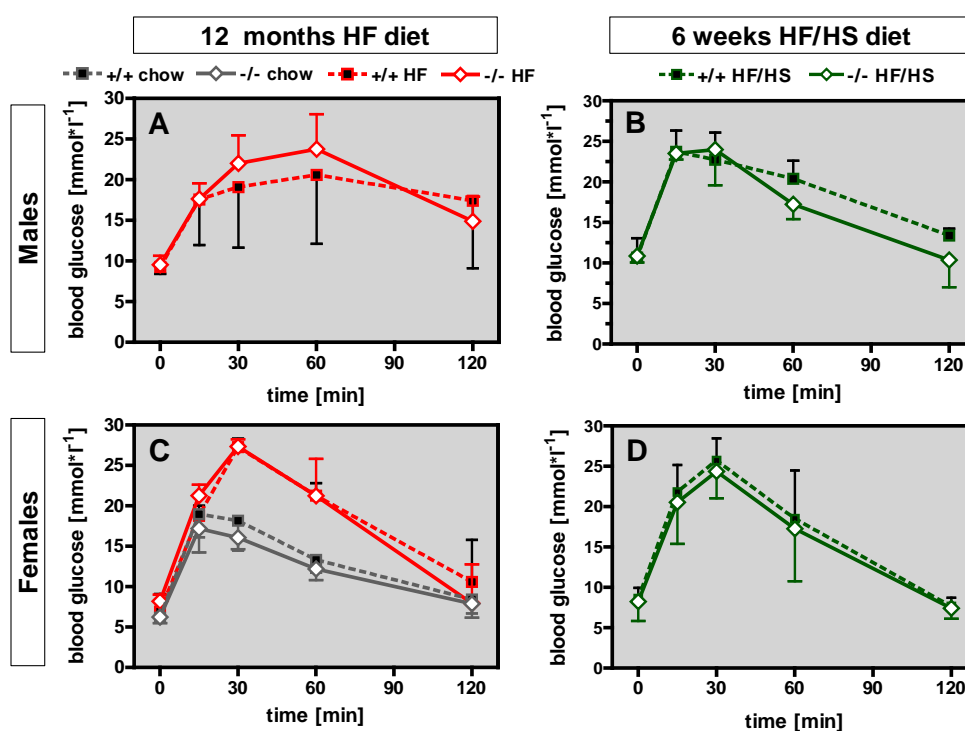
Fig. 3-28. Intraperitoneal glucose tolerance test (i.p.GTT) of male (top) and female (bottom) *Dj-1*$^{-/-}$ and *Dj-1*$^{+/+}$ mice. After animals were deprived of food for 6 hours, they received an i.p. injection of 2 g glucose*kg^{-1} body mass. Glucose was monitored in tail blood 15, 30, 60 and 120 min after glucose administration. (**A, C**) Mice at 6 weeks of age were placed on HF diet for 12 months (n = 4). For females, age matched chow-fed controls were available (n = 3-5), demonstrating a diet effect for areas under the curve (ANOVA p < 0.0001). (**B, D**) 8-month-old mice were placed on HF/HS diet for 6 weeks (n = 4). Values are means ± SD.

3.5 Influence of *Dj-1* deficiency on leptin sensitivity

The hormone leptin is produced and secreted by adipose tissue and plasma leptin levels positively correlate with body fat mass *[Maffei et al. 1995]*. In the central nervous system, the afferent leptin signal exerts an anorectic action representing a negative feedback mechanism for adiposity *[Friedman & Halaas 1998]*. Obesity, however, results in a state of leptin resistance with blunted central leptin action *[Münzberg et al. 2004; Morrison 2008]*.

In *Dj-1$^{-/-}$* and *Dj-1$^{+/+}$* mice, leptin levels were increased by HF diet and significantly correlated with body fat mass in this diet group (Fig. 3-29). Because *Dj-1$^{-/-}$* mice showed an increased proportion of fat mass after 14 weeks of HF diet, we studied whether leptin sensitivity differs from their wildtype littermates.
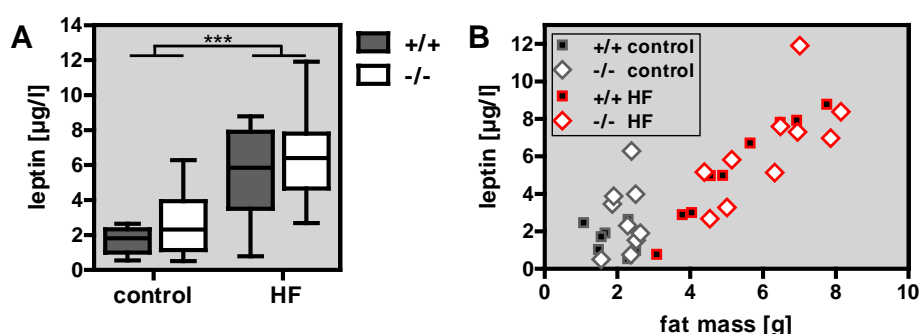
Fig. 3-29. Plasma leptin levels of male *Dj-1$^{-/-}$* and *Dj-1$^{+/+}$* mice maintained on HF or control diet for 14 weeks. (**A**) Plasma was collected from *ad libitum fed* mice (n = 8-10). ANOVA diet effect: ***p < 0.001. (**B**) Leptin levels related to fat mass. Leptin levels of HF diet-fed animals significantly correlate with fat mass (Pearson product-moment correlation: *Dj-1$^{+/+}$* r = 97, p < 0.0001; *Dj-1$^{+/+}$* r = 0.71, p = 0.0225).

3.5.1 Basal STAT3 phosphorylation is attenuated by high-fat diet in *Dj-1$^{-/-}$* mice

The activation of STAT3 to phospho-STAT3 is the most robust molecular marker of leptin action on the leptin receptor *[Münzberg & Myers 2005]* which is blunted in case of leptin resistance. We examined basal STAT3 signaling in lysates of the ventral hypothalamus of male *Dj-1$^{-/-}$* and *Dj-1$^{+/+}$* mice after 14 weeks of HF or control diet-feeding using western blot (Fig. 3-30 A). STAT3 levels positively correlated with phospho-STAT3 (Fig. 3-30 B). Total STAT3 levels were not significantly different between the genotype or diet groups (Fig. 3-30 C). However, phospho-STAT3 is significantly induced by HF diet in wildtype but not in *Dj-1$^{-/-}$* mice (Fig. 3-30 D). Furthermore, the ratio of phospho-STAT3 to STAT3 was affected by diet (Fig. 3-30 E). The tendency towards reduced phospho-STAT3/STAT3 ratios in *Dj-1$^{-/-}$* mice failed to reach statistical significance (p = 0.338). Consequently, wildtype mice are still

leptin sensitive after 14 weeks of HF diet-feeding while leptin sensitivity is lowered in *Dj-1*^{-/-} mice as judged by basal STAT3 phosphorylation.
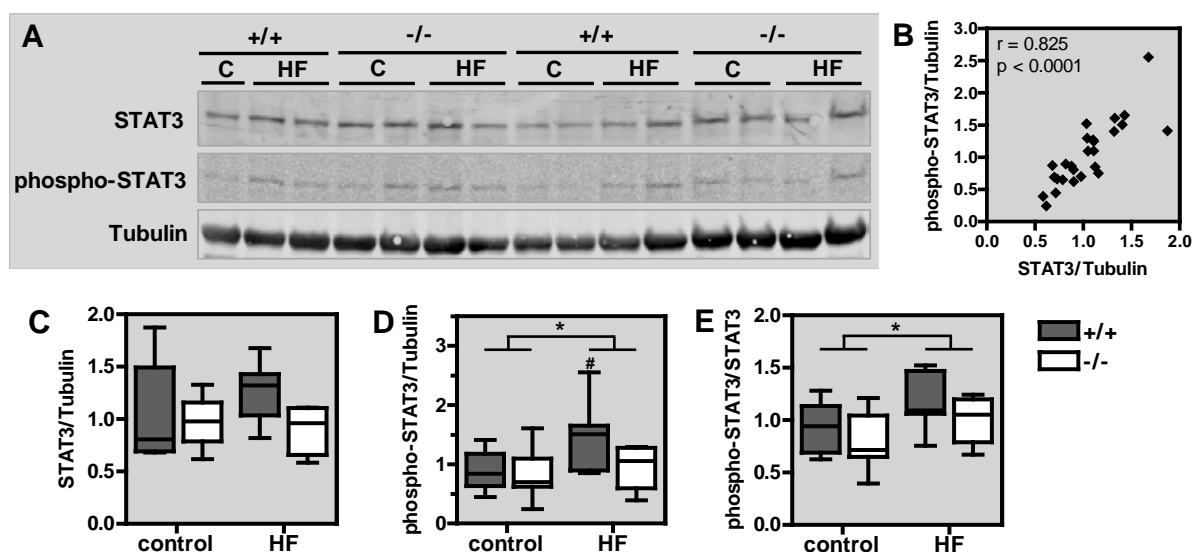
Fig. 3-30. Basal STAT3 phosphorylation in male *Dj-1*^{-/-} and *Dj-1*^{+/+} mice after 14 weeks of HF or control diet feeding. (**A**) Example western blot of protein extracts of the ventral hypothalamus. The three targets were detected on the same membrane. (**B**) Densitometric signals of total STAT3 and phospho-STAT3 were normalized to alpha-tubulin signals and plotted against each other. Pearson product-moment correlation between normalized phospho-STAT3 and STAT3 levels was significant. (**C, D**) Normalized total STAT3 and phospho-STAT3 levels. (**E**) Ratio of phospho-STAT3 to STAT3. ANOVA: significant effect of diet: *$p < 0.05$, Bonferroni post-test: #$p < 0.05$ HF vs. control diet. n = 6-7.

We next analyzed the inducible STAT3 phosphorylation after i.p. leptin administration in 6-month-old male *Dj-1*^{-/-} mice and their wildtype littermates maintained on a normal chow diet. Shortly before the onset of the dark phase, mice were injected with either 5 mg*kg[-1] leptin or vehicle. The ventral part of the hypothalamus was taken 30 minutes after injection and subjected to western blot analysis (Fig. 3-31 A). While total STAT3 levels were unchanged (Fig. 3-31 B), leptin injection increased phospho-STAT3 levels approximately 4-fold compared to vehicle injection (Fig. 3-31 C). The magnitude is in accordance with previous reports showing a 3-fold increase of STAT3 phosphorylation in C57BL/6J mice one hour after i.p. leptin administration *[Prpic et al. 2003]*. Leptin-induced phospho-STAT3 levels as well as phosho-STAT3 to STAT3 ratios (Fig. 3-31 D) were comparable between *Dj-1*^{-/-} and *Dj-1*^{+/+} mice. Thus, the sensitivity towards exogenously applied leptin on the level of STAT3 phosphorylation is not affected in *Dj-1*^{-/-} mice under unchallenged conditions.
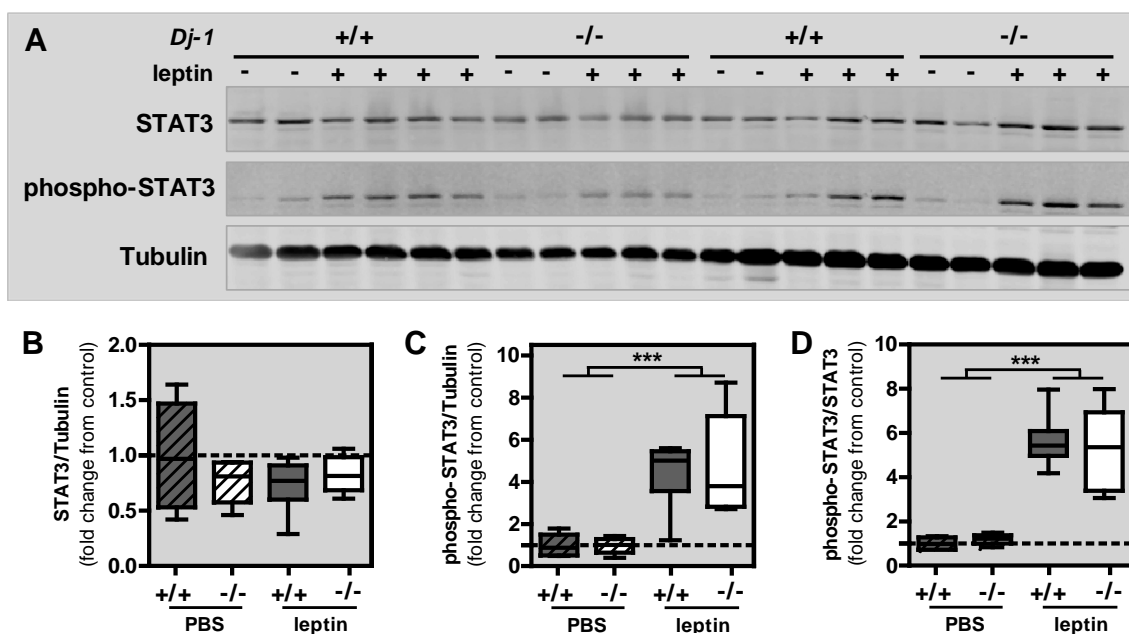
Fig. 3-31. Inducible STAT3 phosphorylation of 6-month-old *Dj-1^-/-* and *Dj-1^+/+* mice after i.p. leptin administration. 30 minutes after animals have received a leptin (5 mg*kg^-1) or vehicle injection, the ventral hypothalamus was dissected. (**A**) Western blot of protein extracts of the ventral hypothalamus. The three targets were detected on the same membrane. Densitometric signals of total STAT3 (**B**) and phospho-STAT3 (**C**) were normalized to alpha-tubulin signals. (**D**) Ratio of phosho-STAT3 to total STAT3 signals. Shown are the fold changes from *Dj-1^+/+* mice with vehicle injection. ANOVA: significant effect of treatment ***p ≤ 0.0001. $n_{vehicle}$ = 4, n_{leptin} = 6-7.

3.5.2 Anorectic leptin action is similar in *Dj-1^-/-* and *Dj-1^+/+* mice

In addition to STAT3 phosphorylation, leptin sensitivity can be concluded from food intake inhibition in response to exogenous leptin *[Scarpace & Zhang 2009]*. We measured the anorectic response after i.p. injections of leptin in male HF and control diet-fed *Dj-1^-/-* and *Dj-1^+/+* mice to follow up whether the diminished leptin sensitivity implied on the level of STAT3 phosporylation translates into a physiological effect. Towards the end of the 14- and 32-week feeding periods, mice received i.p. PBS administrations for three consecutive days followed by 5 mg*kg^-1 leptin the day after. Injections were given shortly before the onset of the dark phase. Food intake was automatically recorded throughout the experiment. Leptin administration led to a decrease of cumulative energy intake in control diet-fed animals apparent after 12 hours (Fig. 3-32 A, C). The anorectic response was blunted in mice after 14 and 32 weeks of HF diet (Fig. 3-32 B, D) indicating HF diet-induced leptin resistance (Supplementary Fig. S7: time courses of cumulative energy intake). On both diets and after both time points, *Dj-1^-/-* mice did not differ from *Dj-1^+/+* mice in their anorectic response to leptin.
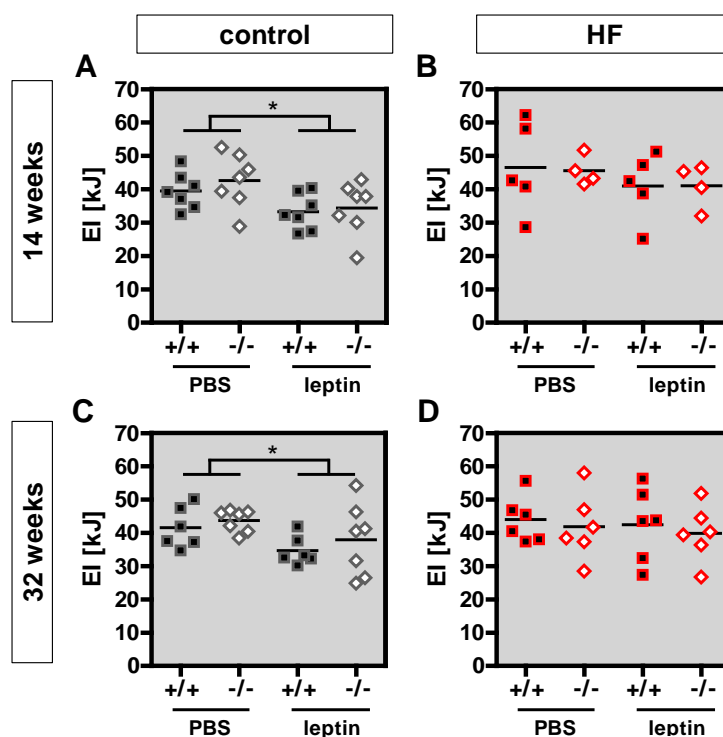
Fig. 3-32. 12-hour energy intake (EI) after i.p. leptin injection compared to PBS injection of male *Dj-1$^{-/-}$* and *Dj-1$^{+/+}$* mice maintained on HF or control diet for 14 or 32 weeks. Mice received i.p. PBS injection for three consecutive days followed by 5 mg*kg^{-1} leptin the day after. Injections were given shortly before the onset of the dark phase. Energy intake was recorded automatically. Data points represent individual mice. Horizontal lines correspond to the mean. EI after PBS injection represents the mean of 3 days. ANOVA: effect of treatment *p < 0.05. n$_{control}$ = 6-8, n$_{HF}$ = 4-6.

73

3.6 High-fat diet has a greater impact on hypothalamic gene regulation in the absence of *Dj-1*

To further investigate the impact of the HF challenge on energy balance regulation in male *Dj-1*$^{-/-}$ mice, we carried out a next generation sequencing-based transcriptome analysis of the ventral hypothalamus after 14 weeks of feeding. Groups were compared pairwise yielding a total of four comparisons: regulation by diet within wildtype mice or *Dj-1*$^{-/-}$ mice and regulation by genotype within HF or control diet-fed groups. RNA expression analysis was performed with two different algorithms (DESeq and edgeR) applying a fold change of > 1.2 (upregulation) or < -1.2 (downregulation) with a p-value threshold of 0.05 corrected for multiple testing. Only hits significant for both algorithms were considered.

Using these criteria, HF compared to control diet-feeding did not lead to differential gene expression in the ventral part of the hypothalamus in neither wildtype nor *Dj-1*$^{-/-}$ mice.

When *Dj-1*$^{-/-}$ mice were compared to wildtype mice, 19 genotype-regulated genes were identified of which 12 were regulated under HF as well as under control diet conditions, 2 were only regulated under control diet and 5 only under HF diet (Table 3-12). Notably, 13 of these genes are localized on chromosome 4, where the *Dj-1* (*Park7*) gene is disrupted by a gene trap vector in *Dj-1*$^{-/-}$ mice. Calculating the distance of these genes from *Dj-1* (*Park7*), the closest gene was located 64 kb upstream. All other genes were downstream of *Dj-1* with the closest located 648 kb and the furthest 5.5 Mb away (Supplementary Table S5).

Taken together, the *Dj-1* deficient genotype influenced the expression of ventral hypothalamic genes while the 14-week HF diet-intervention had no effect under these conditions.

Additional to the stringent statistical methods described above, we applied t-test statistics (p < 0.01 for log+1 transformed normalized expression values) combined with a read fold change of > 1.2 (upregulation) or < -1.2 (downregulation). The resulting lists contained all genes found differentially expressed using DESeq and edgeR algorithms. The highest number of regulated genes (332) was found for the comparison of *Dj-1*$^{-/-}$ and *Dj-1*$^{+/+}$ mice maintained on a HF diet (Fig. 3-33 B, Supplementary Table S9). This was followed by 239 regulated genes between HF and control diet-fed *Dj-1*$^{-/-}$ mice (Fig. 3-33 A, Supplementary Table S7), 185 regulated genes between control diet-fed *Dj-1*$^{-/-}$ and *Dj-1*$^{+/+}$ mice (Fig. 3-33 B, Supplementary Table S8) and 146 regulated genes between HF and control diet-fed wildtype mice (Fig. 3-33 A, Supplementary Table S6). Regarding genes differentially expressed between HF and control diet-fed mice, only the transcription factor *Etv6* (ets variant gene 6 (TEL oncogene)) was regulated by diet in wildtype as well as in *Dj-1*$^{-/-}$ mice while there were 22 genes commonly regulated by genotype in the control as well as in the HF group (Fig. 3-33; Supplementary Table S10). Of the common genotype

regulated genes, 14 were located on chromosome 4. Still, these results indicate that more genes are regulated when *Dj-1* deficiency is combined with HF feeding.

Table 3-10. Genotype-regulated genes under HF and control diet. Male $Dj-1^{-/-}$ and wildtype mice were maintained on either HF or control diet for 14 weeks. The ventral hypothalamus was subjected to RNA sequencing. Listed are genes for which at least one transcript was found differentially expressed with both DESeq and edgeR algorithm ($p < 0.05$, adjusted). A log2 fold change > 0.263 indicates upregulation and < -0.263 downregulation in $Dj-1^{-/-}$ versus $Dj-1^{+/+}$ mice, corresponding to a fold change of > 1.2 or < -1.2, respectively.

Gene symbol	Gene ID	Gene name	mean log2 fold change* within control group	HF group	Chr
Regulated within control and HF group					
5330422M15Rik	77062	RIKEN cDNA 5330422M15 gene	2.3	4.1	4
Eno1	13806	enolase 1, alpha non-neuron	-1.7	-1.8	4
Gm13152	195531	predicted gene 13152	-4.2	-4.8	4
Gm16503	100038537	predicted gene 16503	-6.8	-inf	4
Gm5506	433182	predicted gene 5506	8.5	6.8	18
LOC100045967	100045967	alpha-enolase-like	-6.4	-8.7	2
LOC67527	67527	murine leukemia retrovirus	1.3	1.1	18
Masp2	17175	mannan-binding lectin serine peptidase 2	2.0	2.8	4
Miip	28010	migration and invasion inhibitory protein	-1.1	-1.4	4
Park7	**57320**	**Parkinson disease (autosomal recessive, early onset) 7**	**-4.8**	**-5.1**	**4**
Slc2a5	56485	solute carrier family 2 (facilitated glucose transporter), member 5	-1.3	-1.3	4
Tnfrsf8	21941	tumor necrosis factor receptor superfamily, member 8	-5.1	-4.6	4
Regulated within control group					
2610305D13Rik	112422	RIKEN cDNA 2610305D13 gene	-1.9		4
Ptchd2	242748	patched domain containing 2	-0.9		4
Regulated within HF group					
4921517L17Rik	70873	4921517L17Rik		1.8	2
4930481A15Rik	74931	RIKEN cDNA 4930481A15 gene		-1.2	19
Fbxo44	230903	F-box protein 44		-0.7	4
Rec8	56739	REC8 homolog (yeast)		1.1	14
Ubiad1	71707	UbiA prenyltransferase domain containing 1		0.6	4

*mean log2 fold change of DESeq and edgeR. Chr – Chromosome.

(A) Regulation by diet

(B) Regulation by genotype
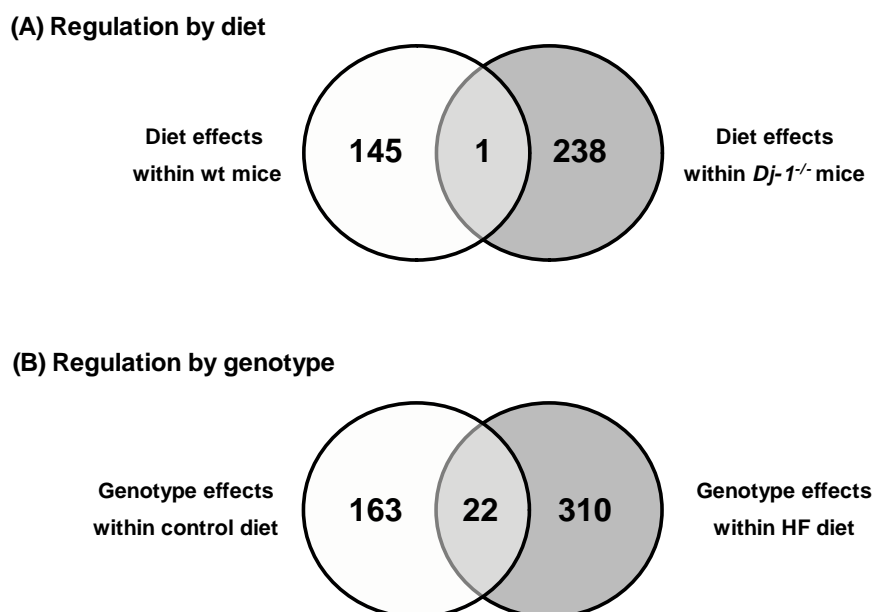
Fig. 3-33. VENN diagram summarizing the number of differentially expressed genes between *Dj-1*$^{-/-}$ and *Dj-1*$^{+/+}$ (wt) mice maintained on a high-fat (HF) or control diet for 14 weeks. Two groups were compared at a time. (**A**) Number of genes regulated by diet within wildtype or *Dj-1*$^{-/-}$ mice. (**B**) Number of genes regulated by genotype within the control or HF diet-fed group. Differentially expressed genes are listed in Supplementary Tables S6-S10.

Using the extended candidate lists from the t-test statistic, we conducted a pathway analysis. We focused on pathways in the category 'Diseases (MeSH)' which we further subclassified into metabolic diseases (including obesity-concomitant phenomena) and diseases related to neurodegeneration or behavior.

Metabolic diseases

Regarding the regulation by diet, genes of seven pathways were overrepresented in both wildtype and *Dj-1*$^{-/-}$ mice, whereby the number of regulated genes associated with these pathways was higher between HF and control diet-fed *Dj-1*$^{-/-}$ compared to wildtype mice (Fig. 3-34 A, Supplementary Table S11). Further metabolic disease pathways were associated with diet-regulated genes in either wildtype or *Dj-1*$^{-/-}$ mice. Only diet-regulated genes in *Dj-1*$^{-/-}$ mice were significantly overrepresented in the pathways 'Obesity/ Overweight/Overnutrition' and 'Body weight' (Fig. 3-34 A) and, interestingly, the pathway 'Mitochondrial Diseases' was associated with the differential genes of this comparison.

Comparing *Dj-1*$^{-/-}$ and wildtype mice, no differentially regulated genes were associated with metabolic disease pathways under control diet-feeding. Under the HF diet regime, several pathways were overrepresented by the genes differentially expressed between

Dj-1^{-/-} and *Dj-1*^{+/+} mice including three pathways linked to body weight regulation ('Body Weight', 'Weight Loss', 'Weight Gain'; Fig. 3-34 B, Supplementary Table S12).

(A) Regulation by diet
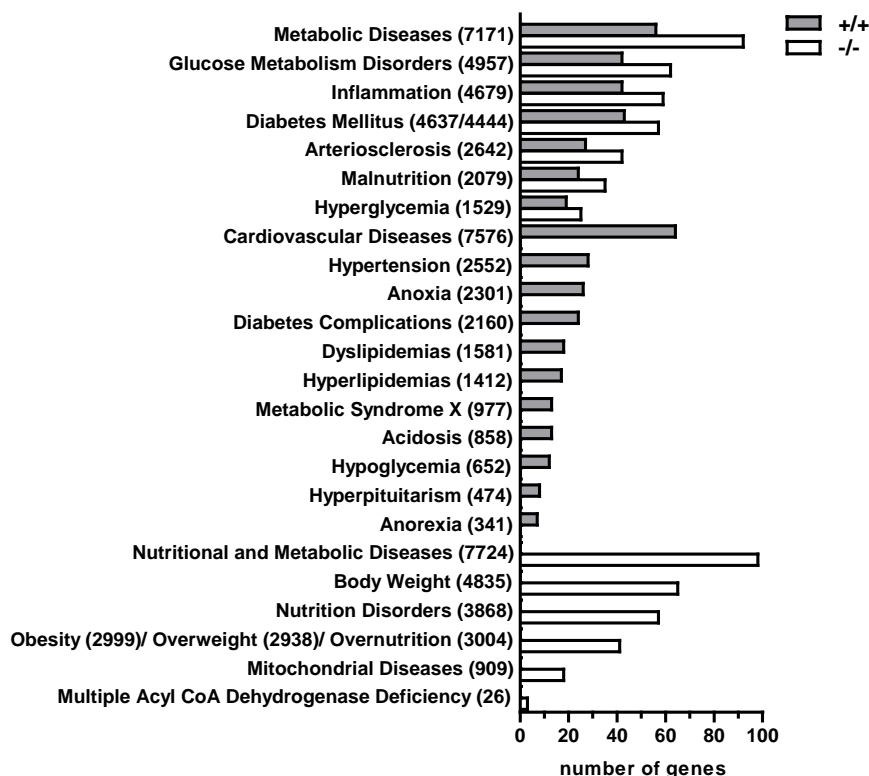
(B) Regulation by genotype
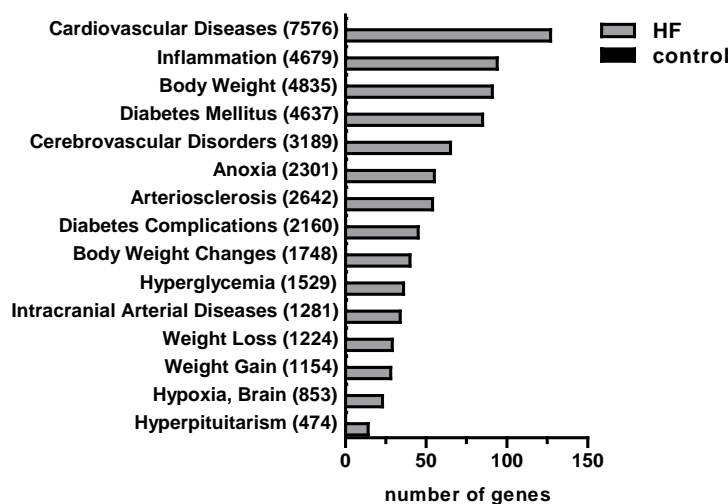
Fig. 3-34. Analysis of pathways associated with metabolic diseases. Shown are pathways for which differentially expressed genes between two groups compared at a time were significantly overrepresented. The length of the bars indicates the number of regulated genes contained in the respective pathway. Shown in parentheses is the number of total genes of the pathway. (**A**) Regulation by diet within wildtype mice (grey bars) or *Dj-1*^{-/-} mice (white bars). The regulated genes contained in the pathways 'Obesity', 'Overweight' and 'Overnutrition' are 100 % congruent. (**B**) Regulation by genotype within HF diet-fed groups (grey bars). No metabolic disease pathways were associated with the differentially expressed genes between control diet-fed *Dj-1*^{-/-} or *Dj-1*^{+/+} mice. See Supplementary Tables S11 and S12 for significance levels and lists of genes.

77

Diseases related to neurodegeneration or behavior

Genes differentially regulated by diet in wildtype mice were overrepresented in five pathways related to neurodegeneration or behavior while no pathway in this category was associated with diet-regulated genes in $Dj-1^{-/-}$ mice (Fig. 3-35 A, Supplementary Table S13).

Comparing $Dj-1^{-/-}$ and wildtype mice, genes of the pathway 'Demyelinating Disease' were overrepresented in both control and HF group being the only emerging pathway under control diet conditions in this category. In contrast, challenging $Dj-1^{-/-}$ and $Dj-1^{+/+}$ mice with a HF diet, genes of further seven pathways were significantly overrepresented in the genotype regulated genes (Fig. 3-35 B, Supplementary Table S14). This indicates that HF diet-feeding has a greater impact on mental health associated gene expression in the absence of $Dj-1$.

(A) Regulation by diet
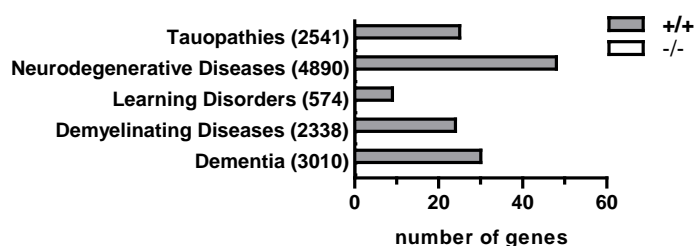
(B) Regulation by genotype
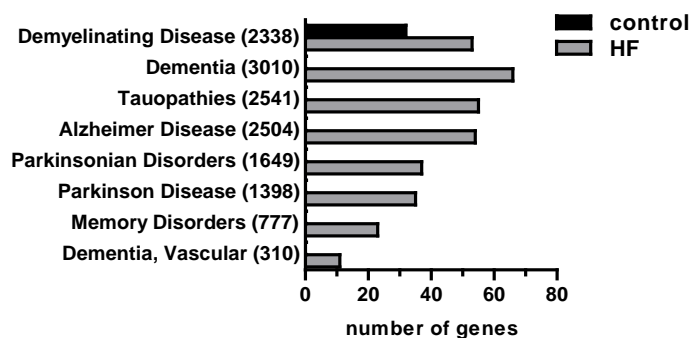
Fig. 3-35. Analysis of pathways related to neurodegeneration and behavior. Shown are pathways for which differentially expressed genes between two groups compared at a time were significantly overrepresented. The length of the bars indicates the number of genotype regulated genes contained in the respective pathway. Shown in parentheses is the number of total genes of the pathway. (**A**) Regulation by diet within wildtype mice (grey bars). No pathways related to neurodegeneration were associated with the differentially expressed genes between control and HF diet-fed $Dj-1^{-/-}$ mice. (**B**) Regulation by genotype within control diet (black bars) or HF diet-fed groups (grey bars). See Supplementary Tables S13 and S14 for significance levels and lists of genes.

3.7 The content of mitochondria is similar between $Dj-1^{-/-}$ and $Dj-1^{+/+}$ mice

Loss of $Dj-1$ is associated with increased mitochondrial H_2O_2 production in the mouse brain and, in older mice, upregulation of antioxidant enzymes *[Andres-Mateos et al. 2007]*. Furthermore, mitochondrial complex activities were increased in $Dj-1^{-/-}$ relative to wildtype mice *[Pham et al. 2010]*. Changes in these parameter could be due to an increased number of mitochondria. However, citrate synthase as a measure of mitochondrial content was either unchanged or increased in the brain of $Dj-1^{-/-}$ mice compared to wildtype mice *[Andres-Mateos et al. 2007; Pham et al. 2010]*. Here, we quantified the mitochondrial genome copy number relative to the nuclear genome copy number using a quantitative PCR with primers directed against exclusive nuclear or mitochondrial genomic targets. The mitochondrial copy number of male 18-week-old $Dj-1^{-/-}$ mice on control diet did not differ from their wildtype littermates neither in brain nor in gastrocnemius muscle or epididymal white adipose tissue (Fig. 3-36).
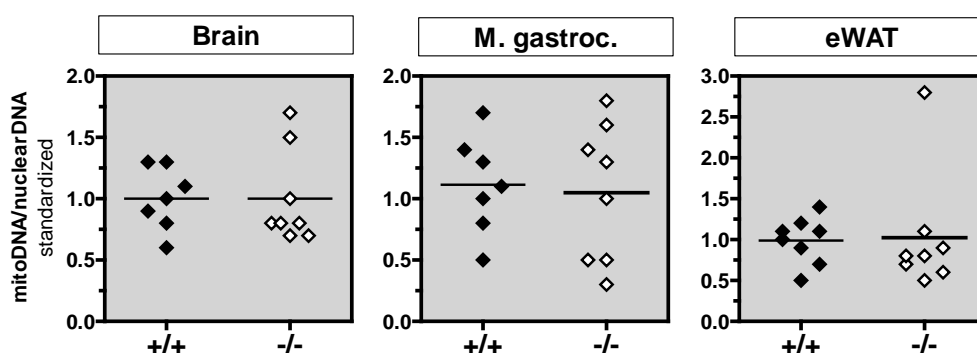
Fig. 3-36. Ratio of mitochondrial to nuclear DNA in the brain, gastrocnemius muscle (M. gastroc) and epididymal white adipose tissue (eWAT) of 18-week-old $Dj-1^{+/+}$ and $Dj-1^{-/-}$ mice.

4 DISCUSSION

4.1 Alterations in the hypothalamic proteome associated with a short-term high-fat diet intervention

The development of obesity is associated with changes in the homeostatic system of energy balance regulation in which the hypothalamus constitutes an important regulator of food intake and energy expenditure (see Chapter 1.2). Once obesity is established, the elevated level of adiposity is actively defended *[Wisse et al. 2007; Leibel 2008]*. In order to increase the understanding of how energy homeostasis is shifted out of balance during the development of overweight, we investigated changes occurring in the hypothalamus of mice after a 10-day HF diet intervention. We concentrated on changes that manifest on the protein level choosing a discovery-oriented proteomics approach and compared hypothalamic protein expression patterns between HF and control diet-fed mice of three strains differing in their susceptibility to DIO. HF diet-associated changes of protein abundances were small in number and extent but, interestingly, the number of candidates correlated positively with the level of adiposity detected in the different strains. In the complex network of energy balance regulation, numerous molecules are involved that orchestrate changes in response to nutritional stimuli. The contribution of individual components is probably small with changes expected to be less than three-fold *[Mobbs et al. 2004]*. On the other hand, we processed the complete hypothalamus which represents a complex tissue containing different cell types (neurons and glia) and highly specialized cells even within one cell population. Examining such a heterogeneous mixture including nuclei with opposing action (see Chapter 1.2.1) might neutralize effects of the applied intervention in specific cells. To attribute HF diet-induced effects on protein abundances to specific neuron populations, microdissection of the respective nuclei would have to be applied.

A small effect size of HF diet-feeding was also observed in a proteome study investigating the protein abundance in the hypothalami of male C57BL/6N mice after 18 weeks of HF feeding. In this study, an additional group of mice received a 'cafeteria' diet which contained higher amounts of simple sugars and salt. Interestingly, more proteins were differentially abundant in the hypothalami of mice fed the 'cafeteria' diet, although the diet-induced gain of body and fat mass was smaller compared to HF diet-fed mice (Supplementary Fig. S9, Supplementary Table 16). Thus, the diet-induced regulation of protein abundance or modification also depends on the type of diet.

Most prominently, DJ-1 (PARK7) was identified to be increased after 10 days of HF diet independently in all strains. In this experiment, we applied two-dimensional difference gel electrophoresis (2D-DIGE) as a quantitative method whereby different proteoforms[8] are separated. The increase of DJ-1 corresponds to one form of DJ-1 (see discussion below) while the total DJ-1 content does neither change on the protein nor on the gene expression level. Gene expression levels of the remaining candidates[9] were also not influenced by the HF diet intervention (Supplementary Table S2). This suggests that HF diet-feeding alters the proteome by post-translational mechanisms rather than transcription and protein synthesis. Unfortunately, it is difficult to identify potential protein modifications from 2D-DIGE analyses retrospectively because mass spectrometrical parameters for protein identification cannot be set for maximal sequence coverage for all proteins in the same run.

Nevertheless, several interesting relations between the regulated proteins become apparent when all candidates are summarized (Fig. 4-1; Table 3-1). Similar to *Dj-1*, mutations in the alpha-synuclein gene are associated with inherited PD *[Thomas & Beal 2011]*. Alpha-synuclein that was found less abundant in C57BL/6N mice upon HF feeding is a ubiquitous protein able to bind lipids and is involved in dopamine synthesis *[Sharon et al. 2001; Perez et al. 2002]*. Alpha-synuclein tends to aggregate, which is promoted by oxidative stress-induced posttranslational modification *[Schildknecht et al. 2013; Xiang et al. 2013]* and aggregated alpha-synuclein is a major component of Lewy bodies which are pathogenic inclusions characteristic of PD *[Spillantini et al. 1997]*. DJ-1 functions as a (co-)chaperone preventing the abnormal aggregation of alpha-synuclein in a redox-dependent manner *[Shendelman et al. 2004; Zhou & Freed 2005; Zhou et al. 2006]*. Moreover, beta-synuclein that was more abundant in HF diet-fed AKR/J mice inhibits alpha-synuclein aggregation *[Hashimoto et al. 2001; Park & Lansbury 2003]*. Thus, the upregulation or modification of DJ-1 and beta-synuclein might counteract alpha-synuclein aggregation which might be induced by changes in the redox state due to the HF diet-intervention (Fig 4-1).

Indeed, a redox-responsive protein was contained in the list of candidates: SH3 domain-binding glutamic acid-rich-like protein 3 (Sh3bgrl3) was more abundant in HF diet-fed AKR/J mice. It is a member of the thioredoxin family and implicated in cellular redox homeostasis through modulating the activities of glutaredoxins which are glutathione-dependent redox enzymes *[Fernandes & Holmgren 2004; Nardini et al. 2004; Xu et al. 2005a]*. This indicates that the redox milieu in the hypothalamus is influenced by the HF diet intervention.

---

[8] This term summarizes 'the different molecular forms in which a protein product of a single gene can be found, including changes due to genetic variations, alternatively spliced RNA transcripts and posttranslational modifications' *[Smith et al. 2013]*.
[9] *Tceal5* was not included in the analysis.
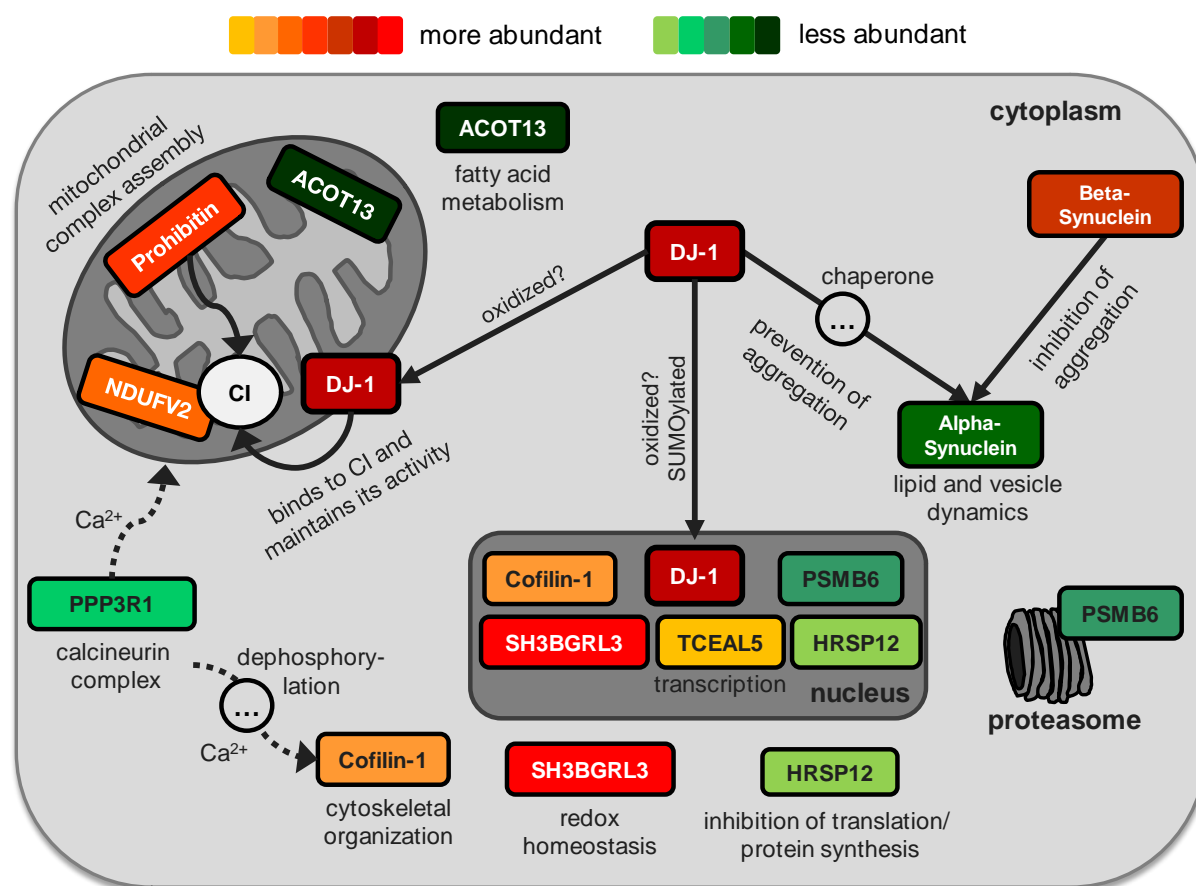
Fig. 4-1. Altered proteins in the hypothalamus of mice after 10 days of high-fat diet-feeding. Possible interactions of candidates arising from the comparison of protein expression patterns between HF and control diet-fed AKR/J, C57BL/6N and SWR/J mice are summarized (see Table 3-1). The subcellular localization is depicted as annotated in the UniProtKB database. The color code denotes the abundance of the proteoform in the HF compared to the control group. See text for further explanations. CI – Complex I. ACOT13 - Acyl-coenzyme A thioesterase 13. HRSP12 - Ribonuclease UK114. NDUFV2 - NADH dehydrogenase [ubiquinone] flavoprotein 2, mitochondrial. PPP3R1 - Calcineurin subunit B type 1. PSMB6 - Proteasome subunit beta type-6. SH3BGRL3 - SH3 domain-binding glutamic acid-rich-like protein 3. TCEAL5 - Transcription elongation factor A protein-like 5.

Mitochondria play an important role in regulating the intracellular homeostasis *[Ryan & Hoogenraad 2007]*. DJ-1 is able to translocate from the cytosol to the nucleus and mitochondria. Within mitochondria, DJ-1 can bind to complex I of the respiratory chain and maintain its correct function (Chapter 1.4) *[Meulener et al. 2005a; Ved et al. 2005; Hayashi et al. 2009; Kwon et al. 2011]*. Interestingly, one core subunit of complex I (Ndufv2) was more abundant in HF diet-fed SWR/J. Prohibitin, that was more abundant in HF diet-fed C57BL/6N mice, is a ubiquitous protein localized in the inner mitochondrial membrane. Prohibitin also interacts with complex I subunits (Fig. 4-1) *[Bourges et al. 2004]* and is involved in mitochondrial complex assembly *[Nijtmans et al. 2002]*. Furthermore, prohibitin is reduced in the substantia nigra of PD patients *[Ferrer et al. 2007]* and the enzymatic activity of complex I

is reduced in PD (reviewed in *Abou-Sleiman et al. [2006]*). Our results indicate that complex I function might also be important in the intracellular changes triggered by HF feeding and might be influenced by DJ-1.

Moreover, mitochondria play an important part in calcium homeostasis and signaling *[Rizzuto et al. 2000; Duchen et al. 2008]*. We found subunit B of calcineurin (Ppp3r1) less abundant in HF diet-fed AKR/J mice. Calcineurin is a Ca^{2+}- and calmodulin-dependent serine/threonine protein phosphatase that mediates cellular responses to intracellular Ca^{2+} signals and consists of a catalytic subunit A and the regulatory subunit B *[Rusnak & Mertz 2000]*. Calcineurin B has been shown to bind to mitochondria, suggesting further roles apart from regulating the catalytic activity of calcineurin A *[Cheng et al. 2012]*.

Finally, cofilin-1 was found higher abundant in HF diet-fed AKR/J mice. Cofilin is a key regulator of actin filament dynamics which is activated by dephosphorylation in response to elevated ROS levels *[Kim et al. 2009a]* or intracellular Ca^{2+} levels *[Meberg et al. 1998; Birkenfeld et al. 2001]*. Calcineurin is indirectly involved in Ca^{2+}-induced cofilin activation *[Wang et al. 2005]*.

In summary, a short-term HF diet-intervention influences the hypothalamic proteome by post-translational mechanisms that likely play an important part of the regulation. Altered proteins are implicated in mitochondrial function, especially related to complex I, as well as redox and calcium homeostasis. To our knowledge, none of the candidates have been shown to be influenced by HF feeding before. Notably, we demonstrate that some of the altered proteins are implicated in PD, suggesting an interaction or overlap of pathways involved in the development of obesity and neurodegenerative diseases.

4.2 High-fat feeding alters the isoform composition of the intracellular DJ-1 pool

DJ-1 undergoes several post-translational modifications and thus exists as a pool of isoforms differing in their pI *[Natale et al. 2010]*. Validation experiments showed that the composition of the DJ-1 pool is altered during HF diet-feeding with low pI isoforms becoming more abundant while more basic forms are decreased. For the hypothalamus, this finding was confirmed with three methods: two-dimensional gel electrophoresis (data not shown) and two IEF methods each of which were combined with semi-quantitative immunodetection of DJ-1.

Remarkably, a similar increase of low pI forms of DJ-1 has been observed in a variety of cells exposed to oxidative stresses such as hydrogen peroxide or paraquat and also in human brain samples under neurodegenerative conditions *[Mitsumoto & Nakagawa 2001; Bandopadhyay et al. 2004; Canet-Aviles et al. 2004; Kinumi et al. 2004; Taira et al. 2004; Zhou & Freed 2005; Choi et al. 2006; Kim et al. 2009b; Natale et al. 2010]*.

The pI of a DJ-1 isoform as detected by IEF does not certainly define the nature of modification. Murine DJ-1 contains 4 cysteines and 8 methionines which have the potential to undergo oxidation. The thiol group (-SH) of cysteines plays an important role in redox signaling as it can exist in a number of oxidation states: sulfenic (-SOH), sulfinic (-SO$_2$H), or sulfonic acid (-SO$_3$H) and as disulfide (-SS-) *[Reddie & Carroll 2008; Paulsen & Carroll 2010]*. In DJ-1, three cysteines are highly conserved (Cys-46, 53, 106) *[Bandyopadhyay & Cookson 2004; Waak et al. 2009]*. Oxidized cysteines have been identified in acidic DJ-1 isoforms, whereby Cys-106 is the most sensitive to oxidation (Fig. 4-2) *[Wilson et al. 2003; Canet-Aviles et al. 2004; Kinumi et al. 2004; Zhou et al. 2006; Inden et al. 2011]*. Cys-106 is critical for a number of functions of DJ-1. Mutations of this residue to other amino acids results in a loss of protective activity against oxidative stress in multiple systems *[Canet-Aviles et al. 2004; Blackinton et al. 2009; Waak et al. 2009; Im et al. 2010; Madian et al. 2012]*. The protective activity, however, seems to be dependent on the oxidation state since overoxidized DJ-1 is thermodynamically instable *[Hulleman et al. 2007]*, prone to aggregation *[Zhou et al. 2006]* and associated with aging and neurodegenerative diseases *[Blackinton et al. 2009; Miyama et al. 2011; Wilson 2011]*. Moreover, Cys-53 and Cys-46 are able to oxidize to a certain extent, disrupting the dimer formation *[Kinumi et al. 2004; Waak et al. 2009]* and methionine residues have been found oxidized to methionine sulfoxide *[Choi et al. 2006; Lin et al. 2012]*.
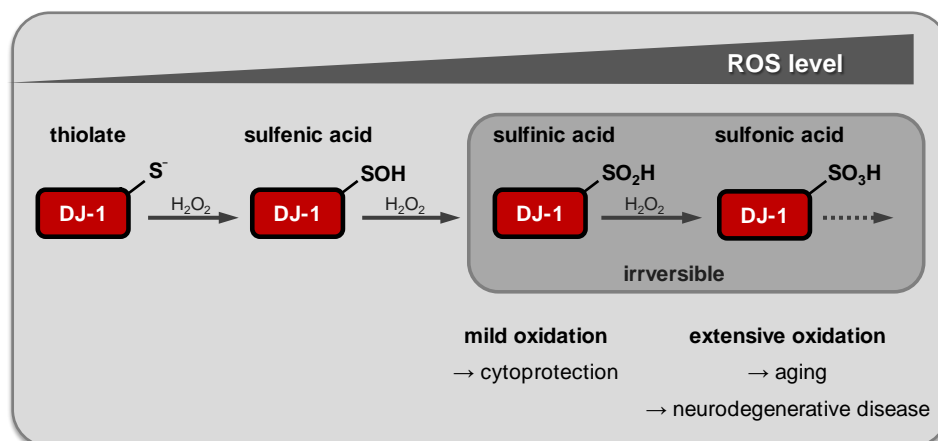
Fig. 4-2. Oxidative modification of DJ-1 Cys-106 with increasing ROS level. The thiolate (S⁻) can react with H_2O_2 to form sulfenic acid (SOH). Further reactions with H_2O_2 leads to formation of sufinic (SO_2H) and sulfonic (SO_3H) acid, which are regarded as irreversible oxoforms. The sulfinic acid of DJ-1 Cys-106 has been related to the cytoprotective activity of DJ-1, while further oxidation is linked to aging and neurodegenerative diseases. Modified from Paulsen & Carroll *[2010]* and Wilson *[2011]*.

Our study is the first to report that an acidic shift of DJ-1 isoforms can be induced by HF diet-feeding in mouse tissue. We detected this phenomenon in the hypothalamus and brain stem, two brain areas that are direct targets for circulating adiposity signals or satiety signals transmitted through the vagus nerve or sympathetic fibers, respectively (Fig. 1-1) *[Schwartz et al. 2000]*. However, a comparable shift occurred in the cerebellum and forebrain, indicating that the whole brain is affected. Moreover, the isoform pattern was altered in liver, pancreas, and skeletal muscle. The latter two showed the most pronounced effect of all tissues investigated, with 5 or 6 of the 7 detected isoforms, respectively, being significantly changed due to HF diet-feeding. Interestingly, this effect was not present in white adipose tissue. Since DJ-1 is ubiquitously expressed, a tissue- or organ-specific role seems unlikely but might nevertheless result from cell-specific DJ-1 binding partners. However, the obtained data suggests that the HF diet-induced shift of the DJ-1 pool towards more acidic isoforms correlates with the metabolic rate of the tissue, which decreases in the order muscle >> brain > liver >> adipose tissue *[Elia 1992]* (no reference was found for pancreas). Although the brain almost exclusively utilizes glucose as energy supply *[Peters et al. 2007]*, increased β-oxidation due to elevated fatty acid availability has been described for the hypothalamus *[Lam et al. 2005]*. Thus, DJ-1 modification might result from the HF diet-induced rise in β-oxidation along with a higher ROS production which is proportional to the metabolic activity of the organ.

The results listed above were detected after 10 days of HF diet-feeding. After two days of feeding, none of the DJ-1 isoforms were differentially abundant in the hypothalamus of HF or control diet-fed mice. After three months of HF diet-feeding, the increase of lower pI DJ-1

isoforms was observed in the hypothalamus but was less pronounced compared to the alterations after 10 days. However, due to high inter-assay coefficients of variation different runs cannot reliably be compared in a quantitative manner *[Besong Agbo et al.* 2013*]*.

These results indicate that the composition of the DJ-1 pool does not change acutely due to the mere presence of increased fatty acid levels but rather depends on a marked increase in body fat or other attributes associated with DIO and possibly age. However, the influence of the duration of exposure to HF diet and/or age on the alteration of the DJ-1 pool composition might be different in other tissues. DJ-1 is also found in blood *[Xu et al. 2010; Lin et al. 2012]*, which would be an interesting target for the evaluation of postprandial effects on DJ-1 modification.

We started to investigate whether the HF diet-induced shift of DJ-1 isoforms results from oxidation. First evidence indicates that the acidic isoforms likely represent indeed higher oxidized forms of DJ-1, as a comparable shift was observed when mouse brain lysate was treated with H_2O_2 (data not shown) [10]. Mass spectrometry based quantitative measurements of modified DJ-1 peptides were still ongoing at the time of writing this thesis.

It is still subject to debate, whether the oxidation of DJ-1 is reversible *in vivo [Blackinton et al. 2009]*. Reversibility of the acidic pI shift of DJ-1 was observed in mouse lung three hours after LPS treatment *[Mitsumoto & Nakagawa 2001]*, in human neuroblastoma cells after paraquat was removed *[Canet-Aviles et al. 2004]* and in a human lung carcinoma cell line four hours after UV radiation *[Shinbo et al. 2006]*, while DJ-1 oxidation could not be reversed in cultured human pneumocytes *[Duan et al. 2008]*. To date, no mechanism is known for the reduction of DJ-1Cys-106-SO$_2$. It was shown that it is not a substrate of sulfiredoxin that reduces cysteine sulfinic acids of peroxiredoxins which are antioxidant enzymes exerting their action through cysteine modification *[Woo et al. 2005; Andres-Mateos et al. 2007; Blackinton et al. 2009; Paulsen & Carroll 2010]*. Methionine sulfoxide can be reduced by the enzyme peptide methionine sulfoxide reductase *[Weissbach et al. 2002]*. Thus, if DJ-1 is functionally restored, it is probably cell-type specific and depends on the site and grade of oxidation or simply occurs by upregulation of protein synthesis and selective degradation of the oxidized form *[Canet-Aviles et al. 2004; Duan et al. 2008]*.

Assuming that DJ-1 is present in higher oxidized forms in tissues of HF diet-fed mice, we can speculate that high fat intake increases the generation of ROS *in vivo*. We manipulated the cellular redox capacity by supplementing the drinking water with N-acetylcysteine (NAC) to test if this influences the DJ-1 pool composition. NAC increases the redox capacity through elevating glutathione, which represents an important antioxidative system in the cell *[Fujii et al. 2011]*. Furthermore, NAC is able to penetrate cell membranes and cross the blood-brain barrier resulting in repletion of neuronal glutathione content *[Farr et*

---

[10] Experiments were carried out by Dr. Gereon Poschmann, MPL, Düsseldorf, Germany.

al. 2003; Berman et al. 2011]. We observed an increase in both reduced and oxidized glutathione in the brain and muscle after NAC treatment to comparable levels between HF and control diet-fed mice. The effect of NAC treatment on the formation of lower pI isoforms of DJ-1 was tested in the hypothalamus using the gel-based IEF method. The result was similar to what was obtained from the comparison of HF and control mice without NAC treatment suggesting that elevated glutathione levels do not influence DJ-1 oxidation at least in the hypothalamus. This experiment should be confirmed with the capillary IEF immunoassay, which is more sensitive and detected higher changes under basal conditions.

Previously, conflicting results were reported regarding the influence of HF diet-feeding on hypothalamic glutathione levels: GSH levels were increased in mice after three days of HF diet-feeding *[Jaillard et al. 2009]* while the GSSG-to-GSx ratio was twice as high in genetically obese compared to lean rats *[Colombani et al. 2009]*. In our study, glutathione levels were comparable between HF and control diet-fed mice in the brain and hypothalamus (data not shown) speaking against a connection of DJ-1 oxidation and glutathione homeostasis. In contrast, GSH was elevated by HF diet-feeding in the gastrocnemius muscle, the tissue in which the alteration of the DJ-1 pool was most pronounced. It was reported that DJ-1 increases GSH levels during oxidative stress through upregulation of glutamate cysteine ligase transcription and activity, which is involved in glutathione synthesis *[Zhou & Freed 2005]*. This function of DJ-1 was not directly shown to be dependent on its oxidation state but DJ-1 oxidation is enhanced when glutathione synthesis is inhibited and GSH levels drop *[Miyama et al. 2011]*. However, the transcription of glutamine cysteine ligase is regulated by several molecules *[Fujii et al. 2011]*. We suppose that oxidized DJ-1 and the supply of reduced glutathione act in parallel rather than in series to regulate redox homeostasis. Thus, it would be of interest to examine the DJ-1 isoform pattern in muscle after NAC treatment which resulted in elevated glutathione levels that were not longer different between HF and control diet-fed mice.

Within a cell, the cytosol contains most of the DJ-1 pool, but it is also found in the nucleus as well as mitochondria *[Nagakubo et al. 1997; Taira et al. 2004; Zhang et al. 2005a]*. Translocation to these two compartments is enhanced in response to oxidative stimuli and it was suggested that cysteine sulfinic acid formation at Cys-106 might be important but not necessarily required for the association of DJ-1 with mitochondria *[Canet-Aviles et al. 2004; Blackinton et al. 2005; Li et al. 2005; Lev et al. 2008; Blackinton et al. 2009; Junn et al. 2009]*. Here, we investigated the isoform distribution in cytosolic and mitochondrial fractions obtained from brain tissue of HF or control diet-fed mice. As expected, total signal intensities were lower in mitochondrial compared to cytosolic fractions. In mitochondria, one main isoform (pI 6.2) was observed, while other isoforms can hardly be detected. This indicates that heavy oxidation of DJ-1 is not a prerequisite to enable mitochondrial translocation. Regarding the individual

DJ-1 isoforms, no differences between HF and control diet-fed mice were observed in either cytosol or mitochondria. This result seems to contradict data obtained from whole tissue. However, the fractionation process involved several centrifugation steps, different buffers were used und protease and phosphatase inhibitors were not present from the beginning - factors which might influence protein modifications. Thus, the result cannot be directly compared to whole tissue. Nevertheless, a tendency towards decreased total DJ-1 content in mitochondria from HF diet-fed mice was observed using conventional western blot analysis as well as the capillary IEF (Fig. 3-11 C and 3-12 F). This finding suggests that the stimulus responsible for mitochondrial translocation is reduced in the brain upon HF feeding. We did not pay attention to the isoform distribution in the nucleus which might be interesting to investigate in future studies.

Finally, it is of interest what consequences the DJ-1 modifications in the context of HF feeding have. It is regarded unlikely, that DJ-1 possesses enzymatic activity *[Honbou et al. 2003; Wilson et al. 2003; Shendelman et al. 2004; Gorner et al. 2007]*. We and others show that acidic (oxidized) DJ-1 forms are present under physiological conditions indicating that severe oxidative stress is not required for oxidative modification *[Mitsumoto & Nakagawa 2001; Duan et al. 2008]*. We observed the HF diet-induced isoform shift of DJ-1 in the brain and peripheral tissues. Possibly, oxidation of DJ-1 is a response to ROS produced during aerobic metabolism *[Mitsumoto & Nakagawa 2001]*, which might be increased due to the systemic fatty acid overload. Oxidized or otherwise modified DJ-1 might then enable to adapt to the changed metabolic situation through several possible mechanisms: the interaction with proteins to regulate their activity or shuttling them to their place of action within the cell or through regulation of transcription (Fig. 4-3).

We analyzed the hypothalamic gene expression of several candidates known to be regulated by DJ-1 or affected by its absence. Of these genes, none were regulated by HF diet on transcript level in our mouse model (Supplementary Table S2). DJ-1 might yet affect other genes in response to HF diet-feeding. Furthermore, we co-immunoprecipitated direct or indirect DJ-1 binding partners from brain lysate of HF or control diet-fed mice[11] (Supplementary Table S15). Subsequent mass spectrometrical quantification revealed no differences in the protein abundances of co-precipitated proteins between the diet groups. Regarding the above hypothesis, the influence of HF diet-feeding on DJ-1 protein interaction is probably not due to stable binding but rather to temporary interaction influencing protein modifications.

---

[11] The experiment was conducted by Dr. Gereon Poschmann, MPL, Düsseldorf, Germany.

Overall, DJ-1 might constitute a sensor of the cellular redox state *[Wilson 2011]* with oxidation as a key regulatory modification relaying this information on to signaling pathways aiming to restore cellular homeostasis and adapt to altered metabolic situations.
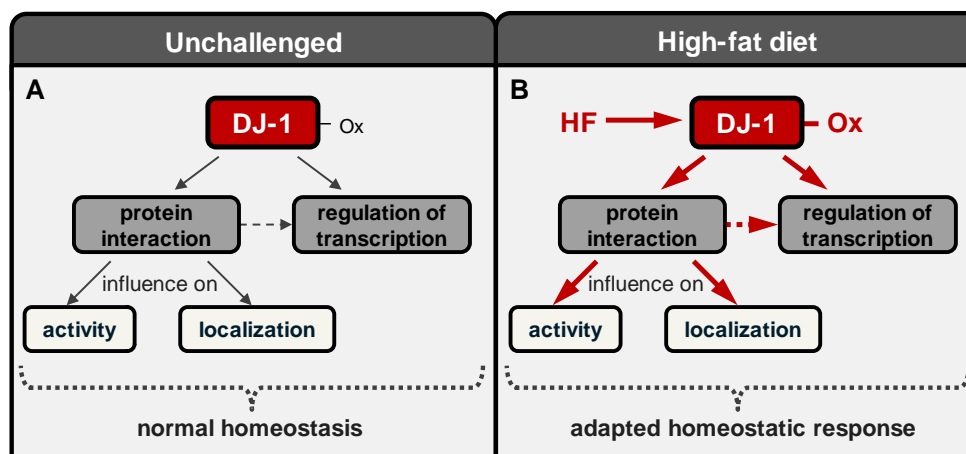
Fig. 4-3. Proposed mechanism of metabolic adaptation to nutrient abundance in the presence of DJ-1. (**A**) Under unchallenged conditions, a small amount of the DJ-1 pool is oxidized which can interact with other proteins to influence their activity or localization within the cell and regulate transcription directly or indirectly. Thereby, DJ-1 contributes to the maintenance of normal cellular homeostasis. (**B**) High-fat (HF) diet-feeding increases DJ-1 oxidation leading to enhanced DJ-1 action which helps to adapt the homeostatic system to the changed metabolic situation.

4.3   Brain mitochondria from high-fat diet-fed mice function normally

Obesity in humans is associated with increased systemic oxidative stress levels *[Keaney et al. 2003; Vincent & Taylor 2006; Vincent et al. 2007]*. We speculate that a change in the redox state is responsible for the HF diet-induced increase of acidic DJ-1 isoforms *in vivo*. Mitochondria release ROS as a physiological consequence of oxidative phosphorylation and several genes implicated in mitochondrial functions were regulated in the hypothalamus in the initial proteome study. Thus, we examined the generation of ROS in isolated brain mitochondria from mice fed a HF or control diet for 10 days. Hydrogen peroxide production rates were similar between the diet groups in the crude mitochondrial fraction as well as in mitochondria treated with sodium carbonate which detaches loosely associated proteins and represent a cleaner fraction (see Chapter 2.8, data not shown). However, mitochondria have been isolated from their physiological context, which might not necessarily allow a conclusion towards ROS production *in vivo* under the specific conditions induced by HF diet-feeding. Characterizing isolated mitochondria from HF and control diet-fed mice *ex vivo* rather shows

that they have the capability to function normally. Furthermore, cells contain other sources of ROS like NADPH oxidases which produce superoxide by transferring electrons from NADPH to molecular oxygen. NADPH oxidase-linked ROS generation is increased in the cerebral cortex of diet-induced obese rats *[Zhang et al. 2005b]*. We applied a method to detect ROS on the tissue level using a membrane-permeable dye which becomes fluorescent upon the reaction with hydrogen peroxide *[Benani et al. 2007]*. As before, hypothalamic ROS levels were not different after 10 days of HF diet as compared to controls *[Schöttl 2011]*.

Moreover, the protein abundance of the antioxidant enzyme SOD2 did not differ between HF and control diet-fed mice which is in line with the unchanged ROS production. However, studies on human cells suggest that few if any antioxidant enzymes are regulated by hydrogen peroxide *[Chuang et al. 2002; Weigel et al. 2002; Desaint et al. 2004]*.

Taken together, our data provide no evidence for altered ROS levels in the brain upon HF feeding. However, these results do not contradict our hypothesis that the HF diet-induced acidic DJ-1 isoform shift is due to changes in the redox state. Although ROS are generally regarded as a source of 'oxidative stress' able to damage macromolecules, an important part of ROS activity is exerted through their action on signaling pathways *[Maher & Schubert 2000]*. Within the hypothalamus, ROS play a role in glucose and lipid sensing *[Leloup et al. 2006; Benani et al. 2007; Colombani et al. 2009]* as well as in insulin-induced food intake inhibition *[Jaillard et al. 2009]*. The action of H_2O_2 as a second messenger to modulate protein function is likely locally restricted. As an example, H_2O_2 is generated in the vicinity of stimulated cell surface receptors and molecules that diffuse away from this place of action are rapidly destroyed *[Rhee et al. 2000; Paulsen & Carroll 2010]*. Measuring the overall H_2O_2 production, thus, is not very conclusive with regard to local concentrations.

Our data provide evidence that brain mitochondria function normally in the presence of increased systemic fatty acid levels. Thus, adaptation mechanisms towards altered substrate supply *in vivo* are thus of a physiological rather than pathophysiological nature.

4.4 Differences in phenotypic parameters of high-fat diet challenged *Dj-1-/-* compared to wildtype mice

Several mutations of the human *DJ-1* gene have been associated with inherited forms of PD *[Bonifati et al. 2003b]*. Surprisingly, none of the *Dj-1* mutant mouse lines resemble the typical PD phenotype with an age-dependent degeneration of dopaminergic neurons in the substantia nigra *[Chen et al. 2005; Goldberg et al. 2005; Kim et al. 2005b; Andres-Mateos et al. 2007; Pham et al. 2010]* and only minor motor deficits *[Chen et al. 2005; Chandran et al. 2008]*. However, DJ-1 is not only expressed in the brain and its molecular functions are very diverse due to the ability to interact with numerous proteins as well as with RNA, a feature that is influenced by changes in the redox state in many cases (see Chapter 1.4).

In this study, DJ-1 emerged as a candidate protein from the comparison of the hypothalamic proteome in response to a short-term HF or control diet intervention. Other proteome studies found DJ-1 upregulated by HF diet and hyperglycemic stimulation in mouse pancreatic islets of Langerhans *[Waanders et al. 2009]* or downregulated in the epididymal white adipose tissue (eWAT) of obese rats *[Joo et al. 2011]*. We therefore investigated the gene-diet interaction in *Dj-1* deficient mice (*Dj-1-/-*) in order to elucidate the physiological function of this protein in energy balance regulation.

Increased fat accumulation in high-fat diet challenged *Dj-1-/-* mice

After 14 weeks of HF-feeding, the body composition of *Dj-1-/-* mice was altered compared to wildtype littermates favoring higher fat accumulation at the expense of lean mass leaving the body mass unchanged. Assessing the level of DIO, body mass is most commonly focused on as the most important outcome, while the body partitioning is often neglected. However, the divergence of energy intake from energy expenditure over time can also be reflected by the relative amounts of fat and lean mass. Since these components show an almost 10-fold difference in their energy density, large shifts in body energy content can occur without altering the body mass *[Leibel 2008]*. Although ANCOVA analysis revealed a higher adiposity in both male and female mice after 14 weeks of HF diet, the level of DIO was much less pronounced in females. In our study, female wildtype mice placed on a HF diet at the age of 4 weeks were protected from DIO for the first 14 weeks after which they started to gain considerable amounts of fat with ongoing HF diet-feeding confirming sex-specific differences in the response to a HF diet *[Hwang et al. 2010]*. The differences in adiposity between male *Dj-1-/-* and *Dj-1+/+* mice were counterbalanced with ongoing HF-feeding. In contrast, female mice showed a higher HF diet-induced fat mass for the subcutaneous depot after 32 weeks of feeding. Probably, the counterbalancing is delayed in female mice and might be fat depot-dependent. Notably, muscle wet weights were reduced in aged male and female *Dj-1-/-* mice

independent of diet. It was formerly reported that the body mass of male $Dj-1^{-/-}$ mice was similar to wildtype mice in the first year after which it decreased progressively with age *[Chandran et al. 2008]*. Since body composition was not measured in this study, possibly, a reduced lean mass is causative for the reduced body mass observed in old $Dj-1^{-/-}$ mice.

The prolonged feeding, however, was conducted with a smaller sample size. During the 32 weeks of HF-feeding, approximately one third of the mice of both sexes did not respond to the HF diet. Animals were categorized as non-responders if their fat mass after 32 weeks of HF diet was not raised above twice the mean of control diet-fed mice (Supplementary Fig. S4) and thus were excluded from further analyses. We can exclude a litter effect because all obesity resistant mice originated from different litters with the size ranging from 3 to 9 pups which was representative of the overall litter size distribution (Supplementary Fig. S3). The percentage of DIO resistance is in accordance with a previous observation showing that 35 % of male C57BL/6J mice fed a HF diet for 20 weeks maintain a body mass comparable to chow diet-fed mice *[Enriori et al. 2007]*.

Glucose tolerance tests and further measurements were performed during the last two weeks of the feeding periods, which resulted in a slight drop of fat mass and/or body mass (Fig. 3-18 and 3-21). However, altered body composition was already present after 12 weeks of HF diet (Supplementary Fig. 5-6), so we can exclude the possibility that this phenotype is due to differences in susceptibility towards stress.

We conclude that the increased adiposity of HF diet-fed $Dj-1^{-/-}$ mice is a transient effect more pronounced during the development and adaptation phase to the HF diet. On the other hand, the decrease in muscle mass becomes distinct with higher age independent of diet. Having shown that the HF diet-induced modification of DJ-1 is most pronounced in skeletal muscle, the role of DJ-1 in this tissue should be focused on in future studies.

Dj-1 deficient mice are hypoactive without detectable changes in energy intake and energy expenditure

We studied which component of energy metabolism contributes to the altered body composition in male $Dj-1^{-/-}$ mice. Energy intake and metabolic rate were comparable in $Dj-1^{-/-}$ and $Dj-1^{+/+}$ mice. However, $Dj-1^{-/-}$ mice gained ~1 g more adipose tissue than wildtype mice within 14 weeks of HF diet. Neglecting lean mass and assuming 29 kJ energy per gram fat *[Klaus 2004]*, the difference amounts to 0.3 kJ per day. This translates into 0.7 % less energy expended (of 46 kJ/day) or 14 mg food consumed more by $Dj-1^{-/-}$ mice on a daily basis. To reliably detect such a small difference, the employed methods are not precise enough.

Energy expenditure is influenced by body mass as well as body composition, which has to be corrected for. We chose to normalize our data to body composition taking into account the differing metabolic activity of fat and lean tissue *[Even & Nadkarni 2012]* because this

method eliminates the body mass dependency (Fig. 3-25). When normalized to body composition, basal metabolic rate (HP$_{30°C,pa}$) was increased in female $Dj-1^{-/-}$ mice after 32 weeks of control diet-feeding and by tendency in male $Dj-1^{-/-}$ mice after 14 weeks HF diet-feeding. Notably, these are the groups in which $Dj-1^{-/-}$ mice displayed higher adiposity. A higher basal metabolic rate in the presence of less metabolic active tissue could be an explanation of the transience of the body composition phenotype.

Parameters of nocturnal spontaneous activity were decreased in $Dj-1^{-/-}$ mice compared to wildtype mice on control diet while the activity of HF diet-fed mice was comparable between the genotypes. Thus, HF feeding results in a drop of activity in wildtype mice but does not decrease further in $Dj-1^{-/-}$ mice. These results were obtained after 14 weeks of feeding. Analysis of activity in HF diet-fed mice after 32 weeks of feeding was inconclusive due to low animal numbers after exclusion of obesity-resistant mice. In male control diet-fed $Dj-1^{-/-}$ mice, however, we also observed a lower activity level compared to wildtype mice at this age (Supplementary Table S4). In female mice, no significant genotype differences were detected at this age due to very high inter-individual variation. Hypoactivity of $Dj-1$ deficient mice has been reported before as diminished horizontal and rearing activity *[Goldberg et al. 2005; Pham et al. 2010]*. Furthermore, old $Dj-1^{-/-}$ mice display reduced grip strength without any differences in gross muscle anatomy *[Chandran et al. 2008]*. Notably, our study shows that the reduced activity of $Dj-1^{-/-}$ mice is associated with a reduced lean mass. Yet, whether the reduced muscle mass is causative or a consequence of the hypoactivity needs further clarification. In favor of the first possibility is the fact that DJ-1 is linked to the regulation of calcium homeostasis in isolated mouse skeletal muscle cells *[Shtifman et al. 2011]*. Loss of $Dj-1$ leads to elevated resting intracellular Ca^{2+} concentrations and decreased Ca^{2+} release from the sarcoplasmic reticulum in response to electrical stimulation, both of which are partially reversed by the antioxidant glutathione or by activating mitochondrial function using resveratrol *[Shtifman et al. 2011]*. Calcium flux, however, is not only crucial for muscle contradiction but also stimulates the synthesis of dopamine in neurons of the substantia nigra which are degenerated in PD *(reviewed in Surmeier et al. [2011])*. Whether loss of $Dj-1$ similarly disrupts calcium homeostasis in the central nervous system remains to be shown.
In summary, the increased adiposity and decreased muscle mass in $Dj-1^{-/-}$ mice after 14 weeks of HF diet-feeding cannot be explained by the energy intake or energy expenditure measurements. Hypoactivity of $Dj-1^{-/-}$ mice likely contributes to this phenotype but this is obviously compensated under control diet conditions where adiposity is similar to wildtype mice. Possibly, an increased basal metabolic rate serves as a mechanism counter-regulating the altered body composition explaining the transience of this phenotype.

Dj-1 deficiency influences glucose levels without affecting glucose tolerance

Altered relative amounts of fat and lean mass may influence glucose metabolism. After 14 weeks of HF or control diet-feeding, we found altered plasma glucose levels in *ad libitum* fed male mice which were dependent of genotype and diet. Wildtype mice maintained similar glucose levels under HF and control diet but in order to do so produce, by trend, higher amounts of insulin under HF diet. Conclusively, HF diet-feeding induced insulin resistance of peripheral tissues which is reflected in increased HOMA-IR levels (not significant). Compared to wildtype mice, control diet-fed *Dj-1$^{-/-}$* mice have slightly lower glucose levels but in the presence of higher insulin levels. This indicates that *Dj-1* deficiency negatively influences peripheral insulin sensitivity already under control diet conditions. HF diet-challenge does not further increase insulin levels in *Dj-1$^{-/-}$* mice but they are not sufficient to retain normal glucose levels as is the case in wildtype mice. HOMA-IR indices on the other hand suggest that HF diet-feeding did not further aggravate insulin resistance in *Dj-1$^{-/-}$* mice. Insulin and HOMA-IR data, however, were not statistically significant due to high intra-group variability. This might be due to the fact that blood was taken from non-fasted mice although the time window of blood collection did not exceed 3.5 hours during the day time. The trend towards attenuated insulin sensitivity in unchallenged *Dj-1$^{-/-}$* mice regressed with age as this effect was not detected after 32 weeks of feeding.

Moreover, glucose clearance measured in an i.p. glucose tolerance test was comparable between *Dj-1$^{-/-}$* or *Dj-1$^{+/+}$* mice regardless of diet or age. Previously, a decreased glucose tolerance in male *Dj-1$^{-/-}$* mice at 12-13 weeks of age and in 8-week-old mice after two weeks of HF diet was described *[Jain et al. 2012]*. The glucose tolerance test differed from ours in the length of fasting before glucose injection (overnight vs. 6 hours), the diets used and the mouse model. In this publication, the impaired glucose tolerance in HF diet-fed *Dj-1$^{-/-}$* mice was accompanied by a blunted increase of insulin secretion 40 min after glucose injection and this finding was linked to a reduced β-cell area in *Dj-1$^{-/-}$* mice *[Jain et al. 2012]*. Considering this, we speculate that a period of peripheral insulin resistance with higher insulin secretion leads to the exhaustion and finally decay of β-cells comparable to type 2 diabetic patients and that this development might be accelerated in *Dj-1$^{-/-}$* mice. However, HF diet-feeding for 32 weeks resulted in higher absolute values of plasma insulin levels without any genotype differences (Table 3-9). This suggests that *Dj-1$^{-/-}$* mice can produce the same amount of insulin with a lower number of β-cells but this theory needs to be proven in further experiments.

Taken together, we suggest that peripheral insulin resistance in *Dj-1$^{-/-}$* mice coincides with the altered body composition observed after 14 weeks of HF feeding and that both phenotypes are transient effects.

Dj-1 deficiency does not influence anorectic leptin action

Another aspect observed in the pathophysiology of obesity is the loss of sensitivity towards leptin, a hormone secreted in proportion to the body fat stores *[Maffei et al. 1995; Considine et al. 1996; Schwartz et al. 1996]*. In the central nervous system, the afferent leptin signal exerts anorectic action representing a negative feedback mechanism for adiposity *[Friedman & Halaas 1998]*. In a state of leptin resistance, the central leptin action is blunted resulting in the disturbance of the negative feedback loop *[Münzberg et al. 2004; Münzberg & Myers 2005; Scarpace & Zhang 2009]*. Having shown that *Dj-1*^{-/-} mice accumulate more fat within 14 weeks of HF diet, we studied whether they differ in leptin sensitivity from their wildtype littermates. HF diet-fed wildtype mice displayed elevated phospho-STAT3 levels in the ventral hypothalamus compared to control diet-fed mice and by tendency a higher phospho-STAT3 to total STAT3 ratio. Since leptin levels are increased in HF diet-fed animals and STAT3 is phosphorylated upon leptin receptor activation, this indicates intact leptin signaling after 14 weeks of HF diet in wildtype mice. In contrast, HF diet-fed *Dj-1*^{-/-} mice displayed phospho-STAT3 levels comparable to control diet-fed mice. This result suggests that in HF diet-fed *Dj-1*^{-/-} mice the magnitude of the central response to circulating leptin levels is lower compared to wildtype mice.

Hence, we tested whether the physiological anorectic response to exogenous leptin is affected in *Dj-1*^{-/-} mice. In control diet-fed animals, the energy intake in the dark phase following i.p. leptin administration was reduced to a similar extent in wildtype and *Dj-1*^{-/-} mice. The anorectic response was attenuated in mice of both genotypes after 14 and 32 weeks of HF diet indicating comparable levels of leptin resistance.

Leptin reduces food intake in lean animals during a time window of 2 to 12 hours after application *[Myers et al. 2010]*. In our study, the mean decrease in energy intake 12 hours after i.p. leptin administration ranged from 14 to 20 % in control diet-fed mice (as compared to energy intake after PBS injections). This magnitude is similar to previous observations in male C57BL/6 mice showing a reduction of 25 % after administration of 2 mg*kg[-1] leptin on two consecutive days *[Enriori et al. 2007]* or a decrease of 11 % after the injection of 10 mg*kg[-1] leptin on three consecutive days *[van Heek et al. 1997]*. The average leptin-induced reduction of energy intake in HF diet-fed mice was 10-11 % after 14 weeks of feeding. A similar effect size was reported after 11 weeks of HF diet-feeding in male mice (13 % after 2 mg*kg[-1] leptin for 3 days) *[Kleinridders et al. 2009]*. After 32 weeks of HF-feeding, mice showed only a mean reduction in energy intake of 4 %. Obviously, a long period of HF feeding is required for the manifestation of leptin resistance in our DIO mouse model.

We observed a very high intra-group variability and high variability between the nocturnal food intake of individual mice. Due to textural differences, the spillage is much higher for HF compared to control diet and this could not be corrected for. For this reason,

mice had to be excluded resulting in low animal numbers. To obtain sufficient animal numbers in the HF groups, this was the only experiment in which obesity-resistant mice were included. They showed a stronger reduction in food intake after leptin injection indicating that leptin signaling is intact (Supplementary Fig. S8). Thus, the difference in energy intake between HF and control diet-fed mice is likely to be higher if the HF group consisted of only obesity-prone mice. Moreover, this indicates that leptin resistance is dependent on body mass and not solely on fat as a dietary constituent as has been suggested before *[Banks et al. 2004]*. Finally, we administered leptin only once. The anorectic response to leptin might be less heterogeneous when leptin is applied repeatedly as in the other studies *[van Heek et al. 1997; Enriori et al. 2007; Kleinridders et al. 2009]*.

Although STAT3 phosphorylation was higher in HF diet-fed wildtype mice compared to $Dj-1^{-/-}$ mice, the anorectic response to exogenous leptin was not different. However, basal STAT3 phosphorylation does not necessarily mirror inducible phospho-STAT3 levels upon exogenous leptin administration. Although leptin-induced STAT3 phosphorylation was similar in unchallenged $Dj-1^{-/-}$ and $Dj-1^{+/+}$ mice, this remains to be tested in HF diet-fed animals.

Conclusively, loss of $Dj-1$ does not influence leptin sensitivity in unchallenged mice and it seems unlikely that it does so under HF conditions.

4.5 High-fat diet has a greater impact on hypothalamic gene regulation in the absence of *Dj-1*

Multiple proteins sense and mediate the various peripheral signals implicated in the regulation of energy balance *[Leibel 2008]*. Moreover, the central response to signals like leptin is mediated through more than one pathway *[Myers et al. 2008]*. We therefore chose an unbiased approach to identify factors involved in energy balance regulation and performed a transcriptome analysis of the ventral hypothalamus comparing HF or control diet fed *Dj-1⁻/⁻* and *Dj-1⁺/⁺* mice. This part of the hypothalamus includes the arcuate nucleus (ARC) and ventromedial nucleus, two main areas involved in energy homeostasis and satiety. The four experimental groups were compared pairwise and the results separated into regulation by diet or regulation by genotype.

Using very stringent statistical methods, no genes were differentially expressed between HF and control diet-fed mice. Possibly, there is a stronger effect in earlier phases during HF diet-feeding but once the body is adapted to the new metabolic situation and defends the state of adiposity *[Wisse et al. 2007; Leibel 2008]*, the influence of HF diet on gene expression decreases. Regarding the genes regulated by genotype in both diet groups, a substantial amount (70 %) locate to chromosome 4 which harbors the *Dj-1* (*Park7*) gene that was disrupted by the introduction of a gene trap vector in *Dj-1⁻/⁻* mice. There are two possible explanations for this: First, this might be an allele effect resulting from the generation of *Dj-1⁻/⁻* mice. ES cell clones were derived from the 129P2/OLaHsd mouse strain, injected into blastocystes of C57BL/6J mice and resulting chimeras were mated with C57BL/6J mice generating heterozygous mice *[Pham et al. 2010]*. Theoretically, every round of backcrossing with C57BL/6J wildtype mice reduces the heterozygosity by 50 %. Mice used in this study had been backcrossed onto C57BL/6J background for 11 generations leaving only 0.1 % of the genome heterozygous. However, this is only true for those parts of the genome that are not in high linkage disequilibrium with the differential gene. Since the *Dj-1* locus is the selection criteria during breeding, loci in high linkage disequilibrium with this locus are also selected for. Thus, the heterozygosity of this region has to be regarded more critical compared to the rest of the genome.

Second, this region might represent a functional gene cluster and the insertion of the gene trap vector into the *Dj-1* locus disrupts a cis-regulatory element of these genes. In this case, effects attributed to the loss of *Dj-1* rather have to be interpreted as the combined effect of several genes. Moreover, conclusions regarding the function of *Dj-1* drawn from this mouse model cannot be transferred to other species, since i.e. in humans *DJ-1* is located on chromosome 1.

Considering that comparing 4-5 animals per genotype-diet group does not have a high statistical power, we reanalyzed the transcriptome data using simple t-tests in order to extend the list of possible candidates. Although we are aware that the false positive rate may be high (and thus, individual genes shall not be discussed), this less stringent statistical approach led to an interesting finding considering the number of regulated genes. Overall, we observed a higher number of genes to be regulated by genotype within the diet groups than by diet within genotype comparisons. Prominently, the combination of *Dj-1* deficiency and HF diet showed the greatest effect on gene expression: The number of genes regulated by diet in *Dj-1*$^{-/-}$ mice exceeded the number in wildtype mice by 40 % and twice as many genes were regulated by genotype within the HF group compared to the control group (Fig. 3-33)[12]. This indicates that the *Dj-1* deficiency combined with a HF diet causes greater adaptation on gene expression level compared to the isolated effects of *Dj-1* deficiency or HF diet-feeding. Still, interesting candidates detected by transcriptome analyses need to be validated for biological relevance in further experiments examining their protein content and activity level.

Additionally, we used the extended candidate list to conduct a pathway analysis focusing on associated disease pathways. Regarding pathways linked to metabolic diseases, several were associated with the genes regulated by diet independent of genotype including 'Hyperglycemia' and 'Diabetes Mellitus' (Fig. 3-34 A). This is remarkable considering that the diet regulated genes did not overlap between wildtype and *Dj-1*$^{-/-}$ mice except for *Etv6*. Furthermore, genes of the pathway 'Inflammation' were overrepresented in diet-regulated genes of wildtype as well as *Dj-1*$^{-/-}$ mice. This phenomenon is in line with current knowledge stating that inflammatory processes occur within the hypothalamus under HF diet consumption and obesity (Chapter 1.2.2) *[De Souza et al. 2005; Posey et al. 2009; Wisse & Schwartz 2009; Thaler et al. 2010; Thaler et al. 2012]*. On the other hand, several pathways linked to the diet-regulated genes were dependent on genotype. Interestingly, the pathways 'Obesity/Overweight/Overnutrition' and 'Body weight' were only associated with diet regulated genes in the absence of *Dj-1*. Moreover, genotype-regulated genes were associated with metabolic disease pathways only under HF diet-feeding. It has to be pointed out that differentially regulated genes linked to certain disease pathways do not necessarily imply the presence of this disease as they might also refer to protective mechanisms depending on the direction of regulation. We rather conclude that more mechanisms counter-regulating obesity might occur in *Dj-1*$^{-/-}$ mice. As mentioned above, diet-induced gene regulation might be more pronounced in earlier phases during the feeding period. Thus, this finding indicates that regulatory mechanisms need longer to settle on a higher state of

---

[12] Excluding genes on chromosome 4, the number of genotype-regulated genes within the HF diet group still exceeded the number in the control group.

adiposity in *Dj-1*$^{-/-}$ mice compared to wildtype mice and reflects the transiently increased adipose tissue.

Several compensatory mechanisms in *Dj-1* deficient mice have previously been described including the upregulation of antioxidant enzymes *[Andres-Mateos et al. 2007]* and increased mitochondrial complex activities *[Pham et al. 2010]*. This is not due to an increased number of mitochondria since we show that the content of mitochondria is similar between *Dj-1* deficient and wildtype mice in brain, skeletal muscle and white adipose tissue under unchallenged conditions. Interestingly, the pathway 'Mitochondrial Diseases' was associated with the diet-regulated genes in *Dj-1*$^{-/-}$ mice. Based on this finding, we speculate that HF feeding has a greater impact on mitochondrial function in the absence of *Dj-1*$^{-/-}$ and that mitochondria play an important role in the adaptation to the metabolic changes induced by HF feeding. Follow-up experiments are needed to substantiate this hypothesis.

Most importantly, several of the regulated genes were associated with pathways linked to neurodegenerative diseases or behavior. Pathways of this category were associated with diet-regulated genes only in wildtype mice implying that HF feeding affects genes that play a role in cognitive function. A negative association of obesity and cognition was suggested in a body of literature (see Chapter 1.3). No pathways related to neurodegeneration or behavior were linked to diet-regulated genes in *Dj-1*$^{-/-}$ mice. Probably, unchallenged *Dj-1*$^{-/-}$ mice already exhibit a gene regulation in the same direction. Regarding genotype-regulated genes, the number of associated pathways was indeed much higher in mice fed a HF diet. Remarkably, genes of the pathways 'Parkinson Disease' and 'Parkinsonian Disorders' were only overrepresented when *Dj-1*$^{-/-}$ and wildtype mice were compared under HF conditions. Since unchallenged *Dj-1* deficient mice do not show a typical Parkinson phenotype, additional cues or challenges like feeding a HF diet are probably needed to trigger neurodegenerative pathologies in this mouse model. Therefore, we propose that behavioral tests are carried out under HF diet challenge in order to detect deficits related to PD in this *Dj-1* deficient mouse line.

Taken together, we observed that the HF diet triggered a more complex gene regulation pattern in the hypothalamus of *Dj-1*$^{-/-}$ mice, suggesting that *Dj-1* is important for mechanisms of HF diet-induced adaptation while in its absence there is a higher need for counter-regulatory mechanisms. Having shown that with prolonged HF feeding the effect of increased body fat accumulation is a transient phenomenon, homeostatic pathways in *Dj-1* deficient mice might need longer to settle on a higher level of defended body mass.

In summary, the susceptibility of *Dj-1$^{-/-}$* mice to DIO is similar to wildtype mice with regard to body mass development but HF diet-feeding resulted in higher fat accumulation in *Dj-1$^{-/-}$* mice at the expense of lean mass. This effect was present in both sexes. Because the diet-induced obese phenotype was less pronounced in females, we concentrated on male mice investigating possible mechanisms underlying this phenotype. The changes in body composition could not be explained by measurable alterations in energy intake or expenditure while locomotor activity was generally lower in *Dj-1$^{-/-}$* mice. Our data imply that *Dj-1* deficiency and HF feeding interact to influence glucose levels and hypothalamic STAT3 phosphorylation without affecting glucose tolerance or anorectic leptin action. Transcriptome analyses of the ventral hypothalamus showed that HF diet-feeding triggers a more complex gene regulation pattern in the absence of *Dj-1*. From these findings, we speculate that DJ-1 exerts a stabilizing function under HF diet challenge and mice cope less efficient with the metabolic changes induced by a HF diet challenge in the absence of *Dj-1*. We earlier concluded that DJ-1 contributes to the maintenance of normal cellular homeostasis (Fig. 4-3 A). DJ-1 senses cellular changes induced by HF diet-feeding and relays this information on to signaling pathways by means of protein modification resulting in the adaptation of homeostasis (Fig. 4-3 B). Thus, in the absence of DJ-1, normal homeostasis needs to be sustained through other mechanisms which compensate the lacking DJ-1 action (Fig. 4-4 A) and prevent a stronger phenotype. When *Dj-1* deficient mice are challenged with a HF diet, these or other compensatory mechanisms need to be upregulated to enable a homeostatic adaptation (Fig. 4-4 B).
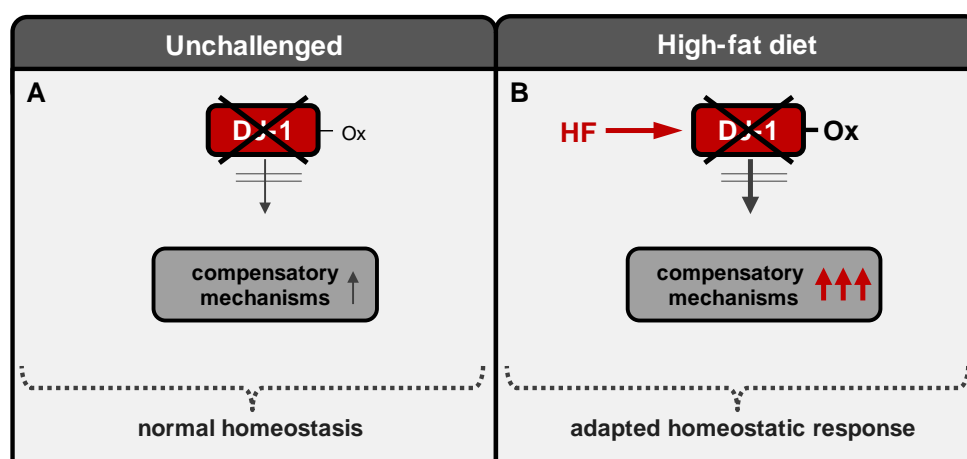
Fig. 4-4. Proposed mechanism of metabolic adaptation to nutrient abundance in the absence of DJ-1. (A) DJ-1 contributes to the maintenance of normal cellular homeostasis. Without DJ-1, normal homeostasis is sustained through other mechanisms compensating the lacking DJ-1 action. **(B)** Upon HF diet-feeding, compensatory mechanisms are upregulated to enable the homeostatic adaptation in the absence of DJ-1.

Most importantly, the altered body composition constitutes a transient effect depending on length of feeding and/or age. Compensational mechanisms are eventually able to counter-balance the accelerated HF diet-induced changes to the level of DIO wildtype mice. Conclusively, in the absence of *Dj-1* it might simply take longer to reach a new steady state of energy balance regulation under HF challenge.

Finally, our study supports a possible convergence or interaction of molecular pathways involved in obesity and neurodegeneration. As mentioned in the introduction, the threshold for developing age-related neurodegenerative diseases may be lowered by obesity-associated metabolic changes (Chapter 1.3). In the future, more experimental studies are needed to investigate the extent to which metabolic derangements affect mental health to eventually answer the question of how important fighting obesity and related disorders is for the prevention of neurodegenerative diseases in humans.

5 REFERENCES

Abbott RD, Ross GW, White LR, Nelson JS, Masaki KH, Tanner CM, Curb JD*, et al.* (2002) Midlife adiposity and the future risk of Parkinson's disease. *Neurology.* 59, 1051-7.

Abou-Sleiman PM, Muqit MM and Wood NW (2006) Expanding insights of mitochondrial dysfunction in Parkinson's disease. *Nature reviews. Neuroscience.* 7, 207-19.

Akerman KE and Wikstrom MK (1976) Safranine as a probe of the mitochondrial membrane potential. *FEBS letters.* 68, 191-7.

Akira S (2003) Toll-like receptor signaling. *The Journal of biological chemistry.* 278, 38105-8.

Aleyasin H, Rousseaux MW, Marcogliese PC, Hewitt SJ, Irrcher I, Joselin AP, Parsanejad M*, et al.* (2010) DJ-1 protects the nigrostriatal axis from the neurotoxin MPTP by modulation of the AKT pathway. *Proc.Natl.Acad.Sci.U.S.A.* 107, 3186-3191.

Andres-Mateos E, Perier C, Zhang L, Blanchard-Fillion B, Greco TM, Thomas B, Ko HS*, et al.* (2007) DJ-1 gene deletion reveals that DJ-1 is an atypical peroxiredoxin-like peroxidase. *Proc.Natl.Acad.Sci.U.S.A.* 104, 14807-14812.

Arch JR, Hislop D, Wang SJ and Speakman JR (2006) Some mathematical and technical issues in the measurement and interpretation of open-circuit indirect calorimetry in small animals. *International journal of obesity.* 30, 1322-31.

Bader V, Ran Z, X, Lubbert H and Stichel CC (2005) Expression of DJ-1 in the adult mouse CNS. *Brain Res.* 1041, 102-111.

Bagdade JD, Bierman EL and Porte D, Jr. (1967) The significance of basal insulin levels in the evaluation of the insulin response to glucose in diabetic and nondiabetic subjects. *The Journal of clinical investigation.* 46, 1549-57.

Bandopadhyay R, Kingsbury AE, Cookson MR, Reid AR, Evans IM, Hope AD, Pittman AM*, et al.* (2004) The expression of DJ-1 (PARK7) in normal human CNS and idiopathic Parkinson's disease. *Brain.* 127, 420-430.

Bandyopadhyay S and Cookson MR (2004) Evolutionary and functional relationships within the DJ1 superfamily. *BMC evolutionary biology.* 4, 6.

Banks WA, Coon AB, Robinson SM, Moinuddin A, Shultz JM, Nakaoke R and Morley JE (2004) Triglycerides induce leptin resistance at the blood-brain barrier. *Diabetes.* 53, 1253-1260.

Bell CG, Walley AJ and Froguel P (2005) The genetics of human obesity. *Nature reviews. Genetics.* 6, 221-34.

Benani A, Troy S, Carmona MC, Fioramonti X, Lorsignol A, Leloup C, Casteilla L*, et al.* (2007) Role for mitochondrial reactive oxygen species in brain lipid sensing: redox regulation of food intake. *Diabetes.* 56, 152-60.

Bence KK, Delibegovic M, Xue B, Gorgun CZ, Hotamisligil GS, Neel BG and Kahn BB (2006) Neuronal PTP1B regulates body weight, adiposity and leptin action. *Nature medicine.* 12, 917-24.

Benjamini Y and Hochberg Y (1995) Controlling the False Discovery Rate: A Practical and Powerful Approach to Multiple Testing. *Journal of the Royal Statistical Society. Series B (Methodological).* 57, 289-300.

Benoit SC, Kemp CJ, Elias CF, Abplanalp W, Herman JP, Migrenne S, Lefevre AL*, et al.* (2009) Palmitic acid mediates hypothalamic insulin resistance by altering PKC-theta subcellular localization in rodents. *The Journal of clinical investigation.* 119, 2577-89.

Berman AE, Chan WY, Brennan AM, Reyes RC, Adler BL, Suh SW, Kauppinen TM*, et al.* (2011) N-acetylcysteine prevents loss of dopaminergic neurons in the EAAC1-/- mouse. *Annals of neurology.* 69, 509-20.

Besong Agbo D, Klafki H, Poschmann G, Seyfarth K, Genius J, Stühler K, Wurst W*, et al.* (2013) Development of a Capillary Isoelectric Focusing Immunoassay to Measure DJ-1 Isoforms in Biological Samples. *Anal Biochem.* 443(2),197-204

Birkenfeld J, Kartmann B, Betz H and Roth D (2001) Cofilin activation during Ca(2+)-triggered secretion from adrenal chromaffin cells. *Biochemical and biophysical research communications.* 286, 493-8.

Bjorbaek C, El-Haschimi K, Frantz JD and Flier JS (1999) The role of SOCS-3 in leptin signaling and leptin resistance. *J Biol.Chem.* 274, 30059-30065.

Blackinton J, Ahmad R, Miller DW, van der Brug MP, Canet-Aviles RM, Hague SM, Kaleem M*, et al.* (2005) Effects of DJ-1 mutations and polymorphisms on protein stability and subcellular localization. *Brain research. Molecular brain research.* 134, 76-83.

Blackinton J, Lakshminarasimhan M, Thomas KJ, Ahmad R, Greggio E, Raza AS, Cookson MR*, et al.* (2009) Formation of a stabilized cysteine sulfinic acid is critical for the mitochondrial function of the parkinsonism protein DJ-1. *J Biol.Chem.* 284, 6476-6485.

Blouet C and Schwartz GJ (2010) Hypothalamic nutrient sensing in the control of energy homeostasis. *Behavioural brain research.* 209, 1-12.

Bonifati V, Rizzu P, Squitieri F, Krieger E, Vanacore N, van Swieten JC, Brice A*, et al.* (2003a) DJ-1(PARK7), a novel gene for autosomal recessive, early onset parkinsonism. *Neurol.Sci.* 24, 159-160.

Bonifati V, Rizzu P, van Baren MJ, Schaap O, Breedveld GJ, Krieger E, Dekker MC*, et al.* (2003b) Mutations in the DJ-1 gene associated with autosomal recessive early-onset parkinsonism. *Science.* 299, 256-259.

Bourges I, Ramus C, Mousson de Camaret B, Beugnot R, Remacle C, Cardol P, Hofhaus G*, et al.* (2004) Structural organization of mitochondrial human complex I: role of the ND4 and ND5 mitochondria-encoded subunits and interaction with prohibitin. *The Biochemical journal.* 383, 491-9.

Broberger C, Johansen J, Johansson C, Schalling M and Hokfelt T (1998) The neuropeptide Y/agouti gene-related protein (AGRP) brain circuitry in normal, anorectic, and monosodium glutamate-treated mice. *Proceedings of the National Academy of Sciences of the United States of America.* 95, 15043-8.

Brown RE (2008) Could there be a fine-tuning role for brain-derived adipokines in the regulation of bodyweight and prevention of obesity? *McGill journal of medicine : MJM : an international forum for the advancement of medical sciences by students.* 11, 177-84.

Bruce-Keller AJ, Keller JN and Morrison CD (2009) Obesity and vulnerability of the CNS. *Biochimica et biophysica acta.* 1792, 395-400.

Canet-Aviles RM, Wilson MA, Miller DW, Ahmad R, McLendon C, Bandyopadhyay S, Baptista MJ*, et al.* (2004) The Parkinson's disease protein DJ-1 is neuroprotective due to cysteine-sulfinic acid-driven mitochondrial localization. *Proc.Natl.Acad.Sci.U.S.A.* 101, 9103-9108.

Chandran JS, Lin X, Zapata A, Hoke A, Shimoji M, Moore SO, Galloway MP*, et al.* (2008) Progressive behavioral deficits in DJ-1-deficient mice are associated with normal nigrostriatal function. *Neurobiol.Dis.* 29, 505-514.

Chen H, Zhang SM, Schwarzschild MA, Hernan MA, Willett WC and Ascherio A (2004) Obesity and the risk of Parkinson's disease. *Am.J Epidemiol.* 159, 547-555.

Chen L, Cagniard B, Mathews T, Jones S, Koh HC, Ding Y, Carvey PM*, et al.* (2005) Age-dependent motor deficits and dopaminergic dysfunction in DJ-1 null mice. *J Biol.Chem.* 280, 21418-21426.

Cheng A, Uetani N, Simoncic PD, Chaubey VP, Lee-Loy A, McGlade CJ, Kennedy BP*, et al.* (2002) Attenuation of leptin action and regulation of obesity by protein tyrosine phosphatase 1B. *Developmental cell.* 2, 497-503.

Cheng J, Tang W, Su Z, Guo J, Tong L and Wei Q (2012) Calcineurin subunit B promotes TNF-alpha-induced apoptosis by binding to mitochondria and causing mitochondrial Ca2+ overload. *Cancer letters.* 321, 169-78.

Choi J, Sullards MC, Olzmann JA, Rees HD, Weintraub ST, Bostwick DE, Gearing M*, et al.* (2006) Oxidative damage of DJ-1 is linked to sporadic Parkinson and Alzheimer diseases. *J Biol.Chem.* 281, 10816-10824.

Choi JY, Jang EH, Park CS and Kang JH (2005) Enhanced susceptibility to 1-methyl-4-phenyl-1,2,3,6-tetrahydropyridine neurotoxicity in high-fat diet-induced obesity. *Free Radic.Biol.Med.* 38, 806-816.

Chuang YY, Chen Y, Gadisetti, Chandramouli VR, Cook JA, Coffin D, Tsai MH*, et al.* (2002) Gene expression after treatment with hydrogen peroxide, menadione, or t-butyl hydroperoxide in breast cancer cells. *Cancer research*. 62, 6246-54.

Clements CM, McNally RS, Conti BJ, Mak TW and Ting JP (2006) DJ-1, a cancer- and Parkinson's disease-associated protein, stabilizes the antioxidant transcriptional master regulator Nrf2. *Proc.Natl.Acad.Sci.U.S.A.* 103, 15091-15096.

Colombani AL, Carneiro L, Benani A, Galinier A, Jaillard T, Duparc T, Offer G*, et al.* (2009) Enhanced hypothalamic glucose sensing in obesity: alteration of redox signaling. *Diabetes.* 58, 2189-97.

Cone RD, Cowley MA, Butler AA, Fan W, Marks DL and Low MJ (2001) The arcuate nucleus as a conduit for diverse signals relevant to energy homeostasis. *International journal of obesity and related metabolic disorders : journal of the International Association for the Study of Obesity.* 25 Suppl 5, S63-7.

Considine RV, Sinha MK, Heiman ML, Kriauciunas A, Stephens TW, Nyce MR, Ohannesian JP*, et al.* (1996) Serum immunoreactive-leptin concentrations in normal-weight and obese humans. *The New England journal of medicine*. 334, 292-5.

Cookson MR (2003) Pathways to Parkinsonism. *Neuron*. 37, 7-10.

Cota D, Proulx K, Smith KA, Kozma SC, Thomas G, Woods SC and Seeley RJ (2006) Hypothalamic mTOR signaling regulates food intake. *Science*. 312, 927-30.

Coupe B and Bouret SG (2012) Weighing on autophagy: a novel mechanism for the CNS regulation of energy balance. *Cell cycle*. 11, 1477-8.

Cullheim S and Thams S (2007) The microglial networks of the brain and their role in neuronal network plasticity after lesion. *Brain research reviews*. 55, 89-96.

da Costa CA (2007) DJ-1: a newcomer in Parkinson's disease pathology. *Current molecular medicine*. 7, 650-7.

Daniels SR (2009) Complications of obesity in children and adolescents. *International journal of obesity*. 33 Suppl 1, S60-5.

Darios F, Corti O, Lucking CB, Hampe C, Muriel MP, Abbas N, Gu WJ*, et al.* (2003) Parkin prevents mitochondrial swelling and cytochrome c release in mitochondria-dependent cell death. *Human molecular genetics*. 12, 517-26.

Das F, Dey N, Venkatesan B, Kasinath BS, Ghosh-Choudhury N and Choudhury GG (2011) High glucose upregulation of early-onset Parkinson's disease protein DJ-1 integrates the PRAS40/TORC1 axis to mesangial cell hypertrophy. *Cell Signal.* 23, 1311-1319.

De Souza CT, Araujo EP, Bordin S, Ashimine R, Zollner RL, Boschero AC, Saad MJ*, et al.* (2005) Consumption of a fat-rich diet activates a proinflammatory response and induces insulin resistance in the hypothalamus. *Endocrinology*. 146, 4192-4199.

Desaint S, Luriau S, Aude JC, Rousselet G and Toledano MB (2004) Mammalian antioxidant defenses are not inducible by H2O2. *The Journal of biological chemistry*. 279, 31157-63.

Doherty GH (2011) Obesity and the ageing brain: could leptin play a role in neurodegeneration? *Current gerontology and geriatrics research*. 2011, 708154.

Duan X, Kelsen SG and Merali S (2008) Proteomic analysis of oxidative stress-responsive proteins in human pneumocytes: insight into the regulation of DJ-1 expression. *Journal of proteome research*. 7, 4955-61.

Duchen MR, Verkhratsky A and Muallem S (2008) Mitochondria and calcium in health and disease. *Cell calcium*. 44, 1-5.

Elia M (1992) Organ and tissue contribution to metabolic rate. In: *Energy metabolism : tissue determinants and cellular corollaries*. Tucker, HN and Kinney, JM (eds.), pp 61-80, Raven Press New York

Emanuelli B, Peraldi P, Filloux C, Sawka-Verhelle D, Hilton D and Van Obberghen E (2000) SOCS-3 is an insulin-induced negative regulator of insulin signaling. *The Journal of biological chemistry*. 275, 15985-91.

Enriori PJ, Evans AE, Sinnayah P, Jobst EE, Tonelli-Lemos L, Billes SK, Glavas MM*, et al.* (2007) Diet-induced obesity causes severe but reversible leptin resistance in arcuate melanocortin neurons. *Cell Metab*. 5, 181-194.

Ernst MB, Wunderlich CM, Hess S, Paehler M, Mesaros A, Koralov SB, Kleinridders A*, et al.* (2009) Enhanced Stat3 activation in POMC neurons provokes negative feedback inhibition of leptin and insulin signaling in obesity. *The Journal of neuroscience : the official journal of the Society for Neuroscience.* 29, 11582-93.

Even PC and Nadkarni NA (2012) Indirect calorimetry in laboratory mice and rats: principles, practical considerations, interpretation and perspectives. *American journal of physiology. Regulatory, integrative and comparative physiology.* 303, R459-76.

Fan J, Ren H, Fei E, Jia N, Ying Z, Jiang P, Wu M*, et al.* (2008a) Sumoylation is critical for DJ-1 to repress p53 transcriptional activity. *FEBS Lett.* 582, 1151-1156.

Fan J, Ren H, Jia N, Fei E, Zhou T, Jiang P, Wu M*, et al.* (2008b) DJ-1 decreases Bax expression through repressing p53 transcriptional activity. *J Biol.Chem.* 283, 4022-4030.

Fan W, Boston BA, Kesterson RA, Hruby VJ and Cone RD (1997) Role of melanocortinergic neurons in feeding and the agouti obesity syndrome. *Nature.* 385, 165-8.

Farooqui AA, Farooqui T, Panza F and Frisardi V (2012) Metabolic syndrome as a risk factor for neurological disorders. *Cellular and molecular life sciences : CMLS.* 69, 741-62.

Farr SA, Poon HF, Dogrukol-Ak D, Drake J, Banks WA, Eyerman E, Butterfield DA*, et al.* (2003) The antioxidants alpha-lipoic acid and N-acetylcysteine reverse memory impairment and brain oxidative stress in aged SAMP8 mice. *Journal of neurochemistry.* 84, 1173-83.

Farr SA, Yamada KA, Butterfield DA, Abdul HM, Xu L, Miller NE, Banks WA*, et al.* (2008) Obesity and hypertriglyceridemia produce cognitive impairment. *Endocrinology.* 149, 2628-36.

Fernandes AP and Holmgren A (2004) Glutaredoxins: glutathione-dependent redox enzymes with functions far beyond a simple thioredoxin backup system. *Antioxidants & redox signaling.* 6, 63-74.

Ferrer I, Perez E, Dalfo E and Barrachina M (2007) Abnormal levels of prohibitin and ATP synthase in the substantia nigra and frontal cortex in Parkinson's disease. *Neuroscience letters.* 415, 205-9.

Friedman JM and Halaas JL (1998) Leptin and the regulation of body weight in mammals. *Nature.* 395, 763-770.

Fu K, Ren H, Wang Y, Fei E, Wang H and Wang G (2012) DJ-1 inhibits TRAIL-induced apoptosis by blocking pro-caspase-8 recruitment to FADD. *Oncogene.* 31, 1311-1322.

Fujii J, Ito JI, Zhang X and Kurahashi T (2011) Unveiling the roles of the glutathione redox system in vivo by analyzing genetically modified mice. *Journal of clinical biochemistry and nutrition.* 49, 70-8.

Gale SM, Castracane VD and Mantzoros CS (2004) Energy homeostasis, obesity and eating disorders: recent advances in endocrinology. *The Journal of nutrition.* 134, 295-8.

Giaime E, Yamaguchi H, Gautier CA, Kitada T and Shen J (2012) Loss of DJ-1 Does Not Affect Mitochondrial Respiration but Increases ROS Production and Mitochondrial Permeability Transition Pore Opening. *PLoS.One.* 7, e40501.

Goldberg MS, Pisani A, Haburcak M, Vortherms TA, Kitada T, Costa C, Tong Y*, et al.* (2005) Nigrostriatal dopaminergic deficits and hypokinesia caused by inactivation of the familial Parkinsonism-linked gene DJ-1. *Neuron.* 45, 489-496.

Gonzalez-Polo R, Niso-Santano M, Moran JM, Ortiz-Ortiz MA, Bravo-San Pedro JM, Soler G and Fuentes JM (2009) Silencing DJ-1 reveals its contribution in paraquat-induced autophagy. *Journal of neurochemistry.* 109, 889-98.

Gorner K, Holtorf E, Waak J, Pham TT, Vogt-Weisenhorn DM, Wurst W, Haass C*, et al.* (2007) Structural determinants of the C-terminal helix-kink-helix motif essential for protein stability and survival promoting activity of DJ-1. *J Biol.Chem.* 282, 13680-13691.

Gunstad J, Paul RH, Cohen RA, Tate DF, Spitznagel MB and Gordon E (2007) Elevated body mass index is associated with executive dysfunction in otherwise healthy adults. *Comprehensive psychiatry.* 48, 57-61.

Guzman JN, Sanchez-Padilla J, Wokosin D, Kondapalli J, Ilijic E, Schumacker PT and Surmeier DJ (2010) Oxidant stress evoked by pacemaking in dopaminergic neurons is attenuated by DJ-1. *Nature.* 468, 696-700.

Hashimoto M, Rockenstein E, Mante M, Mallory M and Masliah E (2001) beta-Synuclein inhibits alpha-synuclein aggregation: a possible role as an anti-parkinsonian factor. *Neuron.* 32, 213-23.

Hayashi T, Ishimori C, Takahashi-Niki K, Taira T, Kim YC, Maita H, Maita C*, et al. (2009) DJ-1 binds to mitochondrial complex I and maintains its activity. *Biochem.Biophys.Res.Commun.* 390, 667-672.

Hebebrand J, Volckmar AL, Knoll N and Hinney A (2010) Chipping away the 'missing heritability': GIANT steps forward in the molecular elucidation of obesity - but still lots to go. *Obesity facts.* 3, 294-303.

Heldmaier G (1975) The influence of the social thermoregulation on the cold-adaptive growth of BAT in hairless and furred mice. *Pflugers Archiv : European journal of physiology.* 355, 261-6.

Heldmaier G and Ruf T (1992) Body temperature and metabolic rate during natural hypothermia in endotherms. *Journal of comparative physiology. B, Biochemical, systemic, and environmental physiology.* 162, 696-706.

Hesse D, Dunn M, Heldmaier G, Klingenspor M and Rozman J (2010) Behavioural mechanisms affecting energy regulation in mice prone or resistant to diet- induced obesity. *Physiology & behavior.* 99, 370-80.

Hill RW, Wyse GA and Anderson M (2012) Food, Energy, and Temperature. In: *Animal Physiology.* Sinauer, A (ed.), pp 166-170, Sinauer Associates, Inc. Publishers Sunderland, Massachusetts

Hod Y (2004) Differential control of apoptosis by DJ-1 in prostate benign and cancer cells. *Journal of cellular biochemistry.* 92, 1221-33.

Hoeks J, Wilde J, Hulshof MF, Berg SA, Schaart G, Dijk KW, Smit E*, et al. (2011) High fat diet-induced changes in mouse muscle mitochondrial phospholipids do not impair mitochondrial respiration despite insulin resistance. *PloS one.* 6, e27274.

Honbou K, Suzuki NN, Horiuchi M, Niki T, Taira T, Ariga H and Inagaki F (2003) The crystal structure of DJ-1, a protein related to male fertility and Parkinson's disease. *The Journal of biological chemistry.* 278, 31380-4.

Horvath TL (2006) Synaptic plasticity in energy balance regulation. *Obesity.* 14 Suppl 5, 228S-233S.

Horvath TL, Sarman B, Garcia-Caceres C, Enriori PJ, Sotonyi P, Shanabrough M, Borok E*, et al. (2010) Synaptic input organization of the melanocortin system predicts diet-induced hypothalamic reactive gliosis and obesity. *Proceedings of the National Academy of Sciences of the United States of America.* 107, 14875-80.

Howard JK, Cave BJ, Oksanen LJ, Tzameli I, Bjorbaek C and Flier JS (2004) Enhanced leptin sensitivity and attenuation of diet-induced obesity in mice with haploinsufficiency of Socs3. *Nature medicine.* 10, 734-8.

Howard JK and Flier JS (2006) Attenuation of leptin and insulin signaling by SOCS proteins. *Trends in endocrinology and metabolism: TEM.* 17, 365-71.

Hu G, Jousilahti P, Nissinen A, Antikainen R, Kivipelto M and Tuomilehto J (2006) Body mass index and the risk of Parkinson disease. *Neurology.* 67, 1955-9.

Huai Q, Sun Y, Wang H, Chin LS, Li L, Robinson H and Ke H (2003) Crystal structure of DJ-1/RS and implication on familial Parkinson's disease. *FEBS letters.* 549, 171-5.

Hulleman JD, Mirzaei H, Guigard E, Taylor KL, Ray SS, Kay CM, Regnier FE*, et al. (2007) Destabilization of DJ-1 by familial substitution and oxidative modifications: implications for Parkinson's disease. *Biochemistry.* 46, 5776-89.

Hwang LL, Wang CH, Li TL, Chang SD, Lin LC, Chen CP, Chen CT*, et al. (2010) Sex differences in high-fat diet-induced obesity, metabolic alterations and learning, and synaptic plasticity deficits in mice. *Obesity (Silver.Spring).* 18, 463-469.

Im JY, Lee KW, Junn E and Mouradian MM (2010) DJ-1 protects against oxidative damage by regulating the thioredoxin/ASK1 complex. *Neurosci.Res.* 67, 203-208.

Inden M, Kitamura Y, Takahashi K, Takata K, Ito N, Niwa R, Funayama R*, et al. (2011) Protection against dopaminergic neurodegeneration in Parkinson's disease-model animals by a modulator of the oxidized form of DJ-1, a wild-type of familial Parkinson's disease-linked PARK7. *Journal of pharmacological sciences.* 117, 189-203.

Irrcher I, Aleyasin H, Seifert EL, Hewitt SJ, Chhabra S, Phillips M, Lutz AK*, et al.* (2010) Loss of the Parkinson's disease-linked gene DJ-1 perturbs mitochondrial dynamics. *Hum.Mol.Genet.* 19, 3734-3746.

Jaillard T, Roger M, Galinier A, Guillou P, Benani A, Leloup C, Casteilla L*, et al.* (2009) Hypothalamic reactive oxygen species are required for insulin-induced food intake inhibition: an NADPH oxidase-dependent mechanism. *Diabetes.* 58, 1544-9.

Jain D, Jain R, Eberhard D, Eglinger J, Bugliani M, Piemonti L, Marchetti P*, et al.* (2012) Age- and diet-dependent requirement of DJ-1 for glucose homeostasis in mice with implications for human type 2 diabetes. *J Mol.Cell Biol.*

Jeong SK, Nam HS, Son MH, Son EJ and Cho KH (2005) Interactive effect of obesity indexes on cognition. *Dementia and geriatric cognitive disorders.* 19, 91-6.

Joo JI, Oh TS, Kim DH, Choi DK, Wang X, Choi JW and Yun JW (2011) Differential expression of adipose tissue proteins between obesity-susceptible and -resistant rats fed a high-fat diet. *Proteomics.* 11, 1429-1448.

Junn E, Jang WH, Zhao X, Jeong BS and Mouradian MM (2009) Mitochondrial localization of DJ-1 leads to enhanced neuroprotection. *J Neurosci.Res.* 87, 123-129.

Junn E, Taniguchi H, Jeong BS, Zhao X, Ichijo H and Mouradian MM (2005) Interaction of DJ-1 with Daxx inhibits apoptosis signal-regulating kinase 1 activity and cell death. *Proc.Natl.Acad.Sci.U.S.A.* 102, 9691-9696.

Kahle PJ, Waak J and Gasser T (2009) DJ-1 and prevention of oxidative stress in Parkinson's disease and other age-related disorders. *Free Radic.Biol.Med.* 47, 1354-1361.

Kaidanovich-Beilin O, Cha DS and McIntyre RS (2012) Crosstalk between metabolic and neuropsychiatric disorders. *F1000 biology reports.* 4, 14.

Kamp F, Exner N, Lutz AK, Wender N, Hegermann J, Brunner B, Nuscher B*, et al.* (2010) Inhibition of mitochondrial fusion by alpha-synuclein is rescued by PINK1, Parkin and DJ-1. *The EMBO journal.* 29, 3571-89.

Karunakaran S, Diwakar L, Saeed U, Agarwal V, Ramakrishnan S, Iyengar S and Ravindranath V (2007) Activation of apoptosis signal regulating kinase 1 (ASK1) and translocation of death-associated protein, Daxx, in substantia nigra pars compacta in a mouse model of Parkinson's disease: protection by alpha-lipoic acid. *FASEB J.* 21, 2226-2236.

Kaushik S, Arias E, Kwon H, Lopez NM, Athonvarangkul D, Sahu S, Schwartz GJ*, et al.* (2012) Loss of autophagy in hypothalamic POMC neurons impairs lipolysis. *EMBO reports.* 13, 258-65.

Kaushik S, Rodriguez-Navarro JA, Arias E, Kiffin R, Sahu S, Schwartz GJ, Cuervo AM*, et al.* (2011) Autophagy in hypothalamic AgRP neurons regulates food intake and energy balance. *Cell Metab.* 14, 173-83.

Keaney JF, Jr., Larson MG, Vasan RS, Wilson PW, Lipinska I, Corey D, Massaro JM*, et al.* (2003) Obesity and systemic oxidative stress: clinical correlates of oxidative stress in the Framingham Study. *Arteriosclerosis, thrombosis, and vascular biology.* 23, 434-9.

Kim JS, Huang TY and Bokoch GM (2009a) Reactive oxygen species regulate a slingshot-cofilin activation pathway. *Molecular biology of the cell.* 20, 2650-60.

Kim MS, Pak YK, Jang PG, Namkoong C, Choi YS, Won JC, Kim KS*, et al.* (2006) Role of hypothalamic Foxo1 in the regulation of food intake and energy homeostasis. *Nature neuroscience.* 9, 901-6.

Kim RH, Peters M, Jang Y, Shi W, Pintilie M, Fletcher GC, DeLuca C*, et al.* (2005a) DJ-1, a novel regulator of the tumor suppressor PTEN. *Cancer Cell.* 7, 263-273.

Kim RH, Smith PD, Aleyasin H, Hayley S, Mount MP, Pownall S, Wakeham A*, et al.* (2005b) Hypersensitivity of DJ-1-deficient mice to 1-methyl-4-phenyl-1,2,3,6-tetrahydropyridine (MPTP) and oxidative stress. *Proc.Natl.Acad.Sci.U.S.A.* 102, 5215-5220.

Kim YC, Kitaura H, Taira T, Iguchi-Ariga SM and Ariga H (2009b) Oxidation of DJ-1-dependent cell transformation through direct binding of DJ-1 to PTEN. *Int.J Oncol.* 35, 1331-1341.

Kinumi T, Kimata J, Taira T, Ariga H and Niki E (2004) Cysteine-106 of DJ-1 is the most sensitive cysteine residue to hydrogen peroxide-mediated oxidation in vivo in human umbilical vein endothelial cells. *Biochemical and biophysical research communications.* 317, 722-8.

Kitamura T, Feng Y, Kitamura YI, Chua SC, Jr., Xu AW, Barsh GS, Rossetti L, *et al.* (2006) Forkhead protein FoxO1 mediates Agrp-dependent effects of leptin on food intake. *Nature medicine*. 12, 534-40.

Klaus S (2004) Adipose tissue as a regulator of energy balance. *Current drug targets*. 5, 241-50.

Kleinridders A, Schenten D, Konner AC, Belgardt BF, Mauer J, Okamura T, Wunderlich FT, *et al.* (2009) MyD88 signaling in the CNS is required for development of fatty acid-induced leptin resistance and diet-induced obesity. *Cell Metab*. 10, 249-259.

Klose J and Kobalz U (1995) Two-dimensional electrophoresis of proteins: an updated protocol and implications for a functional analysis of the genome. *Electrophoresis*. 16, 1034-59.

Krebiehl G, Ruckerbauer S, Burbulla LF, Kieper N, Maurer B, Waak J, Wolburg H, *et al.* (2010) Reduced basal autophagy and impaired mitochondrial dynamics due to loss of Parkinson's disease-associated protein DJ-1. *PLoS.One.* 5, e9367.

Kwon HJ, Heo JY, Shim JH, Park JH, Seo KS, Ryu MJ, Han JS, *et al.* (2011) DJ-1 mediates paraquat-induced dopaminergic neuronal cell death. *Toxicology letters*. 202, 85-92.

Laemmli UK (1970) Cleavage of structural proteins during the assembly of the head of bacteriophage T4. *Nature*. 227, 680-5.

Lam TK, Schwartz GJ and Rossetti L (2005) Hypothalamic sensing of fatty acids. *Nature neuroscience*. 8, 579-84.

Le Naour F, Misek DE, Krause MC, Deneux L, Giordano TJ, Scholl S and Hanash SM (2001) Proteomics-based identification of RS/DJ-1 as a novel circulating tumor antigen in breast cancer. *Clinical cancer research : an official journal of the American Association for Cancer Research*. 7, 3328-35.

Lee AK, Mojtahed-Jaberi M, Kyriakou T, Astarloa EA, Arno M, Marshall NJ, Brain SD, *et al.* (2010) Effect of high-fat feeding on expression of genes controlling availability of dopamine in mouse hypothalamus. *Nutrition*. 26, 411-422.

Lee EB (2011) Obesity, leptin, and Alzheimer's disease. *Annals of the New York Academy of Sciences*. 1243, 15-29.

Lee J, Giordano S and Zhang J (2012) Autophagy, mitochondria and oxidative stress: cross-talk and redox signalling. *The Biochemical journal*. 441, 523-40.

Lehnardt S, Massillon L, Follett P, Jensen FE, Ratan R, Rosenberg PA, Volpe JJ, *et al.* (2003) Activation of innate immunity in the CNS triggers neurodegeneration through a Toll-like receptor 4-dependent pathway. *Proceedings of the National Academy of Sciences of the United States of America*. 100, 8514-9.

Leibel RL (2008) Molecular physiology of weight regulation in mice and humans. *Int.J Obes.(Lond)*. 32 Suppl 7, S98-108.

Leloup C, Magnan C, Benani A, Bonnet E, Alquier T, Offer G, Carriere A, *et al.* (2006) Mitochondrial reactive oxygen species are required for hypothalamic glucose sensing. *Diabetes*. 55, 2084-90.

Lev N, Ickowicz D, Melamed E and Offen D (2008) Oxidative insults induce DJ-1 upregulation and redistribution: implications for neuroprotection. *Neurotoxicology*. 29, 397-405.

Li HM, Niki T, Taira T, Iguchi-Ariga SM and Ariga H (2005) Association of DJ-1 with chaperones and enhanced association and colocalization with mitochondrial Hsp70 by oxidative stress. *Free Radic.Res.* 39, 1091-1099.

Li XL, Aou S, Oomura Y, Hori N, Fukunaga K and Hori T (2002) Impairment of long-term potentiation and spatial memory in leptin receptor-deficient rodents. *Neuroscience*. 113, 607-15.

Lin X, Cook TJ, Zabetian CP, Leverenz JB, Peskind ER, Hu SC, Cain KC, *et al.* (2012) DJ-1 isoforms in whole blood as potential biomarkers of Parkinson disease. *Scientific reports*. 2, 954.

Liu F, Nguyen JL, Hulleman JD, Li L and Rochet JC (2008) Mechanisms of DJ-1 neuroprotection in a cellular model of Parkinson's disease. *J Neurochem*. 105, 2435-2453.

MacKeigan JP, Clements CM, Lich JD, Pope RM, Hod Y and Ting JP (2003) Proteomic profiling drug-induced apoptosis in non-small cell lung carcinoma: identification of RS/DJ-1 and RhoGDIalpha. *Cancer research*. 63, 6928-34.

Madian AG, Hindupur J, Hulleman JD, Diaz-Maldonado N, Mishra VR, Guigard E, Kay CM*, et al.* (2012) Effect of single amino acid substitution on oxidative modifications of the Parkinson's disease-related protein, DJ-1. *Molecular & cellular proteomics : MCP*. 11, M111 010892.

Maffei M, Halaas J, Ravussin E, Pratley RE, Lee GH, Zhang Y, Fei H*, et al.* (1995) Leptin levels in human and rodent: measurement of plasma leptin and ob RNA in obese and weight-reduced subjects. *Nature medicine*. 1, 1155-61.

Maher P and Schubert D (2000) Signaling by reactive oxygen species in the nervous system. *Cellular and molecular life sciences : CMLS*. 57, 1287-305.

Martinat C, Shendelman S, Jonason A, Leete T, Beal MF, Yang L, Floss T*, et al.* (2004) Sensitivity to oxidative stress in DJ-1-deficient dopamine neurons: an ES- derived cell model of primary Parkinsonism. *PLoS.Biol.* 2, e327.

Meberg PJ, Ono S, Minamide LS, Takahashi M and Bamburg JR (1998) Actin depolymerizing factor and cofilin phosphorylation dynamics: response to signals that regulate neurite extension. *Cell motility and the cytoskeleton*. 39, 172-90.

Mensink G, Schienkiewitz A and Scheidt-Nave C - Robert Koch-Institut Berlin (2012) Studie zur Gesundheit Erwachsener in Deutschland (DEGS): Übergewicht und Adipositas in Deutschland: Werden wir immer dicker? June 2012 http://www.rki.de/DE/Content/Gesundheitsmonitoring/Studien/Degs/degs_w1/Symposium/degs_uebergewicht_adipositas.pdf?__blob=publicationFile

Meulener M, Whitworth AJ, Armstrong-Gold CE, Rizzu P, Heutink P, Wes PD, Pallanck LJ*, et al.* (2005a) Drosophila DJ-1 mutants are selectively sensitive to environmental toxins associated with Parkinson's disease. *Curr.Biol.* 15, 1572-1577.

Meulener MC, Graves CL, Sampathu DM, Armstrong-Gold CE, Bonini NM and Giasson BI (2005b) DJ-1 is present in a large molecular complex in human brain tissue and interacts with alpha-synuclein. *J Neurochem*. 93, 1524-1532.

Meyer CW, Klingenspor M, Rozman J and Heldmaier G (2004) Gene or size: metabolic rate and body temperature in obese growth hormone-deficient dwarf mice. *Obesity research*. 12, 1509-18.

Milanski M, Degasperi G, Coope A, Morari J, Denis R, Cintra DE, Tsukumo DM*, et al.* (2009) Saturated fatty acids produce an inflammatory response predominantly through the activation of TLR4 signaling in hypothalamus: implications for the pathogenesis of obesity. *The Journal of neuroscience : the official journal of the Society for Neuroscience*. 29, 359-70.

Miller DW, Ahmad R, Hague S, Baptista MJ, Canet-Aviles R, McLendon C, Carter DM*, et al.* (2003) L166P mutant DJ-1, causative for recessive Parkinson's disease, is degraded through the ubiquitin-proteasome system. *J Biol.Chem.* 278, 36588-36595.

Mitsumoto A and Nakagawa Y (2001) DJ-1 is an indicator for endogenous reactive oxygen species elicited by endotoxin. *Free Radic.Res.* 35, 885-893.

Miyama A, Saito Y, Yamanaka K, Hayashi K, Hamakubo T and Noguchi N (2011) Oxidation of DJ-1 induced by 6-hydroxydopamine decreasing intracellular glutathione. *PLoS.One.* 6, e27883.

Mo JS, Kim MY, Ann EJ, Hong JA and Park HS (2008) DJ-1 modulates UV-induced oxidative stress signaling through the suppression of MEKK1 and cell death. *Cell death and differentiation*. 15, 1030-41.

Mobbs CV, Yen K, Mastaitis J, Nguyen H, Watson E, Wurmbach E, Sealfon SC*, et al.* (2004) Mining microarrays for metabolic meaning: nutritional regulation of hypothalamic gene expression. *Neurochemical research*. 29, 1093-103.

Molteni R, Barnard RJ, Ying Z, Roberts CK and Gomez-Pinilla F (2002) A high-fat, refined sugar diet reduces hippocampal brain-derived neurotrophic factor, neuronal plasticity, and learning. *Neuroscience*. 112, 803-14.

Moraes JC, Coope A, Morari J, Cintra DE, Roman EA, Pauli JR, Romanatto T*, et al.* (2009) High-fat diet induces apoptosis of hypothalamic neurons. *PLoS.One.* 4, e5045.

Mori H, Hanada R, Hanada T, Aki D, Mashima R, Nishinakamura H, Torisu T*, et al.* (2004) Socs3 deficiency in the brain elevates leptin sensitivity and confers resistance to diet-induced obesity. *Nature medicine*. 10, 739-43.

Morris JK, Bomhoff GL, Stanford JA and Geiger PC (2010) Neurodegeneration in an animal model of Parkinson's disease is exacerbated by a high-fat diet. *American journal of physiology. Regulatory, integrative and comparative physiology.* 299, R1082-90.

Morrison CD (2008) Leptin resistance and the response to positive energy balance. *Physiology & behavior.* 94, 660-3.

Morrison CD, Morton GJ, Niswender KD, Gelling RW and Schwartz MW (2005) Leptin inhibits hypothalamic Npy and Agrp gene expression via a mechanism that requires phosphatidylinositol 3-OH-kinase signaling. *American journal of physiology. Endocrinology and metabolism.* 289, E1051-7.

Morrison CD, Pistell PJ, Ingram DK, Johnson WD, Liu Y, Fernandez-Kim SO, White CL*, et al.* (2010) High fat diet increases hippocampal oxidative stress and cognitive impairment in aged mice: implications for decreased Nrf2 signaling. *Journal of neurochemistry.* 114, 1581-9.

Morton GJ, Cummings DE, Baskin DG, Barsh GS and Schwartz MW (2006) Central nervous system control of food intake and body weight. *Nature.* 443, 289-95.

Münzberg H (2008) Differential leptin access into the brain--a hierarchical organization of hypothalamic leptin target sites? *Physiol Behav.* 94, 664-669.

Münzberg H, Flier JS and Bjorbaek C (2004) Region-specific leptin resistance within the hypothalamus of diet-induced obese mice. *Endocrinology.* 145, 4880-4889.

Münzberg H and Myers MG, Jr. (2005) Molecular and anatomical determinants of central leptin resistance. *Nat.Neurosci.* 8, 566-570.

Myers MG, Cowley MA and Münzberg H (2008) Mechanisms of leptin action and leptin resistance. *Annu.Rev.Physiol.* 70, 537-556.

Myers MG, Jr., Leibel RL, Seeley RJ and Schwartz MW (2010) Obesity and leptin resistance: distinguishing cause from effect. *Trends in endocrinology and metabolism: TEM.* 21, 643-51.

Nagakubo D, Taira T, Kitaura H, Ikeda M, Tamai K, Iguchi-Ariga SM and Ariga H (1997) DJ-1, a novel oncogene which transforms mouse NIH3T3 cells in cooperation with ras. *Biochem.Biophys.Res.Commun.* 231, 509-513.

Nakamura K, Nemani VM, Wallender EK, Kaehlcke K, Ott M and Edwards RH (2008) Optical reporters for the conformation of alpha-synuclein reveal a specific interaction with mitochondria. *The Journal of neuroscience : the official journal of the Society for Neuroscience.* 28, 12305-17.

Nardini M, Mazzocco M, Massaro A, Maffei M, Vergano A, Donadini A, Scartezzini P*, et al.* (2004) Crystal structure of the glutaredoxin-like protein SH3BGRL3 at 1.6 Angstrom resolution. *Biochemical and biophysical research communications.* 318, 470-6.

Natale M, Bonino D, Consoli P, Alberio T, Ravid RG, Fasano M and Bucci EM (2010) A meta-analysis of two-dimensional electrophoresis pattern of the Parkinson's disease-related protein DJ-1. *Bioinformatics.* 26, 946-952.

Nijtmans LG, Artal SM, Grivell LA and Coates PJ (2002) The mitochondrial PHB complex: roles in mitochondrial respiratory complex assembly, ageing and degenerative disease. *Cellular and molecular life sciences : CMLS.* 59, 143-55.

Niki T, Takahashi-Niki K, Taira T, Iguchi-Ariga SM and Ariga H (2003) DJBP: a novel DJ-1-binding protein, negatively regulates the androgen receptor by recruiting histone deacetylase complex, and DJ-1 antagonizes this inhibition by abrogation of this complex. *Mol.Cancer Res.* 1, 247-261.

Niswender KD, Baskin DG and Schwartz MW (2004) Insulin and its evolving partnership with leptin in the hypothalamic control of energy homeostasis. *Trends in endocrinology and metabolism: TEM.* 15, 362-9.

Niswender KD and Schwartz MW (2003) Insulin and leptin revisited: adiposity signals with overlapping physiological and intracellular signaling capabilities. *Frontiers in neuroendocrinology.* 24, 1-10.

Ozcan L, Ergin AS, Lu A, Chung J, Sarkar S, Nie D, Myers MG, Jr.*, et al.* (2009) Endoplasmic reticulum stress plays a central role in development of leptin resistance. *Cell Metab.* 9, 35-51.

Palacios N, Gao X, McCullough ML, Jacobs EJ, Patel AV, Mayo T, Schwarzschild MA*, et al.* (2011) Obesity, diabetes, and risk of Parkinson's disease. *Movement disorders : official journal of the Movement Disorder Society*. 26, 2253-9.

Palmiter RD (2007) Is dopamine a physiologically relevant mediator of feeding behavior? *Trends in neurosciences*. 30, 375-81.

Pardo M, Garcia A, Thomas B, Pineiro A, Akoulitchev A, Dwek RA and Zitzmann N (2006) The characterization of the invasion phenotype of uveal melanoma tumour cells shows the presence of MUC18 and HMG-1 metastasis markers and leads to the identification of DJ-1 as a potential serum biomarker. *International journal of cancer. Journal international du cancer*. 119, 1014-22.

Park JY and Lansbury PT, Jr. (2003) Beta-synuclein inhibits formation of alpha-synuclein protofibrils: a possible therapeutic strategy against Parkinson's disease. *Biochemistry*. 42, 3696-700.

Pattingre S, Espert L, Biard-Piechaczyk M and Codogno P (2008) Regulation of macroautophagy by mTOR and Beclin 1 complexes. *Biochimie*. 90, 313-23.

Paulsen CE and Carroll KS (2010) Orchestrating redox signaling networks through regulatory cysteine switches. *ACS Chem.Biol.* 5, 47-62.

Perez RG, Waymire JC, Lin E, Liu JJ, Guo F and Zigmond MJ (2002) A role for alpha-synuclein in the regulation of dopamine biosynthesis. *J Neurosci.* 22, 3090-3099.

Peters A, Pellerin L, Dallman MF, Oltmanns KM, Schweiger U, Born J and Fehm HL (2007) Causes of obesity: looking beyond the hypothalamus. *Progress in neurobiology*. 81, 61-88.

Pham TT, Giesert F, Rothig A, Floss T, Kallnik M, Weindl K, Holter SM*, et al.* (2010) DJ-1-deficient mice show less TH-positive neurons in the ventral tegmental area and exhibit non-motoric behavioural impairments. *Genes Brain Behav.* 9, 305-317.

Picardi PK, Calegari VC, Prada Pde O, Moraes JC, Araujo E, Marcondes MC, Ueno M*, et al.* (2008) Reduction of hypothalamic protein tyrosine phosphatase improves insulin and leptin resistance in diet-induced obese rats. *Endocrinology*. 149, 3870-80.

Picardi PK, Caricilli AM, de Abreu LL, Carvalheira JB, Velloso LA and Saad MJ (2010) Modulation of hypothalamic PTP1B in the TNF-alpha-induced insulin and leptin resistance. *FEBS letters*. 584, 3179-84.

Pinto S, Roseberry AG, Liu H, Diano S, Shanabrough M, Cai X, Friedman JM*, et al.* (2004) Rapid rewiring of arcuate nucleus feeding circuits by leptin. *Science*. 304, 110-5.

Poschmann G, Sitek B, Sipos B and Stuhler K (2012) Application of saturation labeling in lung cancer proteomics. *Methods Mol Biol*. 854, 253-67.

Posey KA, Clegg DJ, Printz RL, Byun J, Morton GJ, Vivekanandan-Giri A, Pennathur S*, et al.* (2009) Hypothalamic proinflammatory lipid accumulation, inflammation, and insulin resistance in rats fed a high-fat diet. *American journal of physiology. Endocrinology and metabolism*. 296, E1003-12.

Prpic V, Watson PM, Frampton IC, Sabol MA, Jezek GE and Gettys TW (2003) Differential mechanisms and development of leptin resistance in A/J versus C57BL/6J mice during diet-induced obesity. *Endocrinology*. 144, 1155-1163.

Quan W, Kim HK, Moon EY, Kim SS, Choi CS, Komatsu M, Jeong YT*, et al.* (2012) Role of hypothalamic proopiomelanocortin neuron autophagy in the control of appetite and leptin response. *Endocrinology*. 153, 1817-26.

Rahman I, Kode A and Biswas SK (2006) Assay for quantitative determination of glutathione and glutathione disulfide levels using enzymatic recycling method. *Nature protocols*. 1, 3159-65.

Ransohoff RM and Perry VH (2009) Microglial physiology: unique stimuli, specialized responses. *Annual review of immunology*. 27, 119-45.

Ravussin Y, Gutman R, Diano S, Shanabrough M, Borok E, Sarman B, Lehmann A*, et al.* (2011) Effects of chronic weight perturbation on energy homeostasis and brain structure in mice. *American journal of physiology. Regulatory, integrative and comparative physiology*. 300, R1352-62.

Reddie KG and Carroll KS (2008) Expanding the functional diversity of proteins through cysteine oxidation. *Current opinion in chemical biology*. 12, 746-54.

Ren H, Fu K, Mu C, Li B, Wang D and Wang G (2010) DJ-1, a cancer and Parkinson's disease associated protein, regulates autophagy through JNK pathway in cancer cells. *Cancer letters.* 297, 101-8.

Ren H, Fu K, Wang D, Mu C and Wang G (2011) Oxidized DJ-1 interacts with the mitochondrial protein BCL-XL. *J Biol.Chem.* 286, 35308-35317.

Rhee SG, Bae YS, Lee SR and Kwon J (2000) Hydrogen peroxide: a key messenger that modulates protein phosphorylation through cysteine oxidation. *Science's STKE : signal transduction knowledge environment.* 2000, pe1.

Rizzuto R, Bernardi P and Pozzan T (2000) Mitochondria as all-round players of the calcium game. *The Journal of physiology.* 529 Pt 1, 37-47.

Romanatto T, Cesquini M, Amaral ME, Roman EA, Moraes JC, Torsoni MA, Cruz-Neto AP*, et al.* (2007) TNF-alpha acts in the hypothalamus inhibiting food intake and increasing the respiratory quotient--effects on leptin and insulin signaling pathways. *Peptides.* 28, 1050-8.

Rui L, Yuan M, Frantz D, Shoelson S and White MF (2002) SOCS-1 and SOCS-3 block insulin signaling by ubiquitin-mediated degradation of IRS1 and IRS2. *The Journal of biological chemistry.* 277, 42394-8.

Rusnak F and Mertz P (2000) Calcineurin: form and function. *Physiological reviews.* 80, 1483-521.

Ryan MT and Hoogenraad NJ (2007) Mitochondrial-nuclear communications. *Annual review of biochemistry.* 76, 701-22.

Scarpace PJ and Zhang Y (2009) Leptin resistance: a prediposing factor for diet-induced obesity. *Am.J Physiol Regul.Integr.Comp Physiol.* 296, R493-R500.

Schildknecht S, Gerding HR, Karreman C, Drescher M, Lashuel HA, Outeiro TF, Di Monte DA*, et al.* (2013) Oxidative and nitrative alpha-synuclein modifications and proteostatic stress: implications for disease mechanisms and interventions in synucleinopathies. *Journal of neurochemistry.*

Schneider CA, Rasband WS and Eliceiri KW (2012) NIH Image to ImageJ: 25 years of image analysis. *Nat Methods.* 9, 671-5.

Schöttl T (2011) Measurement of reactive oxygen species in the murine hypothalamus after high-fat feeding or intraperitoneal glucose injection utilizing different approaches. *Molecular Nutritional Medicine*, TU München Freising, Germany

Schroder M and Kaufman RJ (2005) ER stress and the unfolded protein response. *Mutation research.* 569, 29-63.

Schwartz MW, Peskind E, Raskind M, Boyko EJ and Porte D, Jr. (1996) Cerebrospinal fluid leptin levels: relationship to plasma levels and to adiposity in humans. *Nature medicine.* 2, 589-93.

Schwartz MW, Woods SC, Porte D, Jr., Seeley RJ and Baskin DG (2000) Central nervous system control of food intake. *Nature.* 404, 661-671.

Sharon R, Goldberg MS, Bar-Josef I, Betensky RA, Shen J and Selkoe DJ (2001) alpha-Synuclein occurs in lipid-rich high molecular weight complexes, binds fatty acids, and shows homology to the fatty acid-binding proteins. *Proceedings of the National Academy of Sciences of the United States of America.* 98, 9110-5.

Shendelman S, Jonason A, Martinat C, Leete T and Abeliovich A (2004) DJ-1 is a redox-dependent molecular chaperone that inhibits alpha-synuclein aggregate formation. *PLoS.Biol.* 2, e362.

Shi M, Zabetian CP, Hancock AM, Ginghina C, Hong Z, Yearout D, Chung KA*, et al.* (2010) Significance and confounders of peripheral DJ-1 and alpha-synuclein in Parkinson's disease. *Neuroscience letters.* 480, 78-82.

Shinbo Y, Niki T, Taira T, Ooe H, Takahashi-Niki K, Maita C, Seino C*, et al.* (2006) Proper SUMO-1 conjugation is essential to DJ-1 to exert its full activities. *Cell Death.Differ.* 13, 96-108.

Shinbo Y, Taira T, Niki T, Iguchi-Ariga SM and Ariga H (2005) DJ-1 restores p53 transcription activity inhibited by Topors/p53BP3. *International journal of oncology.* 26, 641-8.

Shintani T and Klionsky DJ (2004) Autophagy in health and disease: a double-edged sword. *Science.* 306, 990-5.

Shtifman A, Zhong N, Lopez JR, Shen J and Xu J (2011) Altered Ca2+ homeostasis in the skeletal muscle of DJ-1 null mice. *Neurobiol.Aging.* 32, 125-132.

Singh-Manoux A, Czernichow S, Elbaz A, Dugravot A, Sabia S, Hagger-Johnson G, Kaffashian S*, et al. (2012) Obesity phenotypes in midlife and cognition in early old age: the Whitehall II cohort study. *Neurology.* 79, 755-62.

Smith LM, Kelleher NL, Consortium for Top Down P, Linial M, Goodlett D, Langridge-Smith P, Ah Goo Y*, et al. (2013) Proteoform: a single term describing protein complexity. *Nature methods.* 10, 186-7.

Sorensen TI, Sonne-Holm S and Christensen U (1983) Cognitive deficiency in obesity independent of social origin. *Lancet.* 1, 1105-6.

Spanswick D, Smith MA, Groppi VE, Logan SD and Ashford ML (1997) Leptin inhibits hypothalamic neurons by activation of ATP-sensitive potassium channels. *Nature.* 390, 521-5.

Spanswick D, Smith MA, Mirshamsi S, Routh VH and Ashford ML (2000) Insulin activates ATP-sensitive K+ channels in hypothalamic neurons of lean, but not obese rats. *Nature neuroscience.* 3, 757-8.

**Speliotes EK, Willer CJ, Berndt SI, Monda KL, Thorleifsson G, Jackson AU, Lango Allen H*, et al.* (2010) Association analyses of 249,796 individuals reveal 18 new loci associated with body mass index. *Nature genetics.* 42, 937-48.

Spillantini MG, Schmidt ML, Lee VM, Trojanowski JQ, Jakes R and Goedert M (1997) Alpha-synuclein in Lewy bodies. *Nature.* 388, 839-40.

Sriram K, Benkovic SA, Miller DB and O'Callaghan JP (2002) Obesity exacerbates chemically induced neurodegeneration. *Neuroscience.* 115, 1335-46.

Stranahan AM, Norman ED, Lee K, Cutler RG, Telljohann RS, Egan JM and Mattson MP (2008) Diet-induced insulin resistance impairs hippocampal synaptic plasticity and cognition in middle-aged rats. *Hippocampus.* 18, 1085-8.

Surmeier DJ, Guzman JN, Sanchez-Padilla J and Schumacker PT (2011) The role of calcium and mitochondrial oxidant stress in the loss of substantia nigra pars compacta dopaminergic neurons in Parkinson's disease. *Neuroscience.* 198, 221-31.

Taira T, Saito Y, Niki T, Iguchi-Ariga SM, Takahashi K and Ariga H (2004) DJ-1 has a role in antioxidative stress to prevent cell death. *EMBO Rep.* 5, 213-218.

Taira T, Takahashi K, Kitagawa R, Iguchi-Ariga SM and Ariga H (2001) Molecular cloning of human and mouse DJ-1 genes and identification of Sp1-dependent activation of the human DJ-1 promoter. *Gene.* 263, 285-92.

Takahashi K, Taira T, Niki T, Seino C, Iguchi-Ariga SM and Ariga H (2001) DJ-1 positively regulates the androgen receptor by impairing the binding of PIASx alpha to the receptor. *J Biol.Chem.* 276, 37556-37563.

Tao X and Tong L (2003) Crystal structure of human DJ-1, a protein associated with early onset Parkinson's disease. *The Journal of biological chemistry.* 278, 31372-9.

Thaler JP, Choi SJ, Schwartz MW and Wisse BE (2010) Hypothalamic inflammation and energy homeostasis: resolving the paradox. *Front Neuroendocrinol.* 31, 79-84.

**Thaler JP, Yi CX, Schur EA, Guyenet SJ, Hwang BH, Dietrich MO, Zhao X*, et al.* (2012) Obesity is associated with hypothalamic injury in rodents and humans. *J Clin.Invest.* 122, 153-162.

Thomas B and Beal MF (2011) Molecular insights into Parkinson's disease. *F1000 medicine reports.* 3, 7.

**Thomas KJ, McCoy MK, Blackinton J, Beilina A, van der Brug M, Sandebring A, Miller D*, et al.* (2011) DJ-1 acts in parallel to the PINK1/parkin pathway to control mitochondrial function and autophagy. *Hum.Mol.Genet.* 20, 40-50.

Toime LJ and Brand MD (2010) Uncoupling protein-3 lowers reactive oxygen species production in isolated mitochondria. *Free radical biology & medicine.* 49, 606-11.

**van der Brug MP, Blackinton J, Chandran J, Hao LY, Lal A, Mazan-Mamczarz K, Martindale J*, et al.* (2008) RNA binding activity of the recessive parkinsonism protein DJ-1 supports involvement in multiple cellular pathways. *Proc.Natl.Acad.Sci.U.S.A.* 105, 10244-10249.

van Heek M, Compton DS, France CF, Tedesco RP, Fawzi AB, Graziano MP, Sybertz EJ*, et al.* (1997) Diet-induced obese mice develop peripheral, but not central, resistance to leptin. *J Clin.Invest.* 99, 385-390.

Varela L and Horvath TL (2012) Leptin and insulin pathways in POMC and AgRP neurons that modulate energy balance and glucose homeostasis. *EMBO reports.*

Vasseur S, Afzal S, Tardivel-Lacombe J, Park DS, Iovanna JL and Mak TW (2009) DJ-1/PARK7 is an important mediator of hypoxia-induced cellular responses. *Proc.Natl.Acad.Sci.U.S.A.* 106, 1111-1116.

Ved R, Saha S, Westlund B, Perier C, Burnam L, Sluder A, Hoener M*, et al.* (2005) Similar patterns of mitochondrial vulnerability and rescue induced by genetic modification of alpha-synuclein, parkin, and DJ-1 in Caenorhabditis elegans. *J Biol.Chem.* 280, 42655-42668.

Velloso LA and Schwartz MW (2011) Altered hypothalamic function in diet-induced obesity. *International journal of obesity.* 35, 1455-65.

Vincent HK, Innes KE and Vincent KR (2007) Oxidative stress and potential interventions to reduce oxidative stress in overweight and obesity. *Diabetes, obesity & metabolism.* 9, 813-39.

Vincent HK and Taylor AG (2006) Biomarkers and potential mechanisms of obesity-induced oxidant stress in humans. *International journal of obesity.* 30, 400-18.

Waak J, Weber SS, Gorner K, Schall C, Ichijo H, Stehle T and Kahle PJ (2009) Oxidizable residues mediating protein stability and cytoprotective interaction of DJ-1 with apoptosis signal-regulating kinase 1. *J Biol.Chem.* 284, 14245-14257.

Waanders LF, Chwalek K, Monetti M, Kumar C, Lammert E and Mann M (2009) Quantitative proteomic analysis of single pancreatic islets. *Proc.Natl.Acad.Sci.U.S.A.* 106, 18902-18907.

Wang Y, Shibasaki F and Mizuno K (2005) Calcium signal-induced cofilin dephosphorylation is mediated by Slingshot via calcineurin. *The Journal of biological chemistry.* 280, 12683-9.

Wang Z, Liu J, Chen S, Wang Y, Cao L, Zhang Y, Kang W*, et al.* (2011) DJ-1 modulates the expression of Cu/Zn-superoxide dismutase-1 through the Erk1/2-Elk1 pathway in neuroprotection. *Ann.Neurol.* 70, 591-599.

Weigel AL, Handa JT and Hjelmeland LM (2002) Microarray analysis of H2O2-, HNE-, or tBH-treated ARPE-19 cells. *Free radical biology & medicine.* 33, 1419-32.

Weissbach H, Etienne F, Hoshi T, Heinemann SH, Lowther WT, Matthews B, St John G*, et al.* (2002) Peptide methionine sulfoxide reductase: structure, mechanism of action, and biological function. *Archives of biochemistry and biophysics.* 397, 172-8.

White CL, Whittington A, Barnes MJ, Wang Z, Bray GA and Morrison CD (2009) HF diets increase hypothalamic PTP1B and induce leptin resistance through both leptin-dependent and -independent mechanisms. *American journal of physiology. Endocrinology and metabolism.* 296, E291-9.

WHO - World Health Organization (2012) Fact sheet N°311: Obesity and overweight. May 2012 http://www.who.int/mediacentre/factsheets/fs311/en/index.html

Wilson MA (2011) The role of cysteine oxidation in DJ-1 function and dysfunction. *Antioxid.Redox.Signal.* 15, 111-122.

Wilson MA, Collins JL, Hod Y, Ringe D and Petsko GA (2003) The 1.1-A resolution crystal structure of DJ-1, the protein mutated in autosomal recessive early onset Parkinson's disease. *Proceedings of the National Academy of Sciences of the United States of America.* 100, 9256-61.

Wisse BE, Kim F and Schwartz MW (2007) Physiology. An integrative view of obesity. *Science.* 318, 928-9.

Wisse BE and Schwartz MW (2009) Does hypothalamic inflammation cause obesity? *Cell Metab.* 10, 241-242.

Woo HA, Jeong W, Chang TS, Park KJ, Park SJ, Yang JS and Rhee SG (2005) Reduction of cysteine sulfinic acid by sulfiredoxin is specific to 2-cys peroxiredoxins. *J Biol.Chem.* 280, 3125-3128.

Xiang W, Schlachetzki JC, Helling S, Bussmann JC, Berlinghof M, Schaffer TE, Marcus K*, et al.* (2013) Oxidative stress-induced posttranslational modifications of alpha-synuclein: Specific modification of alpha-synuclein by 4-hydroxy-2-nonenal increases dopaminergic toxicity. *Molecular and cellular neurosciences.* 54C, 71-83.

Xu C, Zheng P, Shen S, Xu Y, Wei L, Gao H, Wang S*, et al.* (2005a) NMR structure and regulated expression in APL cell of human SH3BGRL3. *FEBS letters.* 579, 2788-94.

Xu J, Zhong N, Wang H, Elias JE, Kim CY, Woldman I, Pifl C*, et al.* (2005b) The Parkinson's disease-associated DJ-1 protein is a transcriptional co-activator that protects against neuronal apoptosis. *Hum.Mol.Genet.* 14, 1231-1241.

Xu X, Martin F and Friedman JS (2010) The familial Parkinson's disease gene DJ-1 (PARK7) is expressed in red cells and plays a role in protection against oxidative damage. *Blood Cells Mol.Dis.* 45, 227-232.

Yang Y, Gehrke S, Haque ME, Imai Y, Kosek J, Yang L, Beal MF*, et al.* (2005) Inactivation of Drosophila DJ-1 leads to impairments of oxidative stress response and phosphatidylinositol 3-kinase/Akt signaling. *Proceedings of the National Academy of Sciences of the United States of America.* 102, 13670-5.

Yeo GS and Heisler LK (2012) Unraveling the brain regulation of appetite: lessons from genetics. *Nature neuroscience.* 15, 1343-9.

Yokota T, Sugawara K, Ito K, Takahashi R, Ariga H and Mizusawa H (2003) Down regulation of DJ-1 enhances cell death by oxidative stress, ER stress, and proteasome inhibition. *Biochem.Biophys.Res.Commun.* 312, 1342-1348.

Zabolotny JM, Bence-Hanulec KK, Stricker-Krongrad A, Haj F, Wang Y, Minokoshi Y, Kim YB*, et al.* (2002) PTP1B regulates leptin signal transduction in vivo. *Developmental cell.* 2, 489-95.

Zeltser LM, Seeley RJ and Tschop MH (2012) Synaptic plasticity in neuronal circuits regulating energy balance. *Nature neuroscience.* 15, 1336-42.

Zhang L, Shimoji M, Thomas B, Moore DJ, Yu SW, Marupudi NI, Torp R*, et al.* (2005a) Mitochondrial localization of the Parkinson's disease related protein DJ-1: implications for pathogenesis. *Hum.Mol.Genet.* 14, 2063-2073.

Zhang X, Dong F, Ren J, Driscoll MJ and Culver B (2005b) High dietary fat induces NADPH oxidase-associated oxidative stress and inflammation in rat cerebral cortex. *Exp.Neurol.* 191, 318-325.

Zhang X, Zhang G, Zhang H, Karin M, Bai H and Cai D (2008) Hypothalamic IKKbeta/NF-kappaB and ER stress link overnutrition to energy imbalance and obesity. *Cell.* 135, 61-73.

Zhong N, Kim CY, Rizzu P, Geula C, Porter DR, Pothos EN, Squitieri F*, et al.* (2006) DJ-1 transcriptionally up-regulates the human tyrosine hydroxylase by inhibiting the sumoylation of pyrimidine tract-binding protein-associated splicing factor. *J Biol.Chem.* 281, 20940-20948.

Zhong N and Xu J (2008) Synergistic activation of the human MnSOD promoter by DJ-1 and PGC-1alpha: regulation by SUMOylation and oxidation. *Hum.Mol.Genet.* 17, 3357-3367.

Zhong Z, Nural H, He P, Civarella G, Beach T, Sue L, Adler C*, et al.* (2009) Disassembled DJ-1 high molecular weight complex in cortex mitochondria from Parkinson's disease patients. *Mol.Neurodegener.* 4, 30.

Zhou M, Diwu Z, Panchuk-Voloshina N and Haugland RP (1997) A stable nonfluorescent derivative of resorufin for the fluorometric determination of trace hydrogen peroxide: applications in detecting the activity of phagocyte NADPH oxidase and other oxidases. *Analytical biochemistry.* 253, 162-8.

Zhou W and Freed CR (2005) DJ-1 up-regulates glutathione synthesis during oxidative stress and inhibits A53T alpha-synuclein toxicity. *J Biol.Chem.* 280, 43150-43158.

Zhou W, Zhu M, Wilson MA, Petsko GA and Fink AL (2006) The oxidation state of DJ-1 regulates its chaperone activity toward alpha-synuclein. *J Mol.Biol.* 356, 1036-1048.

6   SUPPLEMENTARY DATA

6.1   Supplementary figures
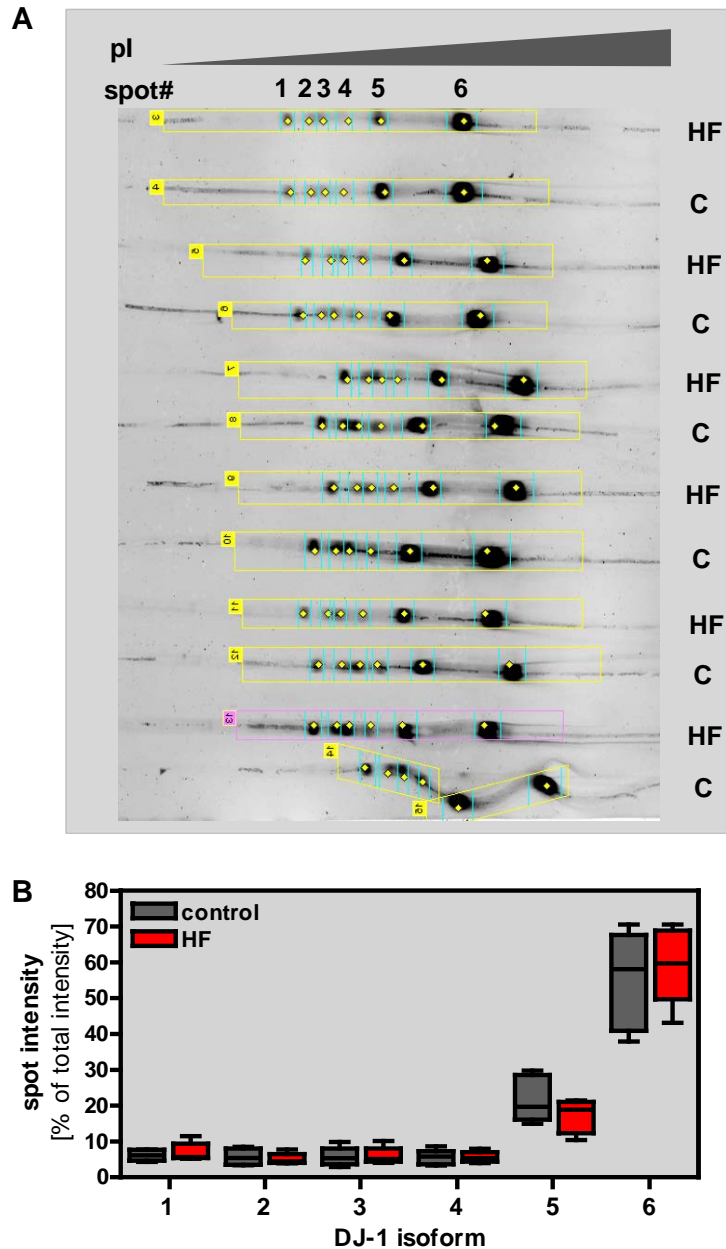
Fig. S1. Comparison of DJ-1 pI isoforms in the epididymal white adipose tissue of male C57BL/6N mice after 10 days of HF or control diet. (**A**) Protein extracts were separated via IEF. Gels were transferred to a membrane followed by immunodetection of DJ-1. (**B**) Densitometric quantification of the signal intensities of individual DJ-1 spots (n = 6). Data was generated by Dr. Gereon Poschmann, MPL, Düsseldorf, Germany.
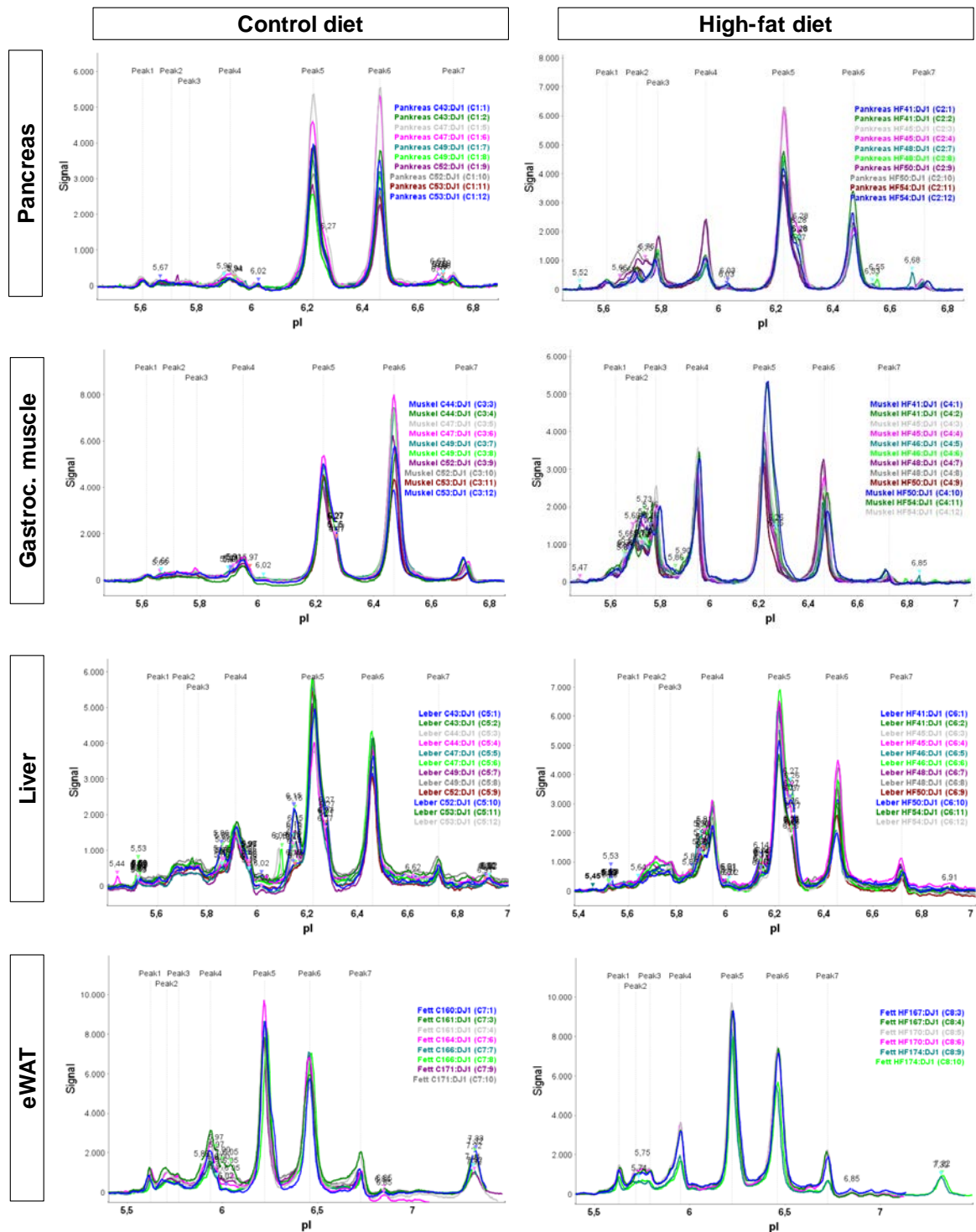
Fig. S2. Comparison of DJ-1 pI isoforms in peripheral tissues of C57BL/6N mice maintained on a HF or control diet for 10 days. Protein extracts were analyzed using an automated capillary IEF immunoassay (NanoPro[TM] 1000, ProteinSimple). Electropherograms show the pI distribution of DJ-1 isoforms detected via chemifluorescence. Samples were measured in duplicates. Each peak likely corresponds to one DJ-1 isoform. $n_{gastrocnemius\ muscle}$ = 5-6, $n_{pancreas}$ = 5, n_{liver} = 6, $n_{epididymal\ WAT}$ = 3. eWAT – epididymal white adipose tissue. Gastroc. muscle – gastrocnemius muscle. Data was generated by Dr. Daniela Besong Agbo and Dr. Hans Klafki, LVR-Klinikum Essen, Germany.
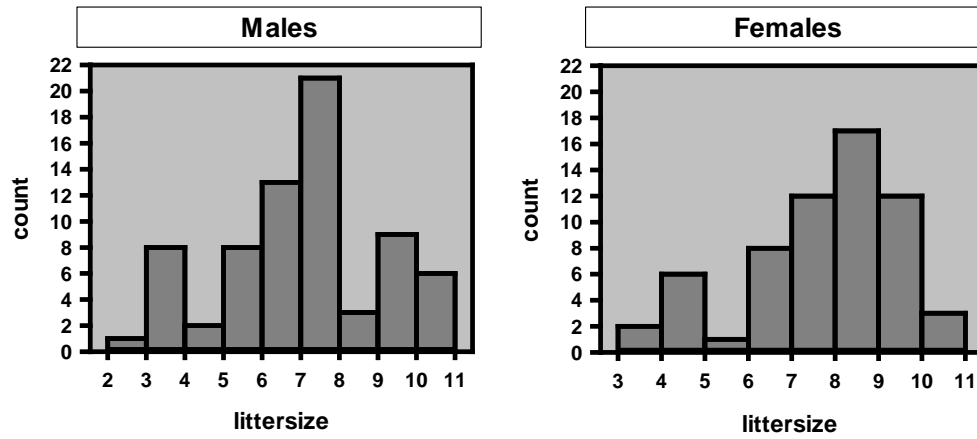
Fig. S3. Histograms of litter sizes of male and female _Dj-1$^{-/-}$_ and _Dj-1$^{+/+}$_ mice employed in the HF diet challenge. Mice derived from heterozygous breeding pairs.
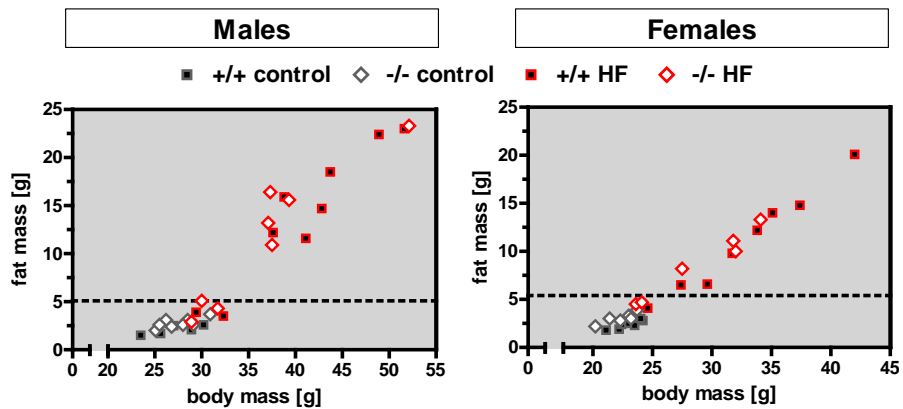
Fig. S4. Fat mass related to body mass in male and female _Dj-1$^{-/-}$_ and _Dj-1$^{+/+}$_ mice after 32 weeks of HF or control diet. The dotted line designates twice the mean fat mass of control diet-fed mice. HF diet-fed mice whose fat mass did not exceed this value were defined as non-responders.
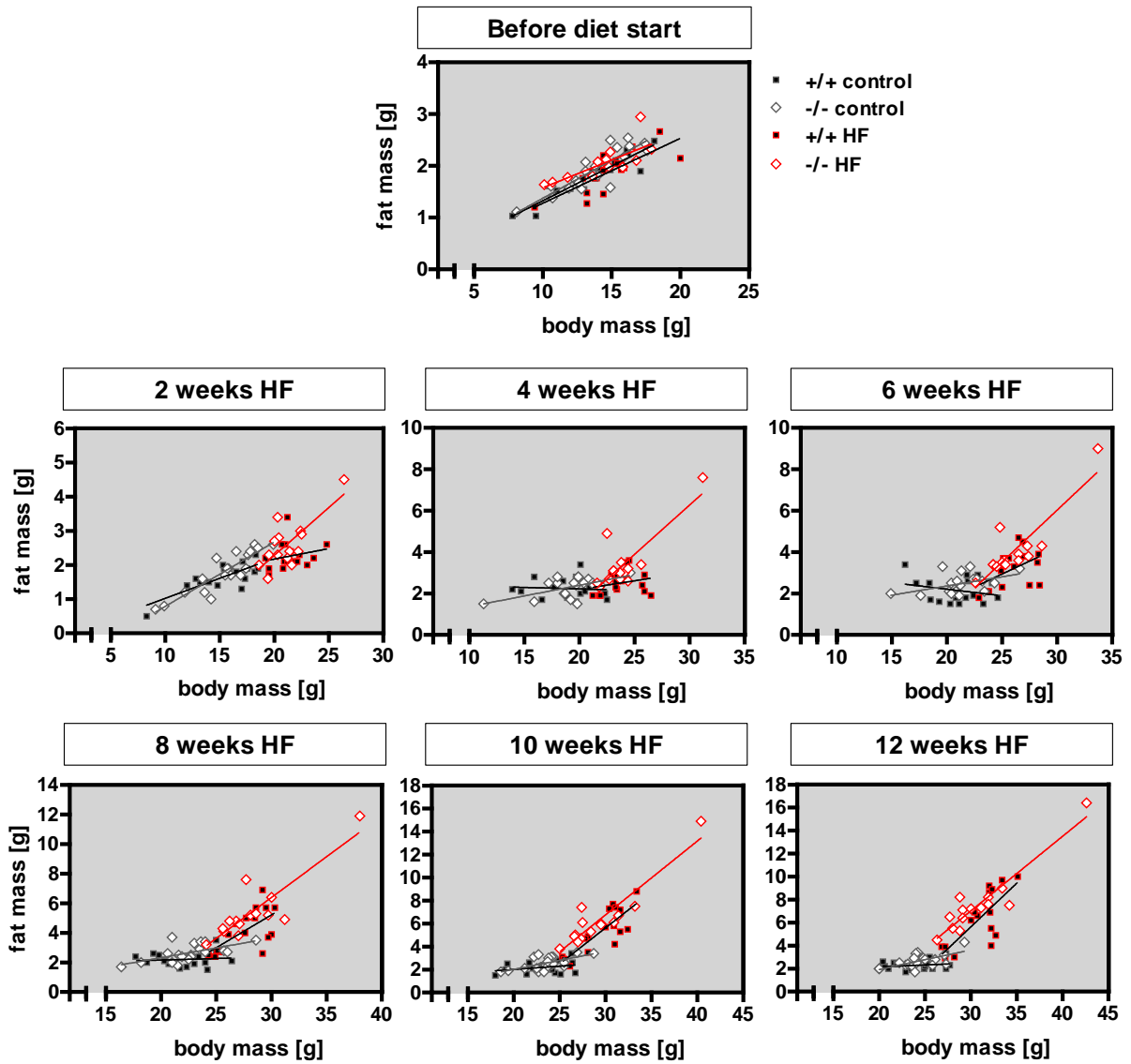
Fig. S5. Fat mass related to body mass in male *Dj-1*^{-/-} and *Dj-1*^{+/+} mice maintained on HF or control diet. Mice were assigned to the diets at 4 weeks of age. Body mass and body composition were determined every two weeks.
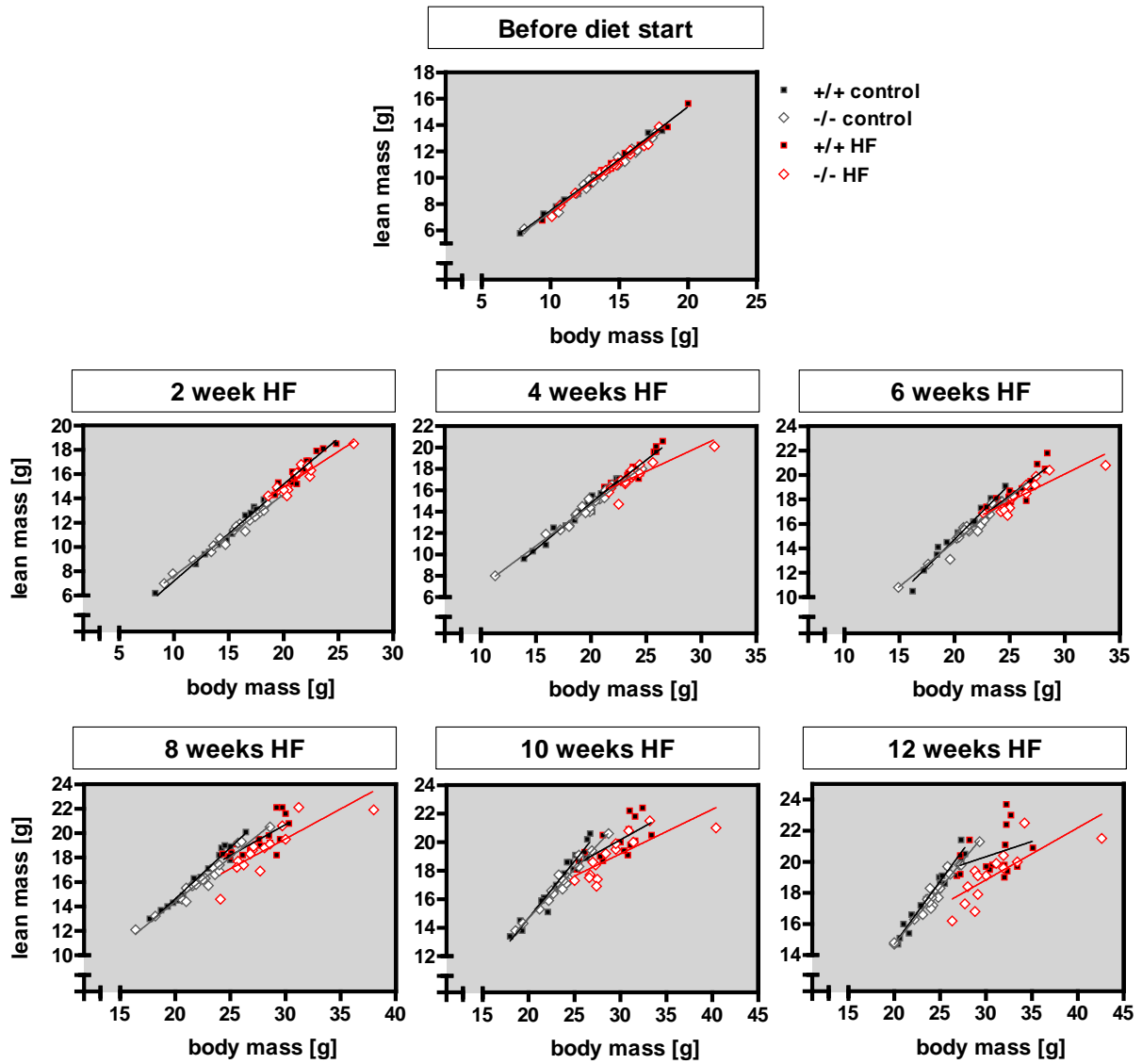
Fig. S6. Lean mass related to body mass in male *Dj-1$^{-/-}$* and *Dj-1$^{+/+}$* mice maintained on HF or control diet. Mice were assigned to the diets at 4 weeks of age. Body mass and body composition were determined every two weeks.
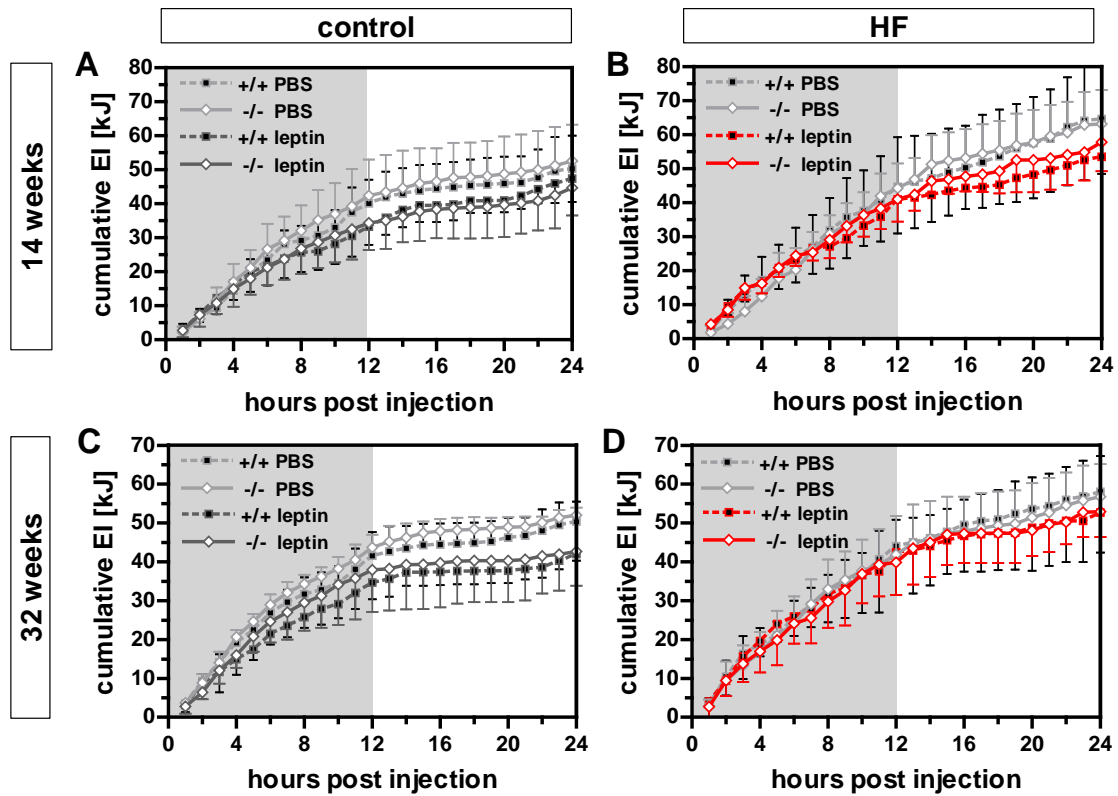
Fig. S7. Cumulative energy intake (EI) after i.p. leptin injection compared to PBS injection of male *Dj-1^-/-* **and *Dj-1^+/+* mice maintained on HF or control diet for 14 or 32 weeks.** Mice received an i.p. PBS injection on three consecutive days followed by 5 mg*kg^-1 leptin the day after. Injections were given shortly before the onset of the dark phase. Energy intake was recorded automatically for 24 hours. EI after PBS injection represents the mean of 3 days. Grey areas indicate dark-phases. Values are means ± SD ($n_{control}$ = 6-8, n_{HF} = 4-6).
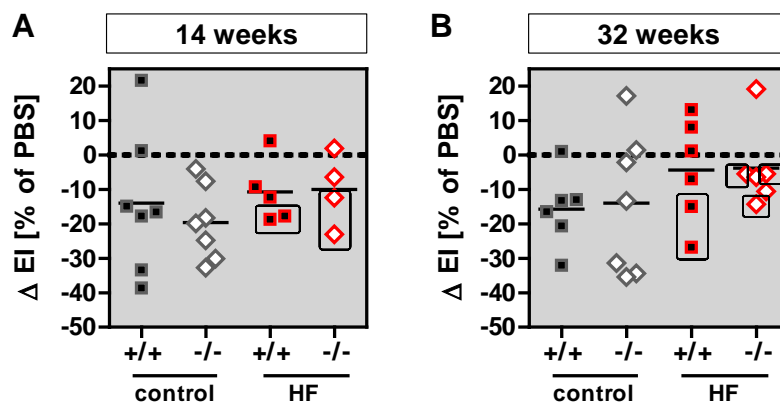
Fig. S8. 12-hour energy intake (EI) after i.p. leptin injection of male *Dj-1^-/-* and *Dj-1^+/+* mice maintained on HF or control diet for 14 or 32 weeks. EI after leptin injection is expressed in percent of the EI after PBS injections (average of 3 days). Data points represent individual animals. Dashed boxes designate mice resistant to DIO. $n_{control}$ = 6-8, n_{HF} = 4-6.
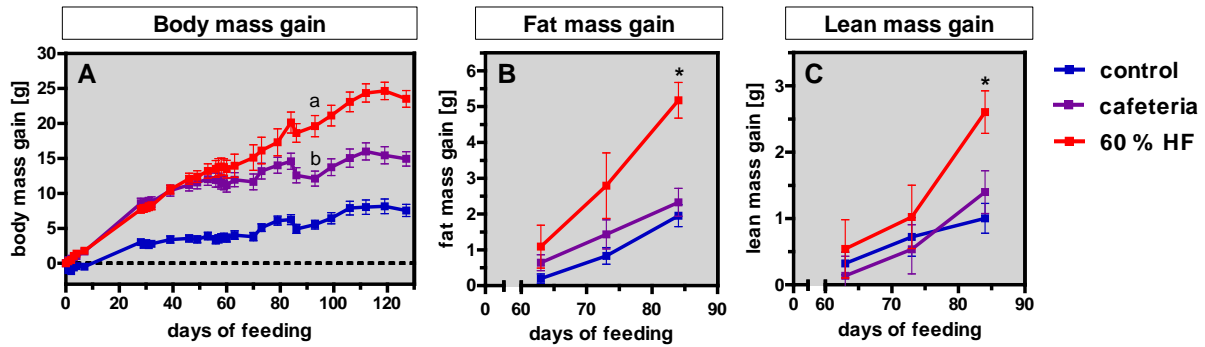
Fig. S9. Gain of body mass, fat and lean mass in male C57BL/6N mice maintained on a high-fat, 'cafeteria' or control diet for 18 weeks. Mice were placed on the diets at 10 weeks of age. Animals on 'cafeteria' diet could choose from three different tasting pellets ('salt', 'biscuit' and 'chocolate'). Diets were obtained from Ssniff Spezialdiäten GmbH, Soest, Germany (control #E15000; 60 % HF #E15741-347, beef-tallow + soybean oil; Cafeteria #S0372-E022/24/26). Body composition was assessed via NMR spectrometry (Minispec; Bruker). Values are means ± SEM (n = 10-12). General linearized model: [a,b]From day 93 on, all groups were significantly different from each other. *p < 0.05 HF vs. control. The experiment was performed at the German Mouse Clinic, Munich, Germany by Dr. Jan Rozman and Monja Willershäuser.

6.2 Supplementary tables

Table S1. Body mass, fat and lean mass of HF or control (C) diet-fed mice of the different cohorts used for follow-up experiments of the initial proteome study.

Experiment	Strain	Ori-gin	Feeding period	n	Diet	Body mass			Fat mass			Lean mass		
						diet start	diet end	gain	diet start	diet end	gain	diet start	diet end	gain
WB	BL/6N	GMC	10 days	11	C	22.4 ± 1.2	23.2 ± 1.2	0.9 ± 1.1	3.8 ± 1.2	4.1 ± 1.0	0.4 ± 0.9	16.5 ± 2.3	16.8 ± 2.1	0.1 ± 0.5
				11	HF	22.4 ± 1.3	25.0 ± 1.5**	2.6 ± 1.2**	3.6 ± 1.6	5.0 ± 1.5	1.4 ± 1.2*	15.5 ± 2.6	17.8 ± 2.2	1.3 ± 1.4*
RNA	BL/6N	TUM	10 days	6	C	23.6 ± 1.6	23.5 ± 1.0	-0.1 ± 0.6	2.3 ± 0.2	2.7 ± 0.6	0.4 ± 0.5	17.7 ± 1.5	17.2 ± 1.4	-0.5 ± 0.7
				6	HF	23.6 ± 1.8	26.4 ± 2.0**	2.8 ± 1.1***	2.3 ± 0.3	4.1 ± 1.3*	1.80 ± 1.2*	17.8 ± 1.7	18.6 ± 2.1	0.9 ± 0.7**
IEF - WB Hyp	AKR/J	TUM	10 days	4	C	25.8 ± 1.7	22.1 ± 2.9	3.8 ± 1.5	4.5 ± 1.0	2.6 ± 1.3	-1.9 ± 0.5	17.6 ± 0.4	15.8 ± 1.5	-1.8 ± 1.1
				4	HF	26.1 ± 1.0	29.4 ± 0.6*	3.4 ± 0.8***	4.2 ± 0.5	7.5 ± 0.8***	3.3 ± 0.7***	18.2 ± 0.9	18.2 ± 0.9*	0.0 ± 0.7*
IEF - WB Hyp	BL/6N	TUM	10 days	4	C	22.6 ± 1.3	21.5 ± 0.5	-1.1 ± 0.9	2.4 ± 0.1	2.3 ± 0.4	-0.1 ± 0.4	16.6 ± 1.1	15.7 ± 0.8	-0.9 ± 0.6
				4	HF	22.2 ± 0.5	25.0 ± 1.4**	2.8 ± 1.2**	1.9 ± 0.3*	4.5 ± 1.4*	2.7 ± 1.2**	17.0 ± 0.8	16.8 ± 0.6	-0.2 ± 0.3
IEF - WB eWAT	BL/6N	TUM	10 days	6	C	25.5 ± 0.8	26.7 ± 0.5	1.2 ± 0.5	2.1 ± 0.2	2.7 ± 0.2	0.6 ± 0.3	19.5 ± 1.0	20.0 ± 0.6	0.4 ± 0.7
				6	HF	26.0 ± 0.9	29.6 ± 2.1*	3.6 ± 1.8*	2.2 ± 0.4*	5.4 ± 2.0*	3.2 ± 1.8*	20.0 ± 0.9	20.3 ± 1.0	0.3 ± 0.8
NanoPro™	BL/6N	TUM	2 days	5	C	21.4 ± 0.7	20.7 ± 0.6	-0.6 ± 0.3	2.3 ± 0.3	2.1 ± 0.2	-0.3 ± 0.3	15.7 ± 0.8	15.5 ± 0.6	-0.1 ± 0.3
				5	HF	21.5 ± 0.7	21.9 ± 0.7*	0.3 ± 0.2***	2.4 ± 0.5	2.7 ± 0.4*	0.3 ± 0.2**	15.9 ± 0.5	15.8 ± 0.5	-0.1 ± 0.4
NanoPro™ & Glutathionf Muscle	BL/6N	TUM	10 days	10	C	23.1 ± 1.3	21.9 ± 0.9	-1.2 ± 0.8	2.3 ± 0.4	2.4 ± 0.5	0.1 ± 0.5	17.4 ± 1.3	16.0 ± 1.0	-1.4 ± 0.7
				10	HF	22.3 ± 1.8	24.5 ± 2.1**	2.3 ± 1.0***	1.8 ± 0.2**	3.9 ± 1.2**	2.1 ± 1.0***	17.0 ± 1.6	17.1 ± 1.5	0.1 ± 0.6***
NanoPro™	BL/6N	GMC	3 months	5	Chow*	34.4 ± 1.4	37.3 ± 1.2	3.6 ± 1.5	10.0 ± 1.1	11.9 ± 1.0	1.8 ± 0.3	20.0 ± 0.8	20.9 ± 0.8	0.8 ± 0.5
				5	HF**	37.0 ± 3.3	52.8 ± 1.8***	16.5 ± 2.2***	12.6 ± 2.2*	23.8 ± 0.9***	11.2 ± 2.2***	20.6 ± 1.4	26.1 ± 0.8***	5.5 ± 1.1***
Fractionation	BL/6N	TUM	10 days	5	C	22.4 ± 1.3	22.4 ± 1.6	0.0 ± 0.4	2.2 ± 0.5	2.4 ± 0.5	0.2 ± 0.2	16.9 ± 1.0	16.3 ± 0.9	-0.6 ± 0.3
				5	HF	21.8 ± 1.3	23.2 ± 1.1	1.3 ± 0.5**	2.4 ± 0.4	3.5 ± 0.5*	1.1 ± 0.3*	16.1 ± 1.1	16.2 ± 1.0	0.1 ± 0.6*
Glutathion Hyp and Brain	BL/6N	TUM	10 days	8	C	24.1 ± 2.1	23.5 ± 1.8	-0.6 ± 0.8	2.0 ± 0.4	2.7 ± 0.5	0.6 ± 0.5	18.6 ± 1.9	17.2 ± 1.2	-1.4 ± 0.9
				8	HF	24.4 ± 1.8	26.8 ± 3.0*	2.4 ± 1.8***	2.4 ± 0.7	5.0 ± 2.3*	2.6 ± 1.6*	18.4 ± 1.3	18.1 ± 0.9	-0.4 ± 0.6
NAC treatment	BL/6N	TUM	10 days	9	C	23.5 ± 1.8	23.6 ± 1.6	0.1 ± 0.6	2.3 ± 0.4	2.8 ± 0.6	0.5 ± 0.5	17.5 ± 1.7	16.9 ± 1.1	-0.5 ± 1.0
				8	HF	22.8 ± 2.0	24.4 ± 3.0	1.6 ± 1.3***	2.2 ± 0.3	3.9 ± 1.3**	1.7 ± 1.1***	17.3 ± 1.6	17.0 ± 1.7	-0.4 ± 0.4
Mito function & NanoPro™ (eWAT)	BL/6N	TUM	10 days	20	C	24.0 ± 1.2	23.7 ± 1.2	-0.3 ± 0.7	2.4 ± 0.7	2.6 ± 0.6	0.3 ± 0.5	18.2 ± 1.1	17.4 ± 1.1	-0.8 ± 0.4
				21	HF	24.3 ± 1.5	26.7 ± 2.2***	2.5 ± 1.3***	2.5 ± 0.6	5.2 ± 1.6***	2.7 ± 1.2***	18.2 ± 1.3	17.8 ± 1.2	-0.4 ± 0.5**

Values are means ± SD. Student's t-test *p < 0.05, **p < 0.01, ***p < 0.001 HF vs. control diet fed mice. WB – Western blot. IEF - Isoelectric focusing. Hyp - hypothalamus. eWAT - epididymal white adipose tissue. NAC – N-acetylcysteine. Mito - mitochondria. GMC - German Mouse Clinic. TUM – TU München, Kleintierforschungszentrum. C – control diet. HF – High-fat diet.

*Altromin International, Lage, Germany (#1314TPF), **60 cal% from fat (tallow), Ssniff Spezialdiäten GmbH, Soest Germany (#E15741-347).

Table S2. Gene expression analysis using qRT-PCR. Analyzed were candidates from the initial proteome study and targets functionally related to DJ-1.

Gene symbol	Gene ID	Gene name	Relative expression levels*				Comment
			control	HF	Ratio HF/C	t-test p-value	
Candidates from the proteome study investigating the hypothalami of mice after 10 days of HF or control diet-feeding							
Park7	57320	Parkinson disease (autosomal recessive, early onset) 7	0.97 ± 0.13	1.02 ± 0.25	1.05	0.6740	upregulated in AKR/J, C57BL/6N and SWR/J
Sh3bgrl3	73723	SH3 domain binding glutamic acid-rich protein-like 3	1.09 ± 0.46	1.11 ± 0.52	1.03	0.9232	upregulted in AKR/J
Sncb	104069	synuclein, beta	1.08 ± 0.40	1.05 ± 0.35	0.97	0.9000	upregulted in AKR/J
Ppp3r1	19058	protein phosphatase 3, regulatory subunit B, alpha isoform (calcineurin B, type I)	1.12 ± 0.22	0.83 ± 0.23	0.74	0.0595	downregulated in AKR/J
Acot13	66834	acyl-CoA thioesterase 13	1.15 ± 0.35	0.92 ± 0.44	0.80	0.3363	downregulated in AKR/J
Phb	18673	Prohibitin	1.09 ± 0.56	1.08 ± 0.53	0.99	0.9718	upregulated in C57BL/6N
Psmb6	19175	proteasome (prosome, macropain) subunit, beta type 6	0.95 ± 0.51	1.18 ± 0.72	1.23	0.5554	downregulated in C57BL/6N
Snca	20617	synuclein, alpha	1.10 ± 0.25	1.05 ± 0.29	0.95	0.7453	downregulated in C57BL/6N
Hrsp12	15473	heat-responsive protein 12	1.00 ± 0.27	1.04 ± 0.47	1.04	0.8775	downregulated in C57BL/6N
Ndufv2	72900	NADH dehydrogenase [ubiquinone] flavoprotein 2, mitochondrial	0.92 ± 0.16	1.17 ± 0.47	1.28	0.2438	upregulted in SWR/J
Targets functionally related to DJ-1							
Pten	19211	phosphatase and tensin homolog	1.02 ± 0.15	1.02 ± 0.19	1.00	0.9867	Kim *et al. [2005a]*
Sod1	20655	superoxide dismutase 1	1.18 ± 0.40	1.10 ± 0.64	0.93	0.7991	Wang *et al. [2011]*
Trp53	22059	transformation related protein 53	0.97 ± 0.23	0.99 ± 0.23	1.02	0.8806	Fan *et al. [2008a]*
Nqo1	18104	NAD(P)H dehydrogenase, quinone 1	1.06 ± 0.20	0.97 ± 0.23	0.91	0.4681	Clements *et al. [2006]*
Gclc	14629	glutamate-cysteine ligase, catalytic subunit	1.15 ± 0.39	1.00 ± 0.43	0.87	0.5458	Zhou & Freed *[2005];* Zhong & Xu *[2008]*
Gclm	14630	glutamate-cysteine ligase, modifier subunit	1.13 ± 0.41	0.80 ± 0.12	0.71	0.0927	Zhou & Freed *[2005]*
Bax	12028	BCL2-associated X protein	0.99 ± 0.16	1.04 ± 0.56	1.05	0.8410	Fan *et al. [2008b]*
Slc25a27	74011	solute carrier family 25, member 27	0.94 ± 0.31	0.99 ± 0.58	1.06	0.8313	Guzman *et al. [2010]*
Slc25a14	20523	solute carrier family 25 (mitochondrial carrier, brain), member 14	1.25 ± 0.42	0.89 ± 0.30	0.71	0.1332	Guzman *et al. [2010]*

*Normalized to *Hsp90* expression. Values are means ± SD.

Table S3. Body mass, fat and lean mass of male and female *Dj-1$^{-/-}$* and *Dj-1$^{+/+}$* mice at 4 weeks of age.

	Males		Females	
	+/+ n = 32	-/- n = 33	+/+ n = 30	-/- n = 27
body mass [g]	14.2 ± 2.7	14.1 ± 2.4	13.0 ± 1.8	12.2 ± 1.9
fat mass [g]	1.8 ± 0.4	2.0 ± 0.4	1.8 ± 0.3	1.9 ± 0.5
lean mass [g]	10.7 ± 2.1	10.5 ± 1.9	9.6 ± 1.3	8.8 ± 1.2*

Values are means ± SD. Student's t-test *p < 0.05.

Table S4. Spontaneous locomotor activity of male and female *Dj-1$^{-/-}$* and *Dj-1$^{+/+}$* mice maintained on control diet for 32 weeks. Animals were kept in the feeding-drinking-activity setup (TSE Systems). Activity parameters of one dark-phase were analyzed after mice had been accustomed to the cages for one day. Total activity refers to beam break counts in X, Y and Z direction, horizontal activity to X and Y direction and rearing activity to Z direction (vertical movement).

	+/+	-/-	t-test p-value
Males			
total activity [counts x10^3]	63.0 ± 16.8	47.5 ± 10.4	**0.0484**
horizontal activity [counts x10^3]	59.5 ± 15.4	45.1 ± 9.9	**0.0482**
rearing activity [counts x10^3]	3.5 ± 1.5	2.4 ± 0.6	0.0791
ambulatory movement [counts x10^3]	41.9 ± 12.9	30.1 ± 8.3	0.0525
fine movement [counts x10^3]	17.6 ± 2.8	15.0 ± 2.0	0.0587
distance [m]	721 ± 193	530 ± 166	0.0600
speed [m*h^{-1}]	59.0 ± 16.3	43.1 ± 14.0	0.0626
Females			
total activity [counts x10^3]	83.1 ± 35.4	60.8 ± 32.1	0.3057
horizontal activity [counts x10^3]	77.9 ± 33.3	57.9 ± 31.3	0.3337
rearing activity [counts x10^3]	5.2 ± 2.5	3.0 ± 1.4	0.1008
ambulatory movement [counts x10^3]	58.0 ± 26.8	41.0 ± 25.7	0.3156
fine movement [counts x10^3]	20.0 ± 6.5	16.8 ± 5.7	0.4258
distance [m]	1031 ± 493	733 ± 420	0.3143
speed [m*h^{-1}]	85.2 ± 41.2	60.1 ± 35.4	0.3138

Values are means ± SD (n_{males} = 7-8, $n_{females}$ = 5-6).

Table S5. Genes located on chromosome 4 found differentially regulated between *Dj-1^{-/-}* and *Dj-1^{+/+}* mice on control as well as on HF diet. Listed are representative transcripts corresponding to these genes sorted by their distance to *Dj-1* (*Park7*).

Transcript accession	Gene symbol	Gene ID	Strand	Start	End	Length	Regulation*	Distance to Park7 [kb]
AK019903	5330422M15Rik	77062	-	150352752	150354072	1321	up	64
NM_020569	**Park7**	**57320**	**-**	**150271242**	**150284030**	**903**	**down**	**0**
NM_023119	Eno1	13806	+	149611306	149622982	1776	down	-648
NM_019741	Slc2a5	56485	+	149493453	149518277	3096	down	-753
NM_010767	Masp2	17175	+	147976653	147978522	744	up	-2287
NM_027873	Ubiad1	71707	-	147808606	147818860	2970	up	-2452
AK160667	Ptchd2	242748	-	147610973	147611838	866	down	-2659
NM_173401	Fbxo44	230903	-	147526909	147534173	1813	down	-2737
NM_001025365	Miip	28010	-	147234887	147242828	1813	down	-3028
NM_145078	2610305D13Rik	112422	-	146986045	147016617	2561	down	-3255
XM_003084609	Gm16503	100038537	+	146914327	146917609	3283	down	-3354
NM_001039209	Gm13152	195531	+	146881712	146887529	1241	down	-3384
NM_009401	Tnfrsf8	21941	-	144858879	144905050	1575	down	-5366

*in *Dj-1^{-/-}* versus *Dj-1^{+/+}* mice

Table S6. Diet-regulated genes in wildtype mice. Mice were maintained on HF or control diet for 14 weeks. The ventral hypothalamus was subjected to RNA sequencing. Listed are genes for which at least one transcript was found differentially expressed (Student's t-test, $p < 0.01$). A log2 fold change > 0.26 indicates upregulation and < -0.26 downregulation in HF versus control diet-fed mice, corresponding to a fold change of > 1.2 or < -1.2, respectively.

Gene symbol	Gene ID	Gene name	Mean log2 fold change*
1110017D15Rik	73721	RIKEN cDNA 1110017D15 gene	-0.41
1200014J11Rik	66874	RIKEN cDNA 1200014J11 gene	0.32
2610035F20Rik	69248	RIKEN cDNA 2610035F20 gene	-1.34
2610037D02Rik	70040	RIKEN cDNA 2610037D02 gene	0.96
2810055G20Rik	77994	RIKEN cDNA 2810055G20 gene	-0.36
2810422O20Rik	69962	RIKEN cDNA 2810422O20 gene	-0.26
3110057O12Rik	269423	RIKEN cDNA 3110057O12 gene	0.94
4930402H24Rik	228602	RIKEN cDNA 4930402H24 gene	0.28
4933427G17Rik	74466	RIKEN cDNA 4933427G17 gene	-0.76
5330422M15Rik	77062	RIKEN cDNA 5330422M15 gene	-1.77
6030400A10Rik	77069	RIKEN cDNA 6030400A10 gene	-0.71
8030443G20Rik	77173	RIKEN cDNA 8030443G20 gene	-0.75
9630017O17	331021	hypothetical protein 9630017O17	-0.56
A230038B01Rik	319276	RIKEN cDNA A230038B01 gene	-0.49
A630072M18Rik	320770	RIKEN cDNA A630072M18 gene	0.59
A730037C10Rik	320604	RIKEN cDNA A730037C10 gene	-0.92
AA960436	101985	expressed sequence AA960436	0.49
Abi3	66610	ABI gene family, member 3	0.58
Adam19	11492	a disintegrin and metallopeptidase domain 19 (meltrin beta)	0.62
Akr1b3	11677	aldo-keto reductase family 1, member B3 (aldose reductase)	0.30
Antxr2	71914	anthrax toxin receptor 2	-0.55
Anxa4	11746	annexin A4	-0.29
Anxa8	11752	annexin A8	-1.26
Apcdd1	494504	adenomatosis polyposis coli down-regulated 1	-0.28
Arhgap25	232201	Rho GTPase activating protein 25	0.76
Arhgap30	226652	Rho GTPase activating protein 30	0.42
Atic	108147	5-aminoimidazole-4-carboxamide ribonucleotide formyltransferase/IMP cyclohydrolase	-0.48
B3galnt2	97884	UDP-GalNAc:betaGlcNAc beta 1,3-galactosaminyltransferase, polypeptide 2	-0.49
B3gnt5	108105	UDP-GlcNAc:betaGal beta-1,3-N-acetylglucosaminyltransferase 5	0.73
B4galnt2	14422	beta-1,4-N-acetyl-galactosaminyl transferase 2	0.71
BC046251	407810	cDNA sequence BC046251	-0.58
BC051142	407788	cDNA sequence BC051142; testis specific basic protein	-0.38
C030013D06Rik	77376	RIKEN cDNA C030013D06 gene	0.67
Ccdc15	245902	coiled-coil domain containing 15	-0.27
Ccdc88a	108686	coiled coil domain containing 88A	-0.44
Ccdc90a	76137	coiled-coil domain containing 90A	0.30
Cd72	12517	CD72 antigen	0.74
Cd9	12527	CD9 antigen	-0.73
Cdk5rap2	214444	CDK5 regulatory subunit associated protein 2	0.38
Cideb	12684	cell death-inducing DNA fragmentation factor, alpha subunit-like effector B	0.55
Clcn2	12724	chloride channel 2	0.28
Coro6	216961	coronin 6	0.51
Crhr1	12921	corticotropin releasing hormone receptor 1	0.52
Crip3	114570	cysteine-rich protein 3	0.35
Csf3r	12986	colony stimulating factor 3 receptor (granulocyte)	1.03

Table S6. Continued.

Gene symbol	Gene ID	Gene name	Mean log2 fold change*
D1Pas1	110957	DNA segment, Chr 1, Pasteur Institute 1	-0.26
Dab2	13132	disabled homolog 2 (Drosophila)	-0.60
Dgki	320127	diacylglycerol kinase, iota	0.39
Dleu2	668253	predicted gene 9069	0.87
Dnmt3b	13436	DNA methyltransferase 3B	0.84
Edn1	13614	endothelin 1	0.57
Entpd7	93685	ectonucleoside triphosphate diphosphohydrolase 7	0.38
Epb4.1l4a	13824	erythrocyte protein band 4.1-like 4a	0.65
Esr2	13983	estrogen receptor 2 (beta)	-0.92
Etv6	14011	ets variant gene 6 (TEL oncogene)	0.56
Exoc6	107371	exocyst complex component 6	0.82
Fbln1	14114	fibulin 1	-0.58
Fhl2	14200	four and a half LIM domains 2	0.36
Fnip2	329679	folliculin interacting protein 2	0.77
Foxp2	114142	forkhead box P2	0.60
Fras1	231470	Fraser syndrome 1 homolog (human)	0.34
Gbp3	55932	guanylate binding protein 3	0.49
Gm10425	100038720	predicted gene 10425	0.41
Gm11974	100041286	predicted gene 11974	-0.30
Gm4980	100503386	predicted gene 4980	0.44
Gm5106	330031	predicted gene 5106	1.84
Gm9958	791294	predicted gene 9958	0.39
Got1l1	76615	glutamic-oxaloacetic transaminase 1-like 1	-0.71
Gpr137c	70713	G protein-coupled receptor 137C	-1.02
Heatr5a	320487	HEAT repeat containing 5A	0.77
Hhex	15242	hematopoietically expressed homeobox	0.48
Hist2h2be	319190	histone cluster 2, H2be	0.30
Il17rd	171463	interleukin 17 receptor D	-0.31
Inadl	12695	InaD-like (Drosophila)	-0.45
Kcnq5	226922	potassium voltage-gated channel, subfamily Q, member 5	0.29
Kctd18	51960	potassium channel tetramerisation domain containing 18	-0.48
Kif27	75050	kinesin family member 27	-0.46
Kif6	319991	kinesin family member 6	-0.65
Lama4	16775	laminin, alpha 4	-0.53
Lamb2	16779	laminin, beta 2	-0.35
Lima1	65970	LIM domain and actin binding 1	-0.43
LOC100046116	100046116	L1 repeat, Gf subfamily, member 21	-0.53
LOC100503272	100503272	predicted gene 11423	0.85
Ltk	17005	leukocyte tyrosine kinase	0.42
Megf6	230971	multiple EGF-like-domains 6	-0.30
Mettl13	71449	methyltransferase like 13	0.79
Mier1	71148	mesoderm induction early response 1 homolog (Xenopus laevis)	-0.57
Mitf	17342	microphthalmia-associated transcription factor	0.56
Mmp16	17389	matrix metallopeptidase 16	-0.47
Mrps10	64657	mitochondrial ribosomal protein S10	0.43
Myb	17863	myeloblastosis oncogene	-0.54
Mzt1	76789	RIKEN cDNA 2410129H14 gene	0.34
Naa20	67877	N-acetyltransferase 5 (ARD1 homolog, S. cerevisiae)	0.69
Nckap5	210356	RIKEN cDNA E030049G20 gene	-0.33
Nfia	18027	nuclear factor I/A	0.73
Nppa	230899	natriuretic peptide precursor type A	-0.37
Nr2e1	21907	nuclear receptor subfamily 2, group E, member 1	0.51

Table S6. Continued.

Gene symbol	Gene ID	Gene name	Mean log2 fold change*
Nrg1	211323	neuregulin 1	0.68
Nsun5	100609	NOL1/NOP2/Sun domain family, member 5	0.44
Nup98	269966	nucleoporin 98	0.36
Onecut1	15379	one cut domain, family member 1	-0.56
Oprm1	18390	opioid receptor, mu 1	-0.31
Osbpl3	71720	oxysterol binding protein-like 3	0.59
Pak4	70584	p21 protein (Cdc42/Rac)-activated kinase 4	-0.42
Pde5a	242202	phosphodiesterase 5A, cGMP-specific	0.58
Plagl1	22634	pleiomorphic adenoma gene-like 1	0.51
Plekhg1	213783	pleckstrin homology domain containing, family G (with RhoGef domain) member 1	0.31
Ptgs1	19224	prostaglandin-endoperoxide synthase 1	0.69
Rac2	19354	RAS-related C3 botulinum substrate 2	1.11
Rapgef4	56508	Rap guanine nucleotide exchange factor (GEF) 4	0.99
Rasd2	75141	RASD family, member 2	0.27
Rbm10	236732	RNA binding motif protein 10; predicted gene 12799	0.37
Rbm4b	66704	RNA binding motif protein 4B	0.49
Rec8	56739	REC8 homolog (yeast)	-0.45
Rfx4	71137	regulatory factor X, 4 (influences HLA class II expression)	-0.27
Rnf135	71956	ring finger protein 135	0.88
Rpa1	68275	replication protein A1	0.64
Runx1	12394	runt related transcription factor 1	0.75
Scarb1	20778	scavenger receptor class B, member 1	0.31
Skp2	27401	S-phase kinase-associated protein 2 (p45)	0.30
Slc12a1	20495	solute carrier family 12, member 1	-0.54
Slc2a4	20528	solute carrier family 2 (facilitated glucose transporter), member 4	0.43
Slc38a3	76257	solute carrier family 38, member 3	0.36
Snap47	67826	synaptosomal-associated protein, 47	0.29
Snapc3	77634	small nuclear RNA activating complex, polypeptide 3	-0.49
Snrnp25	78372	small nuclear ribonucleoprotein 25 (U11/U12)	0.29
Sox12	20667	SRY-box containing gene 12	0.47
Sp110	109032	predicted gene 15753; Sp110 nuclear body protein	0.74
Sv2b	64176	synaptic vesicle glycoprotein 2 b	0.36
Tiam2	24001	T-cell lymphoma invasion and metastasis 2	0.52
Tmc3	233424	transmembrane channel-like gene family 3	1.19
Tmco4	77056	transmembrane and coiled-coil domains 4	-0.79
Tmem216	68642	transmembrane protein 216	0.85
Tmem63a	208795	transmembrane protein 63a	0.83
Tmem88	67020	transmembrane protein 88	0.86
Trip13	69716	thyroid hormone receptor interactor 13	-0.49
Tsen2	381802	tRNA splicing endonuclease 2 homolog (S. cerevisiae)	0.64
Txnip	56338	thioredoxin interacting protein	-0.27
Ubap2	68926	ubiquitin-associated protein 2	1.15
Uckl1os	100271841	uridine-cytidine kinase 1-like 1 opposite strand	-0.47
Vcan	13003	versican	0.40
Vps8	209018	vacuolar protein sorting 8 homolog (S. cerevisiae)	0.30
Wfikkn2	278507	WAP, follistatin/kazal, immunoglobulin, kunitz and netrin domain containing 2	-0.31
Wrap53	216853	WD repeat containing, antisense to TP53	0.37
Ywhaq	22630	tyrosine 3-monooxygenase/tryptophan 5-monooxygenase activation protein, theta polypeptide	0.69
Zic1	22771	similar to Zic protein; zinc finger protein of the cerebellum 1	-1.02

*mean of log2 fold changes of all transcripts found differentially expressed for each gene

Table S7. Diet-regulated genes in *Dj-1*^{-/-} mice. Mice were maintained on HF or control diet for 14 weeks. The ventral hypothalamus was subjected to RNA sequencing. Listed are genes for which at least one transcript was found differentially expressed (Student's t-test, $p < 0.01$). A log2 fold change > 0.26 indicates upregulation and < -0.26 downregulation in HF versus control diet-fed mice, corresponding to a fold change of > 1.2 or < -1.2, respectively.

Gene symbol	Gene ID	Gene name	Mean log2 fold change*
1110014N23Rik	68505	RIKEN cDNA 1110014N23 gene	0.45
1110067D22Rik	216551	RIKEN cDNA 1110067D22 gene	0.32
1600002K03Rik	69770	RIKEN cDNA 1600002K03 gene	0.36
1700052N19Rik	73419	RIKEN cDNA 1700052N19 gene	-0.40
1700112E06Rik	76633	RIKEN cDNA 1700112E06 gene	0.82
2010111I01Rik	72061	RIKEN cDNA 2010111I01 gene	0.31
2310046O06Rik	78323	RIKEN cDNA 2310046O06 gene	0.32
2610019N06Rik	66299	RIKEN cDNA 2610019N06 gene	0.28
2610029G23Rik	67683	RIKEN cDNA 2610029G23 gene	0.32
2900022P04Rik	72868	RIKEN cDNA 2900022P04 gene	0.73
3300002I08Rik	69277	RIKEN cDNA 3300002I08 gene	0.89
3830408C21Rik	100040322	hypothetical protein LOC100040322	0.49
4921525O09Rik	74050	RIKEN cDNA 4921525O09 gene	0.85
4930422G04Rik	71643	RIKEN cDNA 4930422G04 gene	0.36
4930512B01Rik	74724	RIKEN cDNA 4930512B01 gene	0.44
4930579G22Rik	69034	RIKEN cDNA 4930579G22 gene	0.74
9930120I10Rik	77746	RIKEN cDNA 9930120I10 gene	1.19
A230107N01Rik	320919	RIKEN cDNA A230107N01 gene	0.65
A330076C08Rik	320263	RIKEN cDNA A330076C08 gene	0.56
Aasdh	231326	aminoadipate-semialdehyde dehydrogenase	0.72
Aass	30956	aminoadipate-semialdehyde synthase	0.84
Abcb1b	18669	ATP-binding cassette, sub-family B (MDR/TAP), member 1B	0.69
Acad10	71985	acyl-Coenzyme A dehydrogenase family, member 10	0.56
Acss1	68738	acyl-CoA synthetase short-chain family member 1	0.43
Acss2	60525	acyl-CoA synthetase short-chain family member 2	0.45
Adat2	66757	adenosine deaminase, tRNA-specific 2, TAD2 homolog (S. cerevisiae)	0.36
Aldob	230163	aldolase B, fructose-bisphosphate	-0.29
Amigo2	105827	adhesion molecule with Ig like domain 2	0.28
Ano5	233246	anoctamin 5	0.45
Apex2	77622	apurinic/apyrimidinic endonuclease 2	-0.37
Aph1c	68318	anterior pharynx defective 1c homolog (C. elegans)	0.76
Arhgef16	230972	Rho guanine nucleotide exchange factor (GEF) 16	-0.29
Asb4	65255	ankyrin repeat and SOCS box-containing 4	0.46
Atad2	70472	ATPase family, AAA domain containing 2	0.74
Atf1	11908	activating transcription factor 1	0.81/-0.45
Atp13a4	224079	ATPase type 13A4	0.50
Atp13a5	268878	ATPase type 13A5	0.55
Atp5j2	57423	ATP synthase, H+ transporting, mitochondrial F0 complex, subunit f, isoform 2	0.30
Auts2	319974	autism susceptibility candidate 2	-0.45
Bambi-ps1	81913	BMP and activin membrane-bound inhibitor, pseudogene (Xenopus laevis)	0.72
Birc3	11796	baculoviral IAP repeat-containing 3	0.48
Btf3	218490	basic transcription factor 3	0.40
Btf3l4	70533	basic transcription factor 3-like 4	0.46
C330018D20Rik	77422	RIKEN cDNA C330018D20 gene	0.44
C3ar1	12267	complement component 3a receptor 1	0.70

Table S7. Continued.

Gene symbol	Gene ID	Gene name	Mean log2 fold change*
C530005A16Rik	654318	RIKEN cDNA C530005A16 gene	0.31
C630043F03Rik	68285	RIKEN cDNA C630043F03 gene	0.32
Cbfa2t3	12398	core-binding factor, runt domain, alpha subunit 2, translocated to, 3 (human)	-0.30
Ccdc17	622665	coiled-coil domain containing 17	0.58
Ccl9	20308	chemokine (C-C motif) ligand 9	1.14
Ccr5	12774	chemokine (C-C motif) receptor 5	0.95
Cdhr3	68764	RIKEN cDNA 1110049B09 gene	0.50
Cdkn2c	12580	cyclin-dependent kinase inhibitor 2C (p18, inhibits CDK4)	0.61
Chm	12662	similar to choroidermia; choroidermia	0.42
Chmp6	208092	chromatin modifying protein 6	0.58
Clcf1	56708	cardiotrophin-like cytokine factor 1	0.94
Clpx	270166	caseinolytic peptidase X (E.coli)	0.51
Col13a1	12817	collagen, type XIII, alpha 1	0.71
Col1a2	12843	collagen, type I, alpha 2	0.66
Coq2	71883	coenzyme Q2 homolog, prenyltransferase (yeast)	0.61
Cplx1	12889	complexin 1	-0.32
Ctu2	66965	RIKEN cDNA 2310061F22 gene	0.50
Cyp4f13	170716	cytochrome P450, family 4, subfamily f, polypeptide 13	0.61
D10Wsu102e	28109	DNA segment, Chr 10, Wayne State University 102, expressed	0.43
Dach2	93837	dachshund 2 (Drosophila)	-0.69
Dapp1	26377	dual adaptor for phosphotyrosine and 3-phosphoinositides 1	0.39
Dcbld2	73379	discoidin, CUB and LCCL domain containing 2	0.54
Ddx51	69663	DEAD (Asp-Glu-Ala-Asp) box polypeptide 51	0.33
Deaf1	54006	deformed epidermal autoregulatory factor 1 (Drosophila)	0.77
Dhx40	67487	DEAH (Asp-Glu-Ala-His) box polypeptide 40	0.32
Dync2li1	213575	dynein cytoplasmic 2 light intermediate chain 1	0.29
E030016H06Rik	402722	RIKEN cDNA E030016H06 gene	0.60
E130311K13Rik	329659	RIKEN cDNA E130311K13 gene	1.08
Eml6	237711	RIKEN cDNA C230094A16 gene	0.33
Ercc2	13871	excision repair cross-complementing rodent repair deficiency, complementation group 2	0.34
Erg	13876	avian erythroblastosis virus E-26 (v-ets) oncogene related	0.44
Etfa	110842	electron transferring flavoprotein, alpha polypeptide	0.44
Etfb	110826	electron transferring flavoprotein, beta polypeptide	0.39
Etv6	14011	ets variant gene 6 (TEL oncogene)	0.28
Ezh1	14055	enhancer of zeste homolog 1 (Drosophila)	0.34
Fam110b	242297	family with sequence similarity 110, member B	-0.52
Fam179a	320159	family with sequence similarity 179, member A	0.68
Fam184b	58227	family with sequence similarity 184, member B	0.39
Fam198b	68659	RIKEN cDNA 1110032E23 gene	0.83
Fbxo17	50760	F-box protein 17	0.54
Fbxw17	109082	F-box and WD-40 domain protein 17	0.32
Flt3l	14256	FMS-like tyrosine kinase 3 ligand	0.43
Fndc1	68655	fibronectin type III domain containing 1	0.68
Fpgs	14287	folylpolyglutamyl synthetase	-0.34
Fundc2	67391	FUN14 domain containing 2	0.32
Gbp11	634650	guanylate-binding protein 10; RIKEN cDNA 5830443L24 gene	0.79
Ggcx	56316	gamma-glutamyl carboxylase	0.48
Ggta1	14594	glycoprotein galactosyltransferase alpha 1, 3	0.58
Gk5	235533	glycerol kinase 5 (putative)	0.46
Glrx2	69367	glutaredoxin 2 (thioltransferase)	0.27
Gm10574	100038412	predicted gene 10574	0.79

Table S7. Continued.

Gene symbol	Gene ID	Gene name	Mean log2 fold change*
Gm12258	237769	predicted gene 12258	0.42
Gm12472	100038450	predicted gene 12472	0.83
Gm14446	667373	predicted gene 14446	0.53
Gm2149	100039307	predicted gene 2149	-0.27
Gm2897	100040671	alpha7-takusan	0.83
Gm5633	434693	mRNA turnover 4, homolog (S. cerevisiae); predicted gene 5633	-0.41
Gm6287	622116	predicted gene 6287	0.74
Gng5	14707	guanine nucleotide binding protein (G protein), gamma 5	0.41
Gnpda1	26384	glucosamine-6-phosphate deaminase 1	0.29
Gpr107	277463	G protein-coupled receptor 107	0.77
Gpr173	70771	G-protein coupled receptor 173	0.29
Grk4	14772	G protein-coupled receptor kinase 4	-0.34
Gtf2f2	68705	general transcription factor IIF, polypeptide 2	0.39
Gtpbp8	66067	GTP-binding protein 8 (putative)	0.41
Gypc	71683	glycophorin C	0.81
H2-Q7	15018	histocompatibility 2, Q region locus 7	1.69
Heatr6	217026	HEAT repeat containing 6	0.68
Hibadh	58875	3-hydroxyisobutyrate dehydrogenase	0.43
Higd1b	75689	HIG1 domain family, member 1B	0.65
Hist1h4i	319158	histone cluster 1, H4i	0.63
Hk2	15277	hexokinase 2	0.54
Hrh1	15465	histamine receptor H1	0.65
Htr1d	15552	5-hydroxytryptamine (serotonin) receptor 1D	-0.29
Ifi30	65972	interferon gamma inducible protein 30	0.58
Ifngr1	15979	interferon gamma receptor 1	0.27
Igf2bp2	319765	insulin-like growth factor 2 mRNA binding protein 2	-0.60
Il17rc	171095	interleukin 17 receptor C	0.45
Irf4	16364	interferon regulatory factor 4	1.60
Ivd	56357	isovaleryl coenzyme A dehydrogenase	0.58
Lama1	16772	laminin, alpha 1	0.46
Lcp1	18826	lymphocyte cytosolic protein 1	0.33
Ldha	16828	lactate dehydrogenase A	0.28
Lgi4	243914	leucine-rich repeat LGI family, member 4	0.61
Limk2	16886	LIM motif-containing protein kinase 2	0.81
Lmbr1l	74775	limb region 1 like	0.38
Lmnb2	16907	lamin B2	-0.33
Lmo3	109593	LIM domain only 3	0.41
Lnx2	140887	ligand of numb-protein X 2	-0.43
LOC100503212	100503212	uncharacterized LOC100503212	0.80
LOC100504141	100504141	predicted gene, 20083	0.79
LOC100504191	100504191	predicted gene 16576	0.46
LOC100504501	100504501	predicted gene, 20257	1.23
LOC100504662	100504662	predicted gene, 20338	0.37
Lpo	76113	lactoperoxidase	0.64
Lrrc38	242735	leucine rich repeat containing 38	0.76
Med30	69790	mediator complex subunit 30	0.27
Megf11	214058	multiple EGF-like-domains 11	0.32
Mitd1	69028	MIT, microtubule interacting and transport, domain containing 1	-0.51
Mrpl30	107734	mitochondrial ribosomal protein L30	-0.52
Mrpl36	94066	mitochondrial ribosomal protein L36	0.35
N4bp3	212706	RIKEN cDNA C330016O10 gene	-0.37
Naip2	17948	NLR family, apoptosis inhibitory protein 2	1.08

Table S7. Continued.

Gene symbol	Gene ID	Gene name	Mean log2 fold change*
Ncald	52589	neurocalcin delta	0.27
Neat1	66961	RIKEN cDNA 2310043N10 gene	0.47
Nek8	140859	NIMA (never in mitosis gene a)-related expressed kinase 8	-0.51
Nfe2l3	18025	nuclear factor, erythroid derived 2, like 3	0.39
Nfs1	18041	nitrogen fixation gene 1 (S. cerevisiae)	0.40
Nhlrc3	212114	NHL repeat containing 3	0.35
Npr1	18160	natriuretic peptide receptor 1	0.71
Nudt7	67528	nudix (nucleoside diphosphate linked moiety X)-type motif 7	0.60
Nxf3	245610	nuclear RNA export factor 3	0.77
Opcml	330908	opioid binding protein/cell adhesion molecule-like	-0.28
Oscp1	230751	similar to organic solute carrier protein 1	0.51
Oxsm	71147	3-oxoacyl-ACP synthase, mitochondrial	0.41
Pak1ip1	68083	PAK1 interacting protein 1	0.27
Papss2	23972	3'-phosphoadenosine 5'-phosphosulfate synthase 2	0.37
Pcbd1	13180	pterin 4 alpha carbinolamine dehydratase/dimerization cofactor of hepatocyte nuclear factor 1 alpha (TCF1) 1	0.29
Pde4d	238871	phosphodiesterase 4D, cAMP specific	0.63
Pdk1	228026	pyruvate dehydrogenase kinase, isoenzyme 1	0.27
Pdyn	18610	prodynorphin	0.46
Pfdn1	67199	prefoldin 1	0.30
Phtf2	68770	putative homeodomain transcription factor 2	-0.29
Pik3cg	30955	phosphoinositide-3-kinase, catalytic, gamma polypeptide	0.37
Plek	56193	pleckstrin	0.42
Pole	18973	polymerase (DNA directed), epsilon	-0.48
Ppp4r1	70351	protein phosphatase 4, regulatory subunit 1	-0.70
Ptchd2	242748	patched domain containing 2	0.75
Ptpn4	19258	protein tyrosine phosphatase, non-receptor type 4	0.53
Pycr2	69051	pyrroline-5-carboxylate reductase family, member 2	-0.50
Rab2b	76338	RAB2B, member RAS oncogene family	0.34
Rab7l1	226422	RAB7, member RAS oncogene family-like 1	0.79
Rbm39	170791	RNA binding motif protein 39	0.78
Recql	19691	RecQ protein-like	0.29
Rnf38	73469	ring finger protein 38	0.43
Rnpep	215615	arginyl aminopeptidase (aminopeptidase B)	0.52
Rpgrip1	77945	retinitis pigmentosa GTPase regulator interacting protein 1	0.66
Rwdd3	66568	RIKEN cDNA 2510027J23 gene; RWD domain containing 3	0.82
Saal1	78935	serum amyloid A-like 1	0.32
Samsn1	67742	SAM domain, SH3 domain and nuclear localization signals, 1	0.66
Scap	235623	SREBF chaperone	0.34
Sco1	52892	SCO cytochrome oxidase deficient homolog 1 (yeast)	0.29
Sec14l3	380683	SEC14-like 3 (S. cerevisiae)	1.05
Sema3e	20349	sema domain, immunoglobulin domain (Ig), short basic domain, secreted, (semaphorin) 3E	-0.30
Serf1	20365	small EDRK-rich factor 1	-0.33
Sf3a1	67465	splicing factor 3a, subunit 1	0.46
Sfrp4	20379	secreted frizzled-related protein 4	0.44
Slc15a2	57738	solute carrier family 15 (H+/peptide transporter), member 2	0.64
Slc17a8	216227	solute carrier family 17 (sodium-dependent inorganic phosphate cotransporter), member 8	0.47
Slc19a1	20509	solute carrier family 19 (sodium/hydrogen exchanger), member 1	0.47
Slc25a19	67283	solute carrier family 25 (mitochondrial thiamine pyrophosphate carrier), member 19	-0.38
Slc26a2	13521	solute carrier family 26 (sulfate transporter), member 2	0.38

Table S7. Continued.

Gene symbol	Gene ID	Gene name	Mean log2 fold change*
Slc2a12	353169	solute carrier family 2 (facilitated glucose transporter), member 12	0.41
Slc37a4	14385	solute carrier family 37 (glucose-6-phosphate transporter), member 4	0.80
Smpd2	20598	sphingomyelin phosphodiesterase 2, neutral	0.38
Spata6	67946	spermatogenesis associated 6	0.52
Srbd1	78586	S1 RNA binding domain 1	0.33
Stard3	59045	START domain containing 3	0.44
Stat1	20846	signal transducer and activator of transcription 1	0.81
Stat3	20848	signal transducer and activator of transcription 3	0.31
Stat5b	20851	signal transducer and activator of transcription 5B	0.89
Stox1	216021	storkhead box 1	0.40
Surf4	20932	surfeit gene 4	0.37
Svep1	64817	sushi, von Willebrand factor type A, EGF and pentraxin domain containing 1	-0.45
Svop	68666	SV2 related protein	0.35
Tagap	72536	T-cell activation GTPase activating protein 1	0.89
Tctex1d2	66061	Tctex1 domain containing 2	0.41
Tert	21752	telomerase reverse transcriptase	0.98
Tex9	21778	testis expressed gene 9	0.30
Tia1	21841	cytotoxic granule-associated RNA binding protein 1	0.43
Tirap	117149	toll-interleukin 1 receptor (TIR) domain-containing adaptor protein	0.43
Tln1	21894	talin 1	0.35
Tmbim4	68212	transmembrane BAX inhibitor motif containing 4	0.31
Tmbim6	110213	transmembrane BAX inhibitor motif containing 6	0.79
Tmem19	67226	transmembrane protein 19	0.26
Tmem194	210035	transmembrane protein 194	0.36
Trmt11	73681	tRNA methyltransferase 11 homolog (S. cerevisiae)	0.56
Trmt2a	15547	TRM2 tRNA methyltransferase 2 homolog A (S. cerevisiae)	0.36
Twf2	23999	twinfilin, actin-binding protein, homolog 2 (Drosophila)	0.36
Ube2l6	56791	ubiquitin-conjugating enzyme E2L 6	0.60
Ucp2	22228	uncoupling protein 2 (mitochondrial, proton carrier)	0.34
Unc79	217843	unc-79 homolog (C. elegans)	0.36
Vcl	22330	vinculin	-0.29
Wdr19	213081	WD repeat domain 19	0.28
Xrn2	24128	5'-3' exoribonuclease 2	0.53
Yipf3	28064	Yip1 domain family, member 3	0.32
Zbtb4	75580	zinc finger and BTB domain containing 4	0.28
Zbtb49	75079	zinc finger protein 509	0.78
Zfp454	237758	zinc finger protein 454	-0.50
Zfp595	218314	zinc finger protein 595	0.75
Zfp937	245174	predicted gene 4979	0.70
Zfp945	240041	RIKEN cDNA A630033E08 gene	0.36
Zfp951	626391	RIKEN cDNA C230055K05 gene	0.89
Zfp97	22759	zinc finger protein 97	1.02

*mean of log2 fold changes of all transcripts found differentially expressed for each gene

Table S8. Genotype-regulated genes under control diet. *Dj-1*^{-/-} and wildtype mice were maintained on control diet for 14 weeks. The ventral hypothalamus was subjected to RNA sequencing. Listed are genes for which at least one transcript was found differentially expressed (Student's t-test, $p < 0.01$). A log2 fold change > 0.26 indicates upregulation and < -0.26 downregulation in *Dj-1*^{-/-} versus *Dj-1*^{+/+} mice, corresponding to a fold change of > 1.2 or < -1.2, respectively. Genes regulated by genotype under both control and HF diet are listed in Table S10.

Gene symbol	Gene ID	Gene name	Mean log2 fold change*
1700093C20Rik	76623	RIKEN cDNA 1700093C20 gene	-0.56
2210015D19Rik	76508	RIKEN cDNA 2210015D19 gene	-0.29
2410003K15Rik	75593	RIKEN cDNA 2410003K15 gene	-0.30
2410137F16Rik	76798	RIKEN cDNA 2410137F16 gene	0.51
2610035D17Rik	72386	RIKEN cDNA 2610035D17 gene	-0.67
2810055G20Rik	77994	RIKEN cDNA 2810055G20 gene	-0.47
2810422O20Rik	69962	RIKEN cDNA 2810422O20 gene	-0.43
4732440D04Rik	654788	RIKEN cDNA 4732440D04 gene	-0.61
4930434J08Rik	73979	RIKEN cDNA 4930434J08 gene	-1.02
4930507D05Rik	74706	RIKEN cDNA 4930507D05 gene	-0.43
4930579G22Rik	69034	RIKEN cDNA 4930579G22 gene	-0.89
8030443G20Rik	77173	RIKEN cDNA 8030443G20 gene	-0.68
8030456M14Rik	77492	RIKEN cDNA 8030456M14 gene	-0.83
9330160F10Rik	791118	RIKEN cDNA 9330160F10 gene	-0.82
9330161L09Rik	77225	RIKEN cDNA 9330161L09 gene	-0.89
Abcb1b	18669	ATP-binding cassette, sub-family B (MDR/TAP), member 1B	-0.42
Acss1	68738	acyl-CoA synthetase short-chain family member 1	-0.36
Adm	11535	adrenomedullin	-0.71
Amz1	231842	archaelysin family metallopeptidase 1	-0.69
Anks6	75691	similar to sterile alpha motif domain containing 6; ankyrin repeat and sterile alpha motif domain containing 6	-0.79
Antxr1	69538	anthrax toxin receptor 1	-0.39
Antxr2	71914	anthrax toxin receptor 2	-0.54
Apcdd1	494504	adenomatosis polyposis coli down-regulated 1	-0.83
BC055324	381306	cDNA sequence BC055324	-0.47
Bcar1	12927	breast cancer anti-estrogen resistance 1	-1.83
Bdh2	69772	3-hydroxybutyrate dehydrogenase, type 2	-0.60
Bmper	73230	BMP-binding endothelial regulator	-0.59
C230057H02Rik	320575	RIKEN cDNA C230057H02 gene	-1.06
C330011M18Rik	442802	RIKEN cDNA C330011M18 gene	-0.64
Cabin1	104248	calcineurin binding protein 1	-0.37
Cadps2	320405	Ca2+-dependent activator protein for secretion 2	-0.31
Car12	76459	carbonic anyhydrase 12	0.61
Cbfa2t3	12398	core-binding factor, runt domain, alpha subunit 2, translocated to, 3 (human)	0.62
Ccdc122	108811	coiled-coil domain containing 122	-1.35
Ccdc23	69216	coiled-coil domain containing 23	-0.56
Ccl9	20308	chemokine (C-C motif) ligand 9	-1.10
Cd55	13136	CD55 antigen	-1.22
Cdh18	320865	cadherin 18	-0.36
Cdhr3	68764	RIKEN cDNA 1110049B09 gene	-0.69
Cep110	26920	centrosomal protein 110	-0.33
Chuk	12675	conserved helix-loop-helix ubiquitous kinase	-0.50
Clcf1	56708	cardiotrophin-like cytokine factor 1	-1.03
Cnga3	12790	cyclic nucleotide gated channel alpha 3	-0.47
Cpxm2	55987	carboxypeptidase X 2 (M14 family)	-0.64

Table S8. Continued.

Gene symbol	Gene ID	Gene name	Mean log2 fold change*
Crebl2	232430	cAMP responsive element binding protein-like 2	-0.48
Cwc22	80744	CWC22 spliceosome-associated protein homolog (S. cerevisiae)	-0.58
Cwc25	67480	coiled-coil domain containing 49	-0.25
Cyb5rl	230582	cytochrome b5 reductase-like	-0.57
Ddx4	13206	DEAD (Asp-Glu-Ala-Asp) box polypeptide 4	0.36
Dennd1a	227801	DENN/MADD domain containing 1A	-0.28
Dennd3	105841	DENN/MADD domain containing 3	-1.06
Depdc5	277854	DEP domain containing 5	-0.33
Dhrs7	66375	dehydrogenase/reductase (SDR family) member 7	-0.33
Diras2	68203	DIRAS family, GTP-binding RAS-like 2	0.37
Dlc1	50768	deleted in liver cancer 1	-0.49
Drg1	13494	developmentally regulated GTP binding protein 1	-0.41
E330037M01Rik	319775	RIKEN cDNA E330037M01 gene	0.30
Ece1	230857	endothelin converting enzyme 1	-0.65
Eepd1	67484	endonuclease/exonuclease/phosphatase family domain containing 1	-0.37
Efcab4a	213573	EF-hand calcium binding domain 4A	-0.80
Eid1	58521	EP300 interacting inhibitor of differentiation 1	-0.27
Enox	70252	RIKEN cDNA 2010000I03 gene	-0.94
Entpd1	12495	ectonucleoside triphosphate diphosphohydrolase 1	-0.53
Erg	13876	avian erythroblastosis virus E-26 (v-ets) oncogene related	-0.65
Fam103a1	67148	RIKEN cDNA 2610204K14 gene	-0.46
Fam185a	330050	expressed sequence AI847670	-0.47
Fam193a	231128	cDNA sequence BC037112	0.75
Fbn2	14119	similar to fibrillin 2; fibrillin 2	-0.59
Fkbp15	338355	FK506 binding protein 15	-0.58
Gadd45a	13197	growth arrest and DNA-damage-inducible 45 alpha	-0.37
Glrx2	69367	glutaredoxin 2 (thioltransferase)	-0.59
Gm4076	100042862	predicted gene 4076	-0.76
Gm5079	327749	predicted gene 5079	-0.57
Gpr173	70771	G-protein coupled receptor 173	-0.45
Gtf2a2	235459	general transcription factor II A, 2	-0.43
H2afy3	67552	H2A histone family, member Y3	-0.61
Hdgfrp3	29877	hepatoma-derived growth factor, related protein 3	-0.29
Hebp1	15199	heme binding protein 1	-0.49
Hinfp	102423	histone H4 transcription factor	-0.31
Hist1h4i	319158	histone cluster 1, H4i	-0.79
Htatip2	53415	HIV-1 tat interactive protein 2, homolog (human)	-0.33
Idua	15932	iduronidase, alpha-L-	-0.67
Il17rd	171463	interleukin 17 receptor D	-0.41
Ints6	18130	integrator complex subunit 6	-0.41
Khnyn	219094	RIKEN cDNA 9130227C08Rik gene	-0.29
Lair1	52855	leukocyte-associated Ig-like receptor 1	-0.38
Ldha	16828	lactate dehydrogenase A	-0.28
Lgals9	16859	lectin, galactose binding, soluble 9	-0.61
Lman1	70361	lectin, mannose-binding, 1	-0.32
LOC100503962	100503962	predicted gene, 16701	-0.83
Lpo	76113	lactoperoxidase	-0.80
Lrguk	74354	leucine-rich repeats and guanylate kinase domain containing	-0.89
Lzic	69151	leucine zipper and CTNNBIP1 domain containing	0.34
Mapk1ip1l	218975	mitogen-activated protein kinase 1 interacting protein 1-like	0.29
Megf6	230971	multiple EGF-like-domains 6	-1.24

Table S8. Continued.

Gene symbol	Gene ID	Gene name	Mean log2 fold change*
Meis1	17268	Meis homeobox 1	-0.82
Mfn2	170731	similar to mitofusin 2; mitofusin 2	-0.36
Mknk1	17346	MAP kinase-interacting serine/threonine kinase 1	-0.42
Morc4	75746	microrchidia 4	0.60
Mrc2	17534	mannose receptor, C type 2	-1.09
Msn	17698	moesin	-0.30
Mtmr7	54384	myotubularin related protein 7	-0.27
Mtss1	211401	metastasis suppressor 1	-0.32
Mum1	68114	melanoma associated antigen (mutated) 1	-0.33
Mycl1	16918	v-myc myelocytomatosis viral oncogene homolog 1, lung carcinoma derived (avian)	-0.49
Naip2	17948	NLR family, apoptosis inhibitory protein 2	-0.92
Ndufaf2	75597	NADH dehydrogenase (ubiquinone) 1 alpha subcomplex, assembly factor 2	-0.40
Negr1	320840	neuronal growth regulator 1	-0.34
Neurl3	214854	neuralized homolog 3 homolog (Drosophila)	-0.71
Nfia	18027	nuclear factor I/A	0.58
Nono	53610	non-POU-domain-containing, octamer binding protein	-0.40
Nyx	236690	nyctalopin	-0.93
Palld	72333	palladin, cytoskeletal associated protein	-0.49
Papss2	23972	3'-phosphoadenosine 5'-phosphosulfate synthase 2	-0.44
Pard3b	72823	par-3 partitioning defective 3 homolog B (C. elegans)	-0.33
Pcdh17	219228	protocadherin 17	-0.47
Pik3ap1	83490	phosphoinositide-3-kinase adaptor protein 1	-0.43
Prdm16	70673	PR domain containing 16	0.27
Psmg4	69666	proteasome (prosome, macropain) assembly chaperone 4	-0.44
Ptchd2	242748	patched domain containing 2	-0.84
Racgap1	26934	Rac GTPase-activating protein 1; predicted gene 1859	-0.51
Rbmx2	209003	RNA binding motif protein, X-linked 2	0.36
Rfc3	69263	replication factor C (activator 1) 3	-0.39
Rnaset2a	100037283	ribonuclease T2B; ribonuclease T2A	-0.49
Rnf43	207742	ring finger protein 43	-0.92
Rrp1b	72462	ribosomal RNA processing 1 homolog B (S. cerevisiae)	-0.51
Rtkn2	170799	rhotekin 2	0.28
Scn7a	20272	sodium channel, voltage-gated, type VII, alpha	-0.92
Sco1	52892	SCO cytochrome oxidase deficient homolog 1 (yeast)	-0.45
Sec1	56546	secretory blood group 1	-1.03
Serpinb6a	20719	serine (or cysteine) peptidase inhibitor, clade B, member 6a	-0.32
Sgcd	24052	sarcoglycan, delta (dystrophin-associated glycoprotein)	-0.85
Shc4	271849	SHC (Src homology 2 domain containing) family, member 4	-1.04
Slc12a1	20495	solute carrier family 12, member 1	-0.63
Slc17a8	216227	solute carrier family 17 (sodium-dependent inorganic phosphate cotransporter), member 8	-0.67
Slc39a3	106947	solute carrier family 39 (zinc transporter), member 3	-0.65
Sned1	208777	sushi, nidogen and EGF-like domains 1	-0.42
Sntb1	20649	syntrophin, basic 1	-0.81
Sox5	20678	SRY-box containing gene 5	-0.56
Spg7	234847	spastic paraplegia 7 homolog (human)	-0.40
Ssu72	68991	Ssu72 RNA polymerase II CTD phosphatase homolog (yeast)	-0.32
St18	240690	suppression of tumorigenicity 18	-0.52
Stard8	236920	START domain containing 8	0.57
Stim1	20866	similar to Stromal interaction molecule 1; stromal interaction molecule 1	-0.33

Table S8. Continued.

Gene symbol	Gene ID	Gene name	Mean log2 fold change*
Taf1c	21341	TATA box binding protein (Tbp)-associated factor, RNA polymerase I, C	0.35
Tex261	21766	testis expressed gene 261	-0.45
Tia1	21841	cytotoxic granule-associated RNA binding protein 1	-0.53
Tmco4	77056	transmembrane and coiled-coil domains 4	-0.66
Tmem2	83921	transmembrane protein 2	-0.87
Tpst2	22022	protein-tyrosine sulfotransferase 2	-0.78
Trib3	228775	tribbles homolog 3 (Drosophila)	-0.92
Trim23	81003	tripartite motif-containing 23	-0.57
Trip13	69716	thyroid hormone receptor interactor 13	-0.69
Ttll11	74410	tubulin tyrosine ligase-like family, member 11	-0.45
Urb1	207932	URB1 ribosome biogenesis 1 homolog (S. cerevisiae)	-0.78
Vps16	80743	vacuolar protein sorting 16 (yeast)	-0.34
Whsc2	24116	Wolf-Hirschhorn syndrome candidate 2 (human)	0.31
Xpa	22590	xeroderma pigmentosum, complementation group A	-0.42
Zbtb6	241322	RIKEN cDNA A930039A15 gene; zinc finger and BTB domain containing 6	0.27
Zc3h6	78751	zinc finger CCCH type containing 6	-0.71
Zfp2	22678	zinc finger protein 2	-0.42
Zfp300	245368	zinc finger protein 300	-1.17
Zfp408	381410	zinc finger protein 408	-0.61
Zfp715	69930	zinc finger protein 715	-0.42
Zfp862	58894	zinc finger protein 862	-0.44
Zfp945	240041	RIKEN cDNA A630033E08 gene	-0.41

*mean of log2 fold changes of all transcripts found differentially expressed for each gene

Table S9. Genotype-regulated genes under HF diet. *Dj-1*^{-/-} and wildtype mice were maintained on control diet for 14 weeks. The ventral hypothalamus was subjected to RNA sequencing. Listed are genes for which at least one transcript was found differentially expressed (Student's t-test, $p < 0.01$). A log2 fold change > 0.26 indicates upregulation and < -0.26 downregulation in *Dj-1*^{-/-} versus *Dj-1*^{+/+} mice, corresponding to a fold change of > 1.2 or < -1.2, respectively. Genes regulated by genotype under both control and HF diet are listed in Table S10.

Gene symbol	Gene ID	Gene name	Mean log2 fold change*
1200009I06Rik	74190	RIKEN cDNA 1200009I06 gene	-0.58
1500015L24Rik	68994	RIKEN cDNA 1500015L24 gene	0.78
1700001L05Rik	69291	RIKEN cDNA 1700001L05 gene	0.28
1700003D09Rik	69338	RIKEN cDNA 1700003D09 gene	-0.92
1700048O20Rik	69430	RIKEN cDNA 1700048O20 gene	0.37
1700088E04Rik	27660	RIKEN cDNA 1700088E04 gene	-0.32
2210011C24Rik	70134	RIKEN cDNA 2210011C24 gene	-0.94
2310033P09Rik	67862	RIKEN cDNA 2310033P09 gene	-0.52
2410002I01Rik	78777	RIKEN cDNA 2410002I01 gene	-0.43
2410018L13Rik	69732	RIKEN cDNA 2410018L13 gene	-0.86
2610027K06Rik	69909	RIKEN cDNA 2610027K06 gene	-0.69
2700033N17Rik	72603	RIKEN cDNA 2700033N17 gene	-1.37
2700050L05Rik	214764	RIKEN cDNA 2700050L05 gene	-0.68
2810025M15Rik	69953	RIKEN cDNA 2810025M15 gene	-0.43
4833422C13Rik	373852	RIKEN cDNA 4833422C13 gene	-0.65
4930473A06Rik	320226	RIKEN cDNA 4930473A06 gene	-0.45
4930481A15Rik	74931	RIKEN cDNA 4930481A15 gene	-1.47
4930594C11Rik	77633	RIKEN cDNA 4930594C11 gene	0.31
5430407P10Rik	227545	RIKEN cDNA 5430407P10 gene	-0.74
5730433K22Rik	70532	RIKEN cDNA 5730433K22 gene	-0.59
5730577I03Rik	66662	RIKEN cDNA 5730577I03 gene	0.40
6430584L05	330324	hypothetical protein 6430584L05	0.34
9330162G02Rik	319534	RIKEN cDNA 9330162G02 gene	0.51
A230038B01Rik	319276	RIKEN cDNA A230038B01 gene	0.48
A330049M08Rik	230822	RIKEN cDNA A330049M08 gene	-0.68
Abca4	11304	ATP-binding cassette, sub-family A (ABC1), member 4	0.43
Aen	68048	apoptosis enhancing nuclease	-0.36
Afap1l1	106877	actin filament associated protein 1-like 1	0.32
Agphd1	235386	RIKEN cDNA C630028N24 gene	-0.60
Agtrap	11610	angiotensin II, type I receptor-associated protein	0.35
Akap13	75547	A kinase (PRKA) anchor protein 13	1.04
Aldob	230163	aldolase B, fructose-bisphosphate	-0.62
Angptl7	654812	angiopoietin-like 7	0.90
Ank1	11733	ankyrin 1, erythroid	-0.49
Ankdd1a	384945	ankyrin repeat and death domain containing 1A	-0.60
Anxa2	12306	annexin A2	0.30
Apln	30878	apelin	-0.57
Arhgap25	232201	Rho GTPase activating protein 25	-1.00
Arhgap28	268970	Rho GTPase activating protein 28	0.37
Arl5c	217151	ADP-ribosylation factor-like 5C	-1.22
Arl6ip6	65103	ADP-ribosylation factor-like 6 interacting protein 6	0.31
Arnt2	11864	aryl hydrocarbon receptor nuclear translocator 2	-0.28
Arsg	74008	arylsulfatase G	-0.94
Asb14	142687	ankyrin repeat and SOCS box-containing 14	0.75
Atp2b2	11941	ATPase, Ca++ transporting, plasma membrane 2	-0.34
Bai2	230775	brain-specific angiogenesis inhibitor 2	0.29
BC030476	239368	cDNA sequence BC030476	-0.80

139

Table S9. Continued.

Gene symbol	Gene ID	Gene name	Mean log2 fold change*
Bcl11a	14025	B-cell CLL/lymphoma 11A (zinc finger protein)	-0.64
Bola3	78653	bolA-like 3 (E. coli)	-0.59
Btc	12223	betacellulin, epidermal growth factor family member	0.70
Bub1b	12236	budding uninhibited by benzimidazoles 1 homolog, beta (S. cerevisiae)	-1.19
C030029H02Rik	77383	RIKEN cDNA C030029H02 gene	-0.68
C1ql3	227580	C1q-like 3	-0.63
C3ar1	12267	complement component 3a receptor 1	0.27
C78197	97702	expressed sequence C78197	0.81
Calb1	12307	calbindin 1	0.33
Calcrl	54598	calcitonin receptor-like	0.60
Caln1	140904	calneuron 1	-0.55
Camk1d	227541	calcium/calmodulin-dependent protein kinase ID	-0.36
Camta1	100072	calmodulin binding transcription activator 1	-0.34
Car7	12354	carbonic anhydrase 7	-0.56
Ccdc123	72140	coiled-coil domain containing 123	0.39
Ccdc9	243846	coiled-coil domain containing 9	-0.45
Ccr5	12774	chemokine (C-C motif) receptor 5	0.83
Ccrl1	252837	chemokine (C-C motif) receptor-like 1	-0.72
Cd109	235505	CD109 antigen	0.86
Cd44	12505	CD44 antigen	0.38
Cd84	12523	CD84 antigen	0.27
Cd93	17064	CD93 antigen	-0.57
Cdc42se1	57912	CDC42 small effector 1	-0.36
Cdh15	12555	cadherin 15	0.51
Cdk5rap2	214444	CDK5 regulatory subunit associated protein 2	-0.36
Cdr2l	237988	cerebellar degeneration-related protein 2-like	-0.29
Clic6	209195	chloride intracellular channel 6	0.31
Clmn	94040	calmin	-0.29
Clstn1	65945	calsyntenin 1	-0.58
Cmtm7	102545	CKLF-like MARVEL transmembrane domain containing 7	0.28
Cnp	12799	2',3'-cyclic nucleotide 3' phosphodiesterase	-0.44
Cops7a	26894	COP9 (constitutive photomorphogenic) homolog, subunit 7a (Arabidopsis thaliana)	-0.32
Coro2a	107684	coronin, actin binding protein 2A	-0.32
Coro6	216961	coronin 6	-0.51
Cpa4	71791	carboxypeptidase A4	0.54
Cplx1	12889	complexin 1	-0.73
Crat	12908	carnitine acetyltransferase	-0.50
Crem	12916	cAMP responsive element modulator	0.34
Crhr1	12921	corticotropin releasing hormone receptor 1	-0.63
Ctnnbip1	67087	catenin beta interacting protein 1	-0.34
Cyp19a1	13075	cytochrome P450, family 19, subfamily a, polypeptide 1	0.86
D17Wsu92e	224647	DNA segment, Chr 17, Wayne State University 92, expressed	-0.27
Daxx	13163	Fas death domain-associated protein	-0.32
Dffa	13347	DNA fragmentation factor, alpha subunit	-0.36
Dhx29	218629	DEAH (Asp-Glu-Ala-His) box polypeptide 29	-0.30
Diap3	56419	diaphanous homolog 3 (Drosophila)	0.46
Dnajb13	69387	DnaJ (Hsp40) related, subfamily B, member 13	0.60
Dock1	330662	dedicator of cytokinesis 1	-0.47
Dydc2	71200	DPY30 domain containing 2	-1.00
E130311K13Rik	329659	RIKEN cDNA E130311K13 gene	0.55
Echdc2	52430	enoyl Coenzyme A hydratase domain containing 2	-0.38

Table S9. Continued.

Gene symbol	Gene ID	Gene name	Mean log2 fold change*
Ehd2	259300	EH-domain containing 2	-0.48
Eif4a1	13681	eukaryotic translation initiation factor 4A1	0.30
Emid1	140703	EMI domain containing 1	-0.67
Eml6	237711	RIKEN cDNA C230094A16 gene	0.27
Entpd5	12499	ectonucleoside triphosphate diphosphohydrolase 5	-0.33
Ermp1	226090	endoplasmic reticulum metallopeptidase 1	-0.43
Fads6	328035	fatty acid desaturase domain family, member 6	-0.30
Fam107b	66540	family with sequence similarity 107, member B	0.43
Fam111a	107373	RIKEN cDNA 4632417K18 gene	0.90
Fancc	14088	Fanconi anemia, complementation group C	-0.81
Fancm	104806	Fanconi anemia, complementation group M	-0.43
Fasl	14103	Fas ligand (TNF superfamily, member 6)	0.87
Fbln1	14114	fibulin 1	0.30
Fbxo5	67141	F-box protein 5	0.29
Fbxo9	71538	f-box protein 9	-0.34
Fgd6	13998	FYVE, RhoGEF and PH domain containing 6	-0.47
Fibcd1	98970	fibrinogen C domain containing 1	-0.54
Fli1	14247	Friend leukemia integration 1	-0.43
Flt1	14254	FMS-like tyrosine kinase 1	-0.51
Fmnl1	57778	formin-like 1	-0.28
Fmo4	226564	flavin containing monooxygenase 4	1.13
Fnbp1	14269	formin binding protein 1	-0.35
Foxm1	14235	forkhead box M1; RIKEN cDNA 4933413G19 gene	-0.54
Foxn3	71375	forkhead box N3	-0.52
Gabra2	14395	gamma-aminobutyric acid (GABA) A receptor, subunit alpha 2	0.33
Garnl3	99326	GTPase activating RANGAP domain-like 3	-0.45
Gfm1	28030	G elongation factor, mitochondrial 1	-0.34
Ghr	14600	growth hormone receptor	0.44
Gk5	235533	glycerol kinase 5 (putative)	0.62
Gm10425	100038720	predicted gene 10425	-0.64
Gm10742	100038486	predicted gene 10742	-0.90
Gm13157	100041677	similar to novel KRAB box containing protein	-1.65
Gm14418	668066	predicted gene 14418	0.44
Gm3325	100041420	predicted gene 3325; predicted gene 7036	1.04
Gm7173	636104	predicted gene 7173	0.72
Gm8234	666680	predicted gene 8234	0.57
Gm8787	667736	predicted gene 8787	1.32
Gna15	14676	guanine nucleotide binding protein, alpha 15	-0.38
Got2	14719	glutamate oxaloacetate transaminase 2, mitochondrial	-0.31
Gpatch8	237943	G patch domain containing 8	0.27
Gpr153	100129	G protein-coupled receptor 153	-0.39
Gpr37	14763	G protein-coupled receptor 37	-0.43
Gprc5b	64297	G protein-coupled receptor, family C, group 5, member B	-0.31
Grin2c	14813	glutamate receptor, ionotropic, NMDA2C (epsilon 3)	-0.41
Gtpbp2	56055	GTP binding protein 2	-0.34
Herpud2	80517	HERPUD family member 2	-0.35
Hhip	15245	Hedgehog-interacting protein	-0.84
Hlx	15284	H2.0-like homeobox	-0.76
Hyal1	15586	hyaluronoglucosaminidase 1	-0.67
Ide	15925	insulin degrading enzyme	-0.63
Ido2	209176	indoleamine 2,3-dioxygenase 2	0.40
Ikzf4	22781	IKAROS family zinc finger 4; similar to helios	0.37

Table S9. Continued.

Gene symbol	Gene ID	Gene name	Mean log2 fold change*
Impa2	114663	inositol (myo)-1(or 4)-monophosphatase 2	-0.65
Inadl	12695	InaD-like (Drosophila)	0.58
Itgam	16409	integrin alpha M	-0.37
Itgb4	192897	integrin beta 4	-0.56
Itih3	16426	inter-alpha trypsin inhibitor, heavy chain 3	0.27
Itpripl1	73338	inositol 1,4,5-triphosphate receptor interacting protein-like 1	-0.29
Jdp2	81703	Jun dimerization protein 2	-0.37
Kcna6	16494	potassium voltage-gated channel, shaker-related, subfamily, member 6	-0.68
Kctd3	226823	predicted gene 7553; potassium channel tetramerisation domain containing 3	-0.30
Kif13b	16554	kinesin family member 13B	-0.31
Kif5b	16573	kinesin family member 5B	-0.43
Lace1	215951	lactation elevated 1	-0.34
Lap3	66988	leucine aminopeptidase 3	-0.27
Larp6	67557	La ribonucleoprotein domain family, member 6	-0.37
Lekr1	624866	predicted gene 6534	0.35
Limk1	16885	LIM-domain containing, protein kinase	-0.43
Litaf	56722	LPS-induced TN factor	-0.49
LOC100503319	100503319	predicted gene, 17281	-1.12
Lpar1	14745	lysophosphatidic acid receptor 1	-0.62
Lrrc1	214345	leucine rich repeat containing 1	0.33
Lrrc16a	68732	leucine rich repeat containing 16A	-0.47
Lrrc34	71827	leucine rich repeat containing 34	0.30
Lrrc38	242735	leucine rich repeat containing 38	0.36
Lsr	54135	lipolysis stimulated lipoprotein receptor	-0.56
Mad2l2	71890	MAD2 mitotic arrest deficient-like 2 (yeast)	0.50
Map3k6	53608	mitogen-activated protein kinase kinase kinase 6	-0.55
Marveld2	218518	MARVEL (membrane-associating) domain containing 2	-0.93
Max	17187	similar to Myn protein; Max protein	-0.38
Mgat5b	268510	mannoside acetylglucosaminyltransferase 5, isoenzyme B	-0.42
Micall1	27008	microtubule associated monoxygenase, calponin and LIM domain containing -like 1	-0.38
Mknk2	17347	MAP kinase-interacting serine/threonine kinase 2	-0.36
Mmel1	27390	membrane metallo-endopeptidase-like 1	-0.52
Mn1	433938	meningioma 1	-0.67
Mrpl32	75398	mitochondrial ribosomal protein L32	-0.38
Mrps36	66128	mitochondrial ribosomal protein S36predicted gene 4676	-0.79
Mst1r	19882	macrophage stimulating 1 receptor (c-met-related tyrosine kinase)	0.68
Mxd1	17119	MAX dimerization protein 1	-0.36
Myo1d	338367	myosin ID	-0.62
Myo6	17920	myosin VI	-0.40
Myrip	245049	myosin VIIA and Rab interacting protein	-0.36
N4bp3	212706	RIKEN cDNA C330016O10 gene	-0.56
Nfkbiz	80859	nuclear factor of kappa light polypeptide gene enhancer in B-cells inhibitor, zeta	0.35
Nit2	52633	nitrilase family, member 2	-0.32
Nmt2	18108	N-myristoyltransferase 2	-0.67
Npas1	18142	neuronal PAS domain protein 1; similar to neuronal PAS1	-0.57
Nrg1	211323	neuregulin 1	-0.45
Nuak1	77976	NUAK family, SNF1-like kinase, 1	-0.28
Numb	18222	numb gene homolog (Drosophila)	-0.40
Nup98	269966	nucleoporin 98	-0.38
Osbpl5	79196	oxysterol binding protein-like 5	-0.36

Table S9. Continued.

Gene symbol	Gene ID	Gene name	Mean log2 fold change*
Osbpl6	99031	oxysterol binding protein-like 6	-0.48
Otud3	73162	OTU domain containing 3	-0.86
P2rx7	18439	purinergic receptor P2X, ligand-gated ion channel, 7	-0.43
Pax6	18508	paired box gene 6	-0.84
Pcdh1	75599	protocadherin 1	-0.44
Pcp4l1	66425	Purkinje cell protein 4-like 1	-0.56
Pdxdc1	94184	pyridoxal-dependent decarboxylase domain containing 1	-0.26
Pex5l	58869	peroxisomal biogenesis factor 5-like; peroxisomal membrane protein 3	-0.51
Pgr15l	245526	G protein-coupled receptor 15-like	0.28
Pik3cb	74769	phosphatidylinositol 3-kinase, catalytic, beta polypeptide	-0.32
Pik3cd	18707	phosphatidylinositol 3-kinase catalytic delta polypeptide	-0.55
Pla2g7	27226	phospholipase A2, group VII (platelet-activating factor acetylhydrolase, plasma)	-0.54
Plek2	27260	pleckstrin 2	-0.56
Plekhg3	263406	pleckstrin homology domain containing, family G (with RhoGef domain) member 3	-0.37
Plod1	18822	procollagen-lysine, 2-oxoglutarate 5-dioxygenase 1	-0.31
Pnp2	667034	purine-nucleoside phosphorylase 2	0.58
Poc1b	382406	WD repeat domain 51B	-0.29
Ppm1e	320472	protein phosphatase 1E (PP2C domain containing)	-0.30
Ppp1r1b	19049	protein phosphatase 1, regulatory (inhibitor) subunit 1B	-0.61
Pppde2	28075	PPPDE peptidase domain containing 2	-0.42
Prep	19072	prolyl endopeptidase	-0.35
Prmt3	71974	protein arginine N-methyltransferase 3	0.27
Prr5l	72446	proline rich 5 like; hypothetical protein LOC100048398	-0.50
Ptgfrn	19221	prostaglandin F2 receptor negative regulator	-0.41
Pttg1	30939	pituitary tumor-transforming gene 1	-0.60
Qtrtd1	106248	queuine tRNA-ribosyltransferase domain containing 1	-0.57
Rab6b	270192	RAB6B, member RAS oncogene family	-0.32
Rasgrp2	19395	RAS, guanyl releasing protein 2	-0.34
Rbm10	236732	RNA binding motif protein 10; predicted gene 12799	-0.37
Rec8	56739	REC8 homolog (yeast)	1.20
Renbp	19703	renin binding protein	0.64
Reps1	19707	RalBP1 associated Eps domain containing protein	-0.37
Rgs8	67792	regulator of G-protein signaling 8	-0.39
Rhobtb1	69288	Rho-related BTB domain containing 1	-0.63
Rhobtb3	73296	Rho-related BTB domain containing 3	-0.56
Rhog	56212	ras homolog gene family, member G	-0.45
Rnf135	71956	ring finger protein 135	-1.80
Rnf144a	108089	ring finger protein 144A	-0.49
Rprd1b	70470	regulation of nuclear pre-mRNA domain containing 1B	-0.36
Rrp8	101867	ribosomal RNA processing 8, methyltransferase, homolog (yeast)	-0.47
Rsrc1	66880	arginine/serine-rich coiled-coil 1	-0.45
Rsu1	20163	Ras suppressor protein 1	-0.37
Sash1	70097	SAM and SH3 domain containing 1; predicted gene 2082	-0.36
Scpppq1	100271704	secretory calcium-binding phosphoprotein proline-glutamine rich 1	0.66
Sec11c	66286	SEC11 homolog C (S. cerevisiae)	-0.33
Sema3c	20348	sema domain, immunoglobulin domain (Ig), short basic domain, secreted, (semaphorin) 3C	-0.72
Sema3e	20349	sema domain, immunoglobulin domain (Ig), short basic domain, secreted, (semaphorin) 3E	-0.60
Sema5b	20357	sema domain, seven thrombospondin repeats (type 1 and type 1-like), transmembrane domain (TM) and short cytoplasmic domain, (semaphorin) 5B	-0.61
Sept4	18952	septin 4	-0.48

Table S9. Continued.

Gene symbol	Gene ID	Gene name	Mean log2 fold change*
Serpinf1	20317	serine (or cysteine) peptidase inhibitor, clade F, member 1	-0.49
Sh3rf3	237353	SH3 domain containing ring finger 3	-0.81
Shroom1	71774	shroom family member 1	-0.66
Slain1	105439	SLAIN motif family, member 1	-0.45
Slc25a25	227731	solute carrier family 25 (mitochondrial carrier, phosphate carrier), member 25	-0.32
Slc25a45	107375	solute carrier family 25, member 45	-0.46
Slc31a2	20530	solute carrier family 31, member 2	-0.32
Slc38a3	76257	solute carrier family 38, member 3	-0.44
Slc4a9	240215	solute carrier family 4, sodium bicarbonate cotransporter, member 9	-1.42
Slco3a1	108116	solute carrier organic anion transporter family, member 3a1	-0.31
Smad7	17131	MAD homolog 7 (Drosophila)	-0.50
Snx33	235406	sorting nexin 33	-0.36
Socs2	216233	suppressor of cytokine signaling 2	0.27
Spata2	263876	spermatogenesis associated 2	-0.54
Spats2l	67198	RIKEN cDNA 2810022L02 gene	-0.75
St8sia5	225742	ST8 alpha-N-acetyl-neuraminide alpha-2,8-sialyltransferase 5	-0.36
Stag1	20842	stromal antigen 1	0.64
Steap2	74051	six transmembrane epithelial antigen of prostate 2	-0.42
Stk10	20868	serine/threonine kinase 10	-1.29
Stxbp3a	20912	syntaxin binding protein 3A	-0.43
Sumf1	58911	sulfatase modifying factor 1	0.47
Sv2b	64176	synaptic vesicle glycoprotein 2 b	-0.31
Synj2	20975	synaptojanin 2	-0.39
Syt7	54525	synaptotagmin VII	-0.48
Sytl5	236643	synaptotagmin-like 5	-0.49
Tanc1	66860	tetratricopeptide repeat, ankyrin repeat and coiled-coil containing 1	0.40
Tbc1d2b	67016	TBC1 domain family, member 2B	-0.30
Tceal3	594844	transcription elongation factor A (SII)-like 3	0.49
Tcf7	21414	transcription factor 7, T-cell specific	-0.52
Tcf7l2	21416	transcription factor 7-like 2, T-cell specific, HMG-box	-0.50
Tek	21687	endothelial-specific receptor tyrosine kinase	-0.59
Tex10	269536	testis expressed gene 10	0.30
Tgfa	21802	transforming growth factor alpha	-0.31
Thsd1	56229	thrombospondin, type I, domain 1	-0.60
Tiam1	21844	T-cell lymphoma invasion and metastasis 1	-0.36
Tjp2	21873	tight junction protein 2	-0.31
Tmbim1	69660	transmembrane BAX inhibitor motif containing 1	-0.46
Tmem63a	208795	transmembrane protein 63a	-0.81
Tpd52	21985	tumor protein D52	-0.27
Tspan9	109246	tetraspanin 9	-0.39
Ttc9	69480	tetratricopeptide repeat domain 9	-0.31
Tulp4	68842	tubby like protein 4	-0.43
Uap1	107652	UDP-N-acetylglucosamine pyrophosphorylase 1	-0.64
Ubap2	68926	ubiquitin-associated protein 2	-1.09
Ubqln4	94232	ubiquilin 4	-0.32
Ubxn8	108159	UBX domain protein 8	-0.43
Ufsp2	192169	UFM1-specific peptidase 2	-0.28
Ulk2	29869	Unc-51 like kinase 2 (C. elegans)	-0.31
Vash1	238328	vasohibin 1	-0.35
Vps13d	230895	vacuolar protein sorting 13 D (yeast)	-0.33
Wnk4	69847	WNK lysine deficient protein kinase 4	-0.72
Wnt10b	22410	wingless related MMTV integration site 10b	-1.30

Table S9. Continued.

Gene symbol	Gene ID	Gene name	Mean log2 fold change*
Yars	107271	tyrosyl-tRNA synthetase	-0.34
Zbtb43	71834	zinc finger and BTB domain containing 43	-0.56
Zeb2	24136	zinc finger E-box binding homeobox 2	-0.62
Zfp111	56707	zinc finger protein 111	-0.32
Zfp454	237758	zinc finger protein 454	-0.54
Zfp827	622675	zinc finger protein 827	0.33
Zfp933	242747	RIKEN cDNA 2810408P10 gene	-0.92
Zfp951	626391	RIKEN cDNA C230055K05 gene	0.70
Zfp97	22759	zinc finger protein 97	0.40

*mean of log2 fold changes of all transcripts found differentially expressed for each gene

Table S10. Genotype-regulated genes under control as well as HF diet. *Dj-1*^{-/-} and wildtype mice were maintained on control diet for 14 weeks. The ventral hypothalamus was subjected to RNA sequencing. Listed are genes for which at least one transcript was found differentially expressed (Student's t-test, $p < 0.01$). A log2 fold change > 0.26 indicates upregulation and < -0.26 downregulation in *Dj-1*^{-/-} versus *Dj-1*^{+/+} mice, corresponding to a fold change of > 1.2 or < -1.2, respectively.

Gene symbol	Gene ID	Gene name	Mean log2 fold change* within		Chr
			control group	HF group	
2610305D13Rik	112422	RIKEN cDNA 2610305D13 gene	-2.03	-2.51	4
4921517L17Rik	70873	RIKEN cDNA 4921517L17 gene	0.65	1.07	2
5330422M15Rik	77062	RIKEN cDNA 5330422M15 gene	1.96	3.95	4
Eno1	13806	enolase 1, alpha non-neuron	-1.74	-1.74	4
Fbxo44	230903	F-box protein 44	-0.65	-0.89	4
Fcrls	80891	Fc receptor-like S, scavenger receptor	-0.65	-0.65	3
Gm13152	195531	predicted gene 13152	-4.59	-4.86	4
Gm16503	100038537	predicted gene 16503	-6.96	-inf	4
Gm5506	433182	similar to enolase 1, alpha non-neuron	3.49	6.73	18
Kcnab2	16498	potassium voltage-gated channel, shaker-related subfamily, beta member 2	0.69	-0.51	4
Lama1	16772	laminin, alpha 1	-0.35	0.86	17
LOC100045967	100045967	similar to enolase 1, alpha non-neuron	-6.96	-9.43	2
LOC67527	67527	murine leukemia retrovirus	0.95	0.92	18
Masp2	17175	mannan-binding lectin serine peptidase 2	1.62	2.65	4
Miip	28010	migration and invasion inhibitory protein	-1.22	-1.51	4
Park7	57320	Parkinson disease (autosomal recessive, early onset) 7	-5.21	-4.90	4
Phldb1	102693	pleckstrin homology-like domain, family B, member 1	-0.53	-0.51	9
Slc2a5	56485	solute carrier family 2 (facilitated glucose transporter), member 5	-1.74	-1.40	4
Tnfaip8	106869	tumor necrosis factor, alpha-induced protein 8	-0.36	-0.43	18
Tnfrsf1b	21938	tumor necrosis factor receptor superfamily, member 1b	-0.68	-1.44	4
Tnfrsf8	21941	tumor necrosis factor receptor superfamily, member 8	-5.37	-4.79	4
Ubiad1	71707	UbiA prenyltransferase domain containing 1	0.58	0.53	4

*mean of log2 fold changes of all transcripts found differentially expressed for each gene. Chr – Chromosome.

Table S11. Metabolic disease pathways associated with diet-regulated genes. *Dj-1*^{-/-} and wildtpye mice were maintained on HF or control diet for 14 weeks. The ventral hypothalamus was subjected to RNA sequencing. Genes for which at least one transcript was found differentially expressed (Student's t-test, $p < 0.01$) with a log2 fold change > 0.26 (upregulation) or < -0.26 (downregulation) in HF versus control diet-fed mice were subjected to a pathway analysis. Listed are pathways for which the number of differentially expressed genes between HF or control diet-fed wildtype (**A**) or *Dj-1*^{-/-} mice (**B**) exceeded the statistically expected number. Genes shown in bold represent overlapping genes of pathways associated with the diet-regulated genes of both genotype groups.

Pathway	p-value	No. of genes*	total genes**	Gene symbols
(A) Diet effect within wildtype mice (*Dj-1*^{+/+})				
Metabolic Diseases	0.0077	56	7171	Akr1b3, Antxr2, Anxa4, Atic, B4galnt2, Ccdc88a, Cd72, Cd9, Cideb, Clcn2, Crhr1, Csf3r, Dab2, Dleu2, Dnmt3b, Edn1, Esr2, **Etv6,** Exoc6, Fbln1, Fhl2, Foxp2, Hhex, Il17rd, Kcnq5, Kif6, Lama4, Lamb2, Mier1, Mitf, Myb, Nppa, Nr2e1, Nrg1, Onecut1, Oprm1, Pde5a, Plagl1, Ptgs1, Rac2, Rapgef4, Rbm4b, Rec8, Rpa1, Runx1, Scarb1, Skp2, Slc12a1, Slc2a4, Slc38a3, Sv2b, Txnip, Ubap2, Vcan, Ywhaq, Zic1
Glucose Metabolism Disorders	0.0071	42	4957	Akr1b3, Antxr2, Ccdc88a, Cd72, Cd9, Cideb, Crhr1, Csf3r, Dleu2, Dnmt3b, Edn1, Esr2, **Etv6,** Exoc6, Fbln1, Fhl2, Foxp2, Hhex, Il17rd, Kif6, Lama4, Lamb2, Mier1, Myb, Nppa, Nrg1, Onecut1, Oprm1, Pde5a, Plagl1, Ptgs1, Rac2, Rapgef4, Rec8, Runx1, Scarb1, Skp2, Slc12a1, Slc2a4, Slc38a3, Txnip, Vcan
Inflammation	0.0023	42	4679	Adam19, Akr1b3, Anxa4, Atic, Ccdc88a, Cd72, Cd9, Cideb, Clcn2, Crhr1, Csf3r, Dleu2, Edn1, Esr2, **Etv6,** Exoc6, Fbln1, Lama4, Mitf, Myb, Nfia, Nppa, Nr2e1, Nrg1, Nup98, Onecut1, Oprm1, Pak4, Pde5a, Ptgs1, Rac2, Rapgef4, Rasd2, Rpa1, Runx1, Scarb1, Slc12a1, Slc2a4, Slc38a3, Txnip, Vcan, Ywhaq
Diabetes Mellitus	0.0010	43	4637	Akr1b3, Antxr2, Ccdc88a, Cd72, Cd9, Cideb, Crhr1, Csf3r, Dleu2, Dnmt3b, Edn1, Esr2, Etv6, Exoc6, Fbln1, Fhl2, Foxp2, Hhex, Il17rd, Kif6, Lama4, Lamb2, Mier1, Mmp16, Myb, Nppa, Nrg1, Onecut1, Oprm1, Pde5a, Plagl1, Ptgs1, Rac2, Rapgef4, Rec8, Runx1, Scarb1, Skp2, Slc12a1, Slc2a4, Slc38a3, Txnip, Vcan
Arteriosclerosis	0.0034	27	2642	Akr1b3, Anxa4, B4galnt2, Cd9, Clcn2, Crhr1, Dnmt3b, Edn1, Esr2, Etv6, Fbln1, Fhl2, Hhex, Kif6, Mmp16, Myb, Nppa, Nrg1, Oprm1, Pde5a, Plagl1, Ptgs1, Rac2, Scarb1, Slc2a4, Txnip, Vcan
Malnutrition	0.0012	24	2079	Akr1b3, Atic, Cd9, Csf3r, Dnmt3b, Edn1, Esr2, Hhex, Mitf, Myb, Nppa, Nr2e1, Onecut1, Oprm1, Pde5a, Plagl1, Ptgs1, Rpa1, Scarb1, Slc12a1, Slc2a4, Slc38a3, Txnip, Vcan
Hyperglycemia	0.0019	19	1529	Akr1b3, Crhr1, Edn1, Esr2, **Etv6,** Hhex, Lamb2, Nppa, Nrg1, Oprm1, Plagl1, Ptgs1, Rec8, Scarb1, Skp2, Slc12a1, Slc2a4, Txnip, Vcan
Cardiovascular Diseases	0.0002	64	7576	Adam19, Akr1b3, Antxr2, Anxa4, Atic, B4galnt2, Ccdc88a, Cd72, Cd9, Clcn2, Crhr1, Csf3r, D1Pas1, Dab2, Dleu2, Dnmt3b, Edn1, Esr2, Etv6, Exoc6, Fbln1, Fhl2, Foxp2, Fras1, Hhex, Inadl, Kcnq5, Kif6, Lama4, Lamb2, Ltk, Mitf, Mmp16, Mrps10, Myb, Nfia, Nppa, Nr2e1, Nrg1, Nsun5, Onecut1, Oprm1, Osbpl3, Pak4, Pde5a, Plagl1, Ptgs1, Rac2, Rapgef4, Rasd2, Rbm10, Rec8, Rpa1, Runx1, Scarb1, Skp2, Slc12a1, Slc2a4, Slc38a3, Sp110, Txnip, Vcan, Ywhaq, Zic1
Hypertension	0.0009	28	2552	Akr1b3, Crhr1, Dab2, Dleu2, Dnmt3b, Edn1, Esr2, Etv6, Exoc6, Hhex, Inadl, Kcnq5, Mitf, Myb, Nfia, Nppa, Nrg1, Onecut1, Oprm1, Pde5a, Plagl1, Ptgs1, Rpa1, Scarb1, Slc12a1, Slc2a4, Txnip, Vcan
Anoxia	0.0010	26	2301	Akr1b3, Anxa4, Cd9, Crhr1, Csf3r, Edn1, Esr2, Exoc6, Inadl, Lama4, Mitf, Myb, Nppa, Nr2e1, Nrg1, Oprm1, Pde5a, Ptgs1, Rpa1, Runx1, Scarb1, Skp2, Slc12a1, Slc2a4, Txnip, Vcan
Diabetes Complications	0.0020	24	2160	Akr1b3, Csf3r, Edn1, Esr2, Etv6, Exoc6, Hhex, Kif6, Lama4, Lamb2, Mmp16, Nppa, Nrg1, Onecut1, Oprm1, Pde5a, Plagl1, Ptgs1, Rec8, Scarb1, Slc12a1, Slc2a4, Txnip, Vcan
Dyslipidemias	0.0063	18	1581	Akr1b3, Atic, Ccdc88a, Dab2, Edn1, Esr2, Etv6, Kif6, Nppa, Nr2e1, Pde5a, Plagl1, Ptgs1, Scarb1, Slc2a4, Sv2b, Txnip, Vcan
Hyperlipidemias	0.0046	17	1412	Akr1b3, Atic, Dab2, Edn1, Esr2, Etv6, Kif6, Nppa, Nr2e1, Pde5a, Plagl1, Ptgs1, Scarb1, Slc2a4, Sv2b, Txnip, Vcan

Table S11. Continued.

Pathway	p-value	No. of genes*	total genes**	Gene symbols
Metabolic Syndrome X	0.0022	13	977	Cd72, Cideb, Edn1, Esr2, Hhex, Nppa, Pde5a, Ptgs1, Runx1, Scarb1, Slc12a1, Slc2a4, Vcan
Acidosis	0.0020	13	858	Clcn2, Dab2, Edn1, Exoc6, Nppa, Nrg1, Oprm1, Pde5a, Ptgs1, Slc12a1, Slc2a4, Slc38a3, Txnip
Hypoglycemia	0.0006	12	652	Akr1b3, Antxr2, Crhr1, Edn1, Esr2, Lamb2, Nppa, Oprm1, Pde5a, Plagl1, Slc2a4, Txnip
Hyperpituitarism	0.0080	8	474	Crhr1, Edn1, Esr2, Nppa, Pde5a, Plagl1, Scarb1, Slc2a4
Anorexia	0.0046	7	341	Anxa4, Crhr1, Esr2, Nppa, Nrg1, Ptgs1, Slc2a4

(B) Diet effect within *Dj-1⁻ᐟ⁻* mice

Pathway	p-value	No. of genes*	total genes**	Gene symbols
Metabolic Diseases	0.0001	92	7171	Aass, Abcb1b, Acad10, Acss1, Acss2, Aldob, Ano5, Apex2, Atf1, Atp13a4, Birc3, C3ar1, Ccl9, Ccr5, Cdkn2c, Chm, Col1a2, Coq2, Cplx1, Deaf1, Dhx40, Ercc2, Etfa, Etfb, **Etv6,** Flt3l, Fpgs, Ggcx, Ggta1, Gk5, Glrx2, Grk4, Hibadh, Hk2, Hrh1, Ifi30, Ifngr1, Igf2bp2, Il17rc, Irf4, Ivd, Lama1, Lcp1, Ldha, Limk2, Lmbr1l, Lmnb2, Lpo, Med30, Ncald, Neat1, Nek8, Nfs1, Npr1, Papss2, Pcbd1, Pde4d, Pdk1, Pdyn, Pik3cg, Plek, Pole, Rbm39, Recql, Rnpep, Rpgrip1, Scap, Sco1, Sema3e, Sfrp4, Slc15a2, Slc17a8, Slc19a1, Slc25a19, Slc2a12, Slc37a4, Smpd2, Stard3, Stat1, Stat3, Stat5b, Svep1, Svop, Tagap, Tert, Tia1, Tirap, Tmbim4, Tmbim6, Ube2l6, Ucp2, Vcl
Glucose Metabolism Disorders	0.0083	62	4957	Abcb1b, Acad10, Acss1, Acss2, Atf1, C3ar1, Ccl9, Ccr5, Col1a2, Deaf1, Etfa, Etfb, **Etv6,** Flt3l, Fpgs, Ggta1, Gk5, Grk4, Hibadh, Hk2, Hrh1, Ifi30, Ifngr1, Igf2bp2, Il17rc, Irf4, Ivd, Lama1, Lcp1, Ldha, Limk2, Lmnb2, Lpo, Ncald, Neat1, Npr1, Pcbd1, Pde4d, Pdk1, Pdyn, Pik3cg, Plek, Rnpep, Scap, Sema3e, Slc15a2, Slc19a1, Slc25a19, Slc2a12, Slc37a4, Smpd2, Stard3, Stat1, Stat3, Stat5b, Tagap, Tert, Tia1, Tmbim6, Ube2l6, Ucp2, Vcl
Inflammation	0.0088	59	4679	Abcb1b, Aldob, Atf1, Atp5j2, Birc3, C3ar1, Ccl9, Ccr5, Clcf1, Col13a1, Col1a2, Cyp4f13, Ercc2, Erg, **Etv6,** Flt3l, Ggcx, Ggta1, Gk5, Grk4, Hk2, Hrh1, Htr1d, Ifi30, Ifngr1, Il17rc, Irf4, Ivd, Lama1, Lcp1, Ldha, Lpo, Naip2, Nfe2l3, Npr1, Papss2, Pde4d, Pdyn, Pik3cg, Plek, Rnpep, Saal1, Samsn1, Scap, Sec14l3, Serf1, Sfrp4, Slc19a1, Slc37a4, Smpd2, Stat1, Stat3, Stat5b, Svep1, Tert, Tia1, Tirap, Ucp2, Vcl
Diabetes Mellitus	0.0071	57	4444	Abcb1b, Acad10, Acss2, C3ar1, Ccl9, Ccr5, Col1a2, Deaf1, Etfa, Etfb, Flt3l, Fpgs, Ggta1, Gk5, Grk4, Hibadh, Hk2, Hrh1, Ifi30, Ifngr1, Igf2bp2, Irf4, Ivd, Lama1, Lcp1, Ldha, Limk2, Lmnb2, Lpo, Ncald, Neat1, Npr1, Pcbd1, Pde4d, Pdk1, Pdyn, Pik3cg, Plek, Rnpep, Scap, Sema3e, Slc15a2, Slc19a1, Slc25a19, Slc2a12, Slc37a4, Smpd2, Stard3, Stat1, Stat3, Stat5b, Tagap, Tert, Tia1, Ube2l6, Ucp2, Vcl
Arteriosclerosis	0.0005	42	2642	Abcb1b, Birc3, C3ar1, Ccl9, Ccr5, Chm, Col1a2, Dcbld2, Ercc2, Erg, Etv6, Flt3l, Fpgs, Ggcx, Ggta1, Hk2, Hrh1, Htr1d, Ifi30, Ifngr1, Igf2bp2, Ivd, Lama1, Lcp1, Ldha, Lpo, Npr1, Pde4d, Pik3cg, Plek, Rnpep, Scap, Slc19a1, Smpd2, Stard3, Stat1, Stat3, Stat5b, Tert, Tia1, Ucp2, Vcl
Malnutrition	0.0006	35	2079	Aass, Abcb1b, Ccr5, Cdkn2c, Cplx1, Dcbld2, Etfa, Fam184b, Fpgs, Ggcx, Hibadh, Hk2, Hrh1, Ifngr1, Igf2bp2, Ivd, Ldha, Lmbr1l, Lpo, Neat1, Pcbd1, Pik3cg, Plek, Scap, Sfrp4, Slc19a1, Smpd2, Stat1, Stat3, Tert, Tmbim4, Tmbim6, Ucp2, Unc79, Vcl
Hyperglycemia	0.0055	25	1529	Acss2, Ccr5, **Etv6,** Fpgs, Ggta1, Grk4, Hk2, Hrh1, Ifi30, Igf2bp2, Il17rc, Ldha, Lpo, Npr1, Pcbd1, Pik3cg, Plek, Slc15a2, Slc37a4, Stat1, Stat3, Tert, Tmbim6, Ucp2, Vcl
Nutritional and Metabolic Diseases	0.0001	98	7724	Aass, Abcb1b, Acad10, Acss1, Acss2, Aldob, Ano5, Apex2, Asb4, Atf1, Atp13a4, Birc3, C3ar1, Ccl9, Ccr5, Cdkn2c, Chm, Col1a2, Coq2, Cplx1, Dcbld2, Deaf1, Dhx40, Ercc2, Etfa, Etfb, Etv6, Fam184b, Flt3l, Fpgs, Ggcx, Ggta1, Gk5, Glrx2, Grk4, Hibadh, Hk2, Hrh1, Htr1d, Ifi30, Ifngr1, Igf2bp2, Il17rc, Irf4, Ivd, Lama1, Lcp1, Ldha, Limk2, Lmbr1l, Lmnb2, Lpo, Med30, Ncald, Neat1, Nek8, Nfs1, Npr1, Papss2, Pcbd1, Pde4d ,Pdk1, Pdyn, Pik3cg, Plek, Pole, Rbm39, Recql, Rnpep, Rpgrip1, Scap, Sco1, Sema3e, Sfrp4, Slc15a2, Slc17a8, Slc19a1, Slc25a19, Slc26a2, Slc2a12, Slc37a4, Smpd2, Stard3, Stat1, Stat3, Stat5b, Svep1, Svop, Tagap, Tert, Tia1, Tirap, Tmbim4, Tmbim6, Ube2l6, Ucp2, Unc79, Vcl

147

Table S11. Continued.

Pathway	p-value	No. of genes*	total genes**	Gene symbols
Body Weight	0.0010	65	4835	Aass, Abcb1b, Acss1, Acss2, Asb4, Atf1, C3ar1, Ccl9, Ccr5, Cdkn2c, Chm, Clcf1, Col1a2, Cplx1, Dcbld2, Ercc2, Etv6, Fam198b, Flt3l, Fpgs, Ggcx, Ggta1, Gk5, Grk4 H2-Q7, Hibadh, Hk2, Hrh1, Htr1d, Ifi30, Ifngr1, Igf2bp2, Irf4, Ivd, Lama1, Ldha, Lpo, Neat1, Nek8, Npr1, Papss2, Pde4d, Pdyn, Pik3cg, Plek, Rnpep, Scap, Sfrp4, Slc15a2, Slc17a8, Slc19a1, Slc26a2, Slc2a12, Slc37a4, Smpd2, Stat1, Stat3, Stat5b, Tert, Tmbim4, Tmbim6, Ube2l6, Ucp2, Unc79, Vcl
Nutrition Disorders	0.0002	57	3868	Aass, Abcb1b, Acss1, Acss2, Asb4, Atf1, C3ar1, Ccl9, Ccr5, Cdkn2c, Chm, Cplx1, Dcbld2, Ercc2, Etfa, Etv6, Fam184b, Fpgs, Ggcx, Grk4, Hibadh, Hk2, Hrh1, Htr1d, Ifi30, Ifngr1, Igf2bp2, Irf4, Ivd, Lama1, Ldha, Lmbr1l, Lpo, Neat1, Nek8, Npr1, Pcbd1, Pde4d, Pdyn, Pik3cg, Plek, Scap, Sfrp4, Slc19a1, Slc26a2, Slc2a12, Slc37a4, Smpd2, Stat1, Stat3, Stat5b, Tert, Tmbim4, Tmbim6, Ucp2, Unc79, Vcl
Obesity	0.0093	41	2999	Abcb1b, Acss1, Acss2, Asb4, Atf1, C3ar1, Ccl9, Ccr5, Chm, Ercc2, Etv6, Grk4, Hibadh, Hk2, Hrh1, Htr1d, Ifi30, Igf2bp2, Irf4, Lama1, Ldha, Nek8, Npr1, Pde4d, Pdyn, Pik3cg, Plek, Scap, Sfrp4, Slc19a1, Slc26a2, Slc2a12,
				Slc37a4, Smpd2, Stat1, Stat3, Stat5b, Tert, Tmbim6, Ucp2, Vcl
Overweight	0.0065	41	2938	See ‚Obesity'
Overnutrition	0.0095	41	3004	See ‚Obesity'
Mitochondrial Diseases	0.0027	18	909	Apex2, Cdkn2c, Chm, Coq2, Etfa, Etfb, Hk2, Ifi30, Ldha, Lpo, Med30, Nfs1, Rpgrip1, Sco1, Slc25a19, Stat3, Ucp2, Vcl
Multiple Acyl CoA Dehydrogenase Deficiency	0.0019	3	26	Etfa, Etfb, Ldha

*number of differentially expressed genes found in the respective pathway

**total number of genes in the respective pathway

148

Table S12. Metabolic disease pathways associated with genotype-regulated genes. *Dj-1*^{-/-} and wildtpye mice were maintained on HF or control diet for 14 weeks. The ventral hypothalamus was subjected to RNA sequencing. Genes for which at least one transcript was found differentially expressed (Student's t-test, $p < 0.01$) with a log2 fold change > 0.26 (upregulation) or < -0.26 (downregulation) in *Dj-1*^{-/-} versus wildtype mice were subjected to a pathway analysis. Listed are pathways for which the number of differentially expressed genes between *Dj-1*^{-/-} or wildtype mice fed a control (**A**) or HF diet (**B**) exceeded the statistically expected number.

Pathway	p-value	No. of genes*	total genes**	Gene symbols
(A) Genotype effect within control group				
-				
(B) Genotype effect within HF group				
Cardiovascular Diseases	0.0096	127	7576	Abca4, Aen, Agtrap, Akap13, Ank1, Anxa2, Apln, Arnt2, Atp2b2, Bai2, Bcl11a, Btc, Bub1b, C3ar1, Calb1, Calcrl, Caln1, Camta1, Ccr5, Cd109, Cd44, Cd84, Cd93, Cdh15, Clstn1, Cmtm7, Cnp, Coro2a, Crat, Crem, Crhr1, Ctnnbip1, Cyp19a1, Daxx, Dffa, Dydc2, Eno1, Entpd5, Fam111a, Fancc, Fasl, Fbln1, Fli1, Flt1, Foxm1, Foxn3, Ghr, Gna15, Got2, Gprc5b, Grin2c, Hyal1, Ide, Impa2, Inadl, Itgam, Itgb4, Itih3, Jdp2, Kcna6, Kcnab2, Lama1, Lap3, Larp6, Limk1, Litaf, Lpar1, Lrrc16a, Lsr, Map3k6, Marveld2, Masp2, Mmel1, Mn1, Mst1r, Mxd1, Myo6, Nfkbiz, Nrg1, Nuak1, Osbpl6, P2rx7, Park7, Pax6, Pcdh1, Pik3cb, Pik3cd, Pla2g7, Plod1, Ppm1e, Ppp1r1b, Prep, Prmt3, Pttg1, Rasgrp2, Rbm10, Rec8, Renbp, Rgs8, Rhog, Sema3c, Sema3e, Sept4, Serpinf1, Slc25a25, Slc2a5, Slc31a2, Slc38a3, Slco3a1, Smad7, Socs2, Stag1, Tcf7, Tcf7l2, Tek, Tgfa, Tiam1, Tjp2, Tmbim1, Tnfaip8, Tnfrsf1b, Tnfrsf8, Ubqln4, Vash1, Wnk4, Yars, Zeb2
Inflammation	0.0001	94	4679	Abca4, Agtrap, Akap13, Aldob, Ank1, Anxa2, Apln, Atp2b2, BC030476, Bcl11a, Btc, Bub1b, C3ar1, Calb1, Calcrl, Ccr5, Ccrl1, Cd109, Cd44, Cd93, Clmn, Cnp, Coro2a, Crat, Crem, Crhr1, Cyp19a1, Dffa, Eif4a1, Eno1, Entpd5, Fancc, Fasl, Fbln1, Flt1, Fmo4, Ghr, Gk5, Gna15, Got2, Grin2c, Hhip, Hyal1, Ido2, Itgam, Itgb4, Kif5b, Lama1, Limk1, Litaf, LOC67527, Lpar1, Map3k6, Masp2, Max, Mmel1, Mn1, Mst1r, Mxd1, Nfkbiz, Nrg1, Nup98, P2rx7, Park7, Pax6, Pik3cb, Pik3cd, Pla2g7, Ppp1r1b, Prep, Renbp, Rhog, Sept4, Serpinf1, Slc2a5, Slc38a3, Smad7, Socs2, Stag1, Stk10, Sumf1, Tcf7, Tcf7l2, Tek, Tgfa, Tiam1, Tjp2, Tnfaip8, Tnfrsf1b, Tnfrsf8, Uap1, Ubqln4, Wnt10b, Yars
Body Weight	0.0014	91	4835	Abca4, Agtrap, Akap13, Ank1, Anxa2, Apln, Arnt2, Atp2b2, Bcl11a, Btc, Bub1b, C3ar1, Calb1, Calcrl, Camk1d, Ccr5, Cd44, Cd93, Cdh15, Cnp, Cplx1, Crat, Crem, Crhr1, Cyp19a1, Daxx, Dffa, Emid1, Eno1, Fasl, Fbln1, Flt1, Foxm1, Ghr, Gk5, Got2, Gprc5b, Grin2c, Hhip, Hyal1, Ide, Ido2, Itgam, Itih3, Kcna6, Kif5b, Lama1, Lap3, Larp6, Lekr1, Limk1, Litaf, LOC67527, Lpar1, Lsr, Map3k6, Masp2, Max, Mn1, Mst1r, Nrg1, Osbpl5, P2rx7, Park7, Pax6, Pik3cb, Pla2g7, Plod1, Ppp1r1b, Prep, Pttg1, Renbp, Rhog, Serpinf1, Slc25a25, Slc2a5, Smad7, Socs2, Stag1, Sv2b, Syt7, Tcf7, Tcf7l2, Tek, Tgfa, Tnfaip8, Tnfrsf1b, Tnfrsf8, Ubqln4, Vash1, Wnt10b
Diabetes Mellitus	0.0050	85	4637	Abca4, Agtrap, Ank1, Anxa2, Apln, Atp2b2, Bcl11a, Btc, C3ar1, Calb1, Calcrl, Camk1d, Camta1, Car7, Ccr5, Cd44, Cd93, Cdh15, Clstn1, Crat, Crem, Crhr1, Cyp19a1, Daxx, Emid1, Eno1, Entpd5, Fancc, Fasl, Fbln1, Fbxo9, Flt1, Foxm1, Foxn3, Ghr, Gk5, Got2, Hyal1, Ide, Ikzf4, Itgam, Lama1, Larp6, Lekr1, Litaf, Lpar1, Lsr, Masp2, Nrg1, P2rx7, Park7 Pax6, Pik3cb, Pik3cd, Pla2g7, Prep, Pttg1, Rec8, Renbp, Rgs8, Rsu1, Sema3c, Sema3e, Serpinf1, Slc2a5, Slc38a3, Smad7, Socs2, Stk10, Syt7, Tcf7, Tcf7l2, Tek, Tgfa, Tjp2, Tnfaip8, Tnfrsf1b, Tnfrsf8, Tulp4, Uap1, Ubqln4, Vash1, Wnk4, Wnt10b, Zeb2
Cerebrovascular Disorders	0.0014	65	3189	Agtrap, Anxa2, Apln, Arnt2, Atp2b2, Bai2, Bcl11a, C3ar1, Calb1, Calcrl, Camta1, Ccr5, Cd44, Cd93, Cnp, Crem, Crhr1, Cyp19a1, Daxx, Dffa, Eno1, Entpd5, Fancc, Fasl, Fbln1, Flt1, Ghr Got2, Gprc5b, Grin2c, Hyal1, Ide, Impa2, Itgam, Jdp2, Kcnab2, Lama1, Limk1, Lpar1, Lsr, Masp2, Nrg1, P2rx7, Park7, Pax6, Pcdh1, Pik3cb, Pla2g7, Ppp1r1b, Prep, Prmt3, Pttg1, Renbp, Sept4, Serpinf1, Slc2a5, Smad7, Socs2, Tcf7l2, Tek, Tgfa, Tjp2, Tnfrsf1b, Tnfrsf8, Yars

Table S12. Continued.

Pathway	p-value	No. of genes*	total genes**	Gene symbols
Anoxia	0.0001	55	2301	Agtrap, Anxa2, Apln, Arnt2, Bcl11a, Calb1, Calcrl, Cd44, Cd93, Cnp, Cplx1, Crhr1, Cyp19a1, Dffa, Echdc2, Eno1, Fasl, Flt1, Foxm1, Ghr, Got2, Grin2c, Ide, Inadl, Itgam, Kcna6, Lama1, Lpar1, Map3k6, Nrg1, P2rx7, Park7, Pax6, Pik3cd, Pla2g7, Plod1, Prep, Pttg1, Renbp, Sema3e, Sept4, Serpinf1, Smad7, Socs2, Tcf7l2, Tek, Tgfa, Tjp2, Tnfrsf1b, Tnfrsf8, Uap1, Vash1, Wnt10b, Yars, Zeb2
Arteriosclerosis	0.0036	54	2642	Abca4, Agtrap, Anxa2, Apln, Bcl11a, Btc, Bub1b, C3ar1, Calb1, Calcrl, Camta1, Ccr5, Cd44, Cd93, Cdh15, Cnp, Crhr1, Cyp19a1, Eno1, Fasl, Fbln1, Flt1, Foxn3, Ghr, Got2, Ide, Itgam, Itgb4, Itih3, Lama1, Limk1, Lpar1, Lrrc16a, Lsr, Masp2, Myo6, Nrg1, Osbpl6, P2rx7, Park7, Pik3cd, Pla2g7, Prep, Prmt3, Renbp, Serpinf1, Smad7, Tcf7l2, Tek, Tgfa, Tiam1, Tnfrsf1b, Tnfrsf8, Ubqln4
Diabetes Complications	0.0059	45	2160	Agtrap, Ank1, Anxa2, Apln, Bcl11a, Btc, C3ar1, Calb1, Calcrl, Camk1d, Ccr5, Cd44, Clstn1, Crem, Emid1, Entpd5, Fasl, Flt1, Ghr, Got2, Die, Itgam, Lpar1, Lsr, Masp2, Nrg1, P2rx7, Pax6, Pla2g7, Pttg1, Rec8, Renbp, Sema3c, Serpinf1, Slc2a5, Smad7, Tcf7l2, Tek, Tgfa, Tjp2, Tnfaip8, Tnfrsf1b, Tnfrsf8, Vash1, Zeb2
Body Weight Changes	0.0019	40	1748	Abca4, Agtrap, Anxa2, Apln, Atp2b2, Bcl11a, Calb1, Ccr5, Cd44, Cnp, Crat, Crhr1, Cyp19a1, Dffa, Eno1, Fasl, Flt1, Ghr, Got2, Grin2c, Itgam, Kcna6, Lap3, Limk1, Lsr, Mst1r, Nrg1, P2rx7, Pla2g7, Plod1, Renbp, Serpinf1, Slc2a5, Socs2, Sv2b, Tcf7, Tcf7l2, Tgfa, Tnfrsf1b, Tnfrsf8
Hyperglycemia	0.0020	36	1529	Agtrap, Apln, Bcl11a, Btc, Camta1, Ccr5, Cd44, Crat, Crem, Crhr1, Cyp19a1, Eno1, Fasl, Flt1, Foxm1, Ghr, Got2, Ide, Itgam, Nrg1, Nuak1, P2rx7, Pax6, Pik3cb, Pik3cd, Prep, Pttg1, Rec8, Renbp, Rgs8, Serpinf1, Slc2a5, Syt7, Tcf7l2, Tek, Tnfrsf1b
Intracranial Arterial Diseases	0.0003	34	1281	Agtrap, Atp2b2, C3ar1, Calb1, Camta1, Ccr5, Cd44, Cnp, Crem, Cyp19a1, Dffa, Fancc, Fasl, Fbln1, Flt1, Got2, Gprc5b, Hyal1, Ide, Itgam, Jdp2, Limk1, Nrg1, P2rx7, Park7, Pla2g7, Prmt3, Renbp, Sept4, Serpinf1, Tek, Tgfa, Tnfrsf1b, Tnfrsf8
Weight Loss	0.0051	29	1224	Agtrap, Anxa2, Apln, Atp2b2, Bcl11a, Calb1, Ccr5, Cd44, Crat, Crhr1, Cyp19a1, Fasl, Flt1,Ghr, Got2, Itgam, Kcna6, Nrg1, P2rx7, Pla2g7, Renbp, Serpinf1, Slc2a5, Socs2, Sv2b, Tcf7l2, Tgfa, Tnfrsf1b, Tnfrsf8
Weight Gain	0.0043	28	1154	Abca4, Agtrap, Apln, Bcl11a, Calb1, Cd44, Cnp, Crhr1, Dffa, Eno1, Fasl, Flt1, Ghr, Got2, Grin2c, Itgam, Lap3, Limk1, Lsr, Mst1r, Nrg1, Plod1, Renbp, Slc2a5, Socs2, Tcf7, Tcf7l2, Tgfa
Hypoxia, Brain	0.0027	23	853	Agtrap, Anxa2, Apln, Calb1, Ccr5, Cnp ,Crhr1, Fasl, Flt1, Ghr, Got2, Grin2c, Ide, Itgam, Nfkbiz, Nrg1, P2rx7, Ppp1r1b, Slc2a5, Tek, Tgfa, Tjp2, Tnfrsf1b
Hyperpituitarism	0.0085	14	474	Agtrap, Apln, Bcl11a, Bub1b, Calcrl, Crhr1, Cyp19a1, Ghr, Itgam, Lsr, Pttg1, Renbp, Socs2, Tgfa

*number of differentially expressed genes found in the respective pathway
**total number of genes in the respective pathway

Table S13. Pathways related to neurodegeneration or behavior associated with diet-regulated genes. *Dj-1⁻/⁻* and wildtpye mice were maintained on HF or control diet for 14 weeks. The ventral hypothalamus was subjected to RNA sequencing. Genes for which at least one transcript was found differentially expressed (Student's t-test, $p < 0.01$) with a log2 fold change > 0.26 (upregulation) or < -0.26 (downregulation) in HF versus control diet-fed mice were subjected to a pathway analysis. Listed are pathways for which the number of differentially expressed genes between HF or control diet-fed wildtype (**A**) or *Dj-1⁻/⁻* mice (**B**) exceeded the statistically expected number.

Pathway	p-value	No. of genes*	total genes**	Gene symbols
(A) Diet effect within wildtype mice (*Dj-1⁺/⁺*)				
Tauopathies	0.0081	25	2541	Adam19, Akr1b3, Anxa4, Crhr1, Dleu2, Dnmt3b, Edn1, Esr2, Hhex, Mmp16, Myb, Nppa, Nrg1, Oprm1, Pde5a, Ptgs1, Rapgef4, Rpa1, Runx1, Scarb1, Slc2a4, Snapc3, Sv2b, Vcan, Ywhaq
Neurodegenerative Diseases	0.0001	48	4890	Adam19, Akr1b3, Anxa4, Cd72, Cd9, Clcn2, Crhr1, Csf3r, Dleu2, Dnmt3b, Edn1, Esr2, Etv6, Exoc6, Foxp2, Hhex, Inadl, Lamb2, Mier1, Mitf, Mmp16, Myb, Nfia, Nppa, Nrg1, Onecut1, Oprm1, Pak4, Pde5a, Plagl1, Ptgs1, Rac2, Rapgef4, Rasd2, Rfx4, Rnf135, Rpa1, Runx1, Scarb1, Slc2a4, Snapc3, Sv2b, Tsen2, Ubap2, Vcan, Wrap53, Ywhaq, Zic1
Learning Disorders	0.0079	9	574	Crhr1, Dgki, Edn1, Esr2, Foxp2, Oprm1, Pak4, Rapgef4, Rnf135
Demyelinating Diseases	0.0057	24	2338	Akr1b3, Cd72, Cd9, Clcn2, Crhr1, D1Pas1, Dab2, Dleu2, Edn1, Esr2, Fbln1, Lama4, Mmp16, Myb, Nppa, Nrg1, Oprm1, Pde5a, Ptgs1, Rac2, Runx1, Slc12a1, Vcan, Zic1
Dementia	0.0028	30	3010	Adam19, Akr1b3, Anxa4, Clcn2, Crhr1, Dleu2, Dnmt3b, Edn1, Esr2, Etv6, Fbln1, Foxp2, Hhex, Mmp16, Nppa, Nrg1, Oprm1, Pde5a, Ptgs1, Rapgef4, Rasd2, Rpa1, Runx1, Scarb1, Slc2a4, Snapc3, Sv2b, Ubap2, Vcan, Ywhaq
(B) Diet effect within *Dj-1⁻/⁻* mice				
-				

*number of differentially expressed genes found in the respective pathway

**total number of genes in the respective pathway

Table S14. Pathways related to neurodegeneration or behavior associated with genotype-regulated genes. *Dj-1*^{-/-} and wildtpye mice were maintained on HF or control diet for 14 weeks. The ventral hypothalamus was subjected to RNA sequencing. Genes for which at least one transcript was found differentially expressed (Student's t-test, $p < 0.01$) with a log2 fold change > 0.26 (upregulation) or < -0.26 (downregulation) in *Dj-1*^{-/-} versus wildtype mice were subjected to a pathway analysis. Listed are pathways for which the number of differentially expressed genes between *Dj-1*^{-/-} or wildtype mice fed a control (**A**) or HF diet (**B**) exceeded the statistically expected number. Genes shown in bold represent overlapping genes of pathways associated with the genotype-regulated genes of both diet groups.

Pathway	p-value	No. of genes*	total genes**	Gene symbols
(A) Genotype effect within control group				
Demyelinating Diseases	0.0008	32	2338	Abcb1b, Adm, Bmper, Cbfa2t3, Ccl9, Cd55, Chuk, Clcf1, **Eno1,** Entpd1, **Fcrls,** Gadd45a, Htatip2, Lair1, Ldha, Lgals9, **Masp2,** Mfn2, Negr1, Palld, **Park7,** Rnaset2a, Slc12a1, Sox5, Spg7, Stim1, Tia1, Tmem2, **Tnfaip8, Tnfrsf1b, Tnfrsf8,** Xpa
(B) Genotype effect within HF group				
Demyelinating Diseases	0.0004	53	2338	Agtrap, Akap13, Anxa2, Atp2b2, Bcl11a, C3ar1, Calb1, Ccr5, Ccrl1, Cd44, Cd93, Cnp, Crem, Crhr1, Daxx, **Eno1,** Entpd5, Fasl, Fbln1, **Fcrls,** Flt1, Got2, Itgam, Itgb4, Lap3, Limk1, Litaf, Lpar1, **Masp2,** Mmel1, Mst1r, Nfkbiz, Nrg1, P2rx7, **Park7,** Pax6, Pik3cd, Pla2g7, Prep, Renbp, Smad7, Socs2, Stk10, Sumf1, Tcf7, Tcf7l2, Tek, Tgfa, Tjp2, **Tnfaip8, Tnfrsf1b, Tnfrsf8,** Yars
Dementia	0.0002	66	3010	Abca4, Agtrap, Akap13, Anxa2, Atp2b2, Bcl11a, Calb1, Camta1, Ccr5, Cd44, Clstn1, Cnp, Cplx1, Crat, Crem, Crhr1, Cyp19a1, Daxx, Dffa, Eno1, Entpd5, Fasl, Fbln1, Flt1, Foxm1, Gabra2, Got2, Grin2c, Ide, Itgam, Itgb4, Kcna6, Limk1, Masp2, Mmel1, Mn1, Mst1r, Myo6, Myrip, Nrg1, Numb, P2rx7, Park7, Pax6, Pla2g7, Ppp1r1b, Prep, Ptgfrn, Rasgrp2, Renbp, Sema3c, Serpinf1, Slc2a5, Smad7, Sv2b, Tanc1, Tcf7, Tcf7l2, Tgfa, Tiam1, Tjp2, Tnfrsf1b, Tnfrsf8, Ubap2, Zeb2
Tauopathies	0.0009	55	2541	Abca4, Agtrap, Akap13, Atp2b2, Bcl11a, Calb1, Ccr5, Cd44, Clstn1, Cnp, Cplx1, Crat, Crem, Crhr1, Cyp19a1, Daxx, Dffa, Eno1, Entpd5, Fasl, Flt1, Foxm1, Gabra2, Got2, Grin2c, Ide, Itgam, Itgb4, Limk1, Mmel1, Mn1, Myo6, Myrip, Nrg1, Numb, P2rx7, Park7, Pax6, Pla2g7, Ppp1r1b, Prep, Renbp, Sema3c, Serpinf1, Slc2a5, Smad7, Sv2b, Tanc1, Tcf7, Tcf7l2, Tgfa, Tiam1, Tnfrsf1b, Tnfrsf8, Zeb2
Alzheimer Disease	0.0011	54	2504	Abca4, Agtrap, Akap13, Atp2b2, Bcl11a, Calb1, Ccr5, Cd44, Clstn1, Cnp, Cplx1, Crat, Crem, Cyp19a1, Daxx, Dffa, Eno1, Entpd5, Fasl, Flt1, Foxm1, Gabra2, Got2, Grin2c, Ide, Itgam, Itgb4, Limk1, Mmel1, Mn1, Myo6, Myrip, Nrg1, Numb, P2rx7, Park7, Pax6, Pla2g7, Ppp1r1b, Prep, Renbp, Sema3c, Serpinf1, Slc2a5, Smad7, Sv2b, Tanc1, Tcf7, Tcf7l2, Tgfa, Tiam1, Tnfrsf1b, Tnfrsf8, Zeb2
Parkinsonian Disorders	0.0039	37	1649	Agtrap, Atp2b2, Calb1, Ccr5, Cd44, Clstn1, Cnp, Cplx1, Crhr1, Cyp19a1, Daxx, Eno1, Fasl, Flt1, Foxm1, Got2, Gpr37, Ide, Itgam, Limk1, Marveld2, Nrg1 P2rx7, Park7, Pax6, Pla2g7, Ppp1r1b, Prep, Renbp, Rhog, Sema3c, Sept4, Serpinf1, Syt7, Tgfa, Tnfrsf1b, Tnfrsf8
Parkinson Disease	0.0008	35	1398	Agtrap, Atp2b2, Calb1, Ccr5, Cd44, Clstn1, Cplx1, Crhr1, Cyp19a1, Daxx, Eno1, Fasl, Flt1, Got2, Gpr37, Ide, Itgam, Limk1, Marveld2, Nrg1, P2rx7, Park7, Pax6, Pla2g7, Ppp1r1b, Prep, Renbp, Rhog, Sema3c, Sept4, Serpinf1, Syt7, Tgfa, Tnfrsf1b, Tnfrsf8
Memory Disorders	0.0008	23	777	Agtrap, Atp2b2, Bcl11a, Calb1, Camta1, Ccr5, Cplx1, Crem, Cyp19a1, Emid1, Eno1, Grin2c, Ide, Itgam, Kcnab2, Lpar1, Nrg1, P2rx7, Pax6, Ppp1r1b, Prep, Sema3e, Tgfa
Dementia, Vascular	0.0052	11	310	Agtrap, Camta1, Cnp, Fasl, Fbln1, Got2, Ide, Itgam, Renbp, Serpinf1, Tnfrsf8

*number of differentially expressed genes found in the respective pathway
**total number of genes in the respective pathway

Table S15. Proteins immunoprecipitated from mouse brain lysate using an anti DJ-1 antibody. DJ-1 was found in the preciptiates of wildtype samples with a total sequence coverage of 97.9 % and high corresponding ion-intensities. Presented co-preciptiated proteins have been identified and quantified in at least 15 of 18 analysed immunoprecipitates of C57BL/6N mice fed a HF or control diet for 10 days (n = 8) but not in DJ-1 deficient mice and therefore represent potential direct or indirect DJ-1 binding partner proteins. The score for protein identification (posterior error probability, PEP) was < 5.8*10^{-8}. Data was generated by Dr. Gereon Poschmann, MPL, Düsseldorf, Germany.

Gene names	Protein names	UniProt/SwissProtKB accession	MW [kDa]	Peptides	Sequence coverage [%]
2010300C02Rik		E9Q3M9	125.9	17	25.6
Ablim1	Actin-binding LIM protein 1	E9QK41; Q8K4G5; E9Q9C2; E9Q9C1; E9Q9C0; E9Q9C4; E9Q9C7; E9Q030; E9Q9D2; E9Q9D1	96.8	22	32.3
Aco2	Aconitate hydratase, mitochondrial	Q99KI0	85.5	12	21.9
Actb		E9Q5F4	29.4	30	93.6
Actc1; Acta2; Actg2; Acta1	Actin, alpha cardiac muscle 1; Actin, aortic smooth muscle; Actin, gamma-enteric smooth muscle; Actin, alpha skeletal muscle	P68033; P62737; P63268; P68134; D3YZY0	42.0	28	57.6
Actn2	Alpha-actinin-2	Q9JI91	103.8	32	41.4
Actr1b	Beta-centractin	Q8R5C5	42.3	8	35.6
Actr2	Actin-related protein 2	P61161	44.8	11	40.4
Actr3b	Actin-related protein 3B	Q641P0	47.6	12	42.3
Aldoa; Aldoart1	Fructose-bisphosphate aldolase; Fructose-bisphosphate aldolase A	A6ZI44; P05064; D3YWI1; Q9CPQ9; D3YV98	45.1	15	43.8
Ank3		G5E8K5; G5E8K3; G5E8K2; G5E8C5	214.1	37	23.3
Anks1b	Ankyrin repeat and sterile alpha motif domain-containing protein 1B	Q8BIZ1; J3QMR2; J3QM69; J3QM51; E9QPP6	139.1	18	12.2
Ap2a2	AP-2 complex subunit alpha-2	P17427	104.0	34	43.8
Ap2m1	AP-2 complex subunit mu	P84091; Q3TWV4	49.7	27	60.7
Arhgap21		B7ZCJ1; G3UWM5	217.0	12	9.5
Arhgap32	Rho GTPase-activating protein 32	Q811P8; Q811P8-2	229.7	16	11.3
Arhgef11		Q68FM7; E9Q0A3	171.8	23	25.8
Arhgef2	Rho guanine nucleotide exchange factor 2	Q60875; H3BKH9; H3BJ40; H3BJ45; H3BJX8; H3BJU7	112.0	12	15.1
Arpc1a	Actin-related protein 2/3 complex subunit 1A	Q9R0Q6	41.6	11	38.1
Arpc2	Actin-related protein 2/3 complex subunit 2	Q9CVB6; D3YXG6	34.4	10	42.3
Arpc4	Actin-related protein 2/3 complex subunit 4	P59999	19.7	10	50.6
Atp1a2	Sodium/potassium-transporting ATPase subunit alpha-2	Q6PIE5; D3YYN7; D3YVX6	112.2	41	43.3
Atp2a2; Atp2a1	Sarcoplasmic/endoplasmic reticulum calcium ATPase 2; Sarcoplasmic/endoplasmic reticulum calcium ATPase 1	O55143; J3KMM5; Q8R429	114.9	16	17.5
Atp2b2	Plasma membrane calcium-transporting ATPase 2	F8WHB1; Q9R0K7	136.8	16	15.9

Table S15. Continued.

Gene names	Protein names	UniProt/SwissProtKB accession	MW [kDa]	Peptides	Sequence coverage [%]
Atp5c1	ATP synthase subunit gamma, mitochondrial; ATP synthase gamma chain	Q91VR2; Q8C2Q8; A2AKU9; A2AKV3; A2AKV2; A2AKV1	32.9	10	44.6
Bcas1	Breast carcinoma-amplified sequence 1 homolog	Q80YN3; E9Q8Q5; A2AVX1; F7BNZ5	67.4	7	12.2
Bdh1	D-beta-hydroxybutyrate dehydrogenase, mitochondrial	Q80XN0; D3Z2Y8	38.3	7	33.8
Begain	Brain-enriched guanylate kinase-associated protein	F8WIG2; Q68EF6	67.4	8	19.2
Brsk1	Serine/threonine-protein kinase BRSK1	Q5RJI5; D3Z5P0	85.2	11	22.1
C530008M17Rik; Kiaa1211	Uncharacterized protein KIAA1211	E9Q5L4; E9Q3Y7; Q5PR69; Q5PR69-2	142.9	12	16
Camk2g	Calcium/calmodulin-dependent protein kinase type II subunit gamma	Q923T9	59.6	24	52.2
Camkv	CaM kinase-like vesicle-associated protein	Q3UHL1	54.8	12	33.8
Caskin1	Caskin-1	Q6P9K8	150.5	19	22.2
Cct6a	T-complex protein 1 subunit zeta	P80317; E9QPA6	58.0	8	24.9
Cct8	T-complex protein 1 subunit theta	P42932; H3BL49	59.6	7	16.2
Cdh2	Cadherin-2	P15116; D3YYT0	99.8	10	19.8
Cdk5	Cyclin-dependent kinase 5	P49615	33.3	9	33.9
Cit	Citron Rho-interacting kinase	D3YU89;E9QL53;P49025;D3Z1U0; F6SBR5	238.8	16	9.4
Ckmt1	Creatine kinase U-type, mitochondrial	P30275; A2ARP5	47.0	13	41.9
Clasp2	CLIP-associating protein 2	Q08EB6; E9Q8N5; Q8BRT1; F7DCH5	140.9	18	19.2
Cnksr2	Connector enhancer of kinase suppressor of ras 2	Q80YA9; A2AI78	117.4	14	17
Coro1a	Coronin-1A	O89053; G3UYK8	51.0	13	40.1
Coro1b	Coronin-1B	Q9WUM3	53.9	9	24.6
Coro2a	Coronin-2A	B1AVH5; Q8C0P5	61.7	12	21.2
Crmp1	Dihydropyrimidinase-related protein 1	Q6P1J1; P97427	74.2	15	32.2
Ctnnd2	Catenin delta-2	O35927; E9QKH8	135.0	17	18.1
Cyld	Ubiquitin carboxyl-terminal hydrolase CYLD	Q80TQ2	106.9	8	9.9
Dclk2	Serine/threonine-protein kinase DCLK2	Q6PGN3	84.5	9	17.1
Ddx3x; D1Pas1	ATP-dependent RNA helicase DDX3X;Putative ATP-dependent RNA helicase Pl10	Q62167;P16381	73.1	14	30.4
Dlg1	Disks large homolog 1	E9Q9H0;Q811D0; H7BWY4; D3Z3B8; F6UDT8	103.0	19	27
Dlg2	Disks large homolog 2	Q91XM9; E9Q2L2; D3YUZ8; D3YWU0	109.2	32	43.2
Dlg3	Disks large homolog 3	A2BEE9; Q52KF7; P70175	92.1	21	31.5
Dlgap1	Disks large-associated protein 1	Q9D415; D3Z709; D3Z508;D3Z6F4;Q3UVU8	110.4	11	12.9
Dlgap2	Disks large-associated protein 2	Q8BJ42; Q0VF59	119.1	18	22.2
Dlgap3	Disks large-associated protein 3	Q6PFD5; B1AS06	105.9	19	26.8
Dlgap4	Disks large-associated protein 4	B1AZP2; B7ZNS2	107.6	13	15.8

154

Table S15. Continued.

Gene names	Protein names	UniProt/SwissProtKB accession	MW [kDa]	Peptides	Sequence coverage [%]
Dlst	Dihydrolipoyllysine-residue succinyltransferase component of 2-oxoglutarate dehydrogenase complex, mitochondrial	Q9D2G2	49.0	5	14.1
Dmxl2	DmX-like protein 2	B0V2P5; Q8BPN8; F6RYL8	340.7	24	11.4
Dpysl3	Dihydropyrimidinase-related protein 3	E9PWE8; Q62188; Q3TT92; D3YUS0	73.9	12	22.5
Dst	Dystonin	E9PXE5; E9QL23; E9Q9X1; Q91ZU6	834.2	34	6.3
Dstn	Destrin	Q9R0P5	18.5	3	22.4
Epb41l3	Band 4.1-like protein 3	Q9WV92-8; Q9WV92-7	116.8	17	19.6
Erc2	ERC protein 2	Q6PH08	110.6	19	21.2
Etl4;Skt	Sickle tail protein	E9QAU4; A2AQ25; D3Z781	218.4	19	12.9
Fbxo41	F-box only protein 41	Q6NS60	94.3	17	27.6
Fscn1	Fascin	Q61553	54.5	8	23.7
Git1	ARF GTPase-activating protein GIT1	Q68FF6; Q5F258	85.3	9	17
Gja1	Gap junction alpha-1 protein	P23242	43.0	13	46.6
Gm10119; Rps3a; Gm9000	40S ribosomal protein S3a	D3Z6C3; P97351; D3Z7W7	29.8	10	37.9
Gm17352; Rps18; Gm10260; Gm5321	40S ribosomal protein S18	F6YVP7; P62270; G3UZW2; F5H8M6; D3YWV7	17.7	10	48.7
Gm996	Uncharacterized protein C9orf172 homolog	A2AJA9	107.2	23	31.4
Gnai1	Guanine nucleotide-binding protein G(i) subunit alpha-1	B2RSH2	40.4	12	39.3
Gphn	Gephyrin;Molybdopterin adenylyltransferase; Molybdopterin molybdenumtransferase	A0JNY3; Q8BUV3	83.7	15	28.5
Gpm6a	Neuronal membrane glycoprotein M6-a	P35802	31.1	3	12.6
Grin1	Glutamate [NMDA] receptor subunit zeta-1	A2AI21; P35438; A2AI14; A2AI17; A2AI20; A2AI19	108.0	20	19.9
Grin2a	Glutamate [NMDA] receptor subunit epsilon-1	P35436	165.4	10	8.1
Grin2b	Glutamate [NMDA] receptor subunit epsilon-2	G3X9V4; Q01097	166.0	26	20.6
Gsk3b	Glycogen synthase kinase-3 beta	E9QAQ5; Q9WV60	48.0	6	24
Hba; Hba-a1	Hemoglobin subunit alpha	P01942; Q91VB8	15.1	3	25.4
Hbb-b1	Hemoglobin subunit beta-1	A8DUK4; E9Q223; P02088	15.7	8	67.3
Hnrnpm	Heterogeneous nuclear ribonucleoprotein M	Q9D0E1; B8JK32; B8JK33	77.6	7	14.1
Idh3b		Q91VA7	42.2	10	26
Iqsec2	IQ motif and SEC7 domain-containing protein 2	E9QAD8; A4GZ26; Q5DU25; D3Z5I6; D3Z6V7	162.8	22	20.4
Itpka	Inositol-trisphosphate 3-kinase A	Q8R071	50.9	20	51.4
Jmy	Junction-mediating and -regulatory protein	Q9QXM1	110.6	8	12.7
Kif5c	Kinesin heavy chain isoform 5C	P28738	109.3	14	17.8
Klc2	Kinesin light chain 2	Q91YS4; D3YXZ3; O88448	68.4	10	23.6
Lrrc7	Leucine-rich repeat-containing protein 7	E9Q6L9; Q80TE7	172.7	36	30

Table S15. Continued.

Gene names	Protein names	UniProt/SwissProtKB accession	MW [kDa]	Peptides	Sequence coverage [%]
Lsamp	Limbic system-associated membrane protein	Q8BLK3; Q3TYE5	38.1	9	36.7
Macf1	Microtubule-actin cross-linking factor 1	E9PVY8; Q9QXZ0; B1ARU4; E9QA63; F7ACR9; E9QNP1; F6Q750; B1ARU1	831.9	56	10.3
Mal2	Protein MAL2	Q8BI08	19.1	2	17.7
Mark2	Serine/threonine-protein kinase MARK2	E9QMP6; F6ZS70; Q05512; Q3T9A3; E9PYX3; E9Q9N6	86.4	11	18.9
Mtap1a; Map1a	Microtubule-associated protein 1A;MAP1 light chain LC2	A2ARP8; Q9QYR6	325.9	24	13.1
Mtap4; Map4	Microtubule-associated protein; Microtubule-associated protein 4	E9PZ43; E9PWC0; P27546; P27546-2; E9QPW8; F7CK47	97.8	5	6.9
Myh11		E9QPE7; O08638-2	223.4	75	39.1
Myo1b	Unconventional myosin-Ib	Q7TQD7; P46735; E9Q580; E9QNH6	132.1	33	30.9
Myo1c	Unconventional myosin-Ic	Q9WTI7	121.9	22	25.8
Nars	Asparagine--tRNA ligase, cytoplasmic	Q8BP47	64.3	7	14.1
Ncam1	Neural cell adhesion molecule 1	P13595; E9QB01; E9Q589	119.4	12	17.8
Ncdn	Neurochondrin	Q9Z0E0	78.9	15	22.1
Nexn	Nexilin	Q7TPW1	72.1	7	10.7
Nptn	Neuroplastin	P97300; H3BIX4	44.4	6	20.2
Ntm	Neurotrimin	Q8BG33; Q99PJ0; D3Z396; F6RQ26; F6Z2M6	37.9	9	25.9
Ogdh	2-oxoglutarate dehydrogenase, mitochondrial	Q60597	118.2	13	15.5
Pclo	Protein piccolo	E9QK94;Q9QYX7	563.4	45	13.2
Pfkm	6-phosphofructokinase, muscle type	P47857	85.3	17	29
Pfkp	6-phosphofructokinase; 6-phosphofructokinase type C	Q8C605; Q9WUA3	85.5	22	36.2
Phgdh	D-3-phosphoglycerate dehydrogenase	Q61753	56.6	9	21.4
Pkp4	Plakophilin-4	Q68FH0; A2AS45; A2AS44	131.6	27	28.6
Poldip2	Polymerase delta-interacting protein 2	Q91VA6; F6SQH7	41.9	8	24.2
Poldip3	Polymerase delta-interacting protein 3	Q8BG81; Q3UDD3; F6VR84	46.1	7	21.9
Ppfia2	Liprin-alpha-2	B8QI34; Q8BSS9	143.3	9	9
Ppfia3	Liprin-alpha-3	B8QI35; P60469; F6UYF1	133.4	15	16.5
Ppp1cc	Serine/threonine-protein phosphatase PP1-gamma catalytic subunit	P63087	38.5	20	57
Ppp2r2a	Serine/threonine-protein phosphatase 2A 55 kDa regulatory subunit B alpha isoform	Q6P1F6	51.7	8	25.1
Prkcb	Protein kinase C beta type	P68404	76.9	15	30.2
Psd3	PH and SEC7 domain-containing protein 3	E9PUC5; Q2PFD7; F6Z9E6; Q8C0E9	42.3	7	27.1
Ptk2b	Protein-tyrosine kinase 2-beta	Q9QVP9; Q3UDE9; E9Q2A6	115.8	12	13.3
Purb	Transcriptional activator protein Pur-beta	O35295	33.9	9	36.1
Rab14	Ras-related protein Rab-14	Q91V41; A2AL34	23.9	7	37.2

Table S15. Continued.

Gene names	Protein names	UniProt/SwissProtKB accession	MW [kDa]	Peptides	Sequence coverage [%]
Rab1b	Ras-related protein Rab-1B	Q9D1G1	22.2	7	46.3
Rab3a	Ras-related protein Rab-3A	P63011	25.0	7	35.9
Rab6a; Rab6b	Ras-related protein Rab-6A; Ras-related protein Rab-6B	P35279; P61294	23.6	3	16.3
Rapgef4	Rap guanine nucleotide exchange factor 4	Q9EQZ6; A2ASW8; Q9EQZ6-2	115.5	9	11.3
Rbm14	RNA-binding protein 14	Q8C2Q3; E9QL13	69.4	9	17.8
Rimbp2	RIMS-binding protein 2	D3YXR8; Q80U40	119.2	11	16.9
Rims1	Regulating synaptic membrane exocytosis protein 1	Q99NE5; F6VBR4; F6VBT9; F6VBV0; F6Y0S3; F6TZK4	163.2	26	26.5
Rpl10a; Rpl10a-ps2	Ribosomal protein; 60S ribosomal protein L10a	Q5XJF6; P53026; D3YXT2	24.8	6	26.3
Rpl12	60S ribosomal protein L12	P35979	17.8	5	43
Rpl18a	60S ribosomal protein L18a	P62717	20.7	6	24.4
Rpl22	60S ribosomal protein L22	P67984	14.8	4	31.2
Rpl3	60S ribosomal protein L3	P27659	46.1	10	32.3
Rpl30	60S ribosomal protein L30	P62889	12.8	2	24.3
Rpl4	60S ribosomal protein L4	Q9D8E6	47.2	14	34.1
Rpl6; Gm5428	60S ribosomal protein L6	P47911; E9PUX4	33.5	9	24
Rpl7	60S ribosomal protein L7	P14148; F6XI62	31.4	11	44.8
Rplp0;Gm8730	60S acidic ribosomal protein P0	P14869; E9Q070; D3YVM5	34.2	12	45.4
Rps11	40S ribosomal protein S11	P62281	18.4	8	50
Rps13	40S ribosomal protein S13	P62301	17.2	6	38.4
Rps14	40S ribosomal protein S14	P62264	16.3	5	32.5
Sbf1	Myotubularin-related protein 5	B2RXX4; Q6ZPE2	211.4	19	14.1
Sept7	Septin-7	E9Q1G8; E9Q9F5; O55131	50.6	7	20.6
Sfxn3	Sideroflexin-3	Q91V61; Q3U4F0	35.4	8	39.3
Shank1	SH3 and multiple ankyrin repeat domains protein 1	D3YZU1; D3YZU4; D3YZU5	226.3	37	24.7
Shank2	SH3 and multiple ankyrin repeat domains protein 2	D3Z5K8; Q80Z38; D3Z5K9	200.1	38	29.9
Shank3	SH3 and multiple ankyrin repeat domains protein 3	Q4ACU6	192.2	41	31
Shisa7	Protein shisa-7	Q8C3Q5; F6T9T6	58.3	9	18.1
Sipa1l1	Signal-induced proliferation-associated 1-like protein 1	Q8C0T5	197.0	27	22.4
Slc17a7	Vesicular glutamate transporter 1	Q3TXX4	61.6	4	8.4
Slc25a22	Mitochondrial glutamate carrier 1	Q9D6M3; E9Q6M6; E9PY45; E9PV90	34.7	11	55.7
Slc3a2	4F2 cell-surface antigen heavy chain	G3UWA6; P10852	62.2	7	14
Snap91	Clathrin coat assembly protein AP180	E9QLK9; Q61548; E9QQ05; E9Q9A3; Q3TWS4; Q8BQA2	91.9	8	13.8
Sorbs1	Sorbin and SH3 domain-containing protein 1	Q62417	143.1	17	17.1
Sorbs2	Sorbin and SH3 domain-containing protein 2	B9EKP8; E9Q0B0; Q3UTJ2; D3Z080; B2RXQ9; E9Q8K9	145.0	22	24.1
Spire1	Protein spire homolog 1	D3YTL8; Q52KF3; D3Z495	75.0	7	15.5
Spnb4		E9PX29; Q91ZE6	288.8	35	16.9

Table S15. Continued.

Gene names	Protein names	UniProt/SwissProtKB accession	MW [kDa]	Peptides	Sequence coverage [%]
Spta1	Spectrin alpha chain, erythrocyte	P08032	279.9	30	18.5
Srgap2	SLIT-ROBO Rho GTPase-activating protein 2	Q91Z67	120.8	12	14.8
Sucla2	Succinyl-CoA ligase [ADP-forming] subunit beta, mitochondrial	Q9Z2I9	50.1	8	20.5
Suclg1	Succinyl-CoA ligase [ADP/GDP-forming] subunit alpha, mitochondrial	Q9WUM5	36.2	8	27.2
Sv2a	Synaptic vesicle glycoprotein 2A	Q9JIS5	82.6	6	10.9
Syn2	Synapsin-2	Q64332	63.4	12	33.6
Syp	Synaptophysin	Q62277; F6VR28	34.0	2	7.3
Syt1	Synaptotagmin-1	P46096	47.4	16	32.1
Tcp1	T-complex protein 1 subunit alpha	P11983	60.4	13	32.9
Tjp1	Tight junction protein ZO-1	B9EHJ3; P39447	188.9	28	20.4
Tjp2	Tight junction protein ZO-2	Q9Z0U1	131.3	17	17.9
Tmod1	Tropomodulin-1	P49813	40.5	10	34.3
Tpm1		E9Q453; G5E8R0; E9Q455; E9Q456; G5E8R1; G5E8R2	28.5	9	35.5
Trim3	Tripartite motif-containing protein 3	Q9R1R2; Q3TDT0	80.8	13	28.6
Trim46	Tripartite motif-containing protein 46	Q7TNM2; D3YXA6	83.4	13	24.1
Tsc22d4	TSC22 domain family protein 4	D3YZZ4; Q9EQN3; F6VXN4	17.6	3	28
Tubb2b	Tubulin beta-2B chain	Q9CWF2	50.0	35	81.3
Ubc; Ubb; 2810422J05Rik; Rps27a; Uba52; Gm7866	Polyubiquitin-C;Ubiquitin; Ubiquitin-related 1; Ubiquitin-related 2;Polyubiquitin-B; Ubiquitin; Ubiquitin-40S ribosomal protein S27a; Ubiquitin;40S ribosomal protein S27a; Ubiquitin-60S ribosomal protein L40; Ubiquitin;60S ribosomal protein L40	P0CG50; P0CG49; Q5SX22; E9QNP0; E9Q5F6; E9Q4P0; P62983; P62984; J3QK04; E9Q9J0; F6X7C4	82.5	6	60.1
Uqcrc1	Cytochrome b-c1 complex subunit 1, mitochondrial	Q9CZ13	52.9	5	15
Vamp2	Vesicle-associated membrane protein 2	B0QZN5; P63044	17.9	5	42.9
Vdac1	Voltage-dependent anion-selective channel protein 1	Q60932; F2Z471	32.4	8	39.2
Vps35	Vacuolar protein sorting-associated protein 35	Q9EQH3	91.7	8	12.8
Wdr1	WD repeat-containing protein 1	O88342	66.4	11	28.4
Wdr47	WD repeat-containing protein 47	Q8CGF6	102.3	10	13.9
Wdr7	WD repeat-containing protein 7	Q920I9; Q920I9-2	163.5	15	13.6
Ywhae	14-3-3 protein epsilon	P62259	29.2	9	45.9
Ywhag	14-3-3 protein gamma;14-3-3 protein gamma, N-terminally processed	P61982	28.3	12	58.7

MW – Molecular weight.

Table S16. Alterations in the hypothalamic proteome after 18 weeks of HF or 'cafeteria' feeding. Male C57BL/6N mice were either fed a 60 % high-fat (HF), 'cafeteria' or control diet (n = 6). Animals on 'cafeteria' diet could choose from three different tasting pellets ('salt', 'biscuit' and 'chocolate'). After 18 weeks on diet, hypothalami were collected and subjected to two-dimensional difference gel electrophoresis (2D-DIGE). HF or cafeteria diet-fed mice were compared to control diet-fed mice, respectively. Listed are spots with significantly differential volumes that were identified by nano-LC-ESI mass spectrometry. See Supplementary Fig. S9 for body mass and body composition data of mice and information on diets.

Protein name	Gene Symbol	UniProtKB accession no.	Average Ratio*		T-Test p-value		ANOVA + Tukey-Test p-value	
			HF/ control	cafeteria/ control	HF/ control	cafeteria/ control	HF/ control	cafeteria/ control
regulated in high fat and cafeteria group								
Actin, cytoplasmic 1	Actb	P60710	1.74	1.89	**0.000**	**0.000**	**0.000**	**0.000**
Alpha-internexin	Ina	P46660	0.90	0.88	**0.006**	**0.004**	**0.012**	**0.003**
Creatine kinase B-type	Ckb	Q04447	0.92	0.93	**0.048**	**0.023**	0.055	0.064
regulated in high fat group compared to control								
NADH dehydrogenase [ubiquinone] iron-sulfur protein 8, mitochondrial	Ndufs8	Q8K3J1	1.45	1.33	**0.027**	0.092	**0.044**	0.158
Superoxide dismutase [Mn], mitochondrial	Sod2	P09671	1.12	1.02	**0.023**	0.160	**0.020**	0.796
Dynamin-1	Dnm1	P39053	0.90	0.94	**0.036**	0.063	**0.030**	0.238
regulated in cafeteria group compared to control								
Glial fibrillary acidic protein	Gfap	P03995	1.14	1.23	0.100	**0.023**	0.124	**0.016**
26S protease regulatory subunit 6B	Psmc4	P54775	1.04	1.14	0.350	**0.016**	0.610	**0.025**
Stathmin	Stmn1	P54227	1.06	1.11	0.320	**0.034**	0.527	0.101
Dihydropyrimidinase-related protein 2	Dpysl2	O08553	1.07	1.07	0.065	**0.008**	0.078	0.053
Neurofilament medium polypeptide	Nefm	P08553	0.85	0.81	0.087	**0.022**	0.100	**0.037**
Creatine kinase B-type	Ckb	Q04447	0.89	0.86	0.093	**0.010**	0.106	**0.026**
Aconitate hydratase, mitochondrial	Aco2	Q99KI0	0.93	0.89	0.077	**0.030**	0.263	**0.029**
Isocitrate dehydrogenase [NAD] subunit alpha, mitochondrial	Idh3a	Q9D6R2	0.97	0.92	0.380	**0.011**	0.608	0.051

*Ratio of normalized and standardized 2D-DIGE spot volumes. Data generated by Dr. Gereon Poschmann, MPL, Düsseldorf, Germany.

APPENDIX

I   Material

I.I   Diets

A   **Control**

B   **High-fat (HF)**

C   **High-fat/high-sugar (HF/HS)**

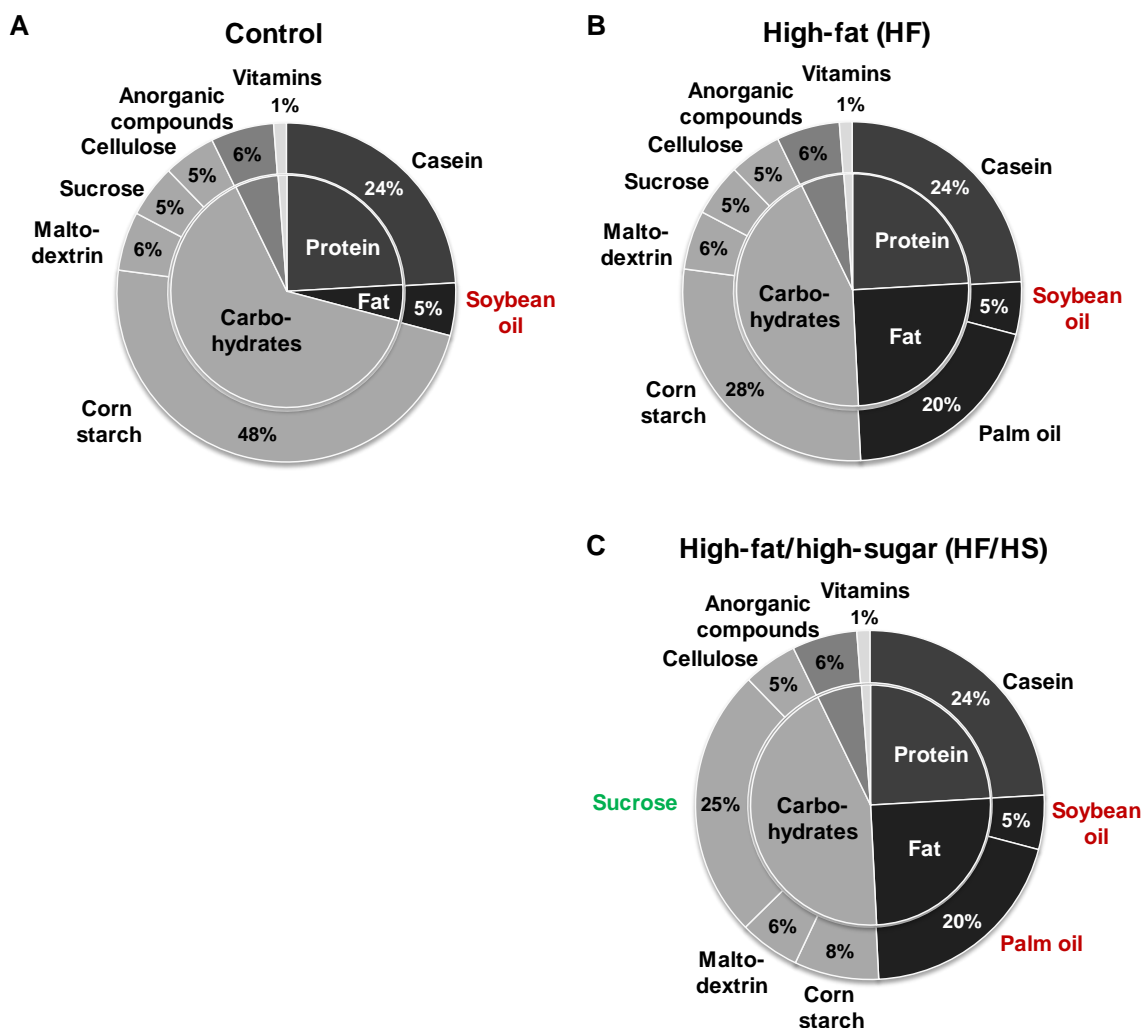**Fig A1. Composition of diets used in this thesis.** The custom-made purified diets were obtained from Ssniff Spezialdiäten GmbH, Soest, Germany: (**A**) Control #S5745-E702, (**B**) HF #S5745-E712 (**C**) HF/HS #S5745-E713). Marcronutrients are given in percent by weight. The amount of fat corresponds to 12 cal% fat for the control diet and 48 cal% for the HF or HF/HS diet.

I.II Antibodies

Table A1. List of primary antibodies.

Target protein	Host	MW [kDa]	Dilution factor	Company	Product code
Actin	mouse	43	10 000	Millipore	MAB1501
Anti-Porin (VDAC)	rabbit	~31	1000	Calbiochem	PC548T
Calnexin	goat	90	1000	Santa Cruz Biotechnology	sc-6465
COXIV	rabbit	17	5000	Cell Signaling	4844
DJ-1	rabbit	23	10 000	Biomol (Epitomics)	2398-1
Histone H3	goat	15	1000	Santa Cruz Biotechnology	sc-8654
OXPHOS Rodent AB Cocktail	mouse		350	MitoSciences	MS604
PMP70	rabbit	70	5000	Abcam	ab3421
phospho-STAT3 (Tyr705)	rabbit	80	1000	Cell Signaling	#9145
STAT3	mouse	80	1000	Cell Signaling	#9139
SOD2	mouse	25	10 000	Abcam	ab16956
Tubulin alpha	mouse	50	7500	Acris	BM753S

MW – Molecular weight. COXIV - cytochrome c oxidase subunit 4. OXPHOS - oxidative phosphorylation. PMP70 - peroxisomal membrane protein 70. SOD2 - superoxide dismutase 2. STAT3 - signal transducer and activator of transcription 3. VDAC - voltage-dependent anion channel.

Secondary antibodies were IRDye 800CW or 680 RD conjugated and obtained from LI-COR® Biosciences, Lincoln, NE, USA (#926-322 11/12/14/21/22).

I.III Primer pairs

Table A2. List of primer sequences applied in gene expression analysis by qRT-PCR.

Gene	Gene ID	Forward (5'-3')	Reverse (5'-3')	Product size (bp)
Acot13	66834	TAATAAACTGGGCACGCTCC	TCCTGTGGTCTTGTTGGTCA	232
Bax	12028	GAAGCTGAGCGAGTGTCTCC	GAAGTTGCCCATCAGCAAACA	145
Gclc	14629	TCATCCCCATTCTGAACTCC	TCAGGATGGTTTGCAATGAA	157
Gclm	14630	TGTTTTGGAATGCACCATGT	AGGCTGTAAATGCTCCAAGG	232
Gfap	14580	TACAGGAAATTGCTGGAGGG	TCACATCACCACGTCCTTGT	207
Hmox1	15368	CTCACAGATGGCGTCACTTC	GCCACATTGGACAGAGTTCA	226
Hrsp12	15473	GCTTACCAAGTCGCTGCTTT	ACCTCCGGAGTCAACATCAG	119
Hsp90	15516	AGGAGGGTCAAGGAAGTGGT	TTTTTCTTGTCTTTGCCGCT	215
Ndufv2	72900	CTGTGTAAATGCACCGATGG	CAAGTTAAAGGCCTGCTTGC	218
Nqo1	18104	GGTAGCGGCTCCATGTACTC	CATCCTTCCAGGATCTGCAT	173
Park7/Dj-1	57320	GATGTGGTGGTTCTTCCAGG	CCTTAGCCAGTGGGTGTGTT	190
Phb	18673	GTAGAAGCCAAACAGGTGGC	GCTGGCAGGTAGGTGATGTT	239
POMC	18976	CCCTCCTGCTTCAGACCTC	CGTTGCCAGGAAACACGG	150
Ppp3r1	19058	GGTGGGCAACAATCTGAAAG	AAAGCAAAAGTGTTGGGTGG	191
Psmb6	19175	TCTGATGGCAGGAATCATCA	TGAACTGCAGACATTCGTCC	188
Pten	19211	GCGTGCAGATAATGACAAGG	TAGCCTCTGGATTTGATGGC	158
Sh3bgrl3	73723	GTCTACAGCACGTCGGTCAC	CCACAGTAGTGGTTCCCGTT	200
Slc25a14	20523	TTGGACCCTGGAACATCATT	GAGGCAACACAAATGCAAAA	214
Slc25a27	74011	CTACCCTCGTGGCTGAGAAT	AGAAATAACAGGGGCGTGTG	161
Snca	20617	GCTCAGAAGACAGTGGAGGG	AGGAGATTGGGTGCAATGAC	216
Sncb	104069	GGAGGAGCTGTGTTCTCTGG	TTACGCCTCTGGCTCGTATT	207
Sod1	20655	GCCAATGTGTCCATTGAAGA	TCAGACCACACAGGGAATGT	200
Trp53	22059	CCGGCTCTGAGTATACCACC	GCACAAACACGAACCTCAAA	154

I.IV Chemicals, materials, equipment, software

Chemicals, materials, and equipement were obtained from the companies Carl Roth (Karlsruhe, Germany), Sigma-Aldrich (St. Louis, MO, USA), Eppendorf (Hamburg, Germany) or Sarstedt (Nümbrecht, Germany) unless otherwise stated. Chemicals had at least p.a. quality.

Table A3. Chemicals and enzymes.

Name	Product code	Company
ADP	A2754	Sigma-Aldrich, St.Louis, MO, USA
Agarose	114046	Serva, Heidelberg, Germany
Albumin Fraction V, ≥ 98%	8076	Carl Roth, Karlsruhe, Germany
Albumin from bovin serum (for isolation of mitochondria)	A3803	Sigma-Aldrich, St.Louis, MO, USA
Amplex® Red	A12222	Invitrogen, Darmstadt, Germany
Antimycin A	A8674	Sigma-Aldrich, St.Louis, MO, USA
Bromphenol blue	A512	Carl Roth, Karlsruhe, Germany
CHAPS	1479	Carl Roth, Karlsruhe, Germany
1,4-Dithiothreitol	6908	Carl Roth, Karlsruhe, Germany
DMSO	4720	Carl Roth, Karlsruhe, Germany
DNA-Ladder 100 bp	T833	Carl Roth, Karlsruhe, Germany
Ethidium bromide solution 1 %	2218	Carl Roth, Karlsruhe, Germany
FCCP	C2920	Sigma-Aldrich, St.Louis, MO, USA
Formaldehyde 37 %	4979	Carl Roth, Karlsruhe, Germany
Formamide	47670	Sigma-Aldrich, St.Louis, MO, USA
Glucose solution 20% (for GTT)	03158931	B. Braun, Melsungen, Germany
Glutamate	G1626	Sigma-Aldrich, St.Louis, MO, USA
Hydrogen peroxide	8070	Carl Roth, Karlsruhe, Germany
ImmoMix	BIO-25020	Bioline, Luckenwalde, Germany
LightCycler® 480 Probes Master	04887301001	Roche, Basel, Switzerland
DL-Malic acid	3034	Carl Roth, Karlsruhe, Germany
D(-)-Mannitol	4175	Carl Roth, Karlsruhe, Germany
2-Mercaptoethanol	4227	Carl Roth, Karlsruhe, Germany
MOPS	6979	Carl Roth, Karlsruhe, Germany
N-Acetyl-L-cysteine	A7250	Sigma-Aldrich, St.Louis, MO, USA
Oligomycin	O4876	Sigma-Aldrich, St.Louis, MO, USA
PBS (for leptin)	10010-015	Invitrogen, Carlsbad, CA, USA
Peroxidase from horeseradish	P8375	Sigma-Aldrich, St.Louis, MO, USA
Phosphatase Inhibitor Cocktail 2	P5726	Sigma-Aldrich, St.Louis, MO, USA
Protease Inhibitor Cocktail	P8340	Sigma-Aldrich, St.Louis, MO, USA
Protein Ladder Page Ruler™ Prestained	SM0671	Thermo Scientific, Waltham, MA, USA
Proteinase K (20 mg/ml)	EO0491	Thermo Scientific, Waltham, MA, USA
Rotiphorese® Gel 30	3029	Carl Roth, Karlsruhe, Germany
Roti®-Quant	K015	Carl Roth, Karlsruhe, Germany
Rotenone	R8875	Sigma-Aldrich, St.Louis, MO, USA
Safranine O	S884	Sigma-Aldrich, St.Louis, MO, USA
SensiMIX SYBR NoROX Kit	QT 650	Bioline, London
D(+)-Sucrose	4621	Carl Roth, Karlsruhe, Germany

Table A3. Continued.

Name	Product code	Company
Succinic acid	S3674	Sigma-Aldrich, St.Louis, MO, USA
5-Sulfosalicylic acid dihydrate	S2130	Sigma-Aldrich, St.Louis, MO, USA
Superoxide Dismutase	S5639	Sigma-Aldrich, St.Louis, MO, USA
TEMED	2367	Carl Roth, Karlsruhe, Germany
Thiourea	HN37	Carl Roth, Karlsruhe, Germany
TRIsure	BIO-38032	Bioline, London, UK
Triton X 100	3051	Carl Roth, Karlsruhe, Germany
Tween® 20	9127	Carl Roth, Karlsruhe, Germany
Urea	3941	Carl Roth, Karlsruhe, Germany

Table A4. Reaction kits.

Name	Product code	Company
Ultrasensitive Mouse Insulin ELISA	10-1249-01	Mercodia, Uppsala, Sweden
Leptin Mouse/Rat ELISA	RD291001200R	BioVendor, Brno-Žabovřesky, Tschechische Republik
Glutathione Assay Kit	703002	Caymann, Ann Arbor, MI, USA
QuantiTect® Reverse Transcription Kit	205311	Qiagen, Hilden, Germany
Wizard® SV Genomic DNA Purification System	A2360	Promega, Fitchburg, WI, USA
SV Total RNA Isolation System	Z3100	Promega, Fitchburg, WI, USA

Table A5. Material and equipment.

Item	Name/Type	Company
Balances	Precision TP-214	Denver Instrument, Brentwood
	Laboratory balance PB	Kern, Balingen, Germany
Blood glucose monitoring system	Freestyle lite	Abbot Diabetes Care, Alamenda, CA, USA
Centrifuges + Rotors	▪ Centrifuge 5417C, R	Eppendorf, Hamburg, Germany
	▪ Centrifuge 5810R	Eppendorf, Hamburg, Germany
	▪ Sorvall® Evolution RC + SS-34 Fixed-Angle Rotor	Thermo scientific, Waltham, MA, USA
	▪ Sorvall® Discovery 90 + Surespin™ 630 Rotor	Thermo Scientific, Waltham, MA, USA
Centrifuges tube	▪ Oak Ridge Centrifuge Tubes, 50ml (3118-0050)	NALGENE® Thermo Scientific, Waltham, MA, USA
	▪ Round Centrifuge Tube, 12ml (3110-0120)	NALGENE® Thermo Scientific, Waltham, MA, USA
Clark electrode system		
▪ Clark electrode	Digital Model 10	Rank Brothers, Cambridge
▪ Data acquisition system	PowerLab 26T	ADInstruments, Bella Vista
▪ Teflon membrane		Collotec, Niddatal, Germany
▪ Water bath	Julabo F12	MAGV, Rabenau-Londorf, Germany
Electrophoresis Systems		
▪ Electrophoresis chamber	▪ MSMINI, MSCHOICE	Biozym, Hessisch Oldendorf, Germany
	▪ Mini-Protean® System	Bio-Rad, Hercuels, CA, USA
	▪ Criterion cell	Bio-Rad, Hercuels, CA, USA
▪ Semi-dry transfer cell	Trans-Blot® SD Semi-Dry	Bio-Rad, Hercuels, CA, USA
▪ Power supply	PowerPac™ Basic	Bio-Rad, Hercuels, CA, USA

Table A5. Contiued.

Item	Name/Type	Company
Feeding-Drinking-Activity System	LabMaster System ▪ Process control Drinking-Feeding 259980 ▪ ActiMot2 302020 series	TSE Systems, Bad Homburg, Germany
Heparin-coated tubes	▪ Microvette® CB300CH	Sarstedt, Nümbrecht, Germany
Homogenizers	▪ Glass-glass potter S 15 ml	Sartorius, Göttingen, Germany
	▪ Glass-teflon potter S 15 ml	Sartorius, Göttingen, Germany
	▪ TissueLyser II (+ stainless steel beads 5 mm)	Quiagen, Hilden, Germany
Indirect calorimetry system	LabMaster System ▪ Process control for valves CaloSys 994600 series ▪ Process control CaloSys 994620 series ▪ Process control Air drying 994620 series ▪ CaloSys Pump 994620-AirP-YP-VC series	TSE Systems, Bad Homburg, Germany
	Climate chamber RMA 3745, Type 3603/16	Feutron®, Langenwetzendorf, Germany
Imaging systems	▪ The Odyssey® Infrared imaging system	LI-COR® Biosciences, Lincoln, NE, USA
	▪ Gel Jet	Intas, Göttingen, Germany
Magnetic Stirrer	RCT basic IKAMAG® safety control	IKA®, Staufen, Germany
Microplate reader	Infinite® M200	Tecan, Männedorf, Switzerland
Multi-well plates	▪ FLUOTRACTM200	Greiner Bio-One, Frickenhausen, Germany
	▪ Twin-tec PCR plate 96	Eppendorf, Hamburg, Germany
	▪ LightCycler® Multiwell plate 96	Roche, Basel, Switzerland
	▪ FrameStar 480	4titude®, Surrey, UK
	▪ Infinite® 200 NanoQuant	Tecan, Männedorf, Switzerland
Nitrocellulose membrane	#926-31092	LI-COR® Biosciences, Lincoln, NE, USA
NMR spectrometer	The Minispec mq7.5 POY Live Mice Analyzer	Bruker, Billerica, MA, USA
pH meter	CyberScan pH 510	Euchtech Instruments, Singapore
Pippets	▪ Research®	Eppendorf, Hamburg, Germany
	▪ Multipette® stream	Eppendorf, Hamburg, Germany
	▪ Matrix 8-Channel Electronic Pipette	Theromo Scientific, Waltham, MA, USA
	▪ Multipette® stream	Eppendorf, Hamburg, Germany
Ultrasonic bath	SONOREX Super RK 106	Bandelin, Berlin, Germany
Ultra Turrax	ULTRA-TURRAX® T 8	IKA®, Staufen, Germany
Shaker	▪ MS 3 basic	IKA®, Staufen, Germany
	▪ VXR basic Vibrax®	IKA®, Staufen, Germany
	▪ UNIMAX 2010	Heidolph, Schwabach, Germany
Syringes	▪ MICROLITER™ Syringe #701	Hamilton, Reno, NV, USA
	▪ MYJECTTOR U-100 Insulin 0.3ml	Terumo, Tokyo, Japan
Thermocycler	▪ FlexCycler Twinblock 48	Analytik Jena, Jena
	▪ Mastercycler® ep realplex epgradient S	Eppendorf, Hamburg
	▪ LightCycler® 96, 480	Roche, Basel, Switzerland

X

Table A6. Software.

Name/Version	Company
Genomatix Genome Analyzer v2.70226	Genomatix Software GmbH, München, Germany
Genomatix Mining Station Sesame 2.3	Genomatix Software GmbH, München, Germany
GraphPad PRISM 4	GraphPad Software, Inc. La Jolla, CA, USA
Intas GDS	Intas, Göttingen
LabChart5	ADInstruments, Bella Vista
ND-1000 V3.1.2	peqLab, Erlangen
Realplex 2.0	Eppendorf, Hamburg
SDSC Biology Workbench 3.2	San Diego Supercomputer Center, University of California, San Diego, CA, USA
Tecan i-control 1.4	Tecan, Männedorf
Tecan Magellan	Tecan, Männedorf

I.V Nano-HPLC-ESI tandem mass spectrometry – Material and settings

Online reversed-phase capillary HPLC:

- UltiMate 3000 HPLC system (Dionex/Thermo Scientific, Idstein, Germany)
- Acclaim PepMap100 column (3 µm C18 particle size, 75 µm inner diameter, 25 cm length) (Dionex /Thermo Scientific, Idstein, Germany)

ESI-tandem mass spectrometry analyses:

- HCT plus ion trap instrument (Bruker Daltonics, Bremen, Germany)
- nanoelectrospray ion source (Bruker Daltonics, Bremen, Germany)
- distal coated SilicaTips (FS360–20–10-D) (New Objective, Woburn, MA, USA)

General mass spectrometric parameters:

- capillary voltage: 1400 V
- end plate offset: 500 V
- dry gas: 8 l/min
- dry temperature: 160°C
- aimed ion charge control (ICC): 150 000
- maximal fill-time: 500 ms

Low-energy collision-induced dissociation (CID):

- fragmentation amplitude: 0.6 V
- MS spectra: sum of seven individual scans from m/z 300-1500; scan rate 8,100 (m/z)/s
- MS/MS spectra: sum of four scans from m/z 100-2200; scan rate 26 000 (m/z)/s

Search parameters for peptide and protein identification:

- Peptide charge states: 2^+, 3^+ and 4^+
- tryptic specificity allowing one missed cleavage
- No fixed modification, oxidation of methionine as variable modification
- Ion trap MS/MS spectra cut off score: 30
- mass tolerance: 0.4 Da and 0.4 Da for MS and MS/MS experiments
- Protein identification: minimum of 2 identified peptides

Software

- Compass 1.3 for esquire/HCT Build 581.4, esquireControl version 6.2 build 62.25 (Bruker Daltonics, Bremen, Germany)
- Software tool Data Analysis (version 4 SP4 build 281) (Bruker Daltonics, Bremen, Germany)

ACKNOWLEDGEMENTS

Ich möchte mich herzlich bei allen bedanken, die zum Gelingen dieser Arbeit beigetragen haben.

Mein Dank gilt zunächst Martin. Ohne dein Mitwirken und deine Bemühungen im Rahmen des NGFN-Netzes wäre dieses Thema nicht zu Stande gekommen. Ich danke dir für deine konstruktiven Denkanstöße und Diskussionen und dafür, dass du unseren Trupp so gut managst und zusammenhältst.

Allen Mitarbeitern der Arbeitsgruppe sei für ihre Unterstützung und für die Schaffung eines so tollen Arbeitsklimas gedankt. Insbesondere danke ich Nadine für ihre unermüdliche Hilfsbereitschaft, Tobias für seine Geduld, Dinge wiederholt zu erklären und die hilfreichen Ratschläge, die er für jedwede technischen und theoretischen Probleme bereit hält, sowie Jan für seine Statistiktipps. Sabine und Anika danke ich für ihre praktischen Ratschläge und die technische Unterstützung.

Ganz besonders bedanken möchte ich mich bei Dr. Gereon Poschmann für sein unerschütterliches Engagement für dieses Projekt und sein stets offenes Ohr für fachliche Fragen. Deine wertvollen Vor- und Ratschläge sowie dein Eifer mit dem du ständig neue Ideen zutage förderst, haben wesentlich zum Gelingen dieses Projektes beigetragen.

Tobi, Jan, Gereon, Flo, Monja, Nadine und Sabine – ein riesiges Dankeschön für eure Korrekturen dieser Arbeit!

Dem Team Neurodegeneration vom Helmholtz Zentrum München unter Leitung von Prof. Dr. Wurst danke ich, dass sie uns die *Dj-1* genetrap Mauslinie für die Zucht zur Verfügung gestellt haben. Ein großer Dank geht hierbei an Dr. Andreas Hofmann für die fachlichen Diskussionen per E-Mail sowie Dr. Daniela Vogt-Weisenhorn für ihre Anregungen und die Gespräche.

Dr. Karol Szafranski und Dr. Marco Groth vom Fritz-Lipmann-Institut, Jena, danke ich für die RNA Sequenzierung und die fachliche Unterstützung bei der Bewältigung der Datenflut.

Prof. Dr. Skerra und seinen Mitarbeitern danke ich für die Bereitstellung des Leptins.

Frau Prof. Dr. Schnieke und Herrn Prof. Dr. Haller danke ich, dass sie die Mühen als Zweitgutachterin bzw. als Vorsitzender der Prüfungskommission auf sich genommen haben.

Nicht zuletzt danke ich meinen Eltern für ihre Unterstützung und ihr fortwährendes Vertrauen darin, „dass ich das schon schaffen werde".

EIDESSTATTLICHE ERKLÄRUNG

Ich erkläre an Eides statt, dass ich die bei der Fakultät Wissenschaftszentrum Weihenstephan für Ernährung, Landnutzung und Umwelt (promotionsführende Einrichtung) der TUM zur Promotionsprüfung vorgelegte Arbeit mit dem Titel

The Role of the Parkinson's Disease associated Protein DJ-1 in the Development of Diet-induced Obesity in Mice

am Lehrstuhl für Molekulare Ernährungsmedizin unter der Anleitung und Betreuung durch Prof. Dr. Martin Klingenspor ohne sonstige Hilfe erstellt und bei der Abfassung nur die gemäß § 6 Abs. 6 und 7 Satz 2 angegebenen Hilfsmittel benutzt habe.

Ich habe keine Organisation eingeschaltet, die gegen Entgelt Betreuerinnen und Betreuer für die Anfertigung von Dissertationen sucht, oder die mir obliegenden Pflichten hinsichtlich der Prüfungsleistungen für mich ganz oder teilweise erledigt.

Ich habe die Dissertation in dieser oder ähnlicher Form in keinem anderen Prüfungsverfahren als Prüfungsleistung vorgelegt.

Ich habe den angestrebten Doktorgrad noch nicht erworben und bin nicht in einem früheren Promotionsverfahren für den angestrebten Doktorgrad endgültig gescheitert.

Die öffentlich zugängliche Promotionsordnung der TUM ist mir bekannt, insbesondere habe ich die Bedeutung von § 28 (Nichtigkeit der Promotion) und § 29 (Entzug des Doktorgrades) zur Kenntnis genommen. Ich bin mir der Konsequenzen einer falschen Eidesstattlichen Erklärung bewusst.

……........
 (Ort, Datum, Unterschrift)

CURRICULUM VITAE

PROMOTION & STUDIUM

seit Dez. 2008	**Promotion an der Technischen Universität München** Lehrstuhl für Molekulare Ernährungsmedizin
Okt. 2003 – *Okt. 2008*	**Studium der Ernährungswissenschaften Friedrich-Schiller-Universität Jena** ▪ Diplomarbeit am Deutschen Institut für Ernährungsforschung Potsdam-Rehbrücke, Abteilung Ernährungstoxikologie *Thema:* „Massenspektrometrische, genetische und kinetische Charakterisierung zweier Formen der murinen Sulfotransferase 1A1" ▪ *Abschluss:* Diplom (Note 1,1) ▪ Diplomarbeitspreis des APFEL e.V. Friedrich-Schiller-Universität Jena

SCHULBILDUNG

1993 – 2002	**Friederiken-Gymnasium Bernburg** ▪ *Abschluss:* Abitur (Note 1,2) ▪ Karl-von-Frisch-Abiturienten-Preis für hervorragende Leistungen im Fach Biologie
1991 - 1993	**Grundschule Karlstraße, Bernburg**
1989 – 1991	**Polytechnische Oberschule Karl-Liebknecht, Bernburg**

PRAKTIKA & NEBENTÄTIGKEITEN

Feb. 2008 – *Sep. 2008*	**Deutsches Institut für Ernährungsforschung Potsdam-Rehbrücke**	Studentische Hilfskraft
März 2007	**Thüringer Landesanstalt für Landwirtschaft, Jena**	Praktikum beim Thüringer Agrarmarketing („Regionale Speisekarte")
Aug. 2006	**Friedrich-Schiller-Universität Jena**	Forschungspraktikum am Lehrstuhl für Ernährungstoxikologie
März/April 2006	**Anhaltinische Pflanzen-zucht GmbH, Bernburg**	Praktikum in der Maisforschung
Okt. 2005 – *Jan. 2006*	**Friedrich-Schiller-Universität Jena**	Studentische Hilfskraft
Aug./Sep. 2005	**Leibnitz-Institut für Naturstoffforschung, Jena**	Praktikum in der Nachwuchsgruppe „Pathogene Pilze"

TAGUNGENG, KONFERENZEN UND WEITERBILDUNGEN

▪	*Dez 2012*	5th Annual Meeting of NGFN-Plus and NGFN-Transfer, Heidelberg	Posterbeitrag
▪	*Mai 2012*	19th European Congress on Obesity (ECO2012), Lyon, France	Posterbeitrag
▪	*März 2012*	49. wissenschaftlicher Kongress der Deutschen Gesellschaft für Ernährung e.V., Freising	Präsentation
▪	*Okt. 2011*	Sattelitensymposium "From Causes of Obesity to Clinical Applications", Essen	
▪	*Okt. 2011*	27. Jahrestagung der Deutschen Adipositas-Gesellschaft, Bochum	Posterbeitrag
▪	*Nov. 2010*	3rd Annual Meeting of NGFN- Plus and NGFN-Transfer, Berlin	Posterbeitrag
▪	*Nov. 2009*	2nd Annual Meeting of NGFN- Plus and NGFN-Transfer, Berlin	Posterbeitrag
▪	*Nov. 2009*	Kompaktkurs „Versuchstiere, Tierversuche und Ersatzmethoden", Berlin	Zertifikat nach FELASA Kat. B
▪	*Juni 2009*	16. Arbeitstagung: Mikromethoden in der Proteinbiochemie, München	
▪	*Mai 2009*	Neurizons, Göttingen	Posterbeitrag
▪	*Feb./März 2009*	Erasmus Intensive Course "Combating Obesity – Strategies for Prevention and Intervention (COSPI)", Grundlsee, Österreich	Präsentation
▪	*Dez. 2008*	1st Annual Meeting of NGFN- Plus and NGFN-Transfer, München	
▪	*Sept. 2008*	NuGO week 2008, Potsdam	
▪	*Feb. 2008*	DIfE Symposium "Genetics and Pathophysiology of Type 2 Diabetes", Potsdam	

PUBLIKATIONEN

Besong Agbo D, Klafki HW, Poschmann G, Seyfarth K, Genius J, Stühler K, Wurst W, Meyer HE, Klingenspor M, Wiltfang J (2013). Development of a Capillary Isoelectric Focusing Immunoassay to Measure DJ-1 Isoforms in Biological Samples. *Analytical Biochemistry*. 443(2):197-204

SONSTIGES

Auslandsaufenthalt   Neuseeland - *Aug. 2002 – Aug. 2003*

Persönliche Angaben
- ▪ *Geburtsdatum:* 27.09.1982
- ▪ *Geburtsort:* Bernburg